Freie Universität Berlin

Kumulative Dissertation

Structural, Metamorphic and Geodynamic Aspects of Sheath-Fold Nappe Formation (Rote Wand Nappe, Tauern Window, Eastern Alps)

Philip Groß

Zur Erlangung des
Doktorgrades der Naturwissenschaften
im

Fachbereich Geowissenschaften
Institut für Geologische Wissenschaften
Fachrichtung Tektonik und Sedimentäre Systeme

4. März 2021

Eidesstattliche Erklärung

Hiermit erkläre ich, Philip Groß, dass diese Arbeit mit dem Titel „Structural, Metamorphic and Geodynamic Aspects of Sheath-Fold Nappe Formation (Rote Wand Nappe, Tauern Window, Eastern Alps)“ ausschließlich auf Grundlage der angegebenen Hilfsmittel und Hilfen selbstständig von mir verfasst wurde. Die Arbeit wurde nicht in einem früheren Promotionsverfahren eingereicht.

Diese Arbeit wurde vom Promotionsausschuss des Fachbereichs Geowissenschaften

am _____ genehmigt.

Erstgutachter: Prof. Dr. Mark R. Handy

Zweitgutachter: Prof. Dr. Timm John

Die Disputation erfolgte am 01. Dezember 2020.

Berlin, den 4. März 2021

Philip Groß

Abstract

The Tauern Window is the largest tectonic window of the Alps. It contains relics of the subduction channel that formed during Cenozoic subduction of the Alpine Tethyan Ocean and the European margin below the Adriatic plate. This thesis documents the structural, kinematic and metamorphic evolution of a segment of this subduction channel exposed in the central Tauern Window.

The thesis presents new structural data that document a tens-of-kilometers-scale recumbent sheath fold in the center of the Tauern Window. The fold comprises an isoclinally folded thrust that transported relicts of the former Alpine Tethys (Glockner Nappe s. str.) onto a distal part of the former European continental margin (Rote Wand Nappe). New petrologic data indicate that the fold formed during early stages of exhumation from maximum burial depth at high-pressure conditions (ca. 2 GPa, 500 °C). Exhumation of the fold to mid-crustal levels is evidenced by near-isothermal decompression to roughly 1 GPa. The fold ascended in the subduction channel between two contemporaneous opposite-sense shear zones; normal-sense (i. e., top-hinterland) at the top of the fold and thrust-sense (i. e., top-foreland) below.

The subduction-related thermal structure of the sheath fold was constrained by Raman spectroscopy on carbonaceous matter (RSCM) thermometry. The greatest peak-temperature conditions are located in the center of the fold at the folded ocean-on-continent thrust. The peak-temperature contours are oriented roughly parallel to the folded nappe contact so that they display a sheath-like pattern that mimics the geometry of the sheath fold itself. This pattern indicates that finite strain during sheath-fold formation decreased laterally from the fold's center. Thus, together with the contemporaneous vertical strain gradients, the fold was shaped at least initially by diapir-like kinematics during exhumation.

Lithostratigraphic correlation of the tectonic units in the central Tauern Window that derive from the European margin documents intense, rift-related segmentation of the margin. The Rote Wand Nappe, which is part of the sheath fold, probably originates from an extensional allochthon that was separated from the main margin by an extensive rift basin above strongly thinned continental basement.

Here it is proposed that this extensional allochthon, when subducted, caused a perturbation of the flow field in the subduction channel. In line with sheath-fold theory, this caused strain localisation at the extensional allochthon, facilitating its initial diapiric ascent to form a proto-sheath fold. While being further exhumed by the normal-sense shear zone at its top, the rest of the fold was amplified in overall, thrust-sense simple-shear to a pronounced sheath-fold geometry. This model and above observations are compatible with forced channel flow as driving force of the upward-directed flow.

This study shows how large structures inherited from rifting — e. g., extensional allochthons — could potentially induce perturbation of flow in subduction channels during the subduction of distal continental margins. Such perturbations can lead to complex kinematics in subduction channels and result in highly non-cylindrical nappes. Further investigation of similar scenarios could contribute to a better understanding of subduction zone dynamics during the transition from oceanic subduction to continent collision.

Zusammenfassung

Das Tauernfenster ist das größte tektonische Fenster der Alpen. Es enthält Reste des Subduktionskanals, der bei der känozoischen Subduktion der Alpinen Tethys und des europäischen Kontinentalrands unter die adriatische Platte gebildet wurde. Diese Arbeit dokumentiert die Entwicklung der Strukturen, der Kinematik und der Metamorphose in einem Segments dieses Subduktionskanals, das nun im zentralen Tauernfenster aufgeschlossen ist.

Die Arbeit zeigt neue Strukturdaten, die eine Zehnerkilometer-große, liegende Zungenfalte im Zentrum des Tauernfensters belegen. Die Falte beinhaltet eine isoklinal verfaltete Überschiebung, entlang der Reste der ehemaligen Alpinen Tethys (Glocknerdecke) auf einen distalen Teil des ehemaligen europäischen Kontinentalrands überschoben worden sind. Neue petrologische Daten zeigen, dass die Falte während der Frühphase der Exhumierung von der größten Versenkungstiefe bei Hochdruckbedingungen (ca. 2 GPa, 500 °C) gebildet wurde. Die Exhumierung der Falte bis in mittlere Krustentiefe zeigt sich durch annähernd isothermale Dekompression bis etwa 1 GPa. Die Falte stieg im Subduktionskanal zwischen zwei gleichzeitigen Scherzonen mit gegensätzlichen Schersinnen auf; also mit abschiebendem Schersinn (d. h. Hangendblock zum Hinterland) im Hangenden der Falte und überschiebendem Schersinn (d. h. Hangendblock zum Vorland) im Liegenden.

Mittels Ramanspektroskopie an kohligem Material (RSCM) wurde die subduktionsbedingte thermische Struktur der Zungenfalte ermittelt. Die höchsten Temperaturen des Metamorphosehöhepunkts finden sich im Zentrum der Falte am verfalteten Überschiebungskontakt zwischen den ozeanischen und kontinentalen Einheiten. Die Temperatur-Konturlinien des Metamorphosehöhepunkts verlaufen etwa parallel zum verfalteten Deckenkontakt. Dies ergibt ein zungenförmiges Muster, welches die Form der Zungenfalte selbst nachahmt. Dieses Muster zeigt, dass die finite Verformung während der Zungenfaltenbildung seitlich vom Faltenkern weg abnahm. Zusammen mit dem gleichzeitigen vertikalen Verformungsgradienten ergibt sich daher, dass die Falte am Anfang der Exhumierung durch diapirartige Kinematik geformt wurde.

Die lithostratigraphische Korrelation der tektonischen Einheiten im zentralen Tauernfenster, die vom europäischen Kontinentalrand stammen, belegt eine intensive, Rift-bedingte Segmentierung des Kontinentalrands. Die Rote Wand-Decke, ein Teil der Zungenfalte, stammt vermutlich von einem extensionalen Allochthon, das durch ein weites Riftbecken über stark ausgedünntem kontinentalem Grundgebirge vom Hauptteil des Kontinentalrands abgetrennt war.

Hier wird vorgeschlagen, dass dieses extensionale Allochthon bei der Subduktion eine Perturbation im Strömungsfeld des Subduktionskanals erzeugt hat. Dies führte — im Einklang mit der Theorie zu Zungenfalten — zur Lokalisierung der Verformung am extensionalen Allochthon, was den initialen diapirartigen Aufstieg und die Bildung einer Proto-Zungenfalte ermöglichte. Während der weiteren Exhumierung durch die abschiebende Scherzone im Hangenden wurde der Rest der Falte durch einfache Scherung mit überschiebender Kinematik zu einer ausgeprägten Zungenfaltengeometrie amplifiziert. Dieses Modell und die oben geschilderten Beobachtungen sind kompatibel mit erzwungener Kanalströmung (oder „Auspressung“) als Antriebskraft der aufwärts gerichteten Stömung.

Diese Studie zeigt, wie große, vom Rifting ererbte Strukturen — z. B. extensionale Allochthone — während der Subduktion von distalen Kontinentalrändern möglicherweise zu Strömungsperturbationen in Subduktionskanälen führen können. Solche Perturbationen können zu komplexer Kinematik in Subduktionskanälen führen und somit die Bildung hochgradig nicht-zylindrischen Decken begünstigen. Weitergehende Untersuchungen ähnlicher Szenarien könnten zu einem besseren Verständnis der Dynamik von Subduktionszonen während des Übergangs von ozeanischer zu kontinentaler Subduktion führen.

Acknowledgements

This work would not have been possible without the support of many colleagues and friends! First of all, I am indebted to my supervisors Jan Pleuger, Mark Handy and Timm John. They gave guidance in the field, greatly helped to improve the manuscripts and were always motivated to discuss the problems I encountered, even so the horrors of Tauern geology (e. g., "Falkenbachlappen"). At the same time, they gave me all the freedom I needed to make my own experiences and mistakes.

Furthermore, I thank Julian Hülscher, Yann-David Brück-Göckelmann and Marc Grund for assistance in the field and insightful discussions. Tim Langner, Marisa Germer and also David are thanked for helping me with RSCM measurements. Anna Giribaldi masterly prepared countless of my samples, which was an invaluable help. I thank Anja Schleicher and Andrea Gottsche for providing XRF measurements. Many thanks to Wolfgang Frank, Ralf Schuster, Benjamin Huet and Christoph Iglseder from the GBA for a great, instructive excursion to the northern Tauern Window and always being willing to discuss and share knowledge, maps and even samples. I thank Philipp Gleißner who shared unpublished age results, Matthias Weger for sending a printed copy of his dissertation and Martina Grundmann for IT-support and providing me a truly powerful computer to work with. Sascha Zertani and Ester Schwarzenbach are thanked for help on the electron microprobe, Martina Menneken and Robin Visser for help in the Raman lab.

In general, I thank all my colleagues and friends from the geology department, who made the time in Berlin truly enjoyable, gave support in numerous ways and were often motivated to have after-work beers. I greatly acknowledge the permission for sampling in the Nationalpark Hohe Tauern granted by the national park administration offices of Kärnten and Salzburg.

Last but not least, I am deeply indebted to my friends, family and to my partner Marisa.

Many thanks to all of you, it was a great journey!

Organization of the Thesis

This thesis consists of five chapters. Two of them (Chapters 3 and 4) were published in or accepted by peer-reviewed journals, one (Chapter 2) is prepared for briefly submission. The following presents the structure of the thesis and explains the contributions of the authors and additional co-workers.

Chapter 1: Introduction

This chapter introduces the main topic of the thesis, explains the framework of the study and gives an overview on the formation mechanisms of sheath folds.

Chapter 2: Geology of the Central Tauern Window

Philip Groß, Jan Pleuger, Mark R. Handy
Will be submitted to Swiss Journal of Geosciences.

This chapter gives an introduction to the geology of the central Tauern Window. The geodynamic evolution model of the region, with special emphasis on Mesozoic rifting, is re-evaluated on the basis of previous and new findings.

Philip Groß conducted most of the fieldwork, carried out the lithostratigraphic correlation, wrote the manuscript and created all figures. Jan Pleuger and Mark Handy helped during much of the fieldwork and greatly improved the text, figures and the lithostratigraphic correlation.

Chapter 3: Crustal-Scale Sheath Folding at HP Conditions in an Exhumed Alpine Subduction Zone (Tauern Window, Eastern Alps)

Philip Groß, Mark R. Handy, Timm John, Gerhard Pestal, Jan Pleuger
Published in Tectonics.

This chapter documents the structure of a sheath fold nappe in the central Tauern Window and its kinematic and metamorphic evolution during exhumation from the Alpine subduction zone.

Philip Groß conducted much of the fieldwork (sampling, mapping, structural measurements), carried out parts of the sample preparation, most of the analytical work (EPMA, Raman spectroscopy) and data evaluation, compiled the map, constructed the cross sections, wrote most of the manuscript and created all figures. Jan Pleuger and Mark Handy contributed to the manuscript text and and field work and together with Timm John greatly improved the text and figures. Gerhard Pestal contributed with geological mapping and valuable ideas on the tectonic structure of the area. Marisa Germer prepared rock powder for XRF analysis. Marc Grund and Yann-David Brück-Göckelmann assisted during fieldwork. Thin and thick sections were largely prepared by Anna Giribaldi.

Chapter 4: Evolving Temperature Field in a Fossil Subduction Channel During the Transition from Subduction to Collision (Tauern Window, Eastern Alps)

Philip Groß, Jan Pleuger, Mark R. Handy, Marisa Germer, Timm John
Published in Journal of Metamorphic Geology.

This chapter documents the evolution of the thermal structure of the sheath fold nappe during subduction, exhumation and collision.

Philip Groß conducted most of the fieldwork (sampling, structural measurements), carried out parts of the sample preparation and the analytical work (Raman spectroscopy). Philip Groß performed the data evaluation and created all the maps and cross sections, wrote the manuscript and created all figures. Jan Pleuger and Mark Handy contributed to the manuscript text and and field work and together with Timm John greatly improved the text and figures. Marisa Germer conducted large parts of the Raman analysis and reviewed the manuscript. Tim Langner and Yann-David Brück-Göckelmann provided additional Raman data. Thin sections were mostly prepared by Anna Giribaldi.

Chapter 5: Conclusions

This chapter summarizes the main conclusions that can be drawn from the entire work.

Chapter 6: Outlook

This last chapter proposes some potential lines of further research that may build on the results of this thesis.

Contents

List of Figures

List of Tables

Chapter 1

Introduction

The Alpine orogen is arguably one of the best-studied mountain chains on earth. Many researchers that investigated this chain gained insights that sometimes fundamentally advanced the understanding of tectonics and mountain building processes or further established new concepts. For example, folds, thrusts, far-travelled nappes and fold nappes were recognized early in the Alps (Trümpy, 2001).

The Alps (Figure 1.1) are the product of two phases of mountain building: The Cretaceous Eoalpine orogeny and the Cenozoic Alpine orogeny (Froitzheim et al., 1994; Schmid et al., 2004). The Eoalpine orogen is mainly exposed in the Eastern Alps, whereas the Alpine orogen (Froitzheim et al., 1994; Schmid et al., 2004) is exposed in the Western and Central Alps and in several tectonic windows further in the East. This study focusses on rocks formed during the Alpine orogeny that are exposed in one of these windows, the so-called Tauern Window. Here, tectonic units reappear on the surface that are prevalent in the Western and Central Alps (i. e., the Penninic and Sub-Penninic nappes) but mostly hidden below the relics of the older Eoalpine orogen (i. e., the Austroalpine nappes) in the Eastern Alps. This first-order observation already shows one of the main characteristics of the structure of the Alpine orogen: The major tectonic units (i. e., nappe systems that derive from paleogeographic domains, sensu Schmid et al., 2004) and can often be traced for hundreds of kilometers along the — partly arcuate — strike of the orogen. These major units are usually composed of several nappes that consequently also largely strike parallel to the orogen and often display a high degree of cylindricity, even though some of them suffered from later refolding which sometimes resulted in complex, non-cylindrical geometries.

In contrast to the typically cylindrical nappes, this thesis uses an example of a sheath fold nappe in the Tauern Window to discuss structural and metamorphic aspects of primary (i. e., single-phase) non-cylindrical nappes and fold nappes. The results show the potential relevance of such structures during subduction, exhumation and collision.

1.1 Framework of this Study

The research presented in this thesis was conducted in the interdisciplinary research project "Understanding subduction by linking surface exposures of subducted and exhumed crust to geophysical images of slabs" that was initiated by Jan Pleuger, Timm John (both FU Berlin) and Frederik Tilmann (GFZ Potsdam). The former two and Mark Handy (FU Berlin) supervised this thesis. Two additional PhD students were involved in the project: Sascha Zertani worked on characterizing the seismic properties of crystalline basement under high-pressure conditions and Stefan Mroczek used a high-density

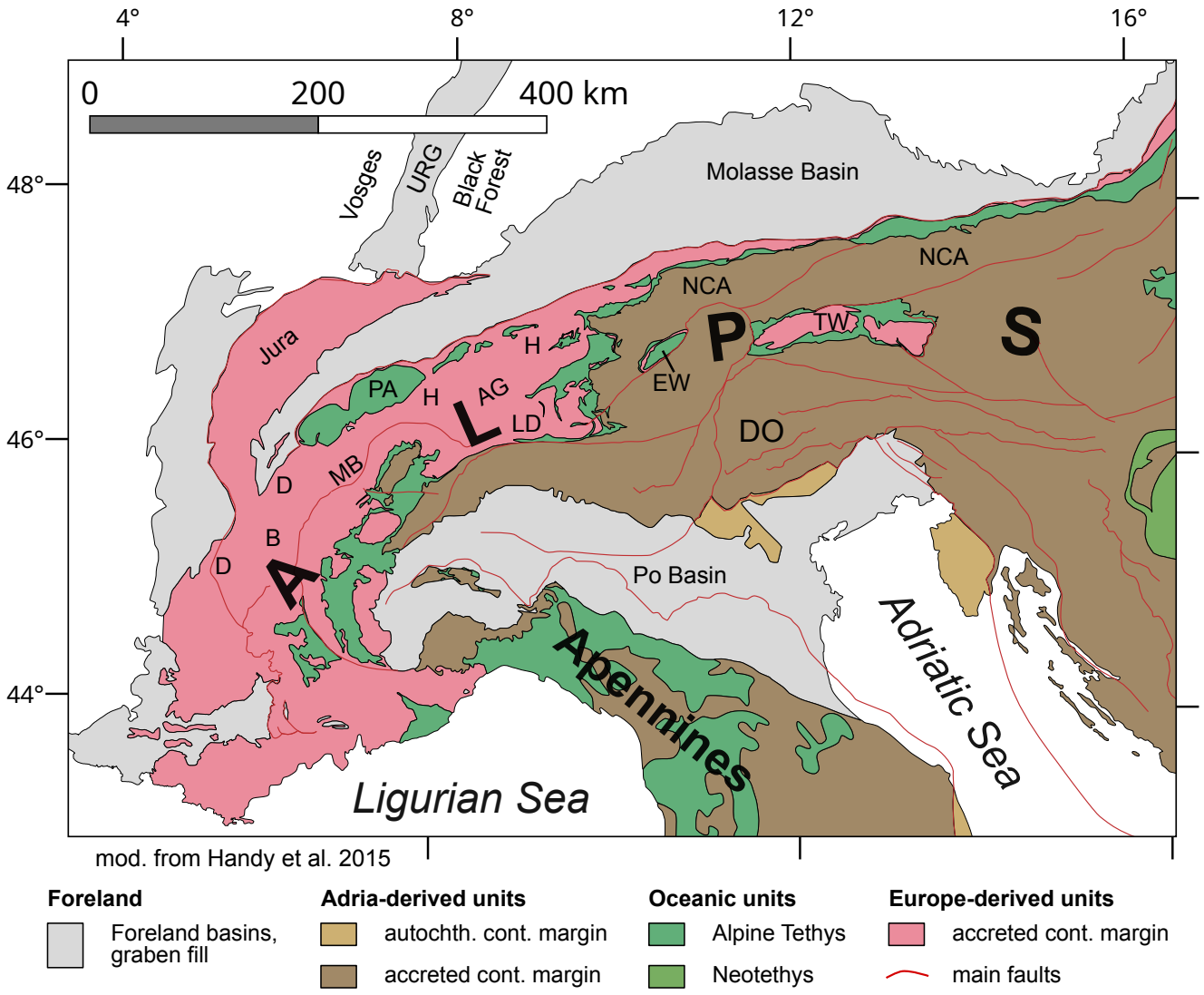

Figure 1.1: Tectonic overview map of the Alps (modified from Handy et al., 2015). AG = Aar and Gotthard massifs, B = Belledonne Massif, D = Dauphinois Zone, DO = Dolomites, EW = Engadine Window, H = Helvetic nappes, LD = Lepontine Dome, MB = Mont-Blanc Massif, NCA = Northern Calcareous Alps, PA = Préalpes, TW = Tauern Window, URG = Upper Rhine Graben.

seismometer deployment (Swath D) to image the crustal structure beneath the Eastern Alps. The project was funded by the Deutsche Forschungsgemeinschaft (DFG; Grants PL 534/4-1, JO 349/11-1, HA 2403/24-1) as part of the priority program SPP2017 “Mountain Building in Four Dimensions (MB-4D)” in the framework of the European AlpArray Working Group.

1.2 Formation of Sheath-Like Fold Geometries

The term sheath fold (Carreras et al., 1977; Cobbold & Quinquis, 1980) describes a non-cylindrical fold that has a complex three-dimensional structure, similar to a sheath, a cone or a tongue, with its hinge line orientation changing by more than 90° (Ramsay & Huber, 1987). Often, the term sheath fold carries a connotation that implies certain kinematics that led to the folding. In the following text, the term

sheath fold is used in a purely descriptive sense of a sheath-like (fold) geometry. Formation mechanisms that are inferred from the geometry are specified additionally.

The folding of a layer to a sheath-like geometry can occur in a number of ways that are very distinct regarding the kinematics and mechanics that caused the folding. These are, e. g., superposition of multiple phases of folding, strain gradients leading to diapir structures, flow perturbation around inclusions or passive shear-amplification of preexisting structures. In the latter two cases the sheath folds form in a single deformation phase in response to an externally-applied shear deformation and require some sort of structural or rheological precursor at which they nucleate.

Folds with a sheath-like geometry are observed relatively frequently in nature. The largest ones described in the literature are usually found in very high-grade, highly-deformed Precambrian or Paleozoic basement and reach sizes of several tens of kilometres (e. g., Bonamici et al., 2011; Chetty et al., 2012; Goscombe, 1991; Vollmer, 1988). While these folds are often thought to be associated with orogenic lower crustal flow, somewhat smaller examples on the scale of some hundreds of metres were reported that formed at relatively low- to medium-grade metamorphic conditions mainly in deformed sedimentary cover rocks, as e. g., in Oman (Cornish & Searle, 2017; Searle & Alsop, 2007) or the Swiss Alps (Lacassin & Mattauer, 1985). Even smaller examples on the metre-scale and below are reported from a wide spectrum of geodynamic settings. Small sheath-like folds occur in intensely-deformed crustal shear zones in crystalline rocks (e. g., Beunk & Page, 2001; Fossen & Rykkelid, 1990; Hanmer & Greene, 2002), carbonates (e. g., Ghosh et al., 1999; Mies, 1993), metapelites and -psammites (e. g., Alsop & Carreras, 2007; Alsop & Holdsworth, 2012; Skjernaa, 1989) and cherts (Minnigh, 1979). Sheath folds are also described in flowing salt (e. g., Talbot & Jackson, 1987b), subglacially-deformed (e. g., Van der Wateren, 1999) and slumped sediments (e. g., Roberts, 1989) and ignimbrite flows (e. g., Branney et al., 2004); for more examples of "exotic" sheath folds, see Alsop et al. (2007). In many cases where sheath folds are observed, including some of the above, the associated formation mechanisms are not entirely clear. The following sections give a short introduction to the characteristics of the different types of folds with sheath-like geometries and their formation mechanisms.

1.2.1 Refolds

Refolds are the result of the superposition of multiple phases of folding (e. g., Ramsay & Huber, 1987). This can lead to complex three-dimensional fold geometries, including sheath-like fold geometries (Figure 1.2). Critical in distinguishing sheath-like refolds from single-phase sheath folds is to test if structural overprinting criteria exist that correspond with a polyphase folding history — like, e. g., a stretching lineation parallel to the fold axes of a first phase that is crenulated by the axial plane foliation of a second phase.

In nature, such structures occur on a great range of different scales. Figure 1.3 shows examples of refolds on the outcrop scale. Entire nappes with a sheath-like geometry that are the product of superposed folding were described and analysed, e. g., in the Central Alps (Maxelon & Mancktelow, 2005; Steck et al., 2019) or in the Bohemian Massif (Jeřábek et al., 2016). Refolds are extensively discussed in the existing literature (e. g., Grasemann et al., 2004; Ramsay & Huber, 1987; Thiessen, 1986) and therefore will not be further discussed here.

1.2.2 Diapirs

Diapirs are dome-, finger- or mushroom-shaped structures that are generally considered to form as Rayleigh-Taylor instabilities due to density contrasts (Talbot & Jackson, 1987b). The density contrast is

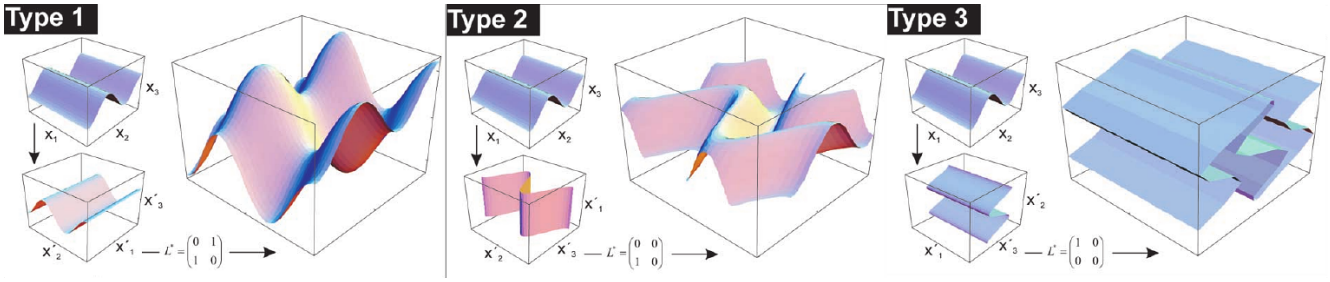

Figure 1.2: Examples of Ramsay-type 1, 2 and 3 refold structures (modified from Grasemann et al., 2004), some of which can display sheath-like geometries.

usually either thermally (e. g., mantle diapir) or compositionally induced (e. g., salt diapirs). Therefore, the flow in a diapir is driven by (internal) body forces rather than externally applied, e. g., as shear force. Diapirs rise ductilely and penetrate the overlying rocks until the driving density contrast vanishes. This flow often involves convection-like counter-flow, which can lead to the incorporation of external material into the diapir (Talbot & Jackson, 1987a). The diverse morphological characteristics of (salt-) diapirs are mainly controlled by the viscosity contrast to the surrounding material and their stage of development. Diapiric flow is best known in the cases of salt domes and mantle diapirs. It has also been attributed to the formation of shale and serpentinite diapirs and highly metamorphic gneiss domes.

In the formation of diapirs, large strain gradients are involved, e. g., between the buoyancy-driven upwards-directed flow of rising material in the diapir stem and the sinking surrounding material. However, externally-imposed strain gradients due to flow perturbations in shear zones can also lead to arcuate folds and diapir- or sheath-like structures (Alsop & Holdsworth, 2007). This process has been described to occur in subduction-exhumation zones (Xypolias & Alsop, 2014). Also the gneissic Adula Nappe in the Central Alps experienced diapir-like kinematics during its exhumation from high-pressure conditions (Kossak-Glowczewski et al., 2017), even though the forces driving the upward flow are unclear in this case.

1.2.3 Structure-Controlled Sheath Folds

The classical model of the formation of sheath folds in shear zones was formulated by Cobbold & Quinquis (1980). This model requires a structural perturbation in a layer, which is passively amplified in homogeneous simple shear (Figure 1.4). The sheath geometry is the result of passive rotation of the perturbation by stretching in the direction of shear. In such a scenario, relatively large shear strains of $\gamma > 10$ are required to produce a sheath geometry. It is important to note that this model is purely kinematic and does not involve rheology contrasts in the deforming material, so that ideally, the layering acts as an entirely passive marker. The geometry of such a sheath fold is only controlled by the geometry of the initial perturbation and the type and amount of strain imposed on it. Compared to sheath folds in nature where rheological layering is often present, this is of course a strong simplification that is only justified in cases with low viscosity contrasts. Analogue experiments by Marques et al. (2008) suggest an upper limit of the viscosity contrast of one order of magnitude between perturbation and matrix to form such structure-controlled sheath folds. Sectioned along the x-z-plane, such sheath folds appear as tight to isoclinal folds with axial planes (sub-)parallel to the shearing plane. Sectioned along the y-z-plane, these sheath folds display nested, concentric, eye-shaped patterns (Figure 1.5).

Figure 1.3: Two arrow-shaped refold patterns (dark) in calcareous micaschist, coin for scale.

Based on a large amount of analysed natural sheath folds, Alsop & Holdsworth (2006) argued that the geometry of passive sheath folds can be used to infer the bulk strain type in which they were formed. This notion was questioned by Marques et al. (2008) based on their analogue experiments that highlighted the significance of the geometry of the initial perturbation and the effect of viscosity layering that can be expected for many naturally-occurring sheath folds (see also comments by Alsop & Holdsworth, 2009 and Marques, 2009). This view was supported in similar experiments by Dell'Ertole & Schellart (2013). In any case, the effect of strain type, amount of finite strain, initial geometry and the interplay of these parameters on the resulting geometry of sheath folds is very complex and still offers potential to be investigated further.

1.2.4 Rheology-Controlled Sheath Folds

Sheath folds can also be generated by flow perturbations around inclusions that form a large rheology contrast (Figure 1.6). In a layered, viscous medium subjected to simple shear parallel to the layers, such folds may nucleate at rotating, rigid inclusions (Adamuszek & Dabrowski, 2017; Marques & Cobbold, 1995; Rosas et al., 2002) or at planar and weak inclusions acting as slip surfaces (Reber et al., 2012). So far, these rheology-controlled types of sheath folds were mainly examined in analogue and numerical experiments which showed that low shear strain is sufficient to form such sheath folds, in contrast to structure-controlled sheath folds that require large shear strains (Cobbold & Quinquis, 1980). The rheology-controlled sheath folds can be regarded as the three-dimensional expression of flanking structures (Reber et al., 2012), which are usually observed in nature in two dimensions only. Therefore, it may well be that many of the nested, concentric and eye-shaped cross-sections of sheath folds observed on the meso- to microscale are in fact flanking structures sectioned along the y-z-plane (Exner & Dabrowski, 2010; Reber et al., 2012).

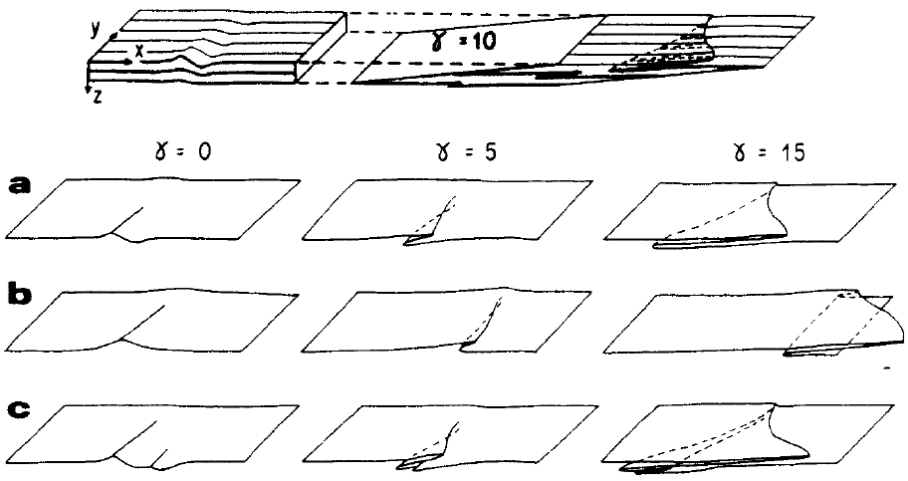

Figure 1.4: Formation of sheath folds from non-cylindric perturbations in dextral simple shear (from Cobbold & Quinquis, 1980).

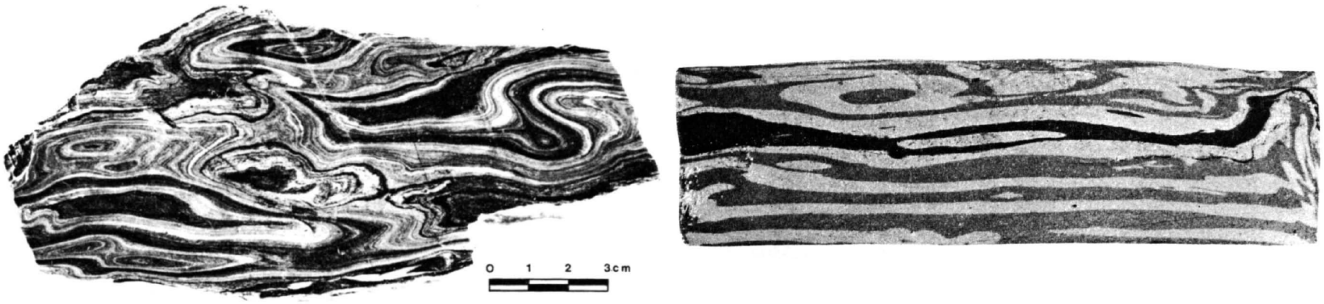

Figure 1.5: Examples of nested, concentric, eye-shaped patterns of sheath folds sectioned along the y-z-plane from nature (left) and experiment (right; from Cobbold & Quinquis, 1980).

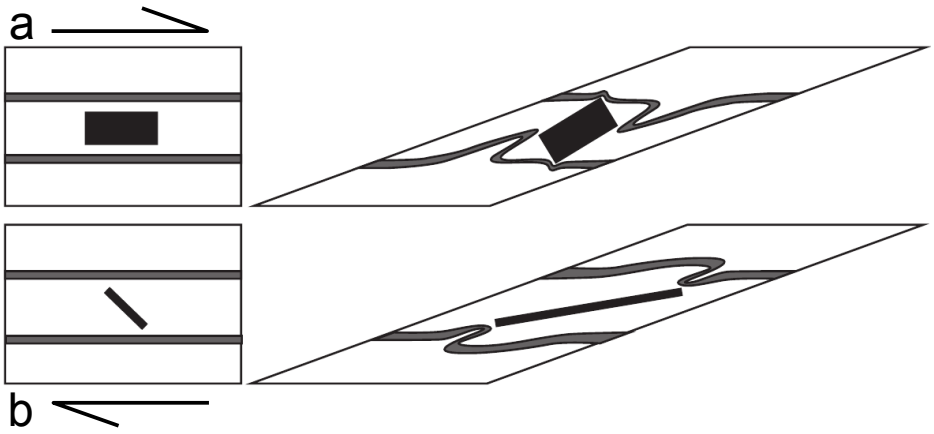

Figure 1.6: Sheath fold-formation from flow perturbation around strong (a) and weak, planar (b) inclusions in dextral simple shear (modified from Adamuszek & Dabrowski, 2017).

Chapter 2

Geology of the Central Tauern Window

Philip Groß, Jan Pleuger, Mark R. Handy
This chapter will be submitted to Swiss Journal of Geosciences.

2.1 Abstract

Many continent-derived tectonic units in the Western and Central Alps indicate hyper-extension during Mesozoic rifting and the formation of the Penninic Ocean. In this study, we reassessed the lithostratigraphic data from the central Tauern Window in the Eastern Alps to reconstruct the post-Variscan evolution of this area and the rift-related geometry of the European continental margin. The lithostratigraphic record of the individual tectonic units in the Alpine nappe stack shows systematic variations in the geodynamic setting. The lower tectonic units (Venediger nappe system, Eclogite Zone and Trögereck Nappe) are characterized by a thick, Lower Cretaceous syn-rift sequence (proximal — Kaserer Formation; distal — Wörth Unit) that overlies strongly-thinned continental basement with some pre-rift sediments. In contrast, the uppermost Europe-derived tectonic unit (Rote Wand Nappe) preserved a thick pre-rift sediment sequence deposited on continental basement, overlain by an extensive Cretaceous syn- to post-rift succession (Brennkogel Formation). In analogy to the Western and Central Alps, we propose that these observations indicate hyper-extension of this eastern part of the European margin during rifting. This involved the formation of an extensional allochthon partly preserved in the Rote Wand Nappe that was separated from the main part of the European margin by a large rift basin on strongly-thinned continental crust. The along-strike discontinuity of the Rote Wand Nappe might reflect the dimensions of the extensional allochthon, indicating intense, rift-related margin-parallel segmentation of the European continental crust.

2.2 Introduction

Studies of the well-preserved Jurassic-Cretaceous rifting phase in the Western and Central Alps provided detailed insights in the processes that led from a stable continent to rifting, breakup and the formation of the Penninic oceanic basin between the European margin in the North and Adriatic margin in the South (e. g., Froitzheim & Manatschal, 1996; Schaltegger et al., 2002). The Penninic and Subpenninic basement nappes of the Alps originate from the paleogeographic domains that were formed during or at least strongly affected by this rifting. The Penninic tectonic units are largely continuous

along the entire Western and Central Alpine Arc to the boundary to the Eastern Alps. However, several studies showed that the laterally continuous nappe systems derived from both margins show features indicative of margin-parallel, rift-related segmentation of the continental crust and hyper-extension (e. g., Ferrando et al., 2004; Froitzheim & Manatschal, 1996; Lemoine et al., 1986; Loprieno et al., 2011; Manatschal & Müntener, 2009; Ribes et al., 2019). These rift-inherited features may be of critical importance during later convergence in controlling the architecture of Alpine-type orogens (e. g., Handy et al., 1996; Mohn et al., 2014; Schmid et al., 1990) and could therefore also affect the degree of cylindricity of such an orogen.

In the Eastern Alps the rocks exposed in the Tauern Window preserve relics of this major rifting phase, although rift-related structures in the Tauern Window were substantially obscured by later subduction, exhumation, collision and indentation. Attempts to reconstruct the geometry of the easternmost part of the rifted European margin exposed in the Alps were made by, e. g., Frisch (1976), Kurz et al. (1998), Ledoux (1984), and Schmid et al. (2013). Kurz (2006) proposed that Europe-derived units in the Tauern Window show signs of hyper-extension: The Rote Wand Nappe, which is a basement lamella with cover, may be interpreted as an extensional allochthon that was separated from the main margin by a narrow strip of transitional crust represented by the Eclogite Zone.

Based on new observations in the central Tauern Window and a reinterpretation of existing data, we propose some refinements on the litho- and tectonostratigraphy that allow us to qualitatively reconstruct the geometry of the eastern part of the rifted European margin in a stage prior to the onset of Adria-Europe convergence and subduction of the Alpine Tethys. Structures inherited from Mesozoic rifting may have affected the kinematics and structural evolution of some units in the central Tauern Window during Alpine subduction and exhumation. Since the correlation of lithological and tectonic units involves integrating a wealth of information from studies published over more than a century, we also include a short review of the history of geological research in the region, introducing the most important previous contributions that are relevant to this study.

2.3 Geographical Overview

This section gives an overview on the geography of the study area in the central Tauern Window and introduces the main geographical features that are used to explain the regional geology and locations of important observations or geological features. Most relevant geographical features are referenced on the overview map in Figure 2.1.

The Tauern Window is the largest tectonic window in the Eastern Alps, extending approximately 170 km from east to west and 30 km from north to south. It is located in the central part of the Eastern Alps in the Austrian states Salzburg, Kärnten and Osttirol and a small part of Northern Italy. This high-altitude mountain region termed Hohe Tauern — eponymous for the Tauern Window — is characterized by an east-west trending main ridge with numerous summits reaching elevations in excess of 3000 meters. In its central part, between the Großvenediger (3666 m) and Hochalm (3360 m) summits, the main ridge is flanked towards the north by more or less north-trending valleys that run towards the Salzach River and that are divided by subordinate ridges. The region south of the main ridge displays a more complex orographic pattern shaped by the Möll and Isel rivers and their tributaries.

The main study area spans the whole width of the Tauern Window in N-S-direction. It is bordered in the north by the Salzach Valley, in the south by the mountain range of the Schober Group and the Möll Valley, in the west by the Kaprun Valley and in the east by the ridge between the Rauris and Hüttwinkl valleys and the Gastein Valley. Towns within the study area are Fusch, Rauris, Wörth, Heiligenblut and

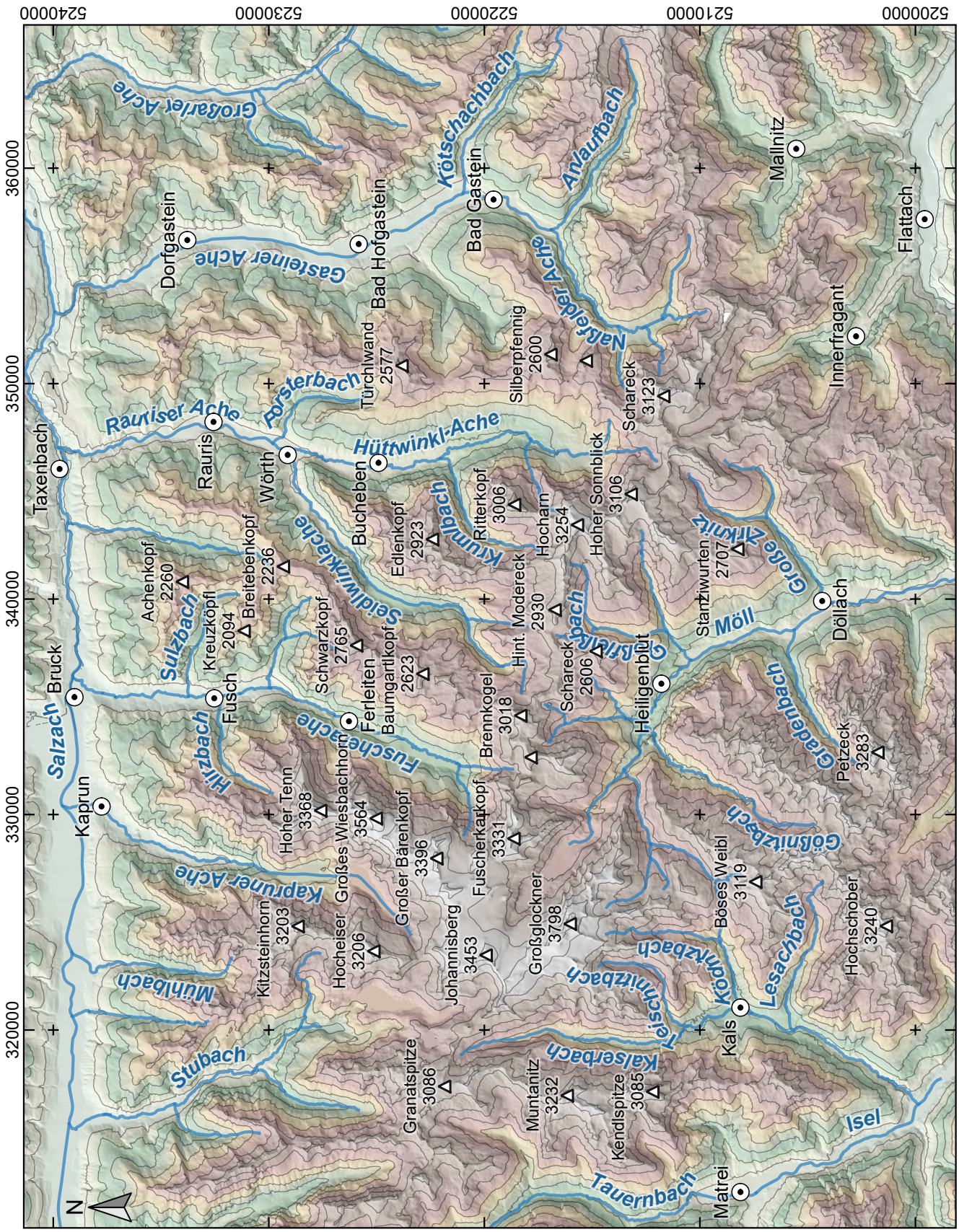

Figure 2.1: Topographic map of the study area. The elevation contour interval is 250 m.

Großkirchheim/Döllach. Large parts of the study area are within the Hohe Tauern National Park that is made accessible by the Großglockner mountain road.

The main valleys north of the main ridge are the Fusch Valley in the west and the Rauris and Hüttwinkl valleys, including their tributary Seidlwinkl Valley, in the east. South of the main ridge, the area is dominated by the Möll Valley and its tributaries: Großfleiß, Kleinfleiß and Zirknitz valleys orographically left and Leiter, Gößnitz and Graden valleys orographically right of the Möll. The main valleys are mostly U-shaped glacial valleys with very steep lower walls, whereas many of the tributaries are hanging valleys.

The most important mountains are Großglockner (3798 m), Austrias highest peak, located in the southwestern corner of the study area, Großes Wiesbachhorn (3564 m, between Fusch and Kaprun valleys), Schwarzkopf (2765 m, between Fusch and Seidlwinkl valleys), Edlenkopf and Ritterkopf (2923m and 3006 m, between Seidlwinkl and Hüttwinkl valleys) and several peaks along the main ridge, most importantly from west to east: Fuscherkarkopf (3331 m), Brennkogel (3018 m), Margrötzenkopf (2734 m), Hinteres Modereck (2930 m), Hocharn (3254 m) and Hoher Sonnblick (3106 m). The huge difference in elevation, often exceeding 2000 m, combined with scarce vegetation in higher altitudes provides great outcrop conditions, which is favourable for a detailed, three-dimensional structural analysis.

2.4 Previous Geological Research

Several authors provided reviews on the history of geological exploration in the region, recently, e. g., Neubauer (2014) and Schuster (2015). In the following, some of those classical publications that are directly relevant to the study presented here are introduced.

Geological research in the Tauern Window and adjacent areas that can be considered as modern — in the sense of a mobilistic, nappe theory-based approach — probably started with Termier (1904) and was significantly promoted by Eduard Suess. After the concept of nappes was introduced by Bertrand (1884), Schardt (1893, 1898) and Lugeon (1902), one of the first comprehensive nappe-based tectonic models of the Alps, including the Tauern Window region, was formulated by Suess, 1909 in his influential "Das Antlitz der Erde". Following Termier (1904, 1906), Suess correctly described the Tauern Window as a tectonic window within the Austroalpine nappe pile in which Penninic nappes are exposed, he wrote:

> Die Tauern sind ein Körper, der mit lepontinischer Umrandung unter den Ostalpen hervortritt. (Suess, 1909, S. 189)

Argand (1909, 1911, 1916) developed a structural-kinematic-paleogeographic model for the Western and Central Alps. Its most important characteristic is the proposition of a direct connection between paleogeography, kinematics and structures that is reflected in the pronounced along-strike cylindricity of these elements. The nappe theory was gradually adopted by several geologists working in the Tauern Window region, which led to subsequent refinement and modernization of the tectonostratigraphy. For example, Staub (1924) described the eastern and western basement domes of the Tauern Window (his "Zentralgneise") to be overlain by a nappe made up of Bündnerschiefer and ophiolites (his "Glocknerdecke"), which is prominently exposed in a central depression between these domes (his "Glocknerdepression"), the main area of interest in the present study. He proposed a correlation of the Glockner Nappe and the Matrei Zone with the Margna-Dent Blanche Nappe and the Venediger crystalline basement with the Monte Rosa Nappe and explicitly stressed the continuity of these units along-strike of the whole orogen (Staub, 1924, p. 86). One of Staub's students, Hottinger (1935),

mapped in the central Tauern Window and provided an early litho- and tectonostratigraphic division of the area, as well as very useful and detailed descriptions of local observations.

One milestone in the geological research in the central Tauern Window was the publication of the geological map of the Großglockner region by Cornelius & Clar (1934), its explanatory report (Cornelius & Clar, 1935) and a later, more detailed description of the geology in this area (Cornelius & Clar, 1939). In these contributions, all relevant lithological units were first described in detail and several aspects of the tectonostratigraphy were recognized as well. The mapping itself appears to be almost entirely correct! Therefore, this map formed the basis of subsequent geological research in the area. Most importantly for this study, Cornelius and Clar suspected that the Glockner Nappe may be wrapped around the Rote Wand Nappe (their "Seidlwinkldecke") in the West and North. This notion was confirmed by Braumüller & Prey (1943) after they mapped northeast of the Cornelius & Clar (1934) map in the area of Wörth, even though they proposed a rather strange and complicated geometry due to still-existing flaws in the available lithostratigraphic concept. The publication of the geological map of the Sonnblickgruppe by Exner (1962) and its explanatory notes (Exner, 1964) extended the area where high-quality lithological and structural observations were available towards the East. These publications included a wealth of structural and lithostratigraphic cross-sections and also provided a careful documentation of characteristic, thin basement nappes, the so called "Gneislamellen". These turned out to be very helpful — also for this study — in tracing the complex structure in the area. Exner wrote, quite adequately:

> Daß unsere Arbeit den Ariadnefaden im Labyrinth der durch komplizierte Falten, Schuppen und Decken entstandenen Lamellen wohl im Prinzip gefunden hat, dieser Faden aber [...] an anderen Stellen durch spätere Querbewegungen um N-S-Achsen noch einmal verwickelt und auch stellenweise einfach abgerissen ist [...], dafür können wir nichts. (Exner, 1964, S. 124)

and further

> Tatsache bleibt, daß ein äußerst komplizierter Verfaltungs-, Gleit- und Schuppenbau in den Tauernschiefern der Sonnblickgruppe vorliegt, vergleichbar am ehesten einem vielfach deformierten und durchgewalzten Teig unter dem Nudelwalker der Hausfrau. (Exner, 1964, S. 124–125)

The work of G. Frasl and W. Frank in the 1950s and 60s (e. g., Frank, 1965, 1969; Frasl, 1958; Frasl & Frank, 1964) provided further improvements of the lithostratigraphy of the central Tauern Window. This gave new insight in the local structure. For example, the idea of a recumbent, isoclinal fold nappe was explicitly formulated by Frank (1965, 1969) and named "Seidlwinklfalte". The lithostratigraphy of the older part of the Rote Wand Nappe, as proposed by these authors (Frasl & Frank, 1964), is in many respects still in use today.

A turning point was the arrival of the theory of plate tectonics to the Eastern Alps. Previously established paleogeographic reconstructions (e. g., Argand, 1911) could now be interpreted in the framework of plate tectonics (e. g., Frisch, 1979; Laubscher, 1969; Laubscher, 1971; Trümpy, 1975. Several studies constrained the degree and distribution of the Barrow-type regional metamorphism (e. g., Cliff et al., 1985; Dachs, 1990; Frank et al., 1987; Hoernes & Friedrichsen, 1974; Scharf et al., 2013b), originally termed "Tauernkristallisation" by Sander (1914). The recognition of high-pressure mineral parageneses (e. g., Dachs & Proyer, 2001; Frank et al., 1987; Holland, 1979) proved the existence of formerly subducted rocks in the Tauern Window. Radiometric age dating successively allowed to precisely assign ages to the different orogenic stages (e. g., Glodny et al., 2005; Kurz et al., 2008; Lambert, 1970;

Oxburgh et al., 1966; Ratschbacher et al., 2004; Zimmermann et al., 1994). Discovery of diagnostic fossils in the metamorphic rocks (e. g., Borowicka, 1966; Höck et al., 2006; Höfer & Tichy, 2005) further improved the lithostratigraphy (e. g., Pestal & Hellerschmidt-Alber, 2011). All these results fed back into refining the geodynamic model of the central Tauern Window (e. g., Frank et al., 1987; Kurz et al., 1998; Schmid et al., 2013).

2.5 Geological Overview and Paleogeographic Models

The Tauern Window is the largest tectonic window in the Eastern Alps. It provides a section through the eastern Alpine nappe stack (e. g., Schmid et al., 2004), reaching from the highest units derived from the former Adriatic plate (Austroalpine nappes) down to the lowest units derived from the European plate (Venediger nappe system). The Austroalpine nappes form the perimeter of the Tauern Window, whereas the Venediger nappe system is exposed in the two basement domes in the Eastern and Western parts of the window. Both nappe systems are separated from each other by the Penninic nappes, an assemblage of several nappes mainly consisting of oceanic basement and a cover of marine sediments, locally called Glockner nappe system, Matrei Zone and Nordrahmenzone (e. g., Pestal et al., 2009). These units are derived from the Jurassic-Cretaceous Alpine Tethyan Ocean that formerly separated the European continent in the North from the Adriatic continent in the South (e. g., Kurz et al., 1996, 1998; Schmid et al., 2004). During Alpine subduction and collision, the Adriatic plate formed the upper plate and the European plate was the lower, down-going plate (e. g., Handy et al., 2010; Stampfli & Borel, 2004). Usually at the base of the Penninic nappes and above the Venediger nappe system, other basement-cover nappes are found in the Tauern Window. These nappes are characterized by continental basement with Permo-Mesozoic cover rocks that are diagnostic of a European affinity (e. g., Rote Wand Nappe, Trögereck Nappe, Wolfendorn Nappe; Kurz et al., 1998).

Several different paleogeographic models have been proposed for the Penninic realm in the Eastern Alps. In recent years, a consensus emerged regarding some issues that were formerly strongly disputed, while other issues remain unresolved so far. Based on clear stratigraphic evidence, the Venediger nappe system is now largely accepted to originate from the European continent (e. g., Froitzheim et al., 1996; Kurz, 2006; Schmid et al., 2004, 2013; Trümpy, 1988), rather than being the eastward continuation of the Briançonnais microcontinent (e. g., Frisch, 1979; Tollmann, 1965). This Middle Penninic continental ribbon is believed to wedge out somewhere between the Engadine and the Tauern windows (Froitzheim et al., 1996; Schmid et al., 2004, 2013; Trümpy, 1988), even though some authors argued that it may find its continuation in some of the thin nappes composed of basement and its Mesozoic cover of the Tauern Window (Kurz, 2006). While the Briançonnais microcontinent separated the Jurassic (Piemontese) and Cretaceous (Valaisan) parts of Alpine Tethys in the West, its disappearance means that in the East, the Alpine Tethys formed a single ocean basin comprising both Jurassic and Cretaceous parts (e. g., Handy et al., 2010; Pleuger et al., 2005; Schmid et al., 2004; Trümpy, 1988). This strongly complicates the interpretation of the Penninic nappes in the east in terms of their paleogeographic origin. Where the continental Middle Penninic nappes are present, they usually serve as a straight-forward structural criterion to decide whether the oceanic Penninic nappes are of North- (below Briançonnais) or South-Penninic (above Briançonnais) origin. Where they are absent, as is the case in the Tauern Window, this distinction requires additional criteria (see, e. g., Schmid et al., 2004, 2013).

In the light of these criteria, the Matrei Zone/Nordrahmenzone is clearly derived from the southern, Jurassic part of Alpine Tethys. It contains numerous slivers from the overlying Austroalpine nappes,

which is typical of the South Penninic units and indicates that it was accreted immediately at the base of the advancing Austroalpine nappes in Cretaceous times. In the case of the Glockner nappe system, these criteria are ambiguous and its paleogeographic origin is disputed (e. g., Schmid et al., 2004, 2005, 2013; Kurz, 2005, 2006). Some authors argue in favor of a Cretaceous North-Penninic origin of the Glockner nappe system, which is mainly based on lithostratigraphic correlation of this unit with the Valais-derived calcareous micaschists in the Central and Western Alps and on the Cenozoic age of high-pressure metamorphism of this unit (e. g., Schmid et al., 2013). Others argue that the transition of the Glockner nappe system to the overlying Matrei Zone and Nordrahmenzone is often stratigraphic rather than tectonic (e. g., Frisch et al., 1987), which in turn means that also the Glockner nappe system is of South-Penninic origin. In our view, the best criterion to differentiate between North- and South-Penninic origin of the Penninic nappes in the Tauern Window is the magmatic age of oceanic crust, which is, however, missing so far.

2.6 Tectono- and Lithostratigraphic Units

The sources from which the new geological bedrock map of the central Tauern Window was compiled are listed in Table 2.1. A main requirement for map compilation was to define and correlate lithological units across the individual maps; these units serve as marker horizons for constraining the structure in the area. Most information provided here was already published by other authors in the long course of geological exploration of the Tauern Window. The purpose of this part is therefore to give an up-to-date summary of the subject, explain the logic of the map compilation and integrate previous concepts with new observations and ideas that developed from this work. The description and nomenclature of the tectonic and lithological units and their geodynamic interpretation given here is largely based on Kurz et al. (1996, 1998), Pestal et al. (2009), Pestal & Hellerschmidt-Alber (2011) and Schmid et al. (2013). Lithostratigraphic columns of the individual tectonic units are given in Figure 2.2.

Map	Reference
Geologische Karte des Grossglocknergebietes	Cornelius & Clar, 1934
Geologische Karte der Umgebung von Gastein	Exner, 1956
Geologische Karte der Sonnblickgruppe	Exner, 1962
Lithological map of the Sonnblick area	Favaro, 2016b
GK50 Blatt 123 Zell am See	Heinisch et al., 1995
GK50 Blatt 153 Grossglockner	Höck & Pestal, 1994
GK50 Blatt 124 Saalfelden am Steinernen Meer, prelim. Geofast map	Kreuss, 2013
GK50 Blatt 179 Lienz	Linner et al., 2013
GK50 Blatt 154 Rauris, unpublished manuscript map	Pestal, 2014
Geologische Karte von Salzburg 1:200000	Pestal et al., 2005

Table 2.1: List of maps used for map compilation.

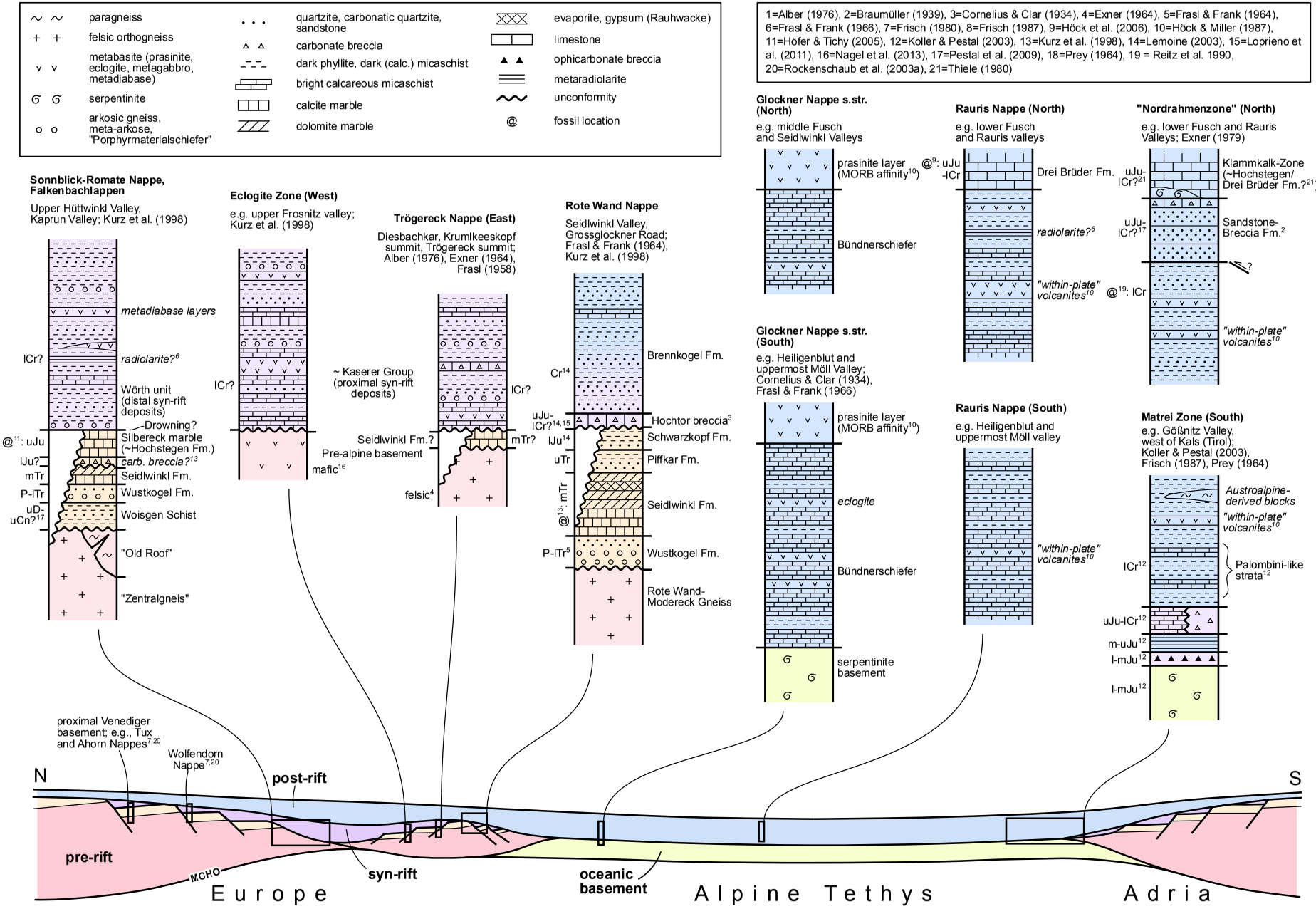
paragneiss
felsic orthogneiss
metabasite (prasinite, eclogite, metagabbro, metadiabase)
serpentinite
arkosic gneiss, meta-arkose, "Porphyrmaterialschiefer"
quartzite, carbonatic quartzite, sandstone
carbonate breccia
dark phyllite, dark (calc.) micaschist
bright calcareous micaschist
calcite marble
dolomite marble
evaporite, gypsum (Rauhwacke)
limestone
ophicarbonate breccia
metaradiolarite
unconformity
fossil location
1=Alber (1976), 2=Braumüller (1939), 3=Cornelius & Clar (1934), 4=Exner (1964), 5=Frasl & Frank (1964), 6=Frasl & Frank (1966), 7=Frisch (1980), 8=Frisch (1987), 9=Höck et al. (2006), 10=Höck & Miller (1987), 11=Höfer & Tichy (2005), 12=Koller & Pestal (2003), 13=Kurz et al. (1998), 14=Lemoine (2003), 15=Loprieno et al. (2011), 16=Nagel et al. (2013), 17=Pestal et al. (2009), 18=Prey (1964), 19 = Reitz et al. 1990, 20=Rockenschaub et al. (2003a), 21=Thiele (1980)
Sonnblick-Romate Nappe, Falkenbachlappen
Upper Hüttwinkl Valley, Kaprun Valley; Kurz et al. (1998)
metadiabase layers
lCr?
radiolarite?6
Wörth unit (distal syn-rift deposits)
Drowning?
@11: uJu
Silbereck marble (~Hochstegen Fm.)
lJu?
carb. breccia?13
mTr
Seidlwinkl Fm.
P-lTr
Wustkogel Fm.
uD-uCn?17
Woisgen Schist
"Old Roof"
"Zentralgneis"
Eclogite Zone (West)
e.g. upper Frosnitz valley; Kurz et al. (1998)
lCr?
Trögereck Nappe (East)
Diesbachkar, Krumlkeeskopf summit, Trögereck summit; Alber (1976), Exner (1964), Frasl (1958)
~ Kaserer Group (proximal syn-rift deposits)
lCr?
Seidlwinkl Fm.?
mTr?
Pre-alpine basement
mafic16
felsic4
Rote Wand Nappe
Seidlwinkl Valley, Grossglockner Road; Frasl & Frank (1964), Kurz et al. (1998)
Brennkogel Fm.
Cr14
uJu-lCr?14,15
Hochtor breccia3
lJu14
Schwarzkopf Fm.
uTr
Piffkar Fm.
@13: mTr
Seidlwinkl Fm.
P-lTr5
Wustkogel Fm.
Rote Wand-Modereck Gneiss
Glockner Nappe s.str. (North)
e.g. middle Fusch and Seidlwinkl Valleys
prasinite layer (MORB affinity10)
@9: uJu-lCr
Bündnerschiefer
Rauris Nappe (North)
e.g. lower Fusch and Rauris valleys
Drei Brüder Fm.
radiolarite?6
"within-plate" volcanites10
"Nordrahmenzone" (North)
e.g. lower Fusch and Rauris Valleys; Exner (1979)
uJu-lCr?21
Klammkalk-Zone (~Hochstegen/ Drei Brüder Fm.?21)
uJu-lCr?17
Sandstone-Breccia Fm.2
?
@19: lCr
"within-plate" volcanites10
Glockner Nappe s.str. (South)
e.g. Heiligenblut and uppermost Möll Valley; Cornelius & Clar (1934), Frasl & Frank (1966)
prasinite layer (MORB affinity10)
eclogite
Bündnerschiefer
serpentinite basement
Rauris Nappe (South)
e.g. Heiligenblut and uppermost Möll valley
"within-plate" volcanites10
Matrei Zone (South)
e.g. Gößnitz Valley, west of Kals (Tirol); Koller & Pestal (2003), Frisch (1987), Prey (1964)
Austroalpine-derived blocks
"within-plate" volcanites10
lCr12
Palombini-like strata12
uJu-lCr12
m-uJu12
l-mJu12
l-mJu12
proximal Venediger basement; e.g., Tux and Ahorn Nappes7,20
Wolfendorn Nappe7,20
N
S
post-rift
pre-rift
MOHO
syn-rift
oceanic basement
Europe
Alpine Tethys
Adria

Figure 2.2 ***(previous page)*****:** Lithostratigraphic columns of the tectonic units in the central Tauern Window. These sections are based on own observations, data from the geological maps in Table 2.1 and Alber (1976), Braumüller (1939), Cornelius & Clar (1934), Exner (1964), Frasl & Frank (1964), Frasl & Frank (1966), Frisch (1980), Frisch et al. (1987), Höck et al. (2006), Höck & Miller (1987), Höfer & Tichy (2005), Koller & Pestal (2003), Kurz et al. (1998), Lemoine (2003), Loprieno et al. (2011), Nagel et al. (2013), Pestal et al. (2009), Prey (1964), Reitz et al. (1990), Rockenschaub et al. (2003) and Thiele (1980). The order of the sections from north to south reflects the present-day position in the Alpine nappe stack from bottom to top, respectively. A large version of this figure is found in Appendix H.

2.6.1 Venediger Nappe System

The lowest major tectonic unit of the Tauern Window is the Venediger Nappe system, prominently exposed in the centers of the eastern and western subdomes (ETD and WTD, respectively). Following, e. g., Schmid et al. (2013), the Venediger Nappe system is derived from the former European margin towards the Penninic Ocean. Therefore, these units are often referred to as Subpenninic Units (e. g., Milnes, 1974; Schmid et al., 2013). During Alpine subduction, the European margin was subjected to imbrication and duplex formation (Lammerer & Weger, 1998). In the tectonostratigraphic subdivision of Schmid et al. (2013), this crustal-scale Venediger duplex comprises at least three horses; from bottom to top: Göss, Hochalm and Sonnblick-Romate Nappes in the eastern Tauern dome; Ahorn, Tux-Granatspitz and Zillertal-Riffl Nappes in the western Tauern dome. These duplex horses are usually defined by characteristic basement-cover sequences. Of the above units, only the Sonnblick-Romate Nappe is relevant to the newly compiled map. Therefore, we describe only this tectonic unit below. The descriptions incorporate, if not referenced otherwise, information mainly from existing maps and from Pestal (2008, 2009), Pestal & Hellerschmidt-Alber (2011), Favaro (2012), Favaro & Schuster (2012) and from own observations. The Sonnblick-Romate Nappe comprises — as the Venediger Nappe units in general — late- to post-Variscan plutons that intruded into an older basement and a post-Variscan metasedimentary cover sequence.

Basement of the Sonnblick-Romate Nappe

The Sonnblick-Romate Nappe consists of two subnappes, the Sonnblick Subnappe in the South and the Romate Subnappe in the North, exposed in two large antiforms. Both are separated by a large synform (Mallnitz Synform) that obscures their true contact (see Exner, 1964, Plate 2), so that the nature and age of juxtaposition depends on the basement-cover relations. The reason for differentiating two subnappes is a striking contrast in their pre-Mesozoic lithology: The Sonnblick Subnappe mainly consists of post-Variscan plutonic rocks ("Zentralgneis") and their country rocks ("Altes Dach" and "Altkristallin"), overlain by only little post-Variscan cover. In the Romate Subnappe, no (pre-) Variscan basement can be found. Instead, the plutonic rocks are immediately overlain by a thick sequence of post-Variscan (Permo-Carboniferous? to Cretaceous) sedimentary rocks. The main reason for grouping these subnappes together is the similarity of their Mesozoic cover rocks, although it must be said that much of this cover is mssing in the Sonnblick unit due to strong deformation.

Altes Dach and Altkristallin of Sonnblick-Romate Nappe (pre- to syn-Variscan) The oldest rocks of the Sonnblick-Romate Nappe are pre- and syn-Variscan rocks with a metamorphic history that predates the intrusion of the late Carboniferous-Permian plutons (e. g., Eichhorn et al., 2000; Veselá et al., 2011). This basement often displays primary intrusive contacts with the plutons and is traditionally referred to as "Altes Dach" or "Altkristallin" (Pestal et al., 2009). Lithologically, this unit is quite

diverse, containing porphyroblast-rich paragneiss, micaschist and amphibolite. The map does not differentiate between these lithologies and groups them together under the common label Altes Dach and Altkristallin.

Zentralgneiss of Romate Subnappe (post-Variscan) The Zentralgneiss of the Romate Subnappe consists of two varieties: a) a fine-grained, albite-rich granite gneiss with augen texture ("Siglitz gneiss"; Exner, 1957; Exner, 1949) and b) a medium- to coarse-grained syenite gneiss, sometimes with flaser texture ("Romate gneiss"; Angel & Staber, 1952). Both varieties are not differentiated in the compiled map.

Zentralgneiss of Sonnblick Subnappe (post-Variscan) The Zentralgneiss of the Sonnblick subnappe is made up primarily of leucocratic granitic augen gneiss and, to a lesser extent, of fine-grained grayish gneiss with large alkali feldspar-phenocrysts. Both are cut by aplitic dikes (Exner, 1964). All three varieties are displayed as one lithological unit in the map.

Post-Variscan Cover of Sonnblick-Romate Nappe

Following Schmid et al. (2013), strata deposited after the Variscan orogeny and the intrusions of late- to post-Variscan plutons are denoted as post-Variscan cover. These authors provided a comprehensive documentation of the occurrence of these lithologies in the whole Tauern Window and highlighted their importance as nappe separators. Favaro & Schuster (2012) gave an overview on the lithologies of the post-Variscan cover, their suspected ages and their distribution in the area of the Mallnitz Synform. Sedimentation of the post-Variscan cover of the Sonnblick-Romate Nappe probably started with Permo-Carboniferous clastics and continued, with some major unconformities, until the Cretaceous.

Woisgenschiefer (Permo-Carboniferous?) The term Woisgenschiefer is used in the sense of Favaro & Schuster (2012) to denote a variety of mainly metapelitic rocks of presumably Carboniferous to Permian age. Woisgenschiefer in the strict sense is silvery chlorite-muscovite schist rich in garnet- and chloritoid-porphyroblasts, but also biotite-porphyroblast and biotite-chlorite-epidote schists are included in this lithological mapping unit. These rocks occur only in the Romate Subnappe but are missing in the Sonnblick Subnappe.

Wustkogel Formation (Permian to Lower Triassic) The main lithologies of the Wustkogel Formation are dark green and fine-grained, phengite-rich augen gneiss (metaarkose) and pale-green phengite-quartzite; a more detailed description will follow below in section 2.6.2. In the Romate Subnappe, the Wustkogel Formation is generally thin (few tens of meters) and unconformably overlies the Woisgenschiefer. It mainly crops out on the western flank of the upper Hüttwinkl Valley (SW of Bucheben), but can also be found on the northern limb of the Falkenbach antiform ("Falkenbachlappen") in the Kaprun Valley. It is completely missing in the Sonnblick Subnappe.

Silbereck Marble (Upper Jurassic) The term Silbereck Marble (locally called Angertal Marble) refers to a succession of white to gray, thick-bedded marbles with variable amounts of white mica that unconformably overlies the Wustkogel Formation, the Woisgenschiefer and the Romate Zentralgneiss (Exner, 1964). Sr-isotope dating (Favaro & Schuster, 2012), biostratigraphic dating (Höfer & Tichy, 2005) and regional correlation with the Hochstegen Marble establish a Late Jurassic age of this lithology. Höfer & Tichy (2005) also clearly confirmed that the contact between the Silbereck Marble and the Romate Zentralgneiss is stratigraphic. In the map, the Silbereck Marble only occurs on the

eastern flanks of the upper Hüttwinkl Valley and in the northeastern limb of the Mallnitz Synform. The Silbereck Marble is missing in the Sonnblick Subnappe.

Wörth Unit (Cretaceous) The name Wörth Unit was proposed by Wolfgang Frank (pers. comm., August 2017) to denote the large mass of dark phyllite extending in E-W direction from the Rauris Valley to the Fusch Valley and even further to the West. Lithologically, the dark phyllites are fairly homogeneous but contain characteristic layers of metadiabase and metatuffite (see below). Both lithological types — dark phyllites and metabasites — are marked as separate units on the map.

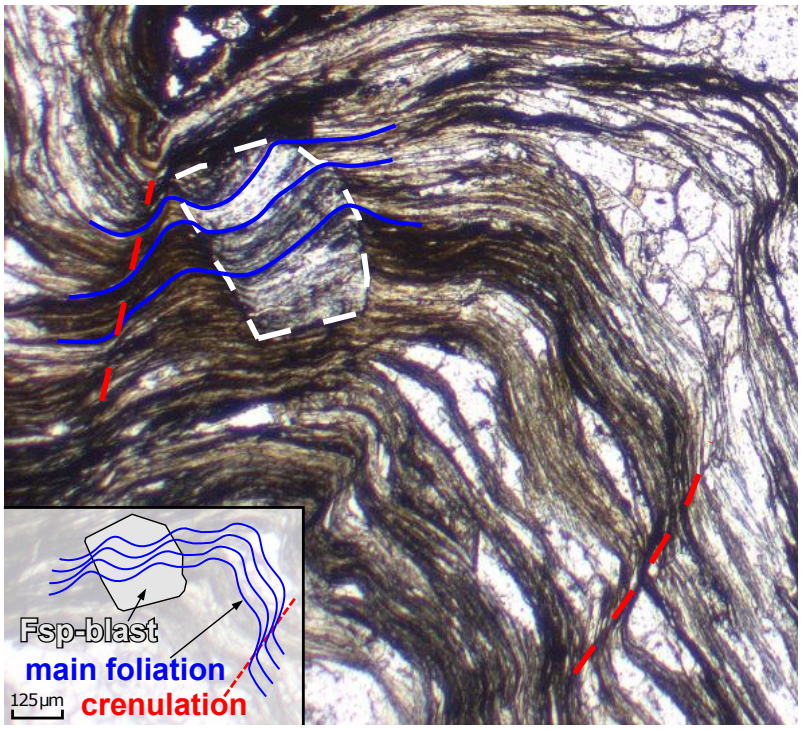

Figure 2.3: Thin section image (parallel polarizers) of a crenulated dark phyllite from the Wörth Unit with a post-kinematic albite porphyroblast (sample PG247, 47.19540°N 12.85067°E).

The dark phyllites are fine-grained and mainly consist of white mica, graphitic organic matter, quartz and some carbonate. In areas with sufficient metamorphic overprint, the rock additionally contains abundant albite porphyroblasts (Figure 2.3). The dark phyllites are intercalated with quartzite banks, layers of dark calcareous micaschist and fine-grained meta-arkosic layers, especially at the base of the Wörth Unit (Frasl, 1958, p. 399; Wolfgang Frank, pers. comm., June 2019). Frasl (1958, p. 399) explicitly mentioned the strong similarity of these gneisses with the gneisses found in the Trögereck Nappe (see below, section 2.6.2).

The layers of metadiabase, -gabbro and -tuffite are fairly discontinuous but still helpful as a marker horizon to trace the large-scale structure. Similar metadiabase and -gabbro layers occur in the Nordrahmenzone, the lithological and tectonic equivalent of the Matrei Zone in the northern Tauern Window (Pestal et al., 2009). These have a geochemical signature of within-plate volcanism (Höck & Miller, 1987), pointing towards a rift-related origin of the Wörth Unit metabasites.

The Wörth Unit is largely identical with what Exner (1957, p. 65) called "Mittlere Schwarzphyllitzone" and with the lower part of the "Weixelbachschuppe" of Frasl (1958, p. 398). Exner noted that this unit can be traced southward into the Rauris and Hüttwinkl valleys, always immediately underlying the

Glockner Nappe s. str.Consequently, the unit overlies the rocks of the Romate Subnappe in the South of the Hüttwinkl Valley. Therefore, and in analogy to the Cretaceous Kaserer Series in the northwestern Tauern Window, a parautochthonous origin (with respect to the Romate-Sonnblick Nappe) of these dark phyllites is likely, making the Wörth Unit the stratigraphically uppermost unit of the post-Variscan cover of the Romate Subnappe. Since it overlies the Upper Jurassic Silbereck Marble, a Cretaceous age is probable.

The Wörth Unit is interpreted here as distal syn-rift deposit that formed on the European margin in Cretaceous times. It appears to be a deep and oxygen-starved and more distal equivalent to the Cretaceous Kaserer Series in the Western Tauern Window (Frisch, 1980; Lammerer, 1986), as well as to the syn-rift portion of the Bündnerschiefer deposits of the Modereck nappe system in the Central Tauern Window (see below, section 2.6.2).

It is unclear whether the Wörth Unit continues south of the Romate Subnappe, and overlies the Sonnblick Subnappe basement, as shown in the compiled map and depicted in existing maps (GK50 Blatt 154 Rauris, Pestal, 2014). Own observations in the Stanziwurten area (sample PG126, 47.02226°N 12.93057°E) confirmed the existence of typical Wörth-like sediments, e. g., dark phyllites, immediately overlying the Sonnblick Nappe basement. But so far, there is no clear evidence that these phyllites actually derive from the Wörth Unit; instead, the dark phyllite on the Sonnblick Nappe basement might be part of the basement itself, which would make them Variscan or older in age.

2.6.2 Modereck Nappe System

The Modereck nappe system comprises several nappes that are derived from the former external European margin towards the Penninic Ocean, paleogeographically situated to the south (e. g., Kurz et al., 1998; Schmid et al., 2013). In the study area, two nappes belong to the Modereck Nappe system: The Rote Wand Nappe and the underlying Trögereck Nappe.

Trögereck Nappe

The Trögereck Nappe, the lower part of the Modereck nappe system in the central Tauern Window, is named after the Trögereck summit in the Stanziwurten area (Exner, 1964), where this nappe is well-exposed. As is typical for the Subpenninic nappes, the Trögereck Nappe comprises a basement-cover sequence. The following compilation of its main lithologies is largely based on own observations and those of Alber (1976), Exner (1964), and Frasl (1958).

Trögereck Gneiss (post-Variscan) The Trögereck Gneiss ("Gneislamelle 3" in Exner, 1964) is the basement of the Trögereck Nappe. The typical appearance of this gneiss is a medium-grained, phengite- and quartz-rich gneiss with microcline augen, up to 0.5 cm in diameter (Figure 2.4). These augen are in fact porphyroclasts that partly preserve the original granitic texture, often including biotite relics (e. g., sample PG152, 47.10798°N 12.87691°E). The phengite-rich matrix is probably the product of strong metamorphic alteration of the protolith. Depending on the degree of alteration and deformation, the rock can be completely transformed to a phengite-schist, containing quartz and medium-sized (ca. 0.5 cm) albite-porphyroblasts. The protolith of the Trögereck Gneiss is often taken to be the Zentralgneiss of the Venediger nappe system (e. g., Exner, 1964). Frasl (1958) argued that large parts of these gneisses are in fact meta-arkoses that derive from eroded Zentralgneiss. In any case, this lithology is distinct from similar rocks of the Trögereck Nappe that belong to the Bündnerschiefer assemblage (details below).

Calcitic and Dolomitic Marble (Middle Triassic) The Trögereck Nappe contains calcitic and dolomitic marble layers. The layers do not exceed a thickness of several meters and are laterally discontinuous. They appear to stratigraphically overlie the Trögereck Gneiss but also occur as lenses in the Bündnerschiefer (Pestal & Hellerschmidt-Alber, 2011). They might be a lateral equivalent of the Triassic Seidlwinkl Formation of the Rote Wand Nappe (see below).

Bündnerschiefer of the Trögereck Nappe (Cretaceous) The stratigraphically upper- most part of the Trögereck Nappe comprises a fairly diverse succession of Bündnerschiefer-type metasediments that resembles parts of the Brennkogel Formation of the Rote Wand Nappe (see below) and the Kaserer Formation in the Western Tauern Window. This unit contains impure, carbonate-bearing arkosic gneiss (Figure 2.5e-f), carbonate breccia, dark phyllite, calcareous micaschist and garnet-micaschist, all with mutual gradual transitions. The metapelites can be relatively rich in organic matter. Additionally, few blocks or layers of garnet-bearing prasinites occur in this succession (see below).

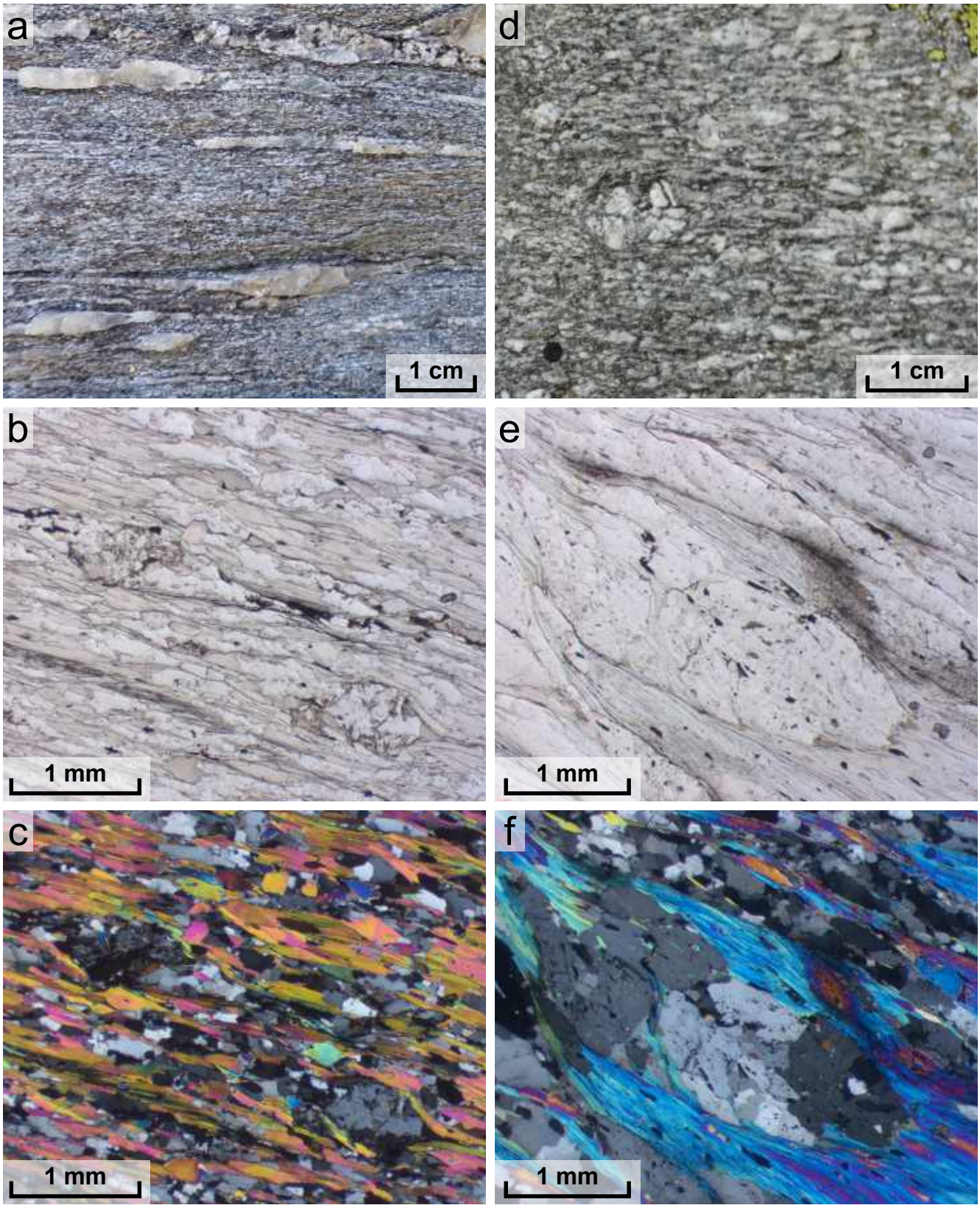
a
1 cm
d
1 cm
b
1 mm
e
1 mm
c
1 mm
f
1 mm

Figure 2.4 ***(previous page)*****:** Comparison of meta-sandstones of different units of the Modereck nappe system. (a) field photograph of fine-grained, phengite- and quartz-rich meta-arkose of the Wustkogel Formation. Thin section images with parallel (b) and crossed (c) polarizers of a similar lithology from the Wustkogel Formation (sample PG75, 47.00636°N 12.92570°E). Note that this rock mainly consists of phengite and quartz, with only few larger feldspar-clasts. (d) field photograph of a relatively coarse-grained arkosic gneiss from the Trögereck Nappe. Thin section images with parallel (e) and crossed (f) polarizers of a similar lithology from the Trögereck Nappe (sample PG78, 47.01618°N 12.92424°E). The rock mainly consists of phengite, quartz and relatively large feldspar clasts. Additionally, few biotite grains are present, e.g., at the tips of the elongated feldspar clasts. No carbonate minerals are present in this rock, which is why it is grouped with the Trögereck Gneiss unit (basement of the Trögereck Nappe).

The meta-arkosic rocks are often transitional to calcareous micaschist, which is the main criterion to distinguish them from the Trögereck gneiss (Frasl, 1958). Where this is not observed, they strongly resemble the Trögereck Gneiss, only that the meta-arkoses of the Bündnerschiefer assemblage partly contain carbonate minerals, which is never the case in the Trögereck Gneiss. Additionally, some rounded clasts are often recognized that may be of detrital origin. It is likely that these meta-arkosic rocks are the erosional product of the Trögereck Gneiss or the Zentralgneiss. Frasl (1958, pp. 369–372) gives an extensive documentation of meta-arkosic gneisses observed in the upper Seidlwinkl Valley. Frasl (1958, p. 372) also proposes that the degree of pleochroism observed in phengite may help distinguish both types of gneisses; gneiss with weakly pleochroic, colorless to pale green phengite usually belongs to the Bündnerschiefer gneiss, whereas strongly pleochroic phengite (colorless to intense green) is characteristic of the basement (Trögereck Gneiss).

A rock association very similar to the Bündnerschiefer assemblage of the Trögereck Nappe is known from the Internal Valais Unit in the Western Alps (e. g., Loprieno et al., 2011). They describe the Complexe Antéflysch Formation as being composed of variegated, clastics-rich and carbonate-bearing metasediments that were intruded by mafic sills and dikes. In analogy, the Bündnerschiefer sequence of the Trögereck Nappe can be interpreted as proximal syn-rift deposit formed at the distal European margin that involved erosion of the Variscan basement, rapid and proximal sedimentation, potentially in a marine environment (carbonates), and some mild, rift-related magmatic activity.

Garnet-Prasinite, Eclogite Relics The Bündnerschiefer assemblage of the Trögereck Nappe contains several layers or lenses of garnet-prasinite, the largest of which were distinguished as a separate unit on the compiled map. In analogy with similar rocks in the Glockner Nappe, these are interpreted as retrogressed eclogites that are derived from small mafic intrusions or volcanics.

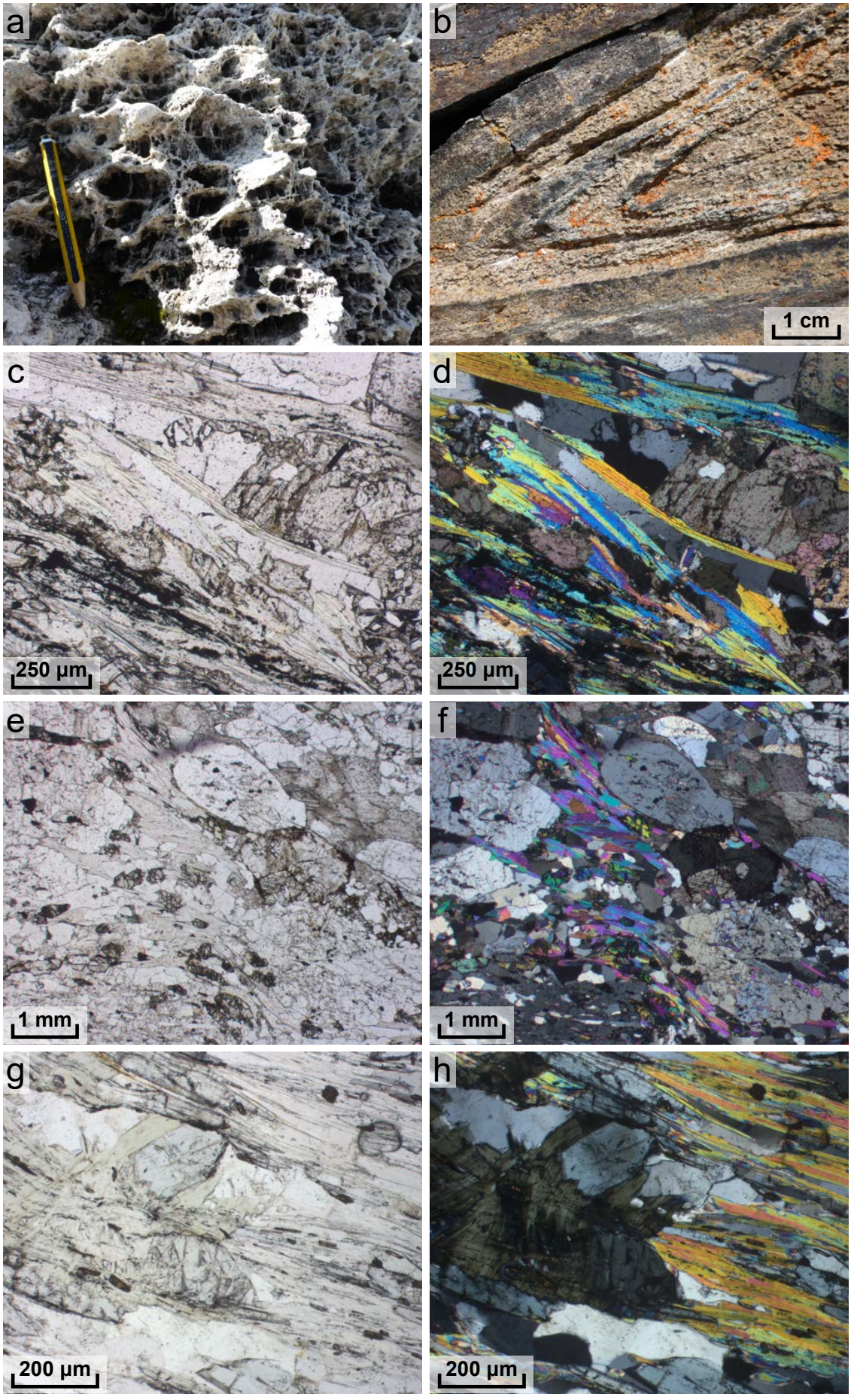
a
b
1 cm
c
250 µm
d
250 µm
e
1 mm
f
1 mm
g
200 µm
h
200 µm

Figure 2.5 ***(previous page)*****:** Lithologies of the Modereck nappe system. (a) cargneule (Rauhwacke) of the Middle Triassic Seidlwinkl Formation . (b) isoclinal fold in carbonate quartzite from the Brennkogel Formation. Thin section images with parallel (c, e, g) and crossed (d, f, h) polarizers of dark micaschist of the Brennkogel Formation (c, d), Bündnerschiefer of the Trögereck Nappe (e, f) and chloritoid-bearing phyllite of the Piffkar Formation (g, h). The dark micaschist of the Brennkogel Formation (c, d; sample PG149, 47.17763°N 12.81997°N) mainly consists of phengite, quartz, carbonate minerals (calcite, ankerite?) and carbonaceous matter, feldspar is very rare. The Bündnerschiefer of the Trögereck Nappe (e, f; sample PG62, 47.08515°N 12.87452°E) mainly consists of abundant feldspar clasts, phengite, carbonate minerals, quartz, carbonaceous matter and some epidote. The chloritoid-bearing phyllite of the Piffkar Formation (g, h; sample PG141, 47.13907°N 12.84402°E) mainly consists of phengite, quartz, chloritoid, chlorite and Ti-rich phases (ilmenite, rutile).

Rote Wand Nappe

The Rote Wand Nappe is the upper nappe of the Modereck nappe system in the central Tauern Window. It comprises a sequence of post-Variscan metasediments that includes Permian to lower Triassic siliciclastics, the "Seidlwinkl Triassic" which is a thick succession of Middle Triassic lagoonal or platform carbonates and evaporites, Upper Triassic to Lower Jurassic metapelites and -psammites and presumably Cretaceous Bündnerschiefer calc-schists. Sometimes the Rote Wand Nappe is also referred to as Modereck Nappe or Rote Wand-Modereck Nappe (e. g., Kurz et al., 1998). The map compilation is based on own observations and descriptions of the lithostratigraphic units by Exner (1964), Favaro & Schuster (2012), Frank (1969), Frasl & Frank (1964), Kurz et al. (1998), Pestal et al. (2009), and Pestal (2008, 2009).

Wustkogel Formation (Permian to Lower Triassic) The Wustkogel Formation is lithologically quite striking and therefore serves as a valuable marker horizon for tracing large-scale fold structures and nappe geometries. It is named after the Wustkogel peak at the southern end of the Seidlwinkl Valley. The Wustkogel Formation is more or less synonymous to what Exner (1964) called "Gneislamelle 4". The lithological content of the Wustkogel formation is similar to that of the Trögereck Gneiss rock assemblage and distinguishing between them is sometimes impossible. The stratigraphically lowest part of the Wustkogel Formation is a fine-grained, dark green phengite-gneiss containing microcline- and/or albite- porphyroblasts and -clasts with a grain size of usually less than 2 mm (Figure 2.4). The rock is probably a paragneiss derived from fine-grained arkosic debris of Zentralgneiss-like material. The characteristic green phengite is strongly pleochroic under the microscope (green-pale pink). Apatite is the dominating accessory mineral and occasionally, pyrite- and magnetite-rich varieties of the gneiss can be found (e. g., Stanziwurten area, 47.00635°N 12.92761°E). The Wustkogel Formation also contains phengite-schist, arkosic gneiss and metakonglomerate (e. g., Exner, 1964; Kurz et al., 1998). The stratigraphically uppermost part is a greenish-white phengite-quartzite. The depositional age of the metasediments ranges from Permian to Early Triassic (Kurz et al., 1998; Pestal et al., 2009).

Seidlwinkl Formation (Middle Triassic) The Seidlwinkl Formation is named after its type locality, the upper Seidlwinkl Valley. In the map, this formation is divided into two distinct units: The stratigraphically lower unit, consisting mainly of bright gray calcite marble and an upper unit, composed of yellow dolomite marble, cargneule (or Rauhwacke) and gypsum. The thickness of the Seidlwinkl formation varies considerably in the study area, ranging from only a few to hundreds of meters. This is caused by extreme thinning and repetition of the stratigraphy by isoclinal folding (more details below). The Early- to Middle-Triassic depositional age of the Seidlwinkl Formation has been established by various fossils (**Frisch1975_wolfendorn**; Borowicka, 1966; Tollmann, 1977).

The lower part of the formation, the Seidlwinkl Marble s. str., is made of relatively coarse, sugary calcite marble of white to light-gray color that is banked on the cm-dm-scale. These banks are typically weathered out and nicely rounded due to preferential erosion along the bank interstices. The rock can contain considerable amounts of white mica, detrital (?) quartz and, occasionally, mm-sized tremolite crystals.

The upper part of the Seidlwinkl Formation consists of light yellow- to orange-colored (or sometimes pinkish) dolomite marble and cargneule (Figure 2.5a), as well as more or less abundant occurrences of massive gypsum. These lithologies are intercalated in a complex manner, presumably reflecting lateral facies changes in the former depositional environment. Usually, the bedding cannot be recognized in outcrop. The dolomite marble consists of large angular fragments of fine-grained dolomite bedded in an equally fine-grained dolomite matrix. Additionally, it contains rounded, detrital (?) quartz and small flakes of white mica.

Piffkar and Schwarzkopf Formations (Upper Triassic to Lower Jurassic)
The Piffkar and Schwarzkopf formations stratigraphically overlie the carbonates of the Seidlwinkl Formation. Even though both are very characteristic, they are treated as a single mapping unit in the map, since they are always closely related and generally have only a small thickness (few tens of meters), except for the northern part of the Rote Wand Nappe.

The Piffkar Formation is characterized by bright, chloritoid-bearing, phengite-poor quartzite on the one hand and, on the other hand, bright-silvery chloritoid-bearing sericite phyllite (Figure 2.5g-h). Both lithologies completely lack carbonate minerals and feldspar and are generally tightly interfolded so that they appear interlayered. Certain amounts of chlorite and kyanite are common as well. Very rarely, relics of garnet can be found in thin section. The main accessory mineral is allanite.

The Schwarzkopf Formation resembles the Piffkar Formation in basically all characteristics mentioned above, except for its very high content of carbonaceous matter, which makes the rocks appear dark in the field. It is mainly made up of dark-silvery, phengite- quartz-phyllites rich in porphyroblastic kyanite that forms up to 1 cm long needles, and can also contain considerable amounts of chloritoid and clinozoisite. The carbonaceous matter is finely dispersed in the matrix and incorporated as tiny flakes inside the kyanite and chloritoid crystals, causing them to look black in hand specimen. Additionally, there are dark gray (phengite-kyanite-chloritoid-) quartzite banks intercalated with the phyllites, but usually these are less frequent than those in the Piffkar Formation. The rocks of the Schwarzkopf Formation also lack carbonate minerals and feldspar completely.

Due to regional correlation with very similar deposits, as outlined, e. g., in Pestal (2008) and Schmid et al. (2013), the Piffkar and Schwarzkopf formations are considered to have a Late Triassic (Keuper) and an Early Jurassic (Liassic) depositional age, respectively. They represent local varieties of the Quarten Formation ("Quartenschiefer") and Gresten Formation in the Swiss Alps. Both formations indicate continuous sedimentation of very similar protolith, the latter under anoxic conditions, maybe during the Toarcian global anoxic event (Schmid et al., 2013; after Takashima et al., 2006).

Bulk rock chemical data (Appendix C) of phyllites from the Piffkar and Schwarzkopf formations prove that both are very similar (with the exception of low (Piffkar Fm.) versus very high (Schwarzkopf Fm.) content of carbonaceous material) and most probably represent a depositional continuum. These phyllites have unusual compositions, which is shown in their fairly high content of Fe and very low content of Ca. Additionally, the almost complete lack of Na makes these metapelites distinct from all other metapelitic lithologies investigated in this study.

Brennkogel Formation (Cretaceous) The Brennkogel Formation forms the uppermost part of the Rote Wand Nappe. It is a few hundred meters thick and has a fairly variable lithological content, mainly comprising dark calcareous micaschist and bright carbonate quartzite as well as meta-conglomerates, -breccias, dark phyllite and dark garnet-chloritoid-micaschist. True meta-arkosic rocks occur only sporadically in this unit and preferentially in its lower part. Usually, these lithologies are tightly interlayered or -folded (Figure 2.5b), which is why they are grouped in a single mapping unit.

The stratigraphic base of the Brennkogel Formation is marked by the Hochtor Breccia. Where present, this lithology serves as a valuable marker horizon. The breccia clasts are usually several centimeters in size, but huge blocks of up to one meter in diameter have been reported (Frasl, 1958). They are mainly derived from the carbonate rocks (especially dolomite) of the Seidlwinkl Formation in the footwall. The matrix is phyllitic or quartzitic (Pestal et al., 2009). Usually, the breccia is strongly tectonized, with deformed clastic components.

Most of the Brennkogel Formation is a dark carbonate-bearing micaschist (Figure 2.5c-d). This lithology typically has rusty-brown spots on the weathered dark-gray cleavage surfaces. Phengite, quartz, carbonate (calcite, ankerite), carbonaceous matter and other opaque phases (hematite?) are ubiquitous. Chlorite, garnet, chloritoid, paragonite, albite, epidote, clinozoisite, rutile and titanite may also occur, depending on bulk chemical composition. Zoned tourmaline is the main accessory mineral and sometimes very abundant. The garnet-bearing varieties often contain pseudomorphs (clinozoisite, albite, chlorite, paragonite) after lawsonite as inclusions in garnet, indicating high-pressure metamorphism (details in Chapter 3).

The quartzite is massive and occurs as dm-m thick banks intercalated with the micaschist (Figure 2.5b). Usually, it is of light-gray or light-brown color, more or less carbonatic and poor in mica. South of the Margarötzenkopf summit, relict cross-bedding was found in one of these quartzite banks. Pestal (2008) describes these quartzite banks to be composed of numerous layers with graded bedding, representing rhythmic flysch-like deposits.

In the upper part of the Brennkogel Formation, intercalations of calcareous micaschist in the dark micaschists are relatively frequent, so that this part of the Brennkogel Formation resembles the metasediments of the Glockner Nappe. The stratigraphic top of the Brennkogel Formation is marked by a tectonic imbrication zone, where large blocks of serpentinite, prasinite and (Triassic) marble are embedded in a matrix of the overlying Brennkogel Formation metasediments. It must be stressed that the Brennkogel and Schwarzkopf formations are very distinct with regard to their lithological content and chemical composition, and no gradational transitions between these units were observed.

The sedimentary age of the Brennkogel Formation is debated and either seen as Liassic (e. g., Cornelius & Clar, 1935; Frasl & Frank, 1964) or Cretaceous (e. g., Lemoine, 2003; Thiele, 1980). Given the striking lithological differences between the Liassic Schwarzkopf Formation and the Brennkogel Formation, and the fact that the Brennkogel Formation has a major unconformity at its base, we follow the argumentation of Schmid et al. (2013) in assigning a (Lower) Cretaceous age to the Brennkogel Formation. However, we propose the following additions to the reasoning of Schmid et al. (2013): As shown above, the Brennkogel Formation of the Rote Wand Nappe consists of two distinct lithological assemblages (dark micaschist with carbonate breccia and dark micaschist with quartzite banks), even though gradual transitions between both types clearly exist. The first type is well-developed, e. g., in the Hochtor and Spielmann peak areas. Predominantly found at the stratigraphic base of the formation, it is characterized by the occurrence of relatively coarse-grained breccias with carbonatic components clearly derived from the Seidlwinkl Formation. This indicates erosion of a Triassic carbonate platform, a short

transport distance and rapid deposition of the eroded material, making mass-wasting due to fault activity in a syn- to post rift environment very likely for the formation of this part of the Brennkogel Formation (e. g., Kurz et al., 1998). The other type is especially well-exposed at the northeastern flank of the eponymous mountain, the Brennkogel, and in the lower slopes of the Fusch Valley near Ferleiten. This type makes up the main part of the formation and is characterized by relatively fine-grained, very mature quartz-rich turbidites that were rhythmically deposited in a basin dominated by organic-rich, fine-grained marly sediments. In addition, layers of calcareous micaschist (as in the Glockner Nappe) are intercalated in the upper parts of this succession. This type of the Brennkogel Formation is more diagnostic of a post-rift environment, where eroding crystalline hinterland delivered mature siliciclastic sediments that were transported to a slowly-filling marine basin via turbidity currents. The Brennkogel Formation is remarkably similar to what is reported for the lithostratigraphy of the external Valais Units in the Western Alps, as reported, e. g., by Loprieno et al. (2011). Their Late Jurassic to Early Cretaceous syn-rift sequence (Pyramides Calcaires Formation of the Brèches du Grand Fond Group) consists of rhythmically-bedded brownish calcschist, black shales, calcareous quartz-sandstones and layers of fine conglomerates with Middle Triassic dolomite clasts; clearly analogous to at least the lower part of the Brennkogel Formation. In contrast, the Liassic syn-rift sequence of the external Valais Units in the Western Alps (Dent d'Arpire Formation), as described by Loprieno et al. (2011), consists entirely of diverse conglomerates and therefore differs from the typical rock assemblage of the lower part of the Brennkogel Formation.

The post-rift sequence of the external Valais Units contains, among others, the Marmontains Formation, which consists of alternating carbonate-free black shales and quartz arenites (Loprieno et al., 2011). This succession is clearly analogous to the Early Cretaceous "Gault-type" deposits in the Central Alps (e. g., Lemoine, 2003) and resembles the upper part of the Brennkogel Formation, except the lack of carbonates, which, however, can be easily explained by deposition below and above the carbonate compensation depth. Therefore, and in analogy to the Western and Central Alps, the Brennkogel Formation probably represents the transition from an Early Cretaceous syn-rift to post-rift setting.

2.6.3 Penninic Nappes

The term Penninic nappes is used throughout the Alps to refer to tectonic units paleogeographically derived from the Alpine Tethys — the Jurassic to Cretaceous Ocean that separated the European continent in the North from the continental part of the Adriatic Plate in the South — and immediately adjacent portions of the continental margins. In the Tauern Window, two distinct Penninic nappe systems are usually distinguished: The upper Matrei Zone and Nordrahmenzone and the lower Glockner nappe system (e. g., Kurz et al., 1998; Schmid et al., 2004). Both Penninic nappes in the Tauern Window consist of metamorphosed marine sediments that contain ophiolite fragments such as serpentinized peridotite and metabasites. During Alpine convergence, the Penninic nappes in the Tauern Window were subducted, exhumed and accreted in the orogenic nappe stack.

Glockner Nappe System

The Glockner nappe system comprises a strongly deformed succession of mainly calcareous micaschist, in which prasinite layers and serpentinite blocks are incorporated. Some parts of the Glockner nappe system experienced high-pressure metamorphism reaching eclogite-facies conditions while other parts did not exceed lower blueschist facies conditions (Groß et al., 2020b, chapter 3). These differences in peak-P systematically correspond to differences in the peak-T attained during subduction-related metamorphism (Glockner nappe s. str. ca. 450-520 °C, Rauris Nappe ca. $<$ 450 °C; Groß et al. subm., chapter

4). Therefore a subdivision of the Glockner nappe system seems plausible, as other authors have already suggested (e. g., Favaro & Schuster, 2012; Pestal & Hellerschmidt-Alber, 2011). Here, we follow the subdivision proposed by Pestal & Hellerschmidt-Alber (2011), who subdivided the Glockner nappe system into a lower Glockner Nappe s. str. and an upper Rauris Nappe. The distinguishing feature is the local occurrence or absence of eclogite-facies parageneses, respectively. Apart from this difference, both nappes contain essentially the same lithologies. Therefore, the following descriptions of the main rock types used in map compilation, except for the eclogite and garnet prasinite, apply to both the Glockner s. str. and Rauris nappes. These descriptions are largely based on Cornelius & Clar (1939), Frank (1969), Frasl (1958), Kurz et al. (1998), and Pestal & Hellerschmidt-Alber (2011) and own observations.

Serpentinite Layers or lenses of serpentinite occur predominantly at the base of the Glockner nappe system near the contact to the underlying Modereck nappe system (Kurz et al., 1998). These blocks range in size from several meters to a few hundreds of meters. The serpentinites are usually interpreted as the alteration product of peridotite derived from oceanic mantle lithosphere (Höck & Miller, 1987). Primary magmatic minerals (olivine, pyroxene) are very rare. Often, the contact area of the serpentinite blocks to the surrounding calcareous micaschist matrix is characterized by metasomatic reaction halos.

Prasinite The Glockner nappe system contains abundant prasinite that occurs as small to very large bodies and layers in the calcareous micaschist. The prasinite consists mainly of actinolite, Na-rich plagioclase (mostly albite), chlorite, epidote, clinozoisite, pyrite and carbonates in variable proportions. Locally, pseudomorphs after lawsonite can be found (Figure 2.6), evidencing retrograde metamorphism from lower blueschist- to greenschist-facies conditions. The prasinite has a geochemical signature indicative of tholeiitic mid-ocean ridge basalt (Höck & Miller, 1987).

Eclogite, Garnet-Prasinite Retrogressed eclogite occurs as lenses or layers in the calcareous micaschist of the Glockner Nappe s. str., in the imbricate zone between Glockner and Modereck nappes and in the Bündnerschiefer of the Trögereck Nappe. The eclogite is always strongly retrogressed so that omphacite is only found sporadically as relics (e. g., Dachs & Proyer, 2001). The rock matrix consists of greenschist-facies minerals (actinolite, albite, chlorite, epidote/clinozoisite, quartz, carbonate) and contains porphyroblastic garnet. Therefore, the rock is more appropriately named a garnet-prasinite. Garnet often contains inclusions of glaucophane and pseudomorphs after lawsonite. They are usually surrounded by a corona of biotite and chlorite, presumably the product of partial garnet breakdown. Dachs & Proyer (2001) determined peak-pressure conditions of ca. 1.7 GPa and 540-570 °Cfor the eclogites from the Gamsgrube and Hochtor localities.

Calcareous Micaschist The volumetrically dominant lithology in the Glockner nappe system is calcareous micaschist. This term denotes a succession of light gray to light brown, carbonate-rich micaschists and phyllites and mica-bearing marbles. Occasionally, layers of dark, graphite-rich phyllite and garnet-micaschist occur as well. The calcareous micaschist essentially consists of only calcite, white mica and quartz. Other minerals are rare and include chlorite and feldspar. In parts of the Rauris Nappe, the calcareous micaschist and calcareous phyllite contain intercalations of particularly fine-grained, thin-bedded quartzite layers that are interpreted as meta-radiolarites (Frasl & Frank, 1966). A special lithology often found at the contact of calcareous micaschist to metabasite is a bright, quartz-rich garnet-white mica-schist that is carbonate-free and often very rich in epidote-group minerals.

The sedimentary age of the main volume of the calcareous micaschist is unconstrained in the central Tauern Window, but was inferred to be Early Cretaceous (Schmid et al., 2013). So far, fossils were

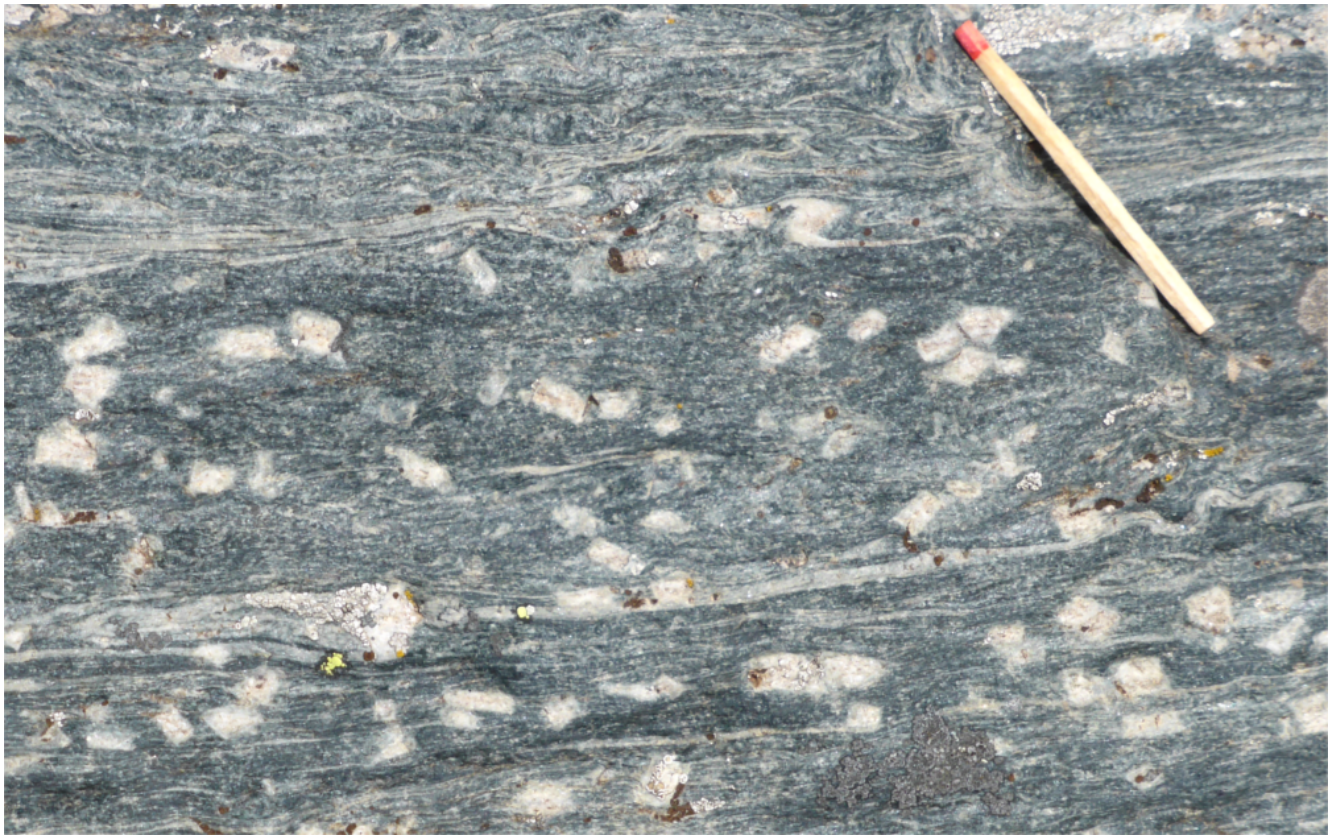

Figure 2.6: Field photograph of a prasinite from the Glockner nappe s. str. The rock contains abundant inclusions of light grey color and rectangular shape that are interpreted as pseudomorphs after lawsonite.

found in only one particular part of the Glockner nappe system, the Drei Brüder Formation (Höck et al., 2006; Kleberger et al., 1981) that probably forms the stratigraphically uppermost part of the Rauris Nappe. In our compiled map, this formation was grouped with the calcareous micaschist unit, even though it shows some characteristics that are different from the "usual" calcareous micaschists. The sedimentary age of the formation was dated by Höck et al. (2006) via trace- and microfossils to range from Tithonian to Berriasian for its lower part to latest Hauterivian or younger for its uppermost part. Provided that the tectonostratigraphy used here is correct, these findings mean that the main mass of calcareous micaschist is indeed Jurassic to earliest Cretaceous in age.

Matrei Zone and Nordrahmenzone

The uppermost Penninic Nappe in the Tauern Window is the Matrei Zone and Nordrahmenzone. The term Matrei Zone originally referred to occurrences of the unit at the southern margin of the Tauern Window, whereas Nordrahmenzone is used for the units at the northern margin. It is an imbricate zone that comprises oceanic metasediments, metabasites and serpentinites from the Alpine Tethys and slivers or olistoliths derived from the overlying Austroalpine nappes, including blocks of siliciclastics and metacarbonates (e. g., Frisch et al., 1987; Koller & Pestal, 2003; Peer & Zimmer, 1980).

This sequence is interpreted as a former accretionary prism that formed during early subduction of the Alpine Tethys below the active Austroalpine margin of the advancing Adriatic plate (Frisch et al., 1987). According to Schmid et al. (2013) and in analogy to the Western and Central Alps, the Matrei Zone/Nordrahmenzone represents the South Penninic (Piemont-Liguria) part of Alpine Tethys in the Tauern Window.

Bündnerschiefer with Exotic Blocks (undifferentiated) This mapping unit is a composite unit that comprises, on the one hand, the mass of Bündnerschiefer of the Matrei Zone and Nordrahmenzone and, on the other hand, numerous other lithologies that are included as blocks or lenses in the Bündnerschiefer matrix. The Bündnerschiefer is mainly made up of dark phyllite and light calcareous phyllite and micaschist, often indistinguishable from those of the Glockner nappe system. The blocks range in size from meters to kilometers and comprise metaradiolarites, prasinites, Permian siliciclastics ("Alpine Verrucano") and Triassic metacarbonates. There was one occurrence of datable fossils in the Bündnerschiefer of the Nordrahmenzone that yielded Early Cretaceous ages for olistolith-bearing dark phyllites (Reitz et al., 1990).

Serpentinite Large serpentinite blocks that occur in the Bündnerschiefer of the Matrei Zone in the southern Tauern Window were marked as separate unit on the map.

Austroalpine Nappes (undifferentiated)

The perimeter of the Tauern Window is formed by the Austroalpine nappes that are not differentiated tectonically or lithologically on the map. They mainly comprise polymetamorphic para- and orthogneisses and amphibolites of the Schober Crystalline in the South and Paleozoic sand-, silt- and claystones of the Grauwackenzone in the North (e. g., Pestal et al., 2009).

2.7 Regional Correlation of Lithostratigraphic and Tectonic Units

Many characteristic lithological assemblages can be correlated across several tectonic units (Figure 1), giving insights in the geodynamic evolution of the central Tauern Window. In the following, a summary of the main stages of the post-Variscan geodynamic evolution of this region is given, as inferred from these correlations. This compilation is largely based on the syntheses of Kurz et al. (1998), Kurz, 2006 and Schmid et al. (2013), but also incorporates recent findings.

2.7.1 Permo-Triassic Sedimentation on the Eroded Variscan Basement

The cessation of the Variscan orogeny in the Alpine region was followed by the sedimentation of an essentially German-type Permo-Triassic sequence. The succession started with the sedimentation of large amounts of siliciclastic material in graben-like intramontane basins that cut Variscan structures in the eroding basement (e. g., Veselá et al., 2008). In the central Tauern Window, this erosional period is evidenced by the siliciclastic metasediments of the Permian to Lower Triassic Wustkogel Formation. These rocks are fairly abundant in the Rote Wand Nappe, but also occur in the Romate Nappe. However, the thickness of these deposits is much less than that of similar deposits in the Western Tauern Window (Veselá et al., 2008) or other parts of central Europe (e. g., Saar-Nahe basin, Henk, 1993). This indicates that, during this period, the Wustkogel Formation of the central Tauern Window occupied a marginal setting to the main graben-bound basins in the region.

This phase of denudation of the Variscan orogen was superseded by a transgression of the Neotethys in mid-Triassic times that resulted in the formation of a shallow epicontinental sea, as evidenced by the lagoonal carbonates of the Seidlwinkl Formation. These deposits are most prominent and thickest

in the Rote Wand Nappe. Thinner successions exist in the Trögereck and Romate nappes, as well as in many other Subpenninic nappes of the Eastern and Western Tauern Window (e. g., Kurz et al., 1998; Schmid et al., 2013.

Regression of the Neotethys during the Late Triassic gave way to the deposition of the siliciclastic rocks of the Piffkar and Schwarzkopf formations that probably formed in a deltaic environment. This assemblage is typical of the Rote Wand Nappe in the central Tauern Window and is also found in other parts of the Modereck nappe system, e. g., in the Wolfendorn (Lammerer, 1986) and Neves areas in the southwestern Tauern Window, as well as in the Mallnitz synform (Favaro & Schuster, 2012). In the other Subpenninic nappes of the Tauern Window, these formations are very sparse. A strikingly similar succession exists in the Mesozoic cover of the Adula Nappe (Cavargna-Sani et al., 2014), including the Lower and Mid-Triassic deposits. In other parts of the Alps, the Quarten and Gresten formations are the non-metamorphic equivalents of the Piffkar and Schwarzkopf formations, respectively.

2.7.2 Mid-Jurassic Rifting and Opening of the Alpine Tethys

The Subpenninic units of the central Tauern Window lack syn-rift sediments that are related to the Early to Middle-Jurassic rifting and opening of the Alpine Tethys. Instead, the stratigraphic record of these units during this time interval is characterized by a substantial unconformity (e. g., Schmid et al., 2013, Figure 2.2) that is interpreted to reflect the erosion of pre-rift strata. Such unconformities are commonly explained by thermally-induced uplift and erosion of the rift shoulders. Some authors argued that the Lower Jurassic syn-rift deposits may be found in the lower parts of the Brennkogel Formation (e. g., Cornelius & Clar, 1935; Frasl & Frank, 1964), a view that is not supported by the observations presented above, which indicate a Cretaceous age for the entire Brennkogel Formation. Therefore, the only sediments in the central Tauern Window that unequivocally record Jurassic rifting and opening of the Alpine Tethys are the deep-marine sediments deposited on the ophiolitic basement of the Matrei Zone, as described by Koller & Pestal (2003). They correlated a succession of ophicarbonate breccia and radiolarite immediately on serpentinized lherzolite with an identical, clearly Jurassic assemblage in the Swiss Alps (e. g., Oberhalbstein and Engadine areas of Eastern Switzerland, Desmurs et al., 2001).

2.7.3 Late Jurassic to Early Cretaceous Carbonatic Shelf

The Early to Middle Jurassic rifting phase of the Alpine Tethys was followed by the formation of relatively deep-marine carbonate deposits on the outer shelf of the European continental margin in Late Jurassic times (Höfer & Tichy, 2005; Kiessling, 1992; Klebelsberg, 1940). This phase is manifested by the laterally equivalent Silbereck, Angertal and Hochstegen marbles that are fairly widespread in several Europe-derived tectonic units of the Western and Eastern Tauern Window. Somewhat similar carbonate deposits called Klammkalk are known from the Penninic Units of the Tauern Window. The Klammkalk is a prominent part of the Nordrahmenzone in the northeastern Tauern Window. It was deposited on the slope of the Adriatic margin (Frisch et al., 1987). Even though datable fossils were not found so far, a similar sedimentation age as the Hochstegen Marble, i. e., Late Jurassic to Early Cretaceous, is likely (Thiele, 1980).

2.7.4 Lower Cretaceous Rift Deposits

Syn-rift sediments that document the Early Cretaceous opening stage of the Alpine Tethys are widespread in the Europe-derived tectonic units of the central Tauern Window. In the Rote Wand Nappe,

this stage is recorded by at least the lower part of the Brennkogel Formation which is characterized by carbonatic escarpment breccias; in the Trögereck Nappe and the Eclogite Zone by the large masses of arkose-rich, Bündnerschiefer; and in the Romate Nappe by the graphitic phyllites that contain fine-grained breccia-horizons and "within-plate" metabasites (Höck & Miller, 1987). In the northwestern Tauern Window, these deposits find their equivalent in the Kaserer Series of the Wolfendorn and Ahorn nappes. This series is rich in coarse-grained arkosic sandstones. It transgressively overlies the Hochstegen Marble and therefore has an Early Cretaceous age (Thiele, 1974).

The differences in terms of sediment composition and grain size observed in the different tectonic units points towards systematic differences in the depositional environments. The coarse-grained, immature siliciclastics of the Kaserer Series and similar deposits of the Trögereck Nappe and Eclogite Zone indicate deposition in the proximity of faults in the crystalline rocks of the Venediger basement. The coarse-grained carbonatic clastics of the Brennkogel Formation indicate proximity to faults affecting a carbonate-dominated hinterland, most likely the Seidlwinkl Formation of the Rote Wand Nappe. In contrast, the organic-rich metapelites of the Wörth Formation can be interpreted as distal deposits in a deep-water, oxygen-starved part of the rift basin.

Here it is proposed that these facies changes represent different settings in a single large rift basin that formed in the European continental margin during Cretaceous rifting. In this scenario, the Kaserer Series was deposited on the northern, proximal part of this basin (i. e., on the side of the stable continent). The Wörth Unit was deposited in a central part of the basin on intensely thinned continental crust. The syn-rift sediments of the Eclogite Zone and the Trögereck Nappe formed on the southern side of the rift basin, also on extremely thinned continental or even transitional basement, in proximity to major normal faults. Both units and the Wörth Unit were affected by mild, rift-related magmatism. The syn- to post-rift sediments of the Brennkogel Formation were deposited on an extensional allochthon (future Rote Wand Nappe) that comprised relatively thick continental basement and Mesozoic cover rocks. It was separated from the main continent by the Early Cretaceous rift basin.

2.7.5 Cretaceous Post-Rift Sedimentation

Sediments deposited after the Early Cretaceous rifting phase are found in the Penninic nappes of the central Tauern Window in the form of the Bündnerschiefer assemblage. These are large amounts of calcareous micaschist that often contain intercalations of dark phyllite and metabasite. These deposits are usually barren of fossils and therefore lack a precise depositional age. However, regional correlation with similar assemblages in the entire Alpine chain indicates largely Late Jurassic to Cretaceous ages of these rocks (Lemoine, 2003). This notion is consistent with the sparse biostratigraphic data: Höck et al. (2006) determined an Early Cretaceous age for a deep-sea fan carbonate sandstone deposit in the uppermost part of the northern Rauris Nappe (Drei Brüder Formation). Reitz et al. (1990) also obtained Early Cretaceous ages for an olistostrome-rich flysch assemblage in the Nordrahmenzone. The upper part of the Brennkogel Formation, which is characterized by deposition of rhythmic, mature quartz turbidites and pelitic marly background sedimentation, may also be interpreted as an Early Cretaceous post-rift sequence.

It is important to note that the age of these sediments only gives minimum ages for the formation of the oceanic lithosphere section on which they were deposited. The precise age of oceanic lithosphere formation is ideally obtained via radiometric crystallization ages of magmatic minerals in oceanic basement rocks (i. e., basalt and gabbro), or via biostratigraphic ages of deposits directly overlying newly-formed oceanic basement — datasets which are missing so far in the entire Tauern Window. This is problematic in the light of correlating the Penninic units in the Tauern Window with those in the

Central and Western Alps, a topic where divergent views exist, as discussed above (e. g., Frisch, 1980; Kurz, 2006; Schmid et al., 2013; Trümpy, 1992). This issue has implications in the interpretation of the Penninic units in terms of their paleogeographic origin.

2.8 The Paleogeography of the Rifted European Margin

The systematic changes in the depositional environment of Lower Cretaceous rift deposits outlined above point towards a pronounced segmentation of the European margin that involved an extensional allochthon at the ocean-continent transition (Figure 2.2). This allochthon was separated from the main continent by an extensional rift basin of presumably Cretaceous age. This interpretation confirms the paleogeographic model of the rifted European margin proposed by Kurz (2006) and Wolfgang Frank (pers. comm., June 2019). It resembles the model by Ledoux (1984) which is based on observations in the northwestern Tauern Window. The correlation of tectonic units with paleogeographic origin is the following:

- Austroalpine nappes — Adriatic margin
- Matrei Zone and Nordrahmenzone — Piemont-Liguria (South Penninic)
- Glockner nappe system — Valais (North Penninic), possibly also relics of Piemont-Liguria (South Penninic)
- Modereck nappe system — extensional allochthon of the European margin
- Eclogite Zone and Trögereck Nappe — rift basin above crustal necking zone
- Venediger nappe system — distal European margin

If we assume in-sequence, foreland-propagating thrusting during subduction and accretion of the European margin, then the stacking order of tectonic units (from bottom to top) corresponds to the map-view succession of paleogeographic domains from North to South. In contrast to the model by Schmid et al. (2013), no out-of-sequence thrust is required to explain the emplacement of the Eclogite Zone in its observed position in the nappe stack. The main difference to their model is the paleogeographic position of the Eclogite Zone and the emphasis on features indicating hyper-extension during the rifting process, i. e., the interpretation of an extensional allochthon.

The view that paleogeographically, the Rote Wand Nappe originates in an extensional allochthon of the European margin raises the question of whether this extensional allochthon might be the eastward continuation of the Briançonnais (Middle Penninic) microcontinent. This would be the case if the main rifting activity during Early Cretaceous times was located between stable Europe and the extensional allochthon, so that this rift basin actually forms the continuation of the North Penninic basin. If the main rifting activity was located south of the extensional allochthon, i. e., somewhere in the already existing Jurassic part of the Penninic Ocean, the extensional allochthon cannot be regarded as equivalent of the Briançonnais microcontinent. As already noted by Kurz (2006), the structural setting of the Rote Wand Nappe, which essentially forms a thin basement lamella with sedimentary cover, is similar to several Briançonnais-derived units in the central Alps, e. g., the Tasna Nappe. On the other hand, it must be noted that the Mesozoic lithostratigraphy of the extensional allochthon, as observed in the Rote Wand Nappe, has a clear affinity to the European margin, rather than to the Briançonnais.

Furthermore, the Wörth unit, that is the most distal and deepest marine Cretaceous syn-rift sedimentary succession between the European margin and the extensional allochthon, is floored by continental basement and not by oceanic lithosphere.

This problem is closely related to the question of whether the Glockner nappe system originates from an oceanic basin that was formed during Jurassic or Cretaceous rifting and spreading, a topic already extensively discussed above (e. g., Kurz, 2005, 2006; Schmid et al., 2004, 2005, 2013). From a lithostratigraphic point of view, the sedimentary succession of the Glockner nappe system is more similar to North Penninic than to South Penninic assemblages in the Central and Western Alps, which implies that the Glockner nappe system is also of North Penninic origin and age. However, as pointed out above and by others (Frisch et al., 1987; Kurz, 2005), the sedimentary record is ambiguous in this respect and unambiguous magmatic ages of oceanic crust formation do not exist in the Tauern Window. Especially the Rauris Nappe of the Glockner nappe system has similarities to the lower parts of the Matrei Zone (e. g., also contains radiolarites; Frasl & Frank, 1966). Therefore, the Rauris Nappe might represent a transitional paleogeographic position, located between the clearly South Penninic Matrei Zone and the Glockner Nappe s. str. that is located further north in the Penninic ocean basin. An episode of upper Jurassic to lower Cretaceous rifting is not only documented in the northern part of Alpine Tethys, but also in the south (e. g., Geier Formation of Reckner Ophiolite and Matrei Zone; Koller & Pestal, 2003). Therefore, we propose that in the area of the later Eastern Alps, lower Cretaceous extension potentially affected large parts of the existing ocean basin and both of its continental margins. This means that the Penninic Units in the Tauern Window (i. e., Glockner nappe system, Matrei Zone) may exhibit Jurassic and Cretaceous ages of oceanic crust formation.

In a study by Nirrengarten et al. (2020) on the ocean-continent transition in the South China Sea, a large extensional allochthon was repeatedly drilled and seismically imaged, exposing several characteristic features of extensional allochthons unaffected by later overprint (Figure 2.7). The extensional allochthon described by Nirrengarten et al. (2020) is expressed in the seismic section as a distal high that consists of continental basement with its pre-rift cover still preserved. Syn-rift sediments on the allochthon are relatively thin and locally missing. This sequence is overlain by marine post-rift deposits similar to the oceanic domain. In the necking zone that separates the extensional allochthon from the main margin, a thick syn-rift sequence directly overlies strongly thinned continental basement, whereas pre-rift sediments are entirely missing due to erosion. Instead, and in contrast to the extensional allochthon, this rift basin contains several rift-related intrusions. The main features observed in the Rote Wand unit, a former extensional allochthon, are remarkably similar to the main characteristics of its present-day counterpart in the South-China Sea.

2.9 Conclusions

Based on a reassessment of lithostratigraphic data from individual nappes in the central Tauern Window (Figure 2.2), we reconstructed the post-Variscan geodynamic evolution of the European continent now exposed in the central Tauern Window. This study largely confirms earlier reconstructions (e. g., Kurz et al., 1998) but also proposes some refinements on the existing models. The deposition of Permian to upper Triassic pre-rift strata was followed by Jurassic rifting and the opening of the Piemont-Liguria ocean basin. Jurassic syn-rift sediments are effectively missing in the Europe derived units; instead, this period is marked by an erosional unconformity of approximately middle Jurassic age. Post-rift subsidence of the European margin enabled the formation of an upper Jurassic carbonatic shelf. This period of relative quiescence was superseded by intense rifting activity during the lower Cretaceous, which led to some magmatic activity and the deposition of large masses of clastic sediments. Following

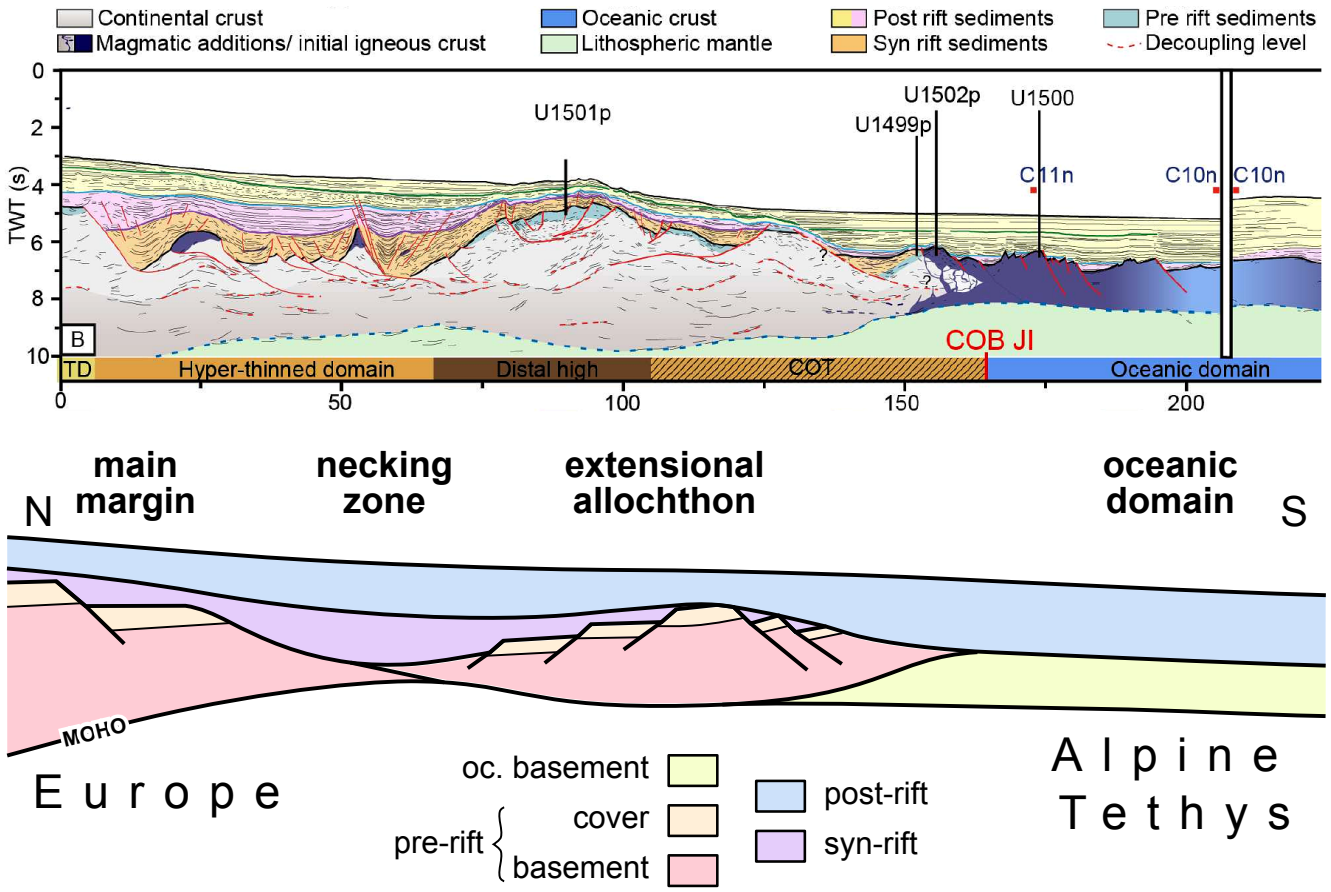

Figure 2.7: Comparison between a present-day example of a hyper-extended margin with an extensional allochthon as documented by Nirrengarten et al. (2020) (top) and our reconstruction of the geometry of the European margin to the Alpine Tethys (bottom) based on lithostratigraphic observations in the central Tauern Window. Note the similarities between thickness of the continental basement and distribution and nature of sediments and magmatic rocks.

Kurz (2006), we propose that during this period, a deep rift basin formed in the distal European margin to the Alpine Tethys, which led to the separation of an extensional allochthon from the main continent (Figure 2.7). During later convergence and subduction of the margin, parts of the margin were sheared off from the down-going European plate. The extensional allochthon formed the Rote Wand Nappe, while the relics of the rift basin can now be found in the Eclogite Zone, the Trögereck Nappe and the Wörth Unit. We document that the lithostratigraphic record of this hyper-extended segment of the European margin, as seen in the aforementioned tectonic units, compares well with the main characteristics of a recent analogue of a hyper-extended continental margin observed in the South-China Sea.

Chapter 3

Crustal-Scale Sheath Folding at HP Conditions in an Exhumed Alpine Subduction Zone (Tauern Window, Eastern Alps)

This chapter was published as:
Groß, P., Handy, M. R., John, T., Pestal, G. & Pleuger, J. (2020b). "Crustal-Scale Sheath Folding at HP Conditions in an Exhumed Alpine Subduction Zone (Tauern Window, Eastern Alps)". In: *Tectonics* 39(2). DOI: 10.1029/2019TC005942.

3.1 Abstract

We investigate a well-preserved paleo subduction channel that preserves a coherent part of the European continental margin exposed in the central Tauern Window (Eastern Alps), with the aim of testing models of sheath fold nappe formation and exhumation. The subduction zone was active during Paleogene convergence of the European and Adriatic plates, after closure of the Alpine Tethyan ocean. New cross sections and structural data together with new petrological data document a recumbent, tens of kilometers-scale sheath fold in the center of the Tauern Window that formed during pervasive top-foreland shear while subducted at high-pressure (HP) conditions (ca. 2.0 GPa, 500 °C) close to maximum burial depth. The fold comprises an isoclinally folded thrust that transported relicts of the former Alpine Tethys onto a distal part of the former European continental margin. The passive margin stratigraphy is still well preserved in the fold and highlights the special character of this segment of the European continental margin. We argue that this segment formed a promontory to the margin, which was inherited from Mesozoic rifting. In accordance with classical sheath fold theory, this promontory may have acted as an initial structural perturbation to nucleate a fold that was passively amplified to a sheath fold during top-foreland shear in the subduction zone. The fold was at least partly exhumed and juxtaposed with the surrounding lower pressure units by opposing top-hinterland and top-foreland shear zones above and below, respectively, that is, in the sense of a nappe fold formed during channel-extrusion exhumation.

3.2 Introduction

Exhuming continental lithosphere from great depths has posed a geodynamic problem ever since the discovery of high-pressure (HP) and ultra-high pressure (UHP) mineral assemblages in continental units in the heart of mountain belts (e. g., Chopin, 1984; Okay et al., 1989). These units, henceforth referred to as HP units, form in the former lower plate of orogens prior to, or at the beginning of, continental collision. The basic challenge has been to determine how crustal units that densified during prograde subduction metamorphism (e. g., Agard et al., 2009; Bousquet et al., 1997) have risen within the orogen and were emplaced next to, and in some cases between, less dense units during crustal thickening. Unfortunately, most HP units have been strongly overprinted during and after exhumation, which has eliminated most, if not all, structures related to subduction and even to exhumation from HP and UHP conditions (e. g., Beltrando et al., 2010; Jolivet et al., 2003; Pleuger & Podladchikov, 2014).

This challenge has been addressed mostly by numerical modelers, who have attempted to fill the information gap with models using various dynamic boundary conditions (reviews by Agard et al., 2018; Hacker et al., 2013; Warren, 2013). One end-member proposal, here termed the "wedge model" after the critical wedge theory of Chapple (1978) and Dahlen et al. (1984), involves the progressive exhumation of deeply subducted nappes from the base of orogenic wedges due to tectonic and erosional unroofing of the overlying nappe stack (Beaumont et al., 1994; Platt, 1986). Thrusting in the wedge-shaped nappe stack is proposed to be "in sequence," that is, to propagate toward the foreland, while the nappe stack unroofs to maintain a force balance between the dipping wedge base, the tapered wedge surface, and the nappe stack itself. Unroofing may be accelerated by uplift of the entire wedge due to removal of negatively buoyant lithospheric mantle from the base of the orogen, either by convective delamination (Houseman et al., 1981) or by tearing and breakoff of a lithospheric slab (Davies & Blanckenburg, 1995). A contrasting model, here termed the "channel" model, involves subducted crustal fragments rising as buoyant bodies along a narrow channel at the top of a descending lithospheric slab (Chemenda et al., 1995; see also Burov et al., 2001). In the case of negatively buoyant HP rock bodies, this ascent may be facilitated by downward narrowing of the channel, which would forcibly extrude the subducted bodies upward between a thrust and normal fault located, respectively, in the footwall and hanging wall of these bodies (Mancktelow, 1995; Vannay & Grasemann, 2001). Yet another way to solve the dilemma of HP rocks within orogens has been to posit that the pressure values recorded in HP units by petrology reflect dynamic pressure rather than lithostatic pressure, P (e. g., Mancktelow, 1995, 2008; Mancktelow, 1993; Moulas et al., 2013; Petrini & Podladchikov, 2000; Rutland, 1965. Dynamic pressure, sometimes called tectonic overpressure or underpressure (depending on the sign), is the difference between mean stress (i. e., $(\sigma 1 + \sigma 3)/2)$ and the lithostatic pressure. If one assumes that mean stress can be equated with thermodynamic pressure, then the pressure values obtained by applying phase petrology to HP rocks in compressional settings correspond to a shallower depth than obtained by assuming the standard geobaric relationship of $P = \rho g z$, where ρ is rock density, g is the acceleration of gravity, and z is depth (Gerya, 2015; Moulas et al., 2013; Schenker et al., 2015). Though dynamic pressure mitigates the problem of exhumation by reducing the depth of subduction, the assumption that mean stress can be equated with thermodynamic pressure is a proposition that remains highly controversial (e. g., Tajčmanová et al., 2014; Wheeler, 2014).

Variants of these end-member hypotheses have been applied to the European Alps (Figure 3.1, inset; Bauville & Schmalholz, 2015; Escher & Beaumont, 1997; Schmid et al., 1996), where Alpine HP and UHP metamorphism affected not only oceanic units but also continental units derived from the margins of both the European and Adriatic plates (Bousquet et al., 2012; Oberhänsli et al., 2004; maps and references therein). These continental units individuated already during Early Mesozoic rifting and

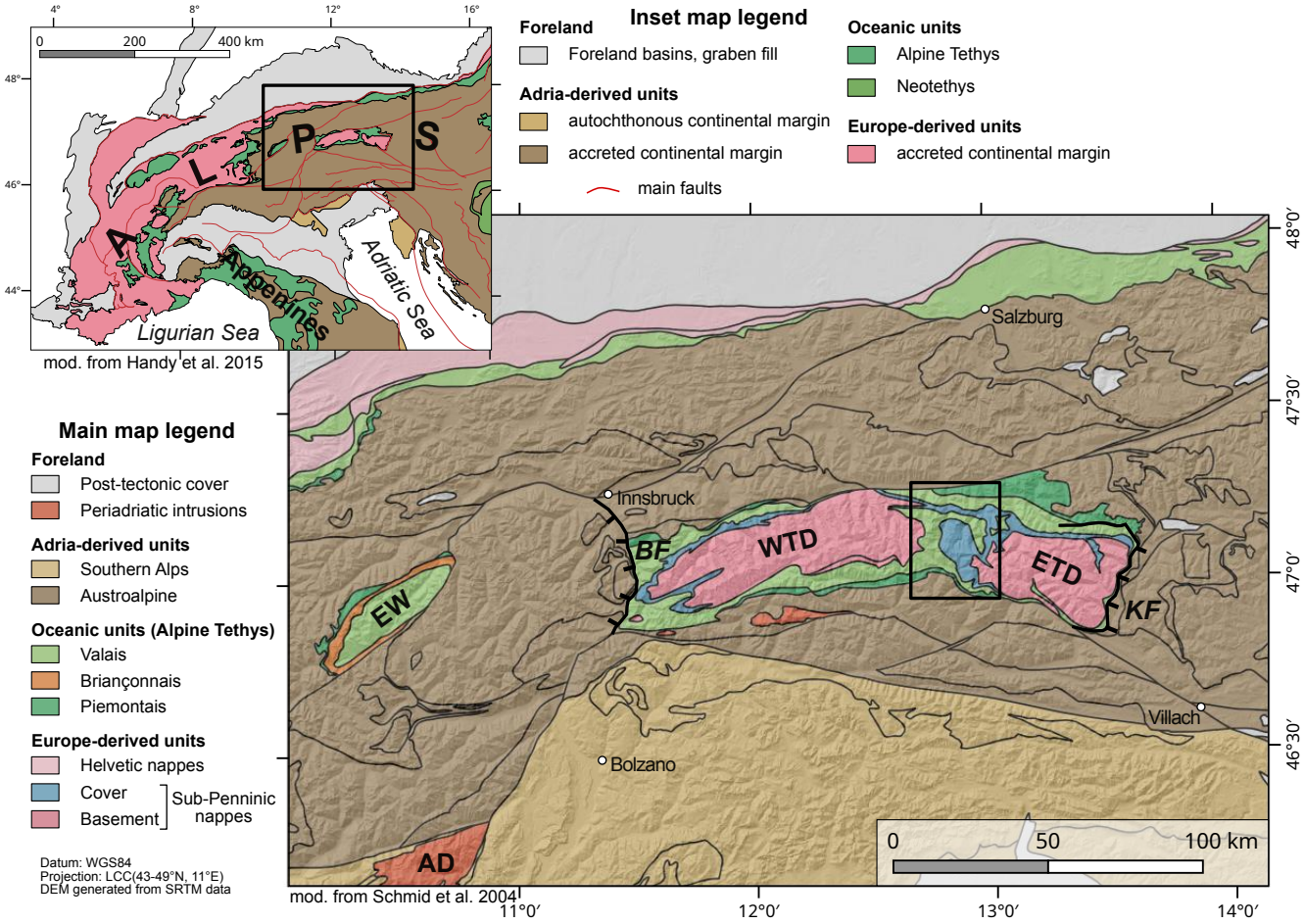

Figure 3.1: Tectonic map of the Eastern Alps and Tauern Window with the Western Tauern Dome (WTD) and Eastern Tauern Dome (ETD). Map modified from Schmid et al. (2004, 2013); inset map of the Alps modified from Handy et al. (2015). Black rectangle outlines the study area and location of the tectonic map in Figure 3.2. AD = Adamello Pluton, EW = Engadin Window, BF = Brenner Fault, KF = Katschberg Fault.

spreading of the Alpine Tethyan ocean (e. g., Froitzheim & Manatschal, 1996). The SE to NW younging of the HP ages in the imbricated oceanic and continental units is interpreted to indicate that these units were subducted and exhumed in a piecemeal fashion during retreating subduction of the European Plate beneath the Adriatic Plate (e. g., Babist et al., 2006; Gebauer, 1999; Handy et al., 2010). The exposure of subduction and exhumation structures is exceptionally good in the Tauern Window of the Eastern Alps (Figure 3.1), where glacially carved mountains with bare outcrop surfaces and a relief of up to 3000 m afford a three-dimensional view of the Adria-Europe suture zone.

In this paper, we present the first clear kinematic and petrological evidence for the formation of a crustal-scale, recumbent sheath fold during Alpine subduction in Paleogene time. We show that this sheath fold — beautifully exposed in the central Tauern Window — contains an isoclinally folded thrust responsible for the emplacement of ocean crust onto fragments of the distal European continental margin. This folded nappe complex was then exhumed as a coherent unit during shearing under blueschist-facies to greenschist-facies retrograde conditions. We then discuss the tectonometamorphic conditions that were conducive for forming the sheath fold and for preserving the original stratigraphy of the continental margin within that fold. The tectonometamorphic evolution of this fold nappe is then used to test the aforementioned ideas on the exhumation of deeply buried crust, including the orogenic wedge and channel-extrusion models.

3.3 Geological Setting

3.3.1 General Overview

The tectonic units investigated in this paper (Figure 3.2) comprise thrust sheets of oceanic lithosphere derived from the Alpine Tethyan ocean (e. g., Schmid et al., 2004), as well as folded and sheared thrust sheets of the distal European continental margin (Kurz et al., 1998). Following Schmid et al. (2013), we refer to these, respectively, as the Glockner nappe system (oceanic origin) and the Modereck nappe system (continental origin). The former is part of the Penninic nappes and the latter of the Sub-Penninic nappes. Parts of the Glockner nappe system contain HP mineral assemblages (e. g., Cornelius & Clar, 1935; Dachs & Proyer, 2001; Frank et al., 1987), indicating that at least some of the oceanic units were subducted to great depth and exhumed during the Alpine orogeny. As shown by Proyer et al. (1999) and Dachs & Proyer (2001) and documented below, the continental Modereck nappe system was also affected by the same HP event.

The overlying Austroalpine nappes forming the perimeter of the Tauern Window are derived from the Adriatic Plate (Figure 3.1), whereas the underlying units in the core of the Tauern Window derive from the European continental margin (Lammerer, 1986; Schmid et al., 2013). All units and nappe contacts, including the aforementioned HP assemblages in the Penninic nappes, were overprinted by a Barrow-type, high T/P metamorphic event, the so-called Tauernkristallisation (Sander, 1914; see also Dachs et al., 2005; Droop, 1985; Hoinkes et al., 1999) in late Oligocene time (e. g., Cliff et al., 1985; Favaro et al., 2015; Höck, 1980). This event varies in metamorphic grade from peak amphibolite facies conditions in the two basement subdomes at either end of the Tauern Window to greenschist facies in the central Tauern Window (e. g., Droop, 1985; Hoernes & Friedrichsen, 1974; Scharf et al., 2013b).

Here, we deal specifically with the internal structure of the Penninic and upper part of the Subpenninic nappes. The aforementioned Glockner and Modereck nappe systems are separated by a thrust that is isoclinally folded, with the Modereck nappe system forming the core of an isoclinal fold (Figure 3.1). Below, we show that this fold, first described by Frank (1965, 1969) and later by Alber (1976) as the Seidlwinkl Fold, is a crustal-scale isoclinal sheath fold nappe that formed under HP conditions in the Alpine subduction zone. The primary geometry of the Seidlwinkl Fold is complicated by folding around a NW-SE trending dome, the Sonnblick Dome, in the eastern Tauern Window (Figure 3.1). The eastern limb of this dome preserves the inverted limb of the Seidlwinkl Fold; this inverted limb lies above the roof thrust of an imbricate stack of Subpenninic basement nappes, the Venediger nappe complex (Figure 3.1).

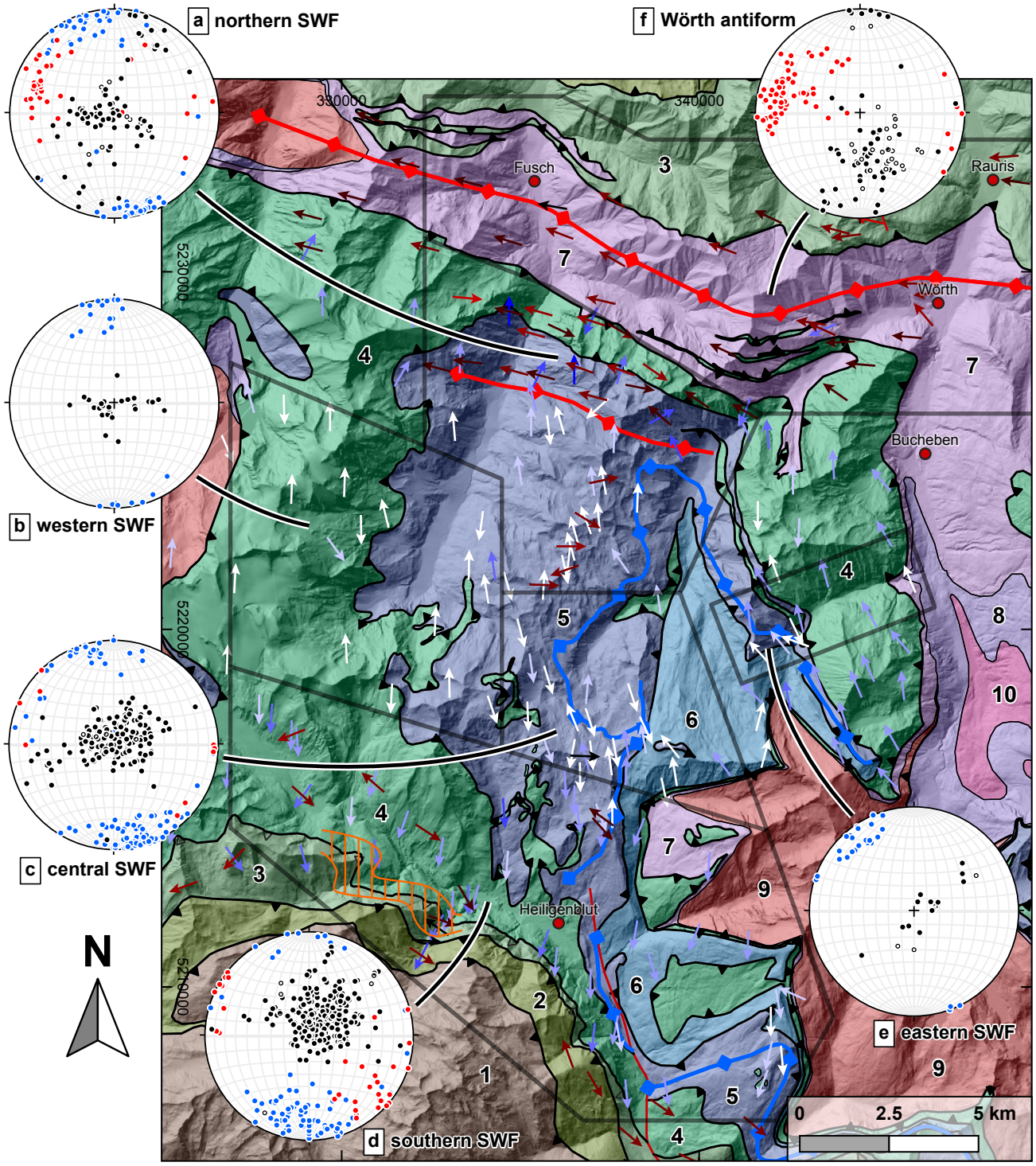

Map Legend

Austroalpine Nappes
1 undifferentiated

Penninic units
2 Matrei Zone
3 Rauris Nappe
4 Glockner Nappe s.str.

Modereck nappe system
5 Rote Wand Nappe
6 Trögereck Nappe

D3 lineations (FA, $L_{stretch}$) — *flat*, *steep*
D4 lineations (FA, L_{cren}, L_{int}) — *steep*
D3 axial plane (antiform)
D4 fold axial plane (antiform)

Venediger nappe system
7 Wörth Unit (post-Variscan cover)
8 pre-Wörth post-Variscan cover
9 Sonnblick and Riffl nappes basement
10 Romate Nappe basement

thrust, inferred
fault (undifferentiated)
area with observed top-S shear zone

Equal Area Plot

Main foliation
Fold axial plane
D3 lineation (FA, $L_{stretch}$)
D4 lineation (FA, L_{cren}, L_{int})

Lineation data plotted on map compiled from: Exner (1957), Exner (1964), Frank (1965), Höck & Pestal (1994). Complete references are in the bibliography.

Figure 3.2 ***(previous page)*****:** Tectonic map of the central Tauern Window with lower hemisphere equal area plots showing poles to the main S3 schistosity, D3 and D4 lineations. Data plotted on the map were compiled from own field measurements and Exner (1957), Exner (1964), Frank (1965), and Höck & Pestal (1994). Structural data in the equal area plots are exclusively from own field observations. SWF = Seidlwinkl sheath fold nappe.

Schmid et al. (2013) used superposed map-scale structures to propose the following succession of tectonometamorphic events for the Tauern Window: D1 — thrusting of the Austroalpine nappes onto the Matrei Zone (southern part of Alpine Tethys); D2 — thrusting of the Glockner nappe system (northern part of Alpine Tethys) onto the Modereck nappe system (distal European margin), forming a composite ocean-on-continent nappe that reached HP conditions within the Alpine subduction zone; D3 — isoclinal folding of this composite HP nappe (the Seidlwinkl fold nappe) and exhumation onto the European margin above a basal thrust; D4 — imbrication of this margin below the original basal thrust to form a duplex of Subpenninic nappes, then subsequent "Tauernkristallisation" Barrovian metamorphism; D5 — doming and orogen-parallel stretching accommodated along oppositely WSW-dipping and SE-dipping, low-angle normal faults at either end of the Tauern Window, respectively, the Brenner and Katschberg Normal Faults (Figure 3.1). The formation of the Tauern Window itself is attributed to a combination of tectonic and erosional unroofing during D5 in response to northward indentation of the Adriatic Plate into the warm and thick Alpine orogenic crust (e. g., Favaro et al., 2017; Ratschbacher et al., 1991; Rosenberg et al., 2007).

In the following, we adopt the numbering above to identify the relative age of the different structures in the central Tauern Window. However, linking the D2 juxtaposition of the Glockner and Modereck nappe systems, as well as the D3 Seidlwinkl folding to the HP metamorphic event in the central Tauern Window, remains an elusive endeavor. Determining this link is crucial to understanding how such folds nucleate and grow, as well as when they form in relation to subduction and exhumation. Metabasites from the Glockner Nappe (Figure 3.2) yield peak pressures of up to ca. 1.7 GPa, 570 °C (Dachs & Proyer, 2001; Proyer et al., 1999). These authors interpreted the metabasites as exotic blocks in a meta-sedimentary matrix that never experienced such high pressure. However, other studies indicate that HP mineral assemblages are widespread in the Penninic units of the central Tauern Window and the continentally derived metasediments of the Modereck nappe system (e. g., Dachs & Proyer, 2001; Frank et al., 1987; Proyer et al., 1999; Schmidt et al., 2014). One of our goals is therefore to reconstruct the tectonometamorphic evolution of HP rocks in the central Tauern Window, with special emphasis on the highly deformed Mesozoic metasediments that form the cover of the continentally derived Modereck nappe system.

3.3.2 Lithostratigraphic Units of the Central Tauern Window

The lithostratigraphy of the nappes in the central Tauern Window established in previous work (e. g., Kurz et al., 1998; Pestal & Hellerschmidt-Alber, 2011; Schmid et al., 2013) is central to our map compilation, cross-section construction, and thermobarometry in the following chapters. The two structural domes at either end of the Tauern Window (ETD and WTD in Figure 3.1) are separated by a structural depression preserving the Seidlwinkl sheath fold that comprises the folded Modereck nappe system and Glockner Nappe (boxed area in Figure 3.1). The lowest tectonic units (Venediger nappe system) exposed in the cores of the domes consist of late-Variscan granitoids ("Zentralgneise") that intruded into pre-Variscan European metamorphic basement ("Altes Dach"). These basement rocks are discordantly overlain by Permo-Triassic (Wustkogel Formation, meta-arkose and meta-sandstone) to presumably

Cretaceous metasediments (graphitic phyllites, named the Wörth Unit by W. Frank, personal communication August 16, 2017). The Venediger nappe system lies structurally below the Eclogite Zone and Modereck nappe system, which represent the most distal part of the former European margin (Kurz et al., 1998; Schmid et al., 2013). In the study area, the Modereck nappe system comprises two nappes: the (lower) Trögereck (Pestal & Hellerschmidt-Alber, 2011; after Exner, 1964) and (upper) Rote Wand nappes. The latter is sometimes referred to as the Seidlwinkl Nappe (Pestal & Hellerschmidt-Alber, 2011) or Rote Wand-Modereck Nappe (Kurz et al., 1998), but we avoid this double name and simply use the term Rote Wand Nappe to prevent any further confusion with the Seidlwinkl fold nappe (above) and Seidlwinkl Formation (below). The Rote Wand Nappe comprises a lamella of gneiss and micaschist overlain by a complete stratigraphic sequence typical of the European continental margin (Kurz et al., 1998). The base of this sequence is Permo-Triassic meta-arkose (Wustkogel Formation, Pestal, 2008) overlain by mid-Triassic lagoonal carbonates and evaporites (Seidlwinkl Formation) and upper Triassic terrestrial pelites and quartzites (Piffkar and Schwarzkopf formations, Pestal, 2008). The stratigraphy of the Rote Wand Nappe is topped by graphite-bearing carbonatic schist and quartzite of the Brennkogel Formation (Frasl & Frank, 1966) of presumably lower Cretaceous age (Schmid et al., 2013). These rocks are interpreted to have been deposited on a distal part of the European margin and were laterally transitional to the "Bündnerschiefer" calc-schists of the adjacent Alpine Tethys (Schmid et al., 2013). The Trögereck Nappe consists of a less well-stratified succession of similar rocks (granitic gneiss, arkosic gneiss, Bündnerschiefer-type calcschist, and marble; Pestal & Hellerschmidt-Alber, 2011) and also lenses of metabasite (exposed, e. g., in the area of the Hinteres Modereck summit; see Appendix F) and may well represent a former syn-rift sedimentary sequence at the European continental margin. In our view, its lithological assemblage is akin to that of the Eclogite Zone further in the west, at the southern rim of the Tauern Window. As a working hypothesis, we therefore consider these two tectonic units to be lateral equivalents.

In most of the Tauern Window, the Glockner nappe system lies on top of the Modereck nappe system. The Glockner nappe system consists of serpentinite bodies at its base overlain by large volumes of calcareous micaschist (Bündnerschiefer) and layers of metabasite (prasinite and relict eclogite) derived from the northern part of Alpine Tethys. Our observations support the proposal by Pestal & Hellerschmidt-Alber (2011) that the Glockner nappe system comprises two nappes: a lower one with eclogite-facies parageneses (Glockner Nappe s. str.) and an upper one with blueschist-facies to greenschist-facies parageneses (Rauris Nappe). The Glockner nappe system is overlain by the Matrei Zone comprising rocks that originate from the older (Jurassic) and originally more southern Piemont part of Alpine Tethys (Handy et al., 2010). We note that the contact between the Rauris part of the Glockner nappe system and the overlying Matrei Zone is often gradational (e. g., Frisch et al., 1987), rendering a clear delineation of the thrust contact between these units difficult. However, they can nevertheless be distinguished where olistoliths or tectonic slivers of Austroalpine rocks are present, which is diagnostic of the Matrei Zone near the originally adjacent distal Adriatic margin (e. g., Frisch et al., 1987). The Matrei Zone is in turn overlain by Austroalpine units.

3.4 Structures

In this section, we describe the microscale to outcrop-scale structures and their orientations, as well as their relationship to crustal-scale structures as shown in a new tectonic map (Figure 3.2), a lithological map (Figure 3.3, Appendix F), and a series of cross sections (Figure 3.3). The appendix provides higher resolution versions of the map (Appendix F), the sections (Appendix G), underlying data, information on sources, map compilation, and cross-section construction (Appendix A.1).

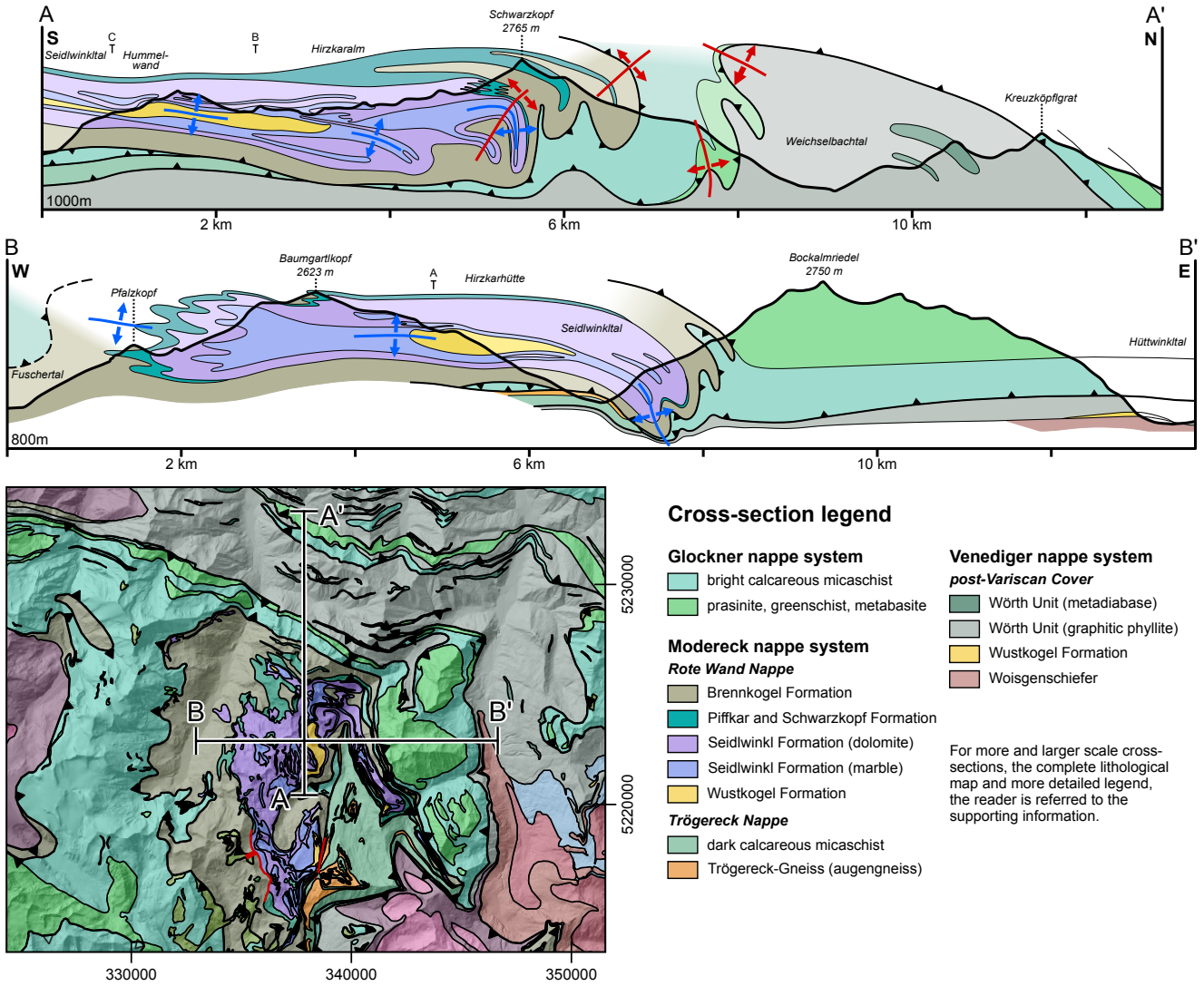

Figure 3.3: Exemplary cross sections through the nose of the isoclinal, recumbent Seidlwinkl sheath fold. Profile A-A' is parallel, and profile B-B' is perpendicular to the nappe transport direction. Note that the fold closes to the north, west, and east. More sections are found in Appendix G.

Structures and their kinematics in the central part of the Tauern Window are directly related to the D1 to D5 regional deformation phases outlined above and previously defined by Kurz et al. (2008) and Schmid et al. (2013) based on their interpretation of map-scale structures.

D1 is marked by the thrust of the Austroalpine nappes onto the oceanic Matrei Zone. D2 is represented by two subduction-related thrusts: (1) the originally intraoceanic thrust of the Matrei Zone (southern part of Alpine Tethys) onto the Glockner nappe system (northern part of Alpine Tethys) and (2) the thrust of the Glockner nappe system onto the Modereck nappe system (distal European margin). This later thrust therefore marks the onset of continental subduction. Additionally, we consider the fault between the Rauris Nappe and the Glockner Nappe s. str. as a D2 thrust along which the Glockner Nappe s. str. was subducted.

On the outcrop scale, D2 in the Glockner and Rote Wand nappes is marked by a relict schistosity, S2, defined by HP mineral parageneses. S2 is parallel to the older compositional layering that we interpret as the original bedding. Both of these foliations are parallel to the D2 thrusts (Figure 3.3).

S2 is preserved in the hinges of D3 isoclinal folds (Figure 3.4a) and in garnet inclusions, for example, lawsonite pseudomorphs and glaucophane (Figure 3.4c).

D3 structures predominate in the study area, more than in any other part of the Tauern Window where D4 and D5 deformations completely transpose older structures. The most obvious D3 structure is the spectacular F3 Seidlwinkl fold nappe, which isoclinally folds the D2 thrust separating the Glockner and Rote Wand nappes, with the latter forming the core of the fold. Its axial plane foliation, S3, is the main foliation in the area. The fold has an arcuate axial trace in map view (Figure 3.2) that is diagnostic of sheath folds (Cobbold & Quinquis, 1980). Indeed, our cross sections confirm this geometry: The D3 sheath fold roots in the south (Appendix G, profile H) and closes toward east and west (Figure 3.3, profile B; Appendix G, profiles B–G) as well as to the north (Figure 3.3, profile A; Appendix G, profile A), which results in a typical sheath fold geometry (Figure 3.4d) and is also consistent with the observed kinematics and microstructural features (see below). We note that these features augment the initial description of the Seidlwinkl Fold by Frank (1969). The fold was first geometrically modeled as a sheath fold by Hilty (2013) without any actual kinematic information to prove its origin as such. Along the lower limb of the Seidlwinkl fold nappe, the tectonostratigraphy is inverted, with the Rote Wand Nappe overlying the Glockner Nappe. The upper boundary of the sheath fold is taken to be the hanging wall of the D2 thrust between the Glockner Nappe s. str. (below) and the Rauris Nappe (above), because this thrust is not affected by D3 folding on the map scale. The Rauris Nappe does not occur in the lower limb of the Seidlwinkl sheath fold, and the Glockner Nappe is only exposed as far north as the steepened southern limb of the D4 Wörth antiform (Figure 3.4d and below). Thus, sheath folding affected only the Rote Wand Nappe and the Glockner Nappe s. str. but not the Rauris Nappe.

Axes of F3 parasitic isoclinal folds with amplitudes on the centimeter to meter scale generally trend N-S in most parts of the Seidlwinkl sheath fold. These minor folds deform lithological boundaries within the nappe as well as the D2 thrust between the Glockner Nappe and Rote Wand Nappe (e. g., Figure 3.3; Appendix G, profiles B–D) and include sheath folds (Figure 3.4b; Kurz et al., 1996). The opening angles of these F3 parasitic folds increase slightly from the core toward the perimeter of the Seidlwinkl fold nappe. In the limbs of these F3 folds, S2 and S3 form a composite S2-S3 foliation; S2 and S3 can only be distinguished in the hinges of F3 folds where S2 is tightly to isoclinally folded. A relict S2 is locally preserved as inclusions in garnet (Figure 3.4c); at garnet rims, this internal foliation is usually truncated by the S3 foliation in the matrix, as previously mentioned. Strain shadows near garnet porphyroblasts normally have a sigmoidal shape and consist of chlorite-quartz-phengite aggregates that are concordant with the S3 schistosity in the adjacent matrix (Figure 3.5). The microstructural observations above indicate that garnet growth initiated during late D2 and ceased before or during an early stage of D3.

A pronounced mineral stretching lineation, L3, is developed parallel to the F3 axes. L3 is defined by a shape-preferred orientation (SPO) of quartz, white mica, feldspar, calcite, or dolomite, depending on the lithology. L3 plunges variably, ranging from moderately S-plunging in the S, to flat-lying in the central part, to steeply N-plunging in the north.

Pervasive D3 shear sense indicators (e. g., shear bands, clasts, and crystallographic preferred orientation of quartz; Figure 3.6a and Appendix D) yield top-N (i. e., top-to-the-foreland) motion in the entire Seidlwinkl sheath fold including the Glockner Nappe s. str., which is consistent with previous findings by Kurz et al. (1996). In the south of the study area, where the top of the fold is exposed (i. e., near the contact of the Glockner Nappe to the overlying Rauris Nappe), we observed sigma clasts (Figure 3.6b) and shear bands that locally overprint the pervasive top-N fabric. These have variable orientations but with predominant top-S (i. e., top-to-the-hinterland) sense of shear with a strong coaxial (flattening) component. In two localities (UTM 33N 330057 5214408 and 329117 5215107), we observed mutually overprinting ductile top-N and top-S shear bands, suggesting that both shear zones were at least partly

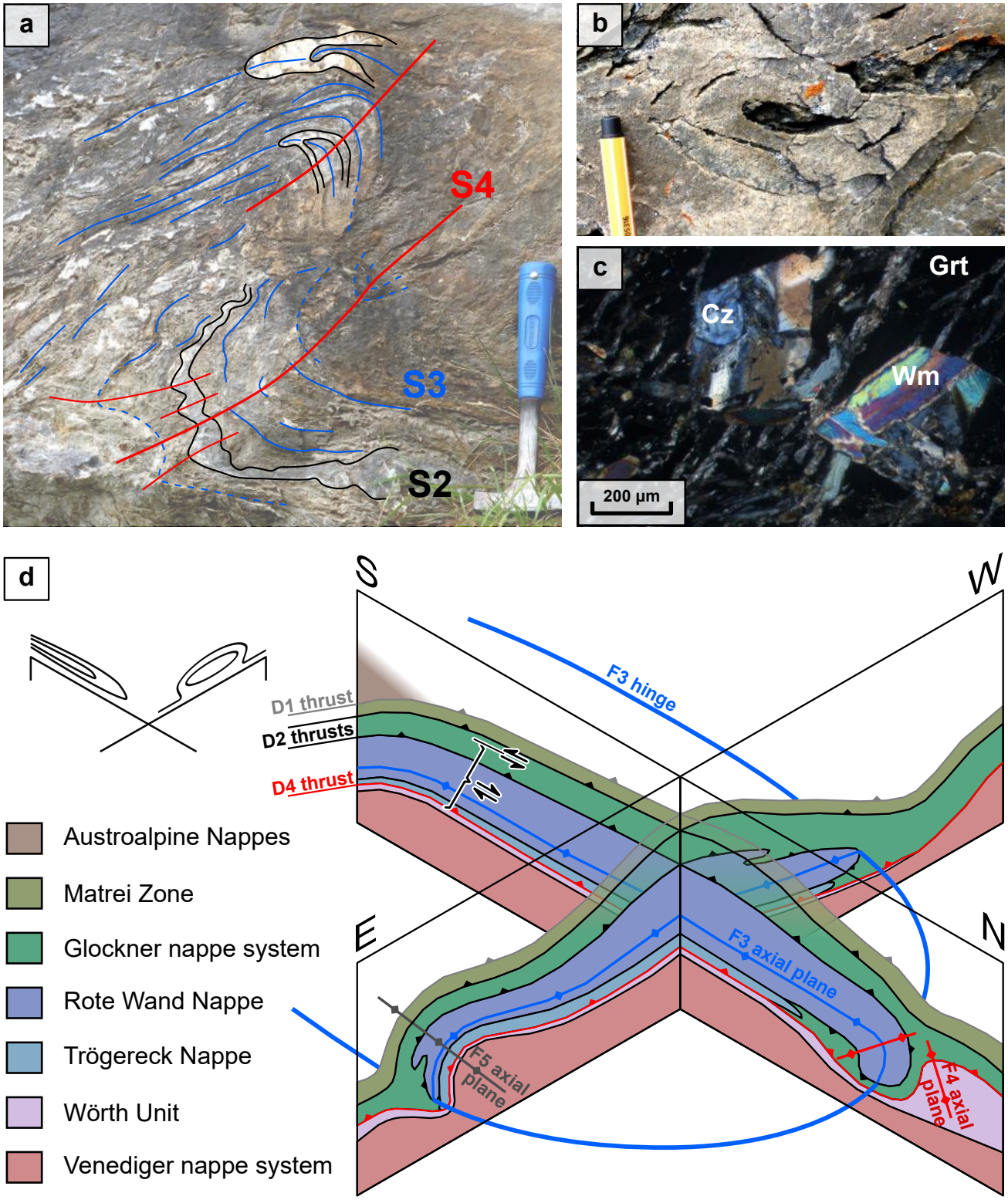

Figure 3.4: Structures of the Seidlwinkl sheath fold: (a) outcrop with cross-cutting relationships of D2, D3, and D4 structures; (b) sheath fold in quartzite with diagnostic eye-shaped pattern of concentrically folded layers in a section roughly perpendicular to the stretching lineation L3 marking the inferred transport direction; (c) microphotograph (crossed polarizers) of pseudomorphs of clinozoisite (Cz) and white mica (Wm) after lawsonite within garnet (Grt) from a garnet micaschist. Similar pseudomorphs also contain chlorite and albite (not shown here). The garnet also contains inclusions of chloritoid, rutile, and tourmaline; (d) block diagram of the Seidlwinkl sheath fold. Note that the D2 thrust is isoclinally folded by F3, which has a strongly curved hinge line. The fold has a concentric eye-shaped pattern and becomes omega-shaped toward its outer parts.

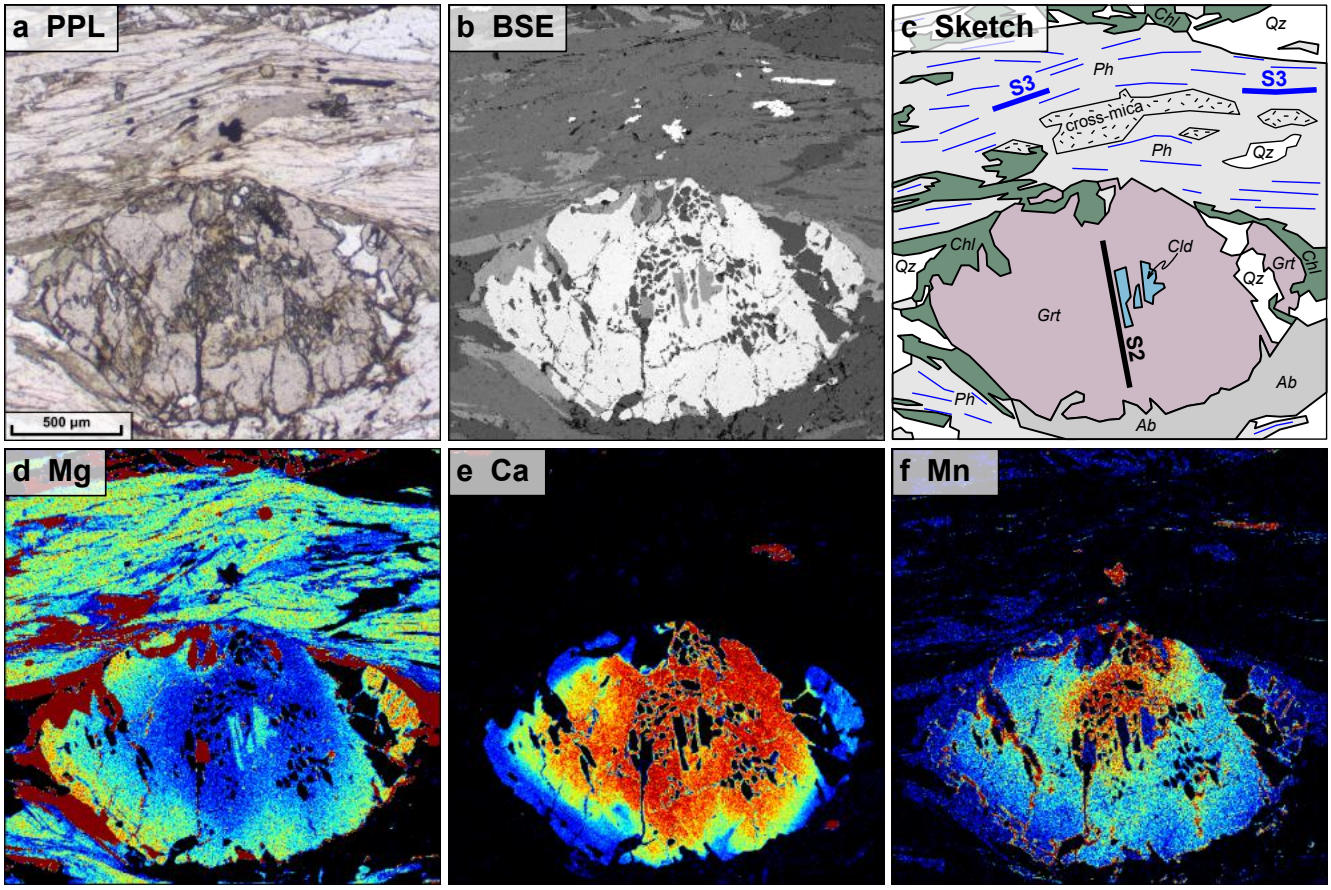

Figure 3.5: Microstructure of a garnet and adjacent areas in garnet micaschist of the Brennkogel Formation, sample PG89. (a) Transmitted light microphotograph with parallel polarizers; (b) backscatter electron image of the same grain; (c) sketch of the same area, showing the distribution of mineral phases and the two schistosities, S2 (Cld-SPO in Grt core) and S3 (main schistosity in matrix). Images (d) to (f) are element distribution maps for Mg, Ca, and Mn obtained with the electron microprobe, respectively. Color scale ranges from very low elemental abundance (black), intermediate abundance (light green), to very high abundance (dark red).

contemporaneous, making the top-S shear zone a syn-D3 to post-D3 structure. Often, a brittle component of motion can be observed on the top-S shear bands, showing late reworking of the originally ductile fault or progressive cooling during continuous top-hinterland shearing. More examples of shear sense indicators on the outcrop-scale and microscale are found in Figures D.1 and D.2 in Appendix D.

Primarily, in the nose of the Seidlwinkl sheath fold, D3 folds are deformed by E-W to SE-NW trending, open to tight F4 folds with a moderately N-dipping S4 axial plane cleavage (Figure 3.2a). This domain of steepened D3 structures occupies the southern limb of the D4 Wörth antiform (Figure 3.3, profile A; Appendix G, profile A), which was first recognized and named by W. Frank (personal communication). F4 fold axes plunge moderately to the W to NW. The Wörth antiform affects the parautochthonous cover of the Venediger basement and lies directly north of the steepened front of the Seidlwinkl fold nappe (Figure 3.3, profile A; Appendix G, profile A). In the hinge zone of the Wörth antiform and north thereof, the Venediger nappes are overthrusted by the Glockner nappe system. This thrust is interpreted as a late D3 to D4 thrust that emplaced the Rauris part of the Glockner nappe system onto the European margin represented by the Venediger nappe complex. The interference of D3 and D4 structures in this region causes meter-scale to kilometer-scale repetitions of lithologies and of the late D3 thrust between the Wörth Unit and the Glockner Nappe s. str.

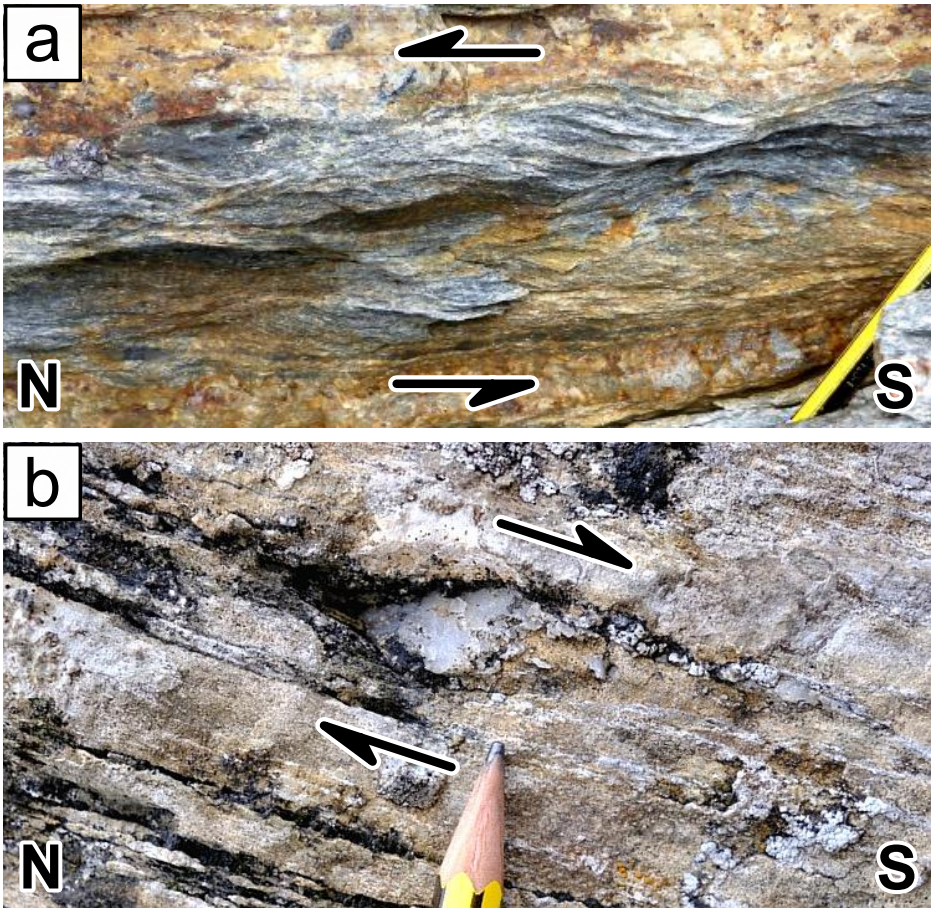

Figure 3.6: Exemplary shear sense indicators in the Seidlwinkl sheath fold. (a) Top-N shear bands to the main schistosity in micaschist (UTM 33N 342182 5208710). (b) Quartz sigma clast in marble indicating top-S sense of shear (UTM 33N 330380 5213630). More examples of shear sense indicators are found in Appendix D.

The largest D5 structures in the study area, the Sonnblick Dome and Mallnitz Synform (Appendix F), deform the Seidlwinkl fold nappe and the main S2-S3 schistosity with its L3 stretching lineation (L3), so that the eastern part of the Seidlwinkl Fold is folded and stretched parallel to the NW-plunging L5 lineation (Favaro et al., 2017; Scharf et al., 2013a; Figure 3.2e).

The age of deformation phases D2 to D5 is bracketed roughly by an 40Ar/39Ar phengite age from the Rote Wand Nappe that is interpreted to be the age of HP metamorphism at 39 Ma (Kurz et al., 2008) and by the onset of Adriatic indentation at ca. 21–23 Ma (Scharf et al., 2013a).

3.5 Metamorphic Record in Metasediments

Microstructures allow us to determine the timing of mineral growth with respect to D3 deformation and formation of the Seidlwinkl sheath fold. In particular, the S3 schistosity is an excellent marker on which to apply pre-, syn-, and post-kinematic growth criteria in order to characterize the tectonometamorphic evolution and establish the physical conditions of nappe emplacement and folding. Pressure (P) and temperature (T) estimates were obtained by applying thermodynamic modeling of phase diagrams and Si-in-phengite isopleths as well as Raman spectroscopy on quartz inclusions (RSQI barometry;

Ashley et al., 2014) and carbonaceous material (RSCM thermometry; calibration of Lünsdorf et al., 2017), methods that were shown to be suitable for our purpose (e. g., Bayet et al., 2018). We used a variety of lithologies including garnet micaschist (early Cretaceous Brennkogel Formation of the Rote Wand and Trögereck nappes and "Bündnerschiefer" of the Glockner Nappe) and chloritoid-bearing micaschist (late Triassic Piffkar Formation) of the Rote Wand Nappe. The Mesozoic age of the protoliths guarantees that the P-T conditions pertain to the Alpine orogeny rather than Variscan and older events, while their microstructures record D3 kinematics. Readers are referred to Appendix A for descriptions of the methods and procedures for obtaining P-T estimates from selected samples.

3.5.1 Microstructures and Parageneses

Garnet micaschists contain quartz, phengite, and chlorite, with albite, carbonate minerals, (clino-)-zoisite, epidote, paragonite, rutile, and titanite abundant but not ubiquitous, depending on bulk rock composition. Garnets often have inclusions of chloritoid and pseudomorphs after lawsonite (Figure 3.4c) that contain clinozoisite, paragonite, chlorite, and albite.

The garnets (Figure 3.5) commonly show prograde growth zoning, with Mn and Ca decreasing and Mg increasing from core to rim. Sometimes, a complex patchy enrichment in Ca can be observed in the outermost rims, which points toward late reequilibration or breakdown of Ca-bearing phases in the matrix (lawsonite?). The garnet grains are often strongly resorbed or replaced by newly grown chlorite.

In garnet micaschists, phengitic white mica is one of the main phases defining the main S2-S3 composite schistosity in the matrix but occasionally also occurs as cross micas oblique to this main foliation. The cores of grains from both phengite generations commonly are rich in Si with up to 3.47 Si p.f.u., whereas, along cleavage fractures and grain boundaries, the grains are locally replaced by mica with lower phengite content (down to ca. 3.05 Si p.f.u.). Consequently, each sample displays a broad range of mica compositions, from highly phengitic to almost purely muscovitic (Figure 3.7). This exchange is mainly controlled by Tschermak substitution; pyrophyllite substitution usually has a minor effect (K+Na always $>$0.85 p.f.u.).

The chloritoid micaschists contain quartz, phengitic white mica, chloritoid, ilmenite — occasionally with rutile in the core — and accessory allanite. These mineral phases usually have a strong shape-preferred orientation and thus define the main S2-S3 composite schistosity. Chlorite is relatively abundant, and kyanite-bearing varieties can be found as well; carbonate minerals and feldspar are lacking completely.

In chloritoid micaschists, white mica has a variable composition that ranges from phengite-rich mica (up to 3.33 Si p.f.u.) to muscovitic white mica. Samples that allow to discriminate S2-parallel mica from S3-parallel mica, for example, in F3 hinges where S2 and S3 are not parallel (Figure 3.7), revealed that micas from both generations show the same compositional variation between high and low phengite content. This may be caused by partial overprint of both mica generations, which also in this lithology is mainly controlled by Tschermak substitution; pyrophyllite substitution usually has a minor effect (K+Na always $>$0.85 p.f.u.). Chloritoid is relatively Fe rich, with Fe# (=Fe/(Fe+Mg+Mn)) ca. 0.80−0.95.

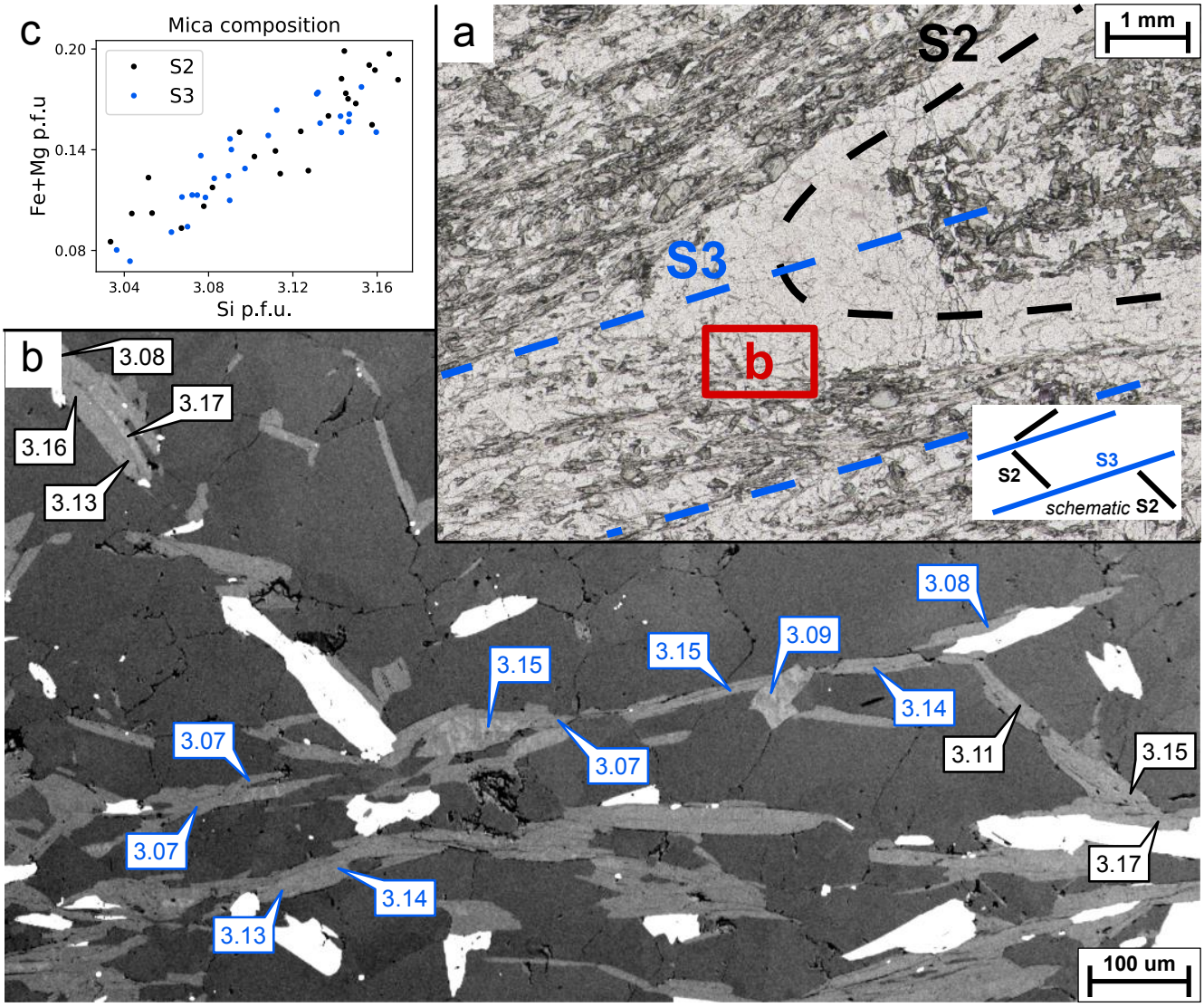

Figure 3.7: Compositional variation of white mica in sample PG130 (chloritoid-bearing micaschist of the Piffkar Formation, UTM Zone 33N: 335018 E, 5219912 N). (a) Thin section image of a fold hinge including sketch of the structural relationships; (b) backscatter electron (BSE) image of a part of the hinge region (red square in (a)), with Si (p.f.u.) content of phengite crystals from two microstructural generations S2 (black) and S3 (blue); (c) composition diagram for all mica analyses in this sample shows that both microstructural generations of white mica have the same range in phengite content.

3.5.2 Constructing a P-T-d Path for the Seidlwinkl Nappe

Microstructural analysis combined with thermodynamic modeling, RSQI, and Si-in-phengite barometry (methodology in Appendix A) allows us to derive a pressure-temperature-deformation (P-T-d) path for selected samples (detailed description in Appendix B). In sample PG89 (Figure 3.8a), peak-P conditions of ca. 1.95 GPa at 520 °C are indicated by the peak assemblage chloritoid and high-Si phengite that grew shortly after the onset of garnet formation. Max-P quartz inclusions in garnet support this interpretation, yielding ca. 1.9 GPa as a pressure minimum during crystallization of garnet. At these conditions, the model predicts the stability of glaucophane and lawsonite, which were not found in the sample. However, the fact that the predicted modal abundance is very low (ca. 1%) and that they may have been completely consumed by retrograde reactions may explain the slight discrepancy between

model and observation. The peak-P event was associated with the development of the S2 schistosity defined as aligned chloritoid inclusions in garnet. The disappearance of chloritoid from the matrix, the beginning of garnet replacement by new chlorite, and the partial replacement of high-Si by low-Si phengite along grain boundaries and cleavage fractures (Figure 3.5) all indicate near-isothermal decompression to P-T conditions below the stability field of chloritoid at around 0.9 GPa and 500 °C. The paragenesis formed during early decompression defines the S3 main foliation. The maximum temperature is limited by the RSCM estimate to ca. 520±30 °C. Retrograde metamorphism was accompanied by the development of the main S3 schistosity defined by the parallel alignment of phengite, chlorite, and quartz.

Sample PG61 shows a similar metamorphic evolution (Figure 3.8b). The thermodynamic model reproduces the observed peak-P mineral assemblage quartz, phengite, chloritoid, chlorite, garnet, and rutile in a well-defined stability field (1.5–1.85 GPa, 500–530 °C). The isopleths of measured maximum Si-in-phengite (max = 3.33 Si p.f.u.) intersect with the peak-assemblage stability field, further constraining peak-P conditions to at least ca. 1.6 GPa and 520 °C for equilibration of the high-Si phengite in the presence of chloritoid, chlorite, and garnet. Isothermal decompression to <1.5 GPa and 530 °C is documented by the incomplete replacement of high-Si by low-Si phengite, the breakdown of rutile to ilmenite (+geikielite), and the almost complete replacement of garnet by post-kinematic chloritoid.

Several aspects complicate straightforward thermodynamic modeling of complete P-T paths in most samples. These problematic aspects are, for example, fractionation of the bulk chemistry due to high garnet contents, pronounced kinetic effects leading to local disequilibria (e. g., metastable feldspar at HP conditions), high contents of ferric iron-rich minerals (epidote), and unclear effect of CO2 activity in lithologies rich in organic carbon and carbonate minerals. Even though it may be possible to resolve these complications with sophisticated and elaborate thermodynamic modeling, we applied a simplified approach to efficiently get rough estimates for peak-P conditions. Given that constructed P-T paths (samples PG89 and PG61) show that (1) garnet formed close to peak-P conditions, (2) decompression was largely isothermal, and (3) no late thermal event exceeded the temperatures reached at peak P, we interpret the RSCM data to represent the T conditions close to peak P. Therefore, for most samples, we estimated the peak-P conditions by using the intersection of the RSCM temperature with either the RSQI pressure or Si-in-phengite isopleth. This procedure was performed on a suite of metasediment samples from the Glockner and Modereck nappe systems covering the whole study area. We consider the precision of peak-P values obtained by this procedure to be sufficient for our purpose of documenting the extent of HP metamorphism in the central Tauern Window. The maximum-burial P-T data for all samples are listed in Table E.1 in Appendix E.

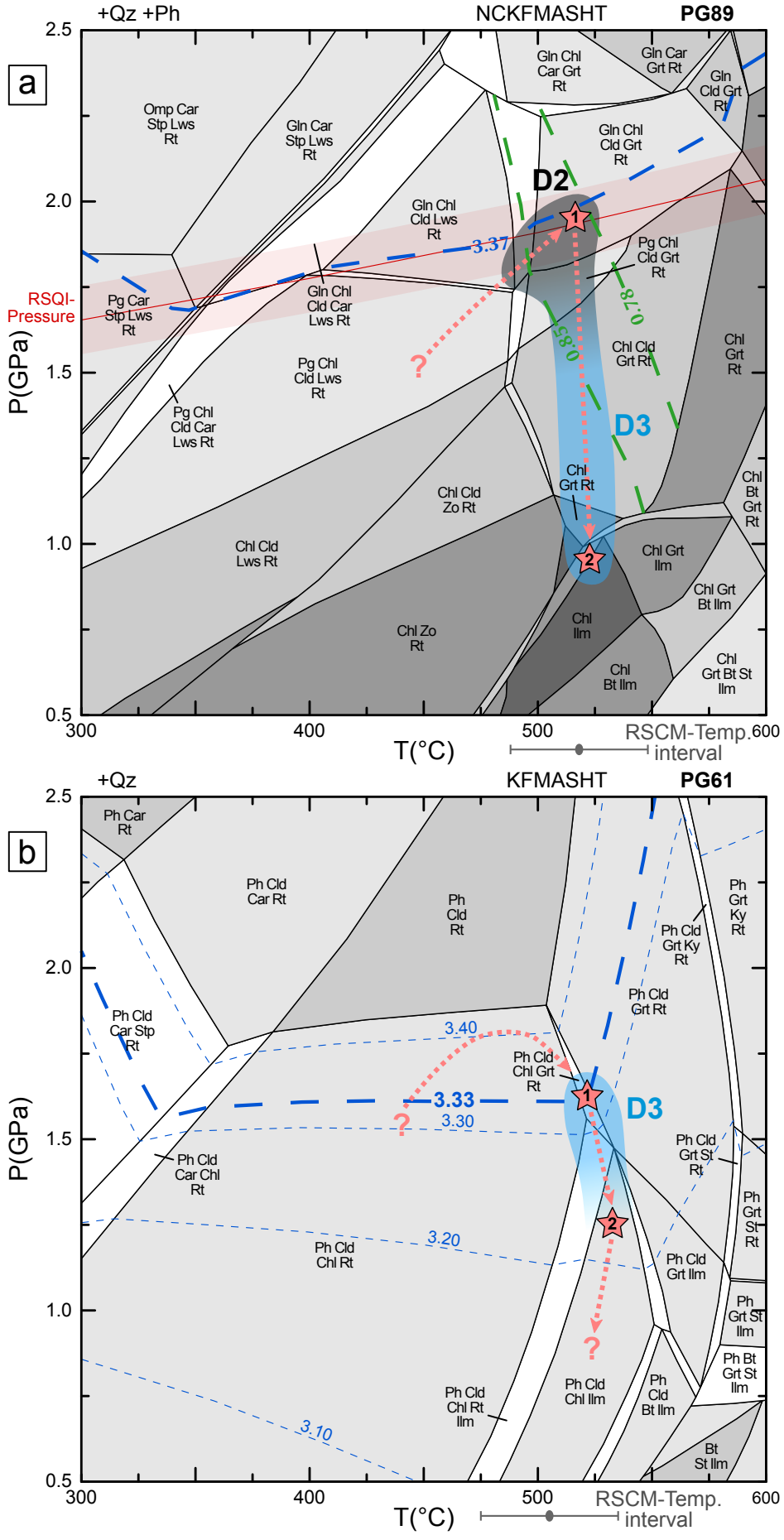
a
+Qz +Ph
NCKFMASHT
PG89
Omp Car Stp Lws Rt
Gln Car Stp Lws Rt
Gln Chl Car Grt Rt
Gln Car Grt Rt
Gln Cld Grt Rt
Gln Chl Cld Grt Rt
Gln Chl Cld Lws Rt
D2
3.37
Pg Chl Cld Grt Rt
RSQI-Pressure
Pg Car Stp Lws Rt
Gln Chl Cld Car Lws Rt
0.78
0.85
Pg Chl Cld Lws Rt
Chl Cld Grt Rt
Chl Grt Rt
D3
Pg Chl Cld Car Lws Rt
Chl Cld Zo Rt
Chl Cld Lws Rt
Chl Grt Ilm
Chl Grt Bt Ilm
Chl Zo Rt
Chl Ilm
Chl Bt Ilm
Chl Grt Bt St Ilm
P(GPa)
T(°C)
RSCM-Temp. interval
b
+Qz
KFMASHT
PG61
Ph Car Rt
Ph Cld Car Rt
Ph Cld Rt
Ph Grt Ky Rt
Ph Cld Grt Ky Rt
Ph Cld Grt Rt
Ph Cld Car Stp Rt
3.40
Ph Cld Chl Grt Rt
3.33
3.30
D3
Ph Cld Grt St Rt
Ph Cld Car Chl Rt
Ph Grt St Rt
3.20
Ph Cld Chl Rt
Ph Cld Grt Ilm
Ph Grt St Ilm
Ph Bt Grt St Ilm
Ph Cld Chl Rt Ilm
Ph Cld Chl Ilm
Ph Cld Bt Ilm
3.10
Bt St Ilm
P(GPa)
T(°C)
RSCM-Temp. interval

Figure 3.8 ***(previous page)*****:** Pseudosections of sample PG89 (a) and PG61 (b) with inferred P-T path (dotted arrows). Dashed lines denote measured (thick) and calculated (thin) compositional isopleths for Si in phengite (blue, in a.p.f.u.) and XFe in chloritoid (green). Red solid line indicates the measured maximum pressure as a function of T as determined from RSQI, with the shaded red area indicating the uncertainty in the P estimate. Gray bracket denotes the measured RSCM temperature with its absolute uncertainty of ±30 ℃. The black and/or blue shaded area shows the range of conditions during and after the D2 and D3 deformation. Red stars represent two distinct metamorphic stages. (a) PG89 stage 1: formation of peak-P mineral assemblage Grt, Cld, and high-Si phengite during regional D2 at ca. 520 ℃ and 1.95 GPa. Stage 2: near-isothermal decompression to <1.0 GPa (destabilization of Grt, Cld, and high-Si phengite). The model system composition is 80.51 SiO_2, 7.58 Al_2O_3, 5.00 FeO, 1.64 MgO, 0.28 CaO, 1.27 K_2O, 0.10 Na_2O, and 0.32 TIO_2 (all in wt%), with H_2O-saturated conditions. (b) PG61 stage 1: formation of peak-P mineral assemblage Qz, Ph, Cld, Chl, Grt, and Rt during D3 at ca. 520 ℃ and at least 1.6 GPa. Stage 2: near-isothermal decompression during and/or after D3 (decrease of Si content in matrix phengite, breakdown of matrix Rt to Ilm, and replacement of Grt by post-D3 Cld). The blue shaded area denotes the activity of the regional deformation phase D3 with respect to P-T conditions, as recorded in sample PG61. The model system composition is 67.43 SiO_2, 16.13 Al_2O_3, 8.70 FeO, 0.61 MgO, 1.51 K_2O, and 0.85 TIO_2 (all in wt%), with H_2O-saturated conditions.

3.5.3 P-T History of the Metasediments and Peak-P Map of the Central Tauern Window

In many investigated metasediment samples, an early low-T high-P (<500 °C, 1.3–2.0 GPa) phase is evidenced by relict pseudomorphs after lawsonite included in garnet (Figure 3.4c). Peak metamorphic conditions were reached in the garnet stability field. Minimum estimates for peak P are in the range of 1.3–2.3 GPa (Figure 3.9), which confirms the existence of an HP event for all samples investigated. For a majority of samples from both the Glockner and the Modereck nappe systems, the peak-P estimates converge to ca. 1.8–2.2 GPa. Somewhat lower peak P obtained for some of the samples, including PG61, may reflect incomplete preservation of the HP assemblages or Si loss of mica due to strong retrograde overprint or relaxation of quartz inclusions. The peak-P values of 1.8–2.2 GPa are somewhat higher than what is reported for metabasites from the Glockner Nappe (ca. 1.8 GPa, Dachs & Proyer, 2001). The pressures derived from Si content of phengite tend to be somewhat lower than the RSQI pressures (Figure 3.9), and additionally, the S3 main foliation of some samples lacks diagnostic HP mineral phases that are still preserved as inclusions in garnet. Both observations reflect early stages of decompressional overprint of phengite and other matrix minerals during D3 top-foreland directed shear, which is not recorded by Qz inclusions in garnet. Later, stages of isothermal decompression to ca. 1.0 GPa and 500 °C under low-strain conditions caused destabilization of garnet, transformation of rutile to ilmenite, and further partial overprint of phengite to almost pure muscovite.

In the map in Figure 3.10, we show the minimum estimates for peak-P conditions in metasediments. The continental Rote Wand and Trögereck nappes and the structurally lower part of the oceanic Glockner nappe system (Glockner Nappe s. str.) reached similar peak-P conditions of ca. 2.0 GPa. These conditions strongly contrast with those reached in the Venediger nappe system in the footwall where a much lower peak P of around 1 GPa at 530 °C is reported (Selverstone, 1993; Selverstone et al., 1984). The same applies to the Matrei Zone in the hanging wall where a peak P of 1.3–2.0 GPa at 360−370 °C has been inferred (Koller & Pestal, 2003) based on analogy of mineral assemblages and lithology with the Reckner Ophiolite (Dingeldey et al., 1997). However, the exact upper structural limit of eclogite-facies parageneses in the Glockner nappe system is ambiguous and has not been settled prior to

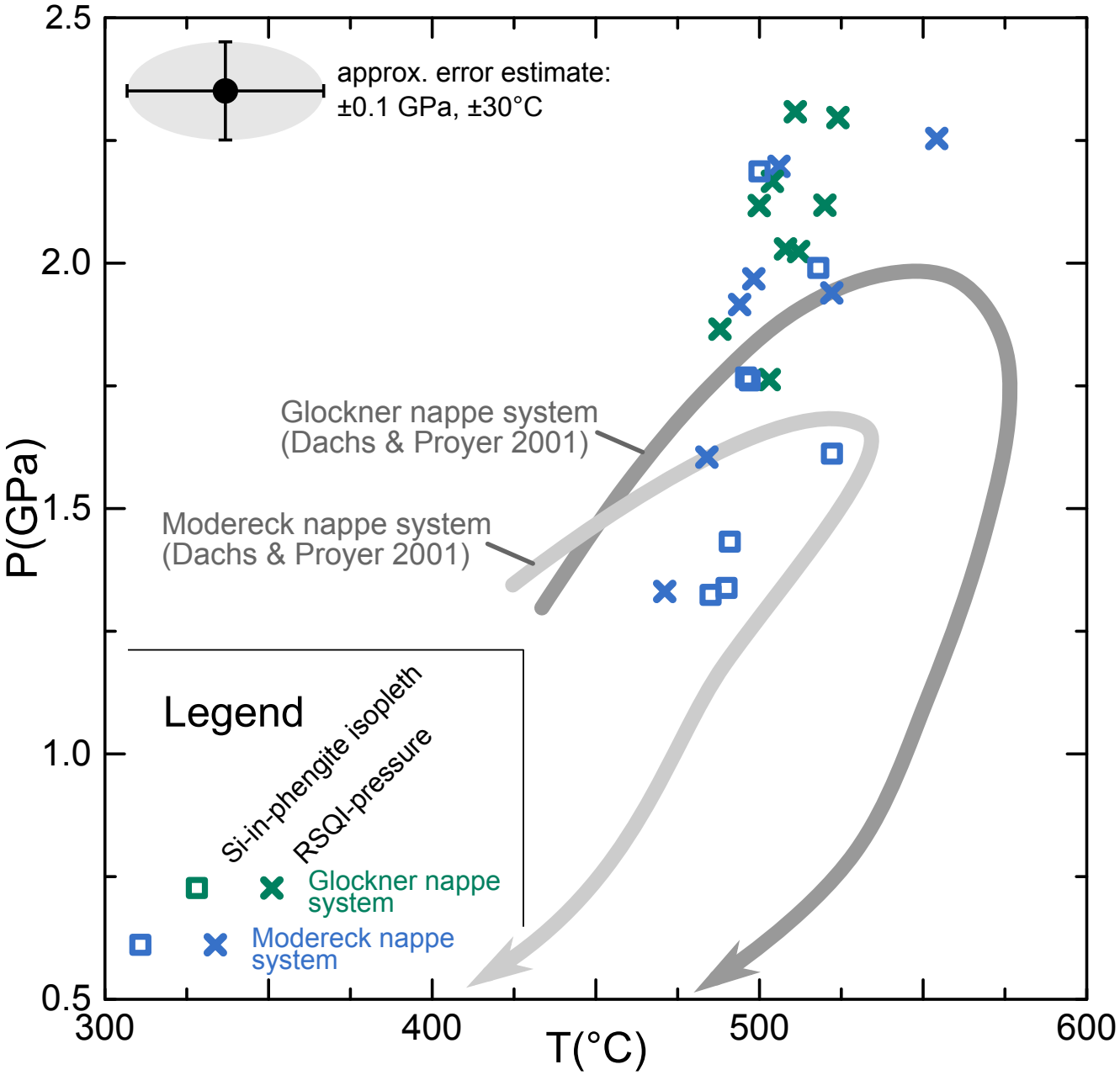

Figure 3.9: Peak-pressure metamorphic conditions obtained for metasediments from the Modereck and Glockner nappe systems using RSQI barometry and Si-in-phengite isopleths. RSQI values are minimum estimates.

this study. Following other authors (Frasl & Frank, 1964; Pestal & Hellerschmidt-Alber, 2011), we subscribe to the idea of a nappe boundary that separates the HP and low-pressure parts of the Glockner nappe system (i. e., between Glockner Nappe s. str. and Rauris Nappe, respectively). In the southern part of our study area, to the best of our knowledge, this nappe boundary has never been mapped before. We place it at the top of a thick prasinite layer that has a well-defined mid-ocean ridge basalt affinity (Höck, 1980) and is laterally largely continuous and can be found north and south of the central Tauern culmination. Structurally below this prasinite body, variegated parageneses contain HP metamorphic minerals with, for example, eclogite relicts in metabasites, lawsonite pseudomorphs in garnet, and two phengites in metasediments (own observations, Cornelius & Clar, 1934; Frank et al.,

1987). In the prasinite body itself lawsonite pseudomorphs were described (Frank et al., 1987); in addition, we found sparse remnants of strongly retrogressed eclogite. In the part of the Glockner nappe system structurally above the prasinite layer, no eclogite-facies parageneses have been found. This upper structural limit of eclogite-facies parageneses in the southern Tauern Window corresponds with the fabric boundary between pervasive top-N D3 shear fabrics below and top-S, syn- to post-D3 fabrics above.

3.6 Discussion

The results above indicate that the Seidlwinkl sheath fold nappe developed under retrograde conditions that involved a near-isothermal drop in pressure from a peak value of approximately 2.0 GPa to a residual pressure of roughly 1.0 GPa. Mylonitic shearing in this part of the Alpine subduction zone was pervasive, with the shear sense uniformly top-N (cf. Kurz et al., 1996), that is, transport direction of the upper, hanging wall limb toward the orogenic foreland. In the following, we address how the inherited geometry of the passive European margin caused sheath nappe folding during subduction and how this nappe fold was exhumed from within the subduction zone.

3.6.1 Formation of the Seidlwinkl Sheath Fold in the Alpine Subduction Zone

As shown in sections 3.3 and 3.4 above, the Seidlwinkl Fold is very non-cylindrical, with its axis curving almost 180° (Figures 3.2 and 3.3d). Yet its Triassic-to-lower Cretaceous cover derived from the former European passive margin survived subduction and collision remarkably intact. In most parts of the fold, this stratigraphic sequence is significantly thinned but only locally boudinaged, particularly the middle-Triassic dolomites. Mylonitic thinning and boudinage of the cover sequence are greater in the fold's lower limb.

The sheath fold does not exist along strike to the east and west in the Tauern Window, where only upward-younging passive-margin stratigraphy of the Modereck nappe system has been mapped around the perimeter of the Venediger nappe system (see, e. g., GK200 Salzburg, Pestal et al., 2005). Either the lower limb of the Seidlwinkl fold nappe was left behind to the south during top-N shearing and thrusting of the detached upper limb (i. e., a fold nappe in the sense of Heim, 1878, 1922), or a lower limb never existed in the eastern and western parts of the Tauern Window. So far, no relicts of an overturned limb have been found in the eastern and western Tauern Window, though we cannot rule out the possibility that such relics exist somewhere below the erosional surface.

This leaves us with the challenge of explaining why the sheath fold developed only in the central Tauern Window. Several mechanisms for the formation of sheath folds have been proposed so far: (a) amplification and/or rotation of a predeformational heterogeneity in the layer(s) during simple shearing (Cobbold & Quinquis, 1980). Possible heterogeneities include local variations in layer thickness or mechanical properties or even a preexisting fold initially oriented oblique to the noncoaxial shearing plane; (b) perturbation of a highly noncoaxial flow field around strong inclusions (Marques & Cobbold, 1995; Rosas et al., 2002); or (c) perturbation near the tip of a planar, weak inclusion in a matrix of stronger, noncoaxially shearing rock (Exner & Dabrowski, 2010; Reber et al., 2012). All of these models involve overall simple shearing and fold amplification near a structural-rheological heterogeneity, but they do not explain how the heterogeneity forms to begin with. Moreover, non-cylindrical nappes can develop where local strain rate varies perpendicular to the slip direction, as shown in studies of

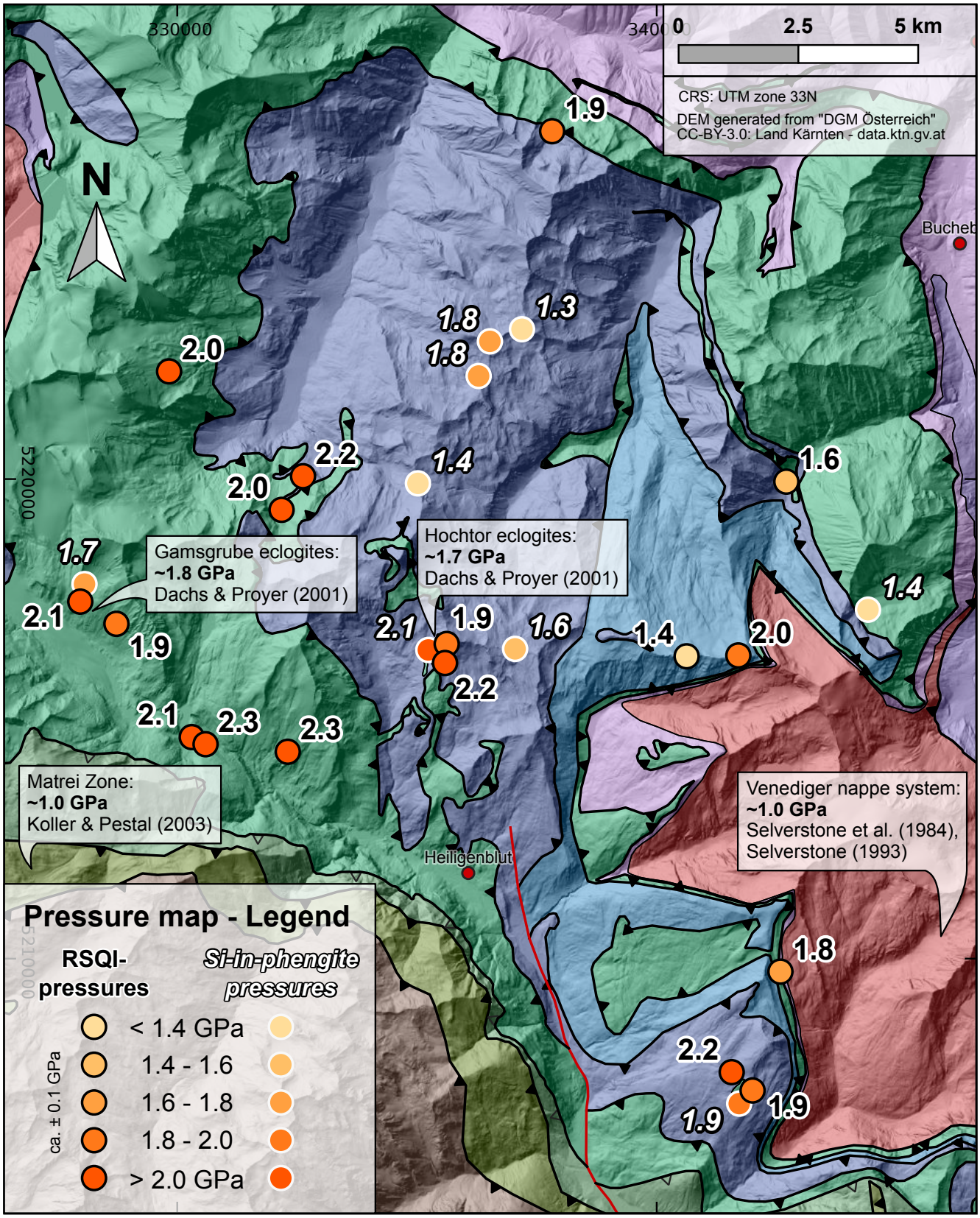

Figure 3.10: Distribution of peak-P estimates in metasediments of the central Tauern Window. RSQI values are minimum estimates. Tectonic units as in Figure 3.2.

sheath folds formed during exhumation (Xypolias & Alsop, 2014) and as proposed for the Adula Nappe in the Central Alps (Kossak-Glowczewski et al., 2017). We cannot rule out the possibility that such gradients contributed to the formation of the Seidlwinkl sheath fold. However, any model for this fold must account for coeval top-foreland shearing in the main body of the fold and top-hinterland flow in its roof. We propose that sheath fold formation ultimately reflects lateral variations in thickness and composition of the rifted European margin. This in turn engendered along-strike differences in detachment level and fold style as the margin obliquely entered the Alpine subduction zone (Figure 3.11). The obliquity of subduction corresponds to the acute angle between the Paleogene NNW-SSE directed Adria-Europe convergence and the structural grain of the European passive margin, which formed during E-W rifting (Kurz et al., 1998) and opening of the northern part of Alpine Tethys (e. g., Frisch, 1979; Handy et al., 2010). In this scenario, the basement (Wustkogel gneiss) and cover of the Rote Wand Nappe in the core of the Seidlwinkl fold nappe originated as a rifted segment of the distal European continental margin (Figure 3.11a). This segment with relatively thick continental basement was separated from the main part of the European continental margin (future Venediger nappe system) by a rift basin with only thin basement (future Eclogite Zone and Trögereck Nappe). In this configuration, the rifted segment (future Rote Wand Nappe) formed a promontory of the margin that later acted as the nucleus for the Seidlwinkl sheath fold. As the passive margin approached the subduction zone, the ocean continent transition was likely a first-order mechanical heterogeneity due to the pronounced viscous strength contrast between thin continental units (mostly continental basement, siliciclastics, prerift platform carbonates, and postrift hemipelagic clastics of the Rote Wand Nappe) and oceanic lithosphere (serpentinized exhumed mantle and overlying mafics and hemipelagic sediments of the Glockner Nappe s. str.). Subduction of a promontory of the distal continental margin formed the composite ocean continent nappe stack, which then detached along the base of the Permian clastics (Wustkogel Formation) as the promontory entered the subduction zone (Figure 3.11b). Thrusting gave way to buckling and the formation of an embryonic Seidlwinkl Fold while the composite nappe stack was still at sufficiently low temperatures to favor high strength contrasts (>5) between the layers of the nappe stack (e. g., Evans & Kohlstedt, 1995; Ramberg, 1964). The fold became tighter with progressive noncoaxial shearing close to peak-pressure conditions at great depth in the subduction channel, where increasing temperature led to a drop in viscous strength contrast. Continued uniform, top-N shearing of all parts of the fold promoted passive amplification of the fold and accentuation of its non-cylindrical sheath geometry (e. g., Dell'Ertole & Schellart, 2013; Marques et al., 2008) shortly after the attainment of peak-pressure conditions (Figure 3.11c). In essence, the formation of the Seidlwinkl sheath fold is the result of lateral variations in the structure of the European continental margin that provided an initial perturbation for nucleation of the fold. Modeling studies show that the width of such an initial perturbation controls the width of the subsequent sheath fold (Brun & Merle, 1988). This seems reasonable in light of our observations: The fold has an E-W width on the order of 20–30 km, which suggests that the width of the promontory — measured parallel to the later subduction zone — had a similar extent (Figure 3.11a). Several tens of kilometres is a common size for extensional allochthons or similar features ("H-blocks" of Péron-Pinvidic & Manatschal, 2010). However, we note that this model for the formation of the Seidlwinkl sheath fold is necessarily speculative in the absence of better preserved relicts. Recently, field-based studies have identified similar, highly non-cylindrical nappes in the Alps (Kossak-Glowczewski et al., 2017; Steck et al., 2019).

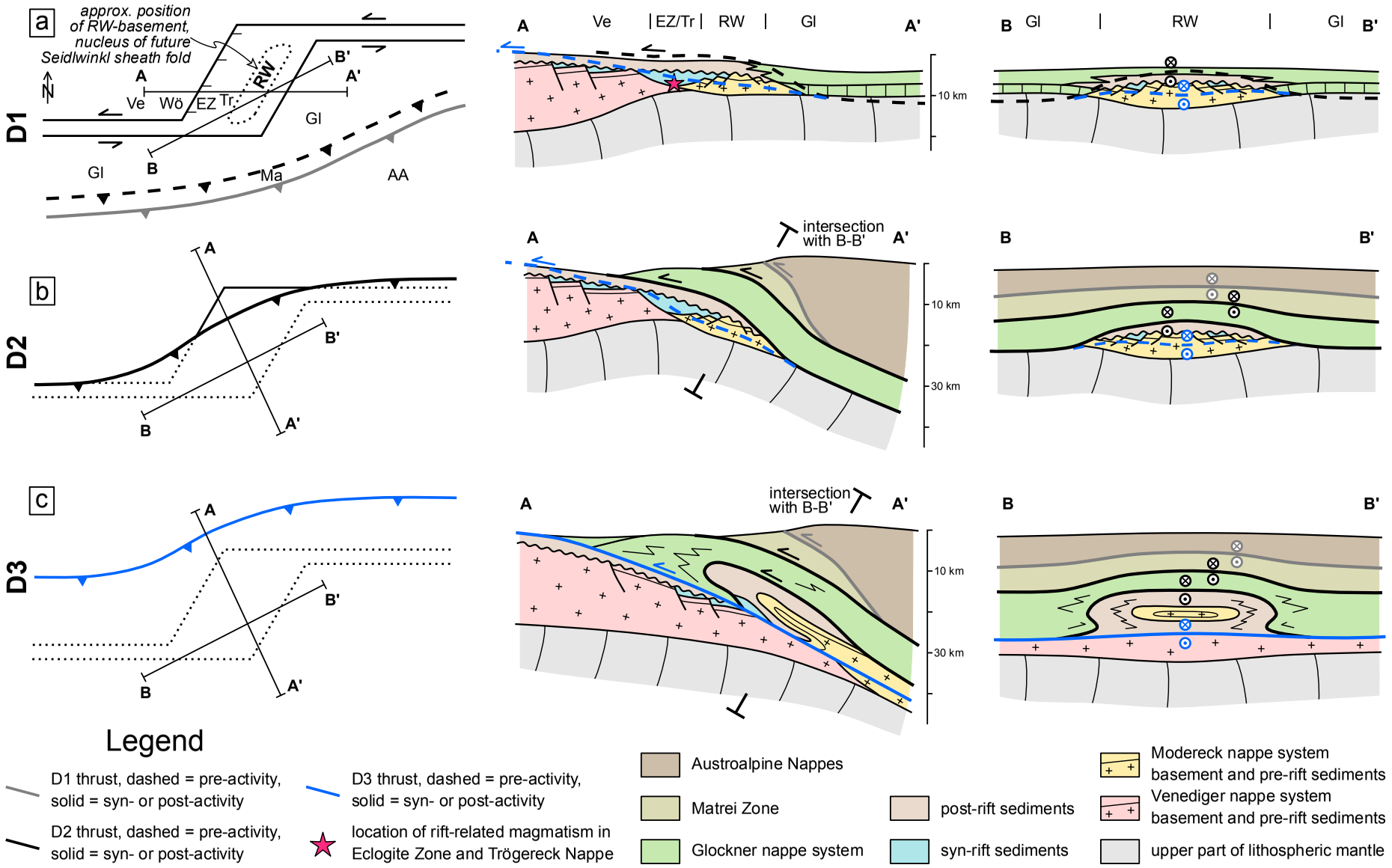
a
approx. position of RW-basement, nucleus of future Seidlwinkl sheath fold
D1
N
A
B
A'
B'
Ve
Wö
EZ
Tr
RW
Gl
Ma
AA
b
D2
c
D3
A
Ve
EZ/Tr
RW
Gl
A'
B
B'
10 km
30 km
intersection with B-B'
Legend
D1 thrust, dashed = pre-activity, solid = syn- or post-activity
D2 thrust, dashed = pre-activity, solid = syn- or post-activity
D3 thrust, dashed = pre-activity, solid = syn- or post-activity
location of rift-related magmatism in Eclogite Zone and Trögereck Nappe
Austroalpine Nappes
Matrei Zone
Glockner nappe system
post-rift sediments
syn-rift sediments
Modereck nappe system basement and pre-rift sediments
Venediger nappe system basement and pre-rift sediments
upper part of lithospheric mantle

Figure 3.11 ***(previous page)*****:** Formation of the Seidlwinkl sheath fold nappe. First column shows the evolving paleogeography in map view (inspired by Weissert & Bernoulli, 1985): (a) D1 convergence and oceanic subduction; (b) D2 prior to the baric peak; and (c) D3 after the baric peak in map view. Second and third columns are schematic cross sections of the margin corresponding to the traces on the maps. (a) Early subduction of Alpine Tethys. The future Rote Wand Nappe originated as a rifted segment of continental basement and cover and was separated from the main part of the margin by a rift basin (future Trögereck Nappe and Eclogite Zone); (b) beginning subduction of the distal European margin. The Rote Wand rift segment was thrust below the Glockner nappe system and further subducted; (c) Glockner and Rote Wand nappes become a composite sheath fold nappe fold in a noncoaxial shear zone. The width of the Rote Wand rift segment (=structural perturbation; sections B-B') dictates the width of the sheath fold. Abbreviations: Ve = Venediger nappe system (European margin), Wö = Wörth Unit, EZ = Eclogite Zone, Tr = Trögereck Nappe, RW = Rote Wand Nappe, Gl = Glockner nappe system, Ma = Matrei Zone, AA = Austroalpine nappes (Adriatic margin). Maps and sections are not drawn to scale; thickness of the units is exaggerated for clarity.

3.6.2 Exhuming the Seidlwinkl Sheath Fold Nappe

Our new data show that imbricated and folded continental crust (Modereck nappe system) and oceanic crust (Glockner Nappe s. str.) experienced identical HP conditions of ca. 2 GPa during Alpine subduction, followed by the incorporation of these units in the Seidlwinkl sheath fold nappe during decompressional metamorphism. They were eventually emplaced to their current position in the nappe stack between other units that experienced lower peak pressures of ca. 1 GPa, that is, in the Matrei Zone and Rauris Nappe above and the Venediger nappes below (Koller & Pestal, 2003; Selverstone, 1993; Selverstone et al., 1984). This 1 GPa difference in peak pressure is consistent with the observation that the HP Seidlwinkl Fold, which underwent pervasive top-N shearing, is bounded in its upper limb by a normal-sense shear zone that at least partly overprinted the lower-P Rauris Nappe. We propose that these shear zones — a thrust below and a normal fault above — were responsible for differential exhumation of the fold with its HP assemblages in the sense of a channel-extrusion model. This exhumation model requires that the two opposite-sense shear zones between which the rocks were exhumed were active simultaneously and that normal-sense shearing started at peak-pressure conditions. Contemporaneity of the opposite-sense shear zones is indicated at the top of the Seidlwinkl Fold by mutually overprinting top-N and top-S shear bands. We therefore interpret this top-S normal-sense shearing to have begun later than the initiation of D2 top-N shearing in the Glockner nappe system but to have been broadly coeval with D3 top-N thrusting in the Seidlwinkl Fold. We regard the parallelism of syn-decompressional, D3 top-N shearing planes in the entire Seidlwinkl Fold with the normal-sense, top-S shearing planes of the Rauris Nappe as a viable kinematic criterion for broadly contemporaneous activity of opposite-sense shearing during exhumation. This also means that the top-S shear zone was active during decompression but does not unequivocally prove that top-S shearing started at peak-pressure conditions, which, however, we consider plausible.

These kinematics raise the question of the forces driving exhumation of the HP Seidlwinkl Fold. Buoyancy forces have been suggested for the exhumation of HP nappes (e. g., Chemenda et al., 1995) in subduction channels. However, this is implausible in the case of the Seidlwinkl fold nappe because the density contrasts between the HP lithologies in this fold nappe (mostly carbonaceous Bündnerschiefer) and the lithologies of underlying and overlying units (marbles and granitoids) are negligible and may even favor negative buoyancy of the HP lithologies. Moreover, it has been argued that exhumation of HP rocks mainly by buoyancy requires large-scale extension of the upper plate driven by slab rollback (e. g., Brun & Faccenna, 2008), which may not have been the case during the final stages of subduction of Alpine Tethys and incipient exhumation of the Seidlwinkl sheath fold.

Another commonly invoked exhumation mechanism for HP rocks is channel extrusion, which involves their exhumation within a subduction channel with parallel or tapered walls. This extrusion is forced by convergence of the walls and/or noncoaxial shearing parallel to the walls (e. g., Escher & Beaumont, 1997; Grujic et al., 1996; Grujic & Mancktelow, 1995; Mancktelow, 1995, 2008; Vannay & Grasemann, 2001). In such models, flow in the channel is driven by a pressure gradient parallel to the channel that is related to the variable rates of convergence and shearing, respectively, across and along the channel. The walls of the channel are assumed to be strong compared to the channel. The models usually show exhumation of HP rocks between coeval shear zones with opposite shearing senses, similar to those observed in the Seidlwinkl fold nappe and its roof. Thus, the channel-extrusion model elegantly explains how the Seidlwinkl Fold formed during top-foreland shearing while being exhumed in the footwall of a top-hinterland shear zone.

A consequence of the channel flow model is that the pressure gradient along the channel required to sustain upward flow of the extruding rock inevitably causes a dynamic pressure component in addition to the lithostatic pressure. The combined lithostatic and dynamic pressure in the channel is higher than in the stronger walls. The magnitude of this dynamic pressure component depends on the geometry of the channel (length, thickness, and angle between the confining walls), the strain rate, the channel viscosity, and the viscosity contrast between weak channel and walls (Mancktelow, 1995, 2008). The tectonically induced pressure gradient must be sustained for the duration of exhumation; otherwise, the upward flow of the exhuming material ceases. Mancktelow (2008) calculated dynamic pressures on the order of several hundred MPa for a tapered channel geometry, assumed natural shear displacement rate and viscosity contrasts.

Applying models like this to the Seidlwinkl fold nappe is speculative endeavor because only the top part of the subduction channel is exposed at the surface today; the original channel geometry cannot be restored. This precludes using the approach above to calculate the dynamic pressure and its contribution to pressure recorded by mineral parageneses in the Seidlwinkl sheath fold. The units overlying and underlying the HP-bearing Seidlwinkl fold nappe comprise weak carbonates and calc-schists that could not have acted as strong confining channel walls, suggesting that the component of dynamic pressure was small. However, at greater depth within the channel, the dynamic pressure may have been higher if the adjacent wall rocks (basement?) are assumed to have been more viscous. A parameter study exploring the potential range of conditions at depth is beyond the scope of this study.

Dynamic pressure variations can also be expected near rheological heterogeneities that cause variations in the differential stress. In the case investigated here, pronounced lithological and rheological heterogeneities are not apt to cause pronounced changes in recorded pressures. For example, peak pressures in weak metasediments are very similar to those reported for stronger metabasite lenses and layers (Dachs & Proyer, 2001). If this observation is not caused by sampling bias, it indicates that dynamically induced variations in peak P within the Seidlwinkl sheath fold nappe are probably smaller than the uncertainties of the available pressure estimates.

3.7 Conclusion

We have documented a recumbent, crustal-scale sheath fold in the central Tauern Window. The fold itself is a composite structure, comprising an isoclinally folded thrust of the former Alpine Tethys (Glockner Nappe s. str.) onto the former European continental margin (Rote Wand Nappe). The pervasive foliation in the area is parallel to the axial plane of the fold and carries a N-S oriented stretching lineation with top-N (to foreland) shear indicators. New petrological data show that both the oceanic

and continental nappes experienced identical peak-pressure conditions of roughly 2.0 GPa and 500 °C, followed by isothermal decompression during top-N shearing. These conditions are remarkably higher than the peak-P conditions reported for the tectonic units in the footwall and hanging wall of the sheath fold.

The kinematic observations are compatible with the classical theory of sheath fold formation by passive amplification of a preexisting perturbation under high-strain simple shear deformation (Cobbold & Quinquis, 1980). Based on regional lithostratigraphic correlation, we propose that this initial perturbation was inherited from lateral variations in the structure and stratigraphy of the rifted European margin. A rifted segment of the passive margin — similar to an extensional allochthon as suggested by Kurz (2006) — composed of Rote Wand Nappe basement and cover formed a structural promontory that was passively amplified to a sheath fold geometry with progressive top-foreland directed shearing in the Alpine subduction zone.

The Seidlwinkl sheath fold nappe is bounded at its top by a top-hinterland (top-S) shear zone with a strong component of flattening. This top-hinterland shear zone also generally coincides with the boundary between the eclogite-bearing (Glockner s. str.) and eclogite-free (Rauris) units. The fold itself exhibits intense and pervasive top-foreland (top-N) kinematics. These opposite-sense shear zones accommodated differential exhumation of the HP sheath fold nappe relative to the surrounding low-pressure tectonic units (Rauris Nappe above, Venediger nappe system below) in the sense of channel-extrusion exhumation models, where the weak, exhuming rock body is separated from the units above and below by a normal fault and a thrust, respectively. At greater depths in the subduction channel not accessible to observation, we infer that the exhuming sheath fold nappe may have been surrounded by stronger wall rocks and therefore have experienced a nonlithostatic pressure gradient driving its exhumation (Mancktelow, 2008).

This study highlights how features inherited from passive margins may dictate the geometry of nappes formed during accretion and subduction of continental margins. In comparable settings, the lateral variability of margins will strongly affect the internal configuration of subduction zones and collisional orogens like the Alps or Himalayas. Orogen-scale two-dimensional cross sections or seismological profiles do not fully account for such lateral heterogeneity and might therefore misleadingly imply a higher degree of cylindricity than in nature.

Chapter 4

Evolving Temperature Field in a Fossil Subduction Channel During the Transition from Subduction to Collision (Tauern Window, Eastern Alps)

This chapter was published as:
Groß, P., Pleuger, J., Handy, M. R., Germer, M. & John, T. (2020d). "Evolving temperature field in a fossil subduction channel during the transition from subduction to collision (Tauern Window, Eastern Alps)". In: *Journal of Metamorphic Geology*. DOI: https://doi.org/10.1111/jmg.12572.

4.1 Abstract

We investigate the evolution of the three-dimensional thermal structure of a paleo-subduction channel exposed in the Penninic units of the central Tauern Window (Eastern Alps). Structural and petrological observations reveal a sheath fold with an amplitude of some 20 km that formed under high-pressure conditions (ca. 2 GPa). The fold is a composite structure that isoclinally folded the thrust of an ophiolitic nappe derived from Alpine Tethys Ocean onto a unit of the distal European continental margin, also affected by the high-pressure conditions. This structural assemblage is preserved between two younger domes at either end of the Tauern Window. The domes deform isograds of the T-dominated Barrovian metamorphism that itself overprints the high-pressure metamorphism partly preserved in the sheath fold. Using Raman spectroscopy on carbonaceous material (RSCM), we are able to distinguish peak-temperature domains related to the original, subduction metamorphism from domains associated with the later temperature-dominated (Barrovian) metamorphism. The distribution of RSCM temperatures in the Barrovian domain indicates a lateral and vertical decrease of peak temperature with increasing distance from the centres of the thermal domes. This represents a downward-increase of paleo-temperature, in line with previous studies. However, we observe the opposite paleo-temperature trend in the lower limb of the sheath fold, namely an upward increase. We interpret this inverted paleo-temperature domain as the relic of a subduction-related temperature field. Towards the central part of the sheath fold's upper limb, RSCM temperatures increase to a maximum of ca. 520 °C. Further

upsection in the hanging wall of the sheath fold, paleo-peak-temperatures decrease to where they are indistinguishable from the peak temperatures of the overprinting Barrovian metamorphism. Peak-temperature contours of the subduction-related metamorphism are oriented roughly parallel to the folded nappe contacts and lithological layering. The contours close towards the northern, western and eastern parts of the fold, resulting in an eye-shaped, concentric pattern in cross-section. The temperature contour geometry therefore mimics the fold geometry itself, indicating that these contours were also folded in a sheath-like manner. We propose that this sheath-like pattern is the result of a two-stage process that reflects a change of the mode of nappe formation in the subduction zone from thrusting to fold nappe formation. First, thrusting of a hot oceanic nappe onto a colder continental nappe created an inverted peak-thermal gradient. Second, sheath folding of this composite nappe structure together with the previously established peak-temperature pattern during exhumation. This pattern was preserved because temperatures decreased during retrograde exhumation metamorphism and remained less than the subduction-related peak temperatures during the later Barrovian overprint. The fold ascended with diapir-like kinematics in the subduction channel.

4.2 Introduction

Mountain building in subduction-collision zones is typically characterised by two distinct modes of plate convergence. First, oceanic lithosphere is consumed during subduction which eventually leads in a second stage to continental collision after complete closure of the ocean. The transition from subduction to collision is accompanied by a rearrangement of crustal deformation patterns and the thermal structure of the involved lithosphere. Temperature (T) controls several key parameters, e. g., rock strength, metamorphic reactions and fluid flow, which are all critical for the dynamics of orogens and subduction zones. These parameters, on the other hand, feed back to the temperature distribution and thermal budget (e. g., Goffé et al., 2003). However, direct observation of any transient thermal state and its dynamics on the large scale is not possible and studies on this topic have to use either indirect observations with geophysical methods or numerical simulations. Both approaches are strongly dependent on boundary conditions and other assumptions and therefore require comparison with natural examples. These data are obtained by reconstructing the thermal state of tectonic units exhumed from subduction zones and now accessible at the surface. Many studies have either explored the thermal evolution of subducted units with time (e. g., classical geochronological studies; Steck & Hunziker, 1994) or the thermal structure integrated over a certain timespan (e. g., Wiederkehr et al., 2011), but combining both aspects to reconstruct the evolution of the thermal structure, possibly in three dimensions, remains very challenging (Luth & Willingshofer, 2008).

In the Alps, a classical area to study processes related to the subduction-collision transition, many tectonic units experienced Alpine pressure- (P-) dominated subduction-zone metamorphism. In the Western Alps, several studies revealed the geometry of the orogen-scale, subduction-related metamorphic structure (e. g., Agard et al., 2002; Babist et al., 2006; Beltrando et al., 2010; Bousquet et al., 2008). In other regions of the Alps, however, the subduction-related thermal imprint has been obscured by a second, later thermal event and most studies focussed on reconstructing the thermal structure of this Barrovian metamorphism (e. g., Cliff et al., 1985; Droop, 1985; Hoernes & Friedrichsen, 1974; Scharf et al., 2013b). This is particularly the case for many of the Penninic and Sub-Penninic units in the Lepontine Dome and the Tauern Window, where the nappe boundaries are crosscut by Barrovian isograds (Oberhänsli et al., 2004). The thermal structure of the regional, collision-related Barrovian metamorphism is overprinted by late collision-related deformation structures. For example, large-scale folds in

the Tauern Window (e. g., Hoinkes et al., 1999) and backfolds in the Lepontine Dome deformed post-nappe isograds (e. g., Steck & Hunziker, 1994). Moreover, external fold-and-thrust belts are generally characterised by large-scale cylindricity of thrust nappes and along-strike continuity of metamorphic isograds (e. g., Bousquet et al., 2008; Frey et al., 1999). For instance, the pattern of peak metamorphic temperatures in the Helvetic nappes was passively folded when the Aiguilles Rouges and Aar massifs were uplifted along basement thrusts (Girault et al., 2020).

Like the cylindrical Jura and Helvetic external belts, some Penninic and Sub-Penninic nappes of the Central and Western Alps that formed during subduction and exhumation occur along the strike of the orogen, suggesting that they were originally also cylindrical. Polyphase post-nappe refolding, however, resulted in generally non-cylindrical nappe geometries (e. g., Maxelon & Mancktelow, 2005; Milnes, 1974; Steck et al., 2019). Given the spatial coincidence of thermal and deformational structure in collisional settings, the question arises if a similar relationship exists in the non-cylindrical (fold) nappes that formed in subduction settings. In other words, do non-cylindrical (fold) nappes also exhibit a non-cylindrical thermal structure that in some way corresponds with the nappe geometry?

We attempt to answer this question by investigating a highly non-cylindrical fold nappe in the Tauern Window in three dimensions. We show that even for a multi-phase metamorphic evolution, the thermal structure of the earlier, subduction-related event can be partly reconstructed. We apply Raman spectroscopy on carbonaceous matter to yield metamorphic peak-T. The pattern of peak-T corresponds well with the originally non-cylindrical geometry of the Seidlwinkl fold nappe. Additionally, the results show how the subduction-related peak-T distribution is overprinted by the post-exhumation Barrovian metamorphism that was most intense in the European basement of the Eastern Alps.

4.3 Geological Overview and Thermal History of the Tauern Window

The Tauern Window is the largest tectonic window in the Alps, exposing units that display a polyphase metamorphic history with older P-dominated and younger T-dominated Alpine metamorphism (e. g., Droop, 1985; Hoernes & Friedrichsen, 1974; Hoinkes et al., 1999; Oberhänsli et al., 2004). This change from P- to T-dominated overprints reflects the large-scale Alpine evolution from a subduction- to a collision-dominated orogenesis. The Tauern Window itself formed mainly in Neogene time during relatively late stages of continental collision by a combination of crustal-scale indentation, doming and lateral escape (e. g., Ratschbacher et al., 1991; Rosenberg et al., 2007; Scharf et al., 2013a; Schmid et al., 2013). Normal faulting at the eastern end western ends of the window together with erosional denudation in response to doming removed the Austroalpine lid (Favaro et al., 2017) and led to the emergence of the underlying Penninic and Sub-Penninic nappes. These nappes had witnessed intense metamorphism and deformation during earlier Paleogene subduction and collision.

Table 4.1: Regional deformation phases in the Tauern Window after Schmid et al. (2013).

Phase	Events
D1	Early subduction of Alpine Tethys
D2	Late subduction of Alpine Tethys, HP metamorphism in Glockner and Rote Wand nappes
D3	Exhumation, Formation of Seidlwinkl sheath fold
D4	Accretion of European margin, Formation of Venediger Duplex
D5	Indentation, doming in the Tauern Window

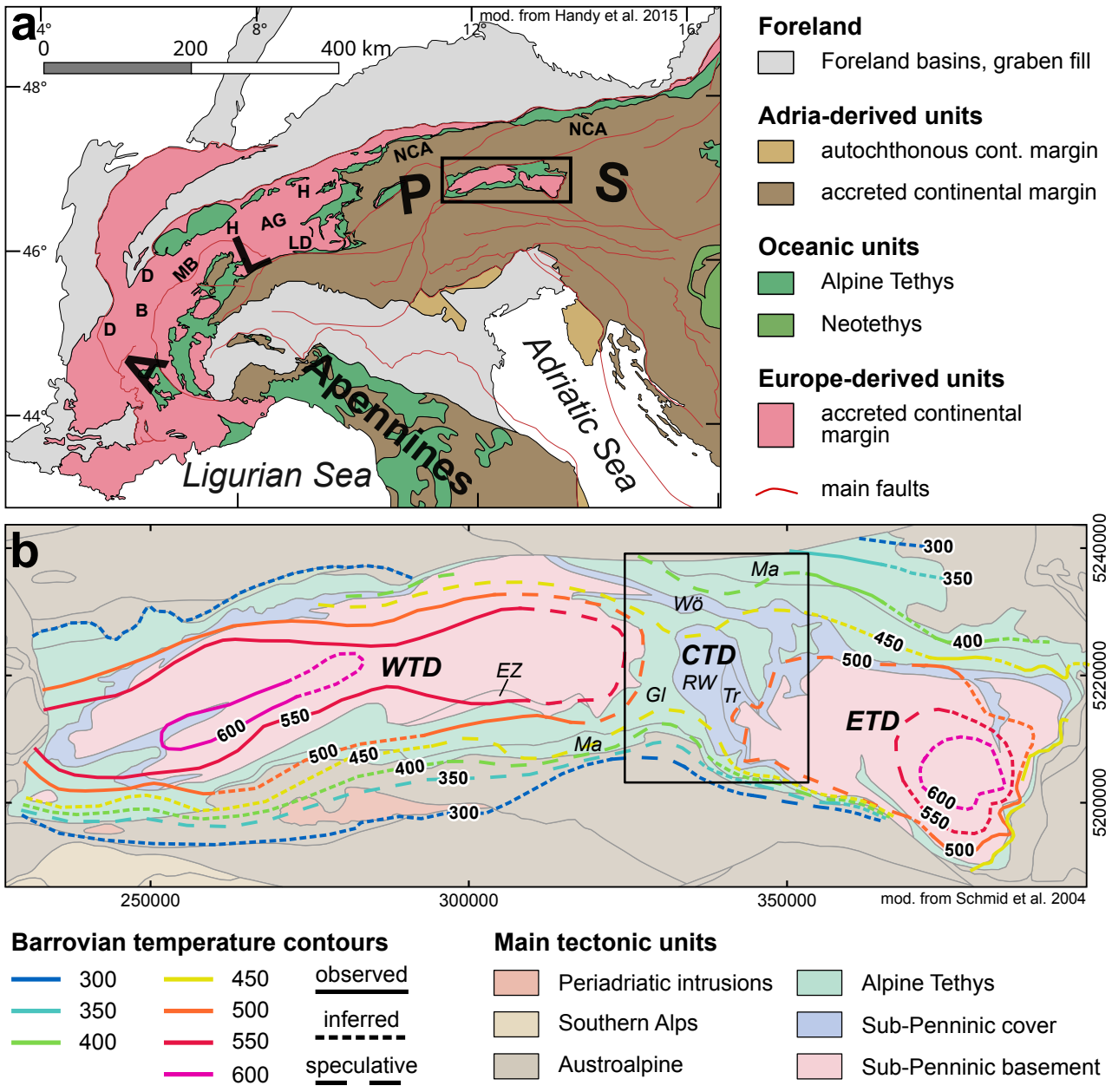

Figure 4.1: (a) Tectonic overview map of the Alps (modified from Handy et al., 2015). Black rectangle denotes location of map in (b). AG = Aar and Gotthard massifs, B = Belledonne Massif, D = Dauphinois Zone, H = Helvetic nappes, LD = Lepontine Dome, MB = Mont-Blanc Massif, NCA = Northern Calcareous Alps. (b) Tectonic map of the Tauern Window region (modified from Schmid et al., 2004) and peak-T contours of regional metamorphism compiled from Bousquet et al. (2012), Dachs (1990), Droop (1985), Hoernes & Friedrichsen (1974), and Rosenberg et al. (2018) — WTD; Favaro et al. (2015), Inger & Cliff (1994), Lambert (1970), Oxburgh et al. (1966), Reddy et al. (1993), and Scharf et al. (2013b) — ETD; Frank et al. (1987), own data — CTD. The contours mainly reflect peak conditions of Barrovian "Tauernkristallisation" metamorphism. The black rectangle delineates the main research area and the location of the Seidlwinkl sheath fold (Figure 4.2). EZ = Eclogite Zone, Wö = Wörth Unit, Tr = Trögereck Nappe, RW = Rote Wand Nappe, Gl = Glockner nappe system, Ma = Matrei Zone (includes the "Nordrahmenzone"). Details on the compilation of peak-T contours are given in Appendix A.5.

The Austroalpine nappes as the uppermost tectonic units surrounding the Tauern Window comprise a nappe stack formed during the Cretaceous Eoalpine orogeny along the Adriatic continental margin (e. g., Froitzheim et al., 1994; Schmid et al., 2004). Below this Eoalpine nappe stack are thrust sheets of oceanic lithosphere that were derived from the Alpine Tethys (also called the Penninic Ocean; e. g., Kurz et al., 1996, 1998; Schmid et al., 2004), as well as thrust sheets of the distal European continental margin (Kurz et al., 2008), termed Penninic and Sub-Penninic nappes, respectively. Following the nomenclature of Schmid et al. (2013), the Penninic nappes can be subdivided into the Matrei Zone (upper, older, Piemont-Liguria part) and the Glockner nappe system (lower, younger, Valais part). The Sub-Penninic nappes comprise, from top to bottom, the Modereck nappe system — in the central Tauern Window composed of the Rote Wand Nappe (above) and Trögereck Nappe (below) — the Eclogite Zone and the Venediger nappe system.

The Alpine Tethys separated the European and Adriatic continents in Jurassic and Cretaceous times but was consumed during Paleogene southward subduction (e. g., Handy et al., 2010; Stampfli & Borel, 2004). Early and late subduction-related structures correspond, respectively, to the regional deformation phases D1 and D2 in the tectonic scheme of Schmid et al. (2013), which we adopt in the following (Table 4.1). During subduction, some of the Penninic and Sub-Penninic nappes were subjected to high-pressure (HP) metamorphism (i. e., Glockner Nappe s. str. Rote Wand Nappe, Trögereck Nappe, Eclogite Zone) and intense deformation which involved the formation of a crustal-scale sheath fold nappe (D3) now exposed in the central Tauern Window (Seidlwinkl sheath fold, Groß et al., 2020b). During the onset of the collisional stage of Alpine orogeny, the more proximal European continental margin was progressively accreted below the Alpine nappe stack (D4), forming the Venediger nappe system (Schmid et al., 2013). The Venediger nappe system is exposed in two structural subdomes, the eastern and western Tauern subdomes (ETD and WTD, respectively; Figure 4.1). The subdomes are separated by an axial depression, the central Tauern depression (CTD). All units were affected by a Barrow-type, high-temperature (HT) metamorphic event in late Oligocene time (e. g., Cliff et al., 1985; Favaro et al., 2015; Höck, 1980) that was overprinted by orogen-parallel extensional shearing and doming (D5; e. g., Favaro et al., 2015; Scharf et al., 2016).

4.3.1 The Seidlwinkl Sheath Fold in the Central Tauern Window

Recent studies document the existence of a crustal-scale, recumbent and isoclinal sheath fold nappe in the central part of the Tauern Window, called the Seidlwinkl sheath fold (Figure 4.2; Groß et al., 2020b). This fold is a composite structure comprising the folded thrust contact of the oceanic Glockner Nappe s. str. with the underlying continental Rote Wand Nappe (D2). During D3, the Glockner Nappe s. str. was wrapped around the Rote Wand Nappe, both units together forming a fold nappe that, also during D3, was thrust over the parautochthonous cover of the Venediger nappe system (Wörth Unit in the ETD, Figure 4.1). The axis of this fold nappe curves almost 180° which results in a sheath fold geometry. The fold formed at HP conditions in the Alpine subduction zone and was exhumed partly in an extrusion channel between opposite-sense shear zones — a normal fault above and a thrust below (Groß et al., 2020b). Continued shortening during D4 led to the accretion of the Sub-Penninic nappes below the Seidlwinkl sheath fold and the formation of the Wörth antiform north of the sheath fold (Figure 4.1).

Sheath folds on the meter to sub-meter scale are common in all kinds of shear zones around the world (e. g., Alsop et al., 2007). However, sheath folds as large as the one discussed here — i. e., on the scale of hundreds of meters to several kilometers — are only rarely described, despite the fact that sufficiently

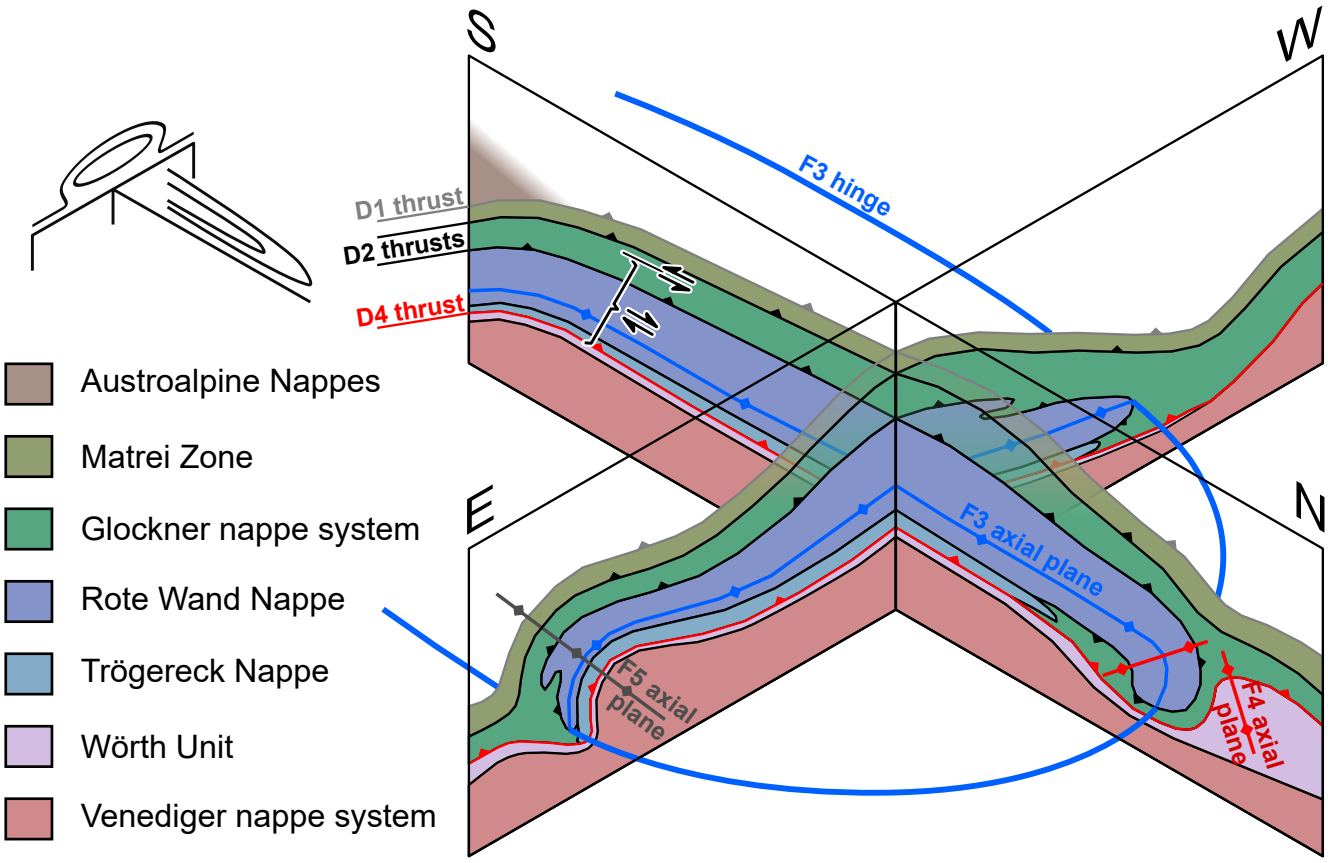

Figure 4.2: Block diagram of the Seidlwinkl sheath fold in the central Tauern Window (modified after Groß et al., 2020b). The fold affected only the HP rocks of the Glockner, Rote Wand and Trögereck nappes. Note that in the E-W section, marker lines outline an eye-shaped pattern in the internal part of the sheath fold and omega-shaped patterns in its outer parts.

large shear zones that could exhibit such structures are fairly common. Very large sheath folds are usually associated with orogenic crustal flow of high-grade and highly-deformed basement (e. g., Bonamici et al., 2011; Chetty et al., 2012; Goscombe, 1991; Henderson, 1981; Vollmer, 1988) and only few have been described from a subduction-exhumation setting (e. g., Lacassin & Mattauer, 1985; Searle & Alsop, 2007), as in this study.

The tectonic units with European affinity discussed here have a common lithostratigraphy, which generally begins with pre-Variscan basement intruded by late-Variscan plutons and overlain unconformably by post-Variscan — mostly Mesozoic — clastic sediments and carbonates (e. g., Kurz et al., 1998; Schmid et al., 2013). This sequence is especially well developed in the Rote Wand Nappe, which forms the core of the Seidlwinkl sheath fold (Frasl & Frank, 1964; Kurz et al., 1998; Pestal & Hellerschmidt-Alber, 2011). This allows a reconstruction of the fold geometry using well-defined stratigraphic marker horizons. The oceanic units discussed below comprise mafic and ultramafic basement and abundant carbonate-bearing marine sediments of Jurassic and/or Cretaceous age (Höck et al., 2006; Koller & Pestal, 2003; Lemoine, 2003; Reitz et al., 1990).

4.3.2 Peak-P-T- and Timing Estimates for Barrovian Metamorphism

A Barrow-type HT metamorphic event termed "Tauernkristallisation" (Sander, 1914) overprinted the Alpine nappe stack in and around the Tauern Window to variable degrees (Hoinkes et al., 1999) in Oligocene time (ca. 30-27 Ma; Christensen et al., 1994; Cliff et al., 1985; Favaro et al., 2015). This event also largely overprinted the older HP assemblages (e. g., Kurz et al., 2008). The large-scale distribution of peak-T conditions of the Barrovian event in the Tauern Window have been mapped in and around the western (Dachs, 1990; Hoernes & Friedrichsen, 1974) and eastern Tauern subdomes (Cliff et al., 1985; Scharf et al., 2013b) and its conditions have been quantified by a variety of thermometrical methods (e. g., oxygen isotope fractionation, calcite-dolomite equilibrium, Raman spectroscopy on carbonaceous material). They all confirmed the concentric Barrovian temperature pattern around the two subdomes of the Tauern Window. The highest peak-T at amphibolite facies conditions ($>$ 600 °C and 0.7 GPa) were reached in the central, structurally lowest parts of the western and eastern Tauern domes. From there, the peak-T radially decrease to values of greenschist-facies conditions at the perimeter of the window and even lower conditions in Austroalpine units outside of the window. However, so far there are only few data in the central Tauern depression (Bickle & Powell, 1977; Dachs & Proyer, 2001; Frank et al., 1987) and the interpretation of these data is ambiguous because of overlapping metamorphic conditions of the Barrovian and subduction-related events (see below). Therefore, the continuation of isotherms of Barrovian metamorphism across the depression between the subdomes, as shown in previous compilations (Bousquet et al., 2012), is speculative. We compiled a new map of existing and own data of peak-T for the Barrovian event in the Tauern Window (Figure 4.1) with focus on the central Tauern depression. Details of this compilation are given in Appendix A.5. This compilation confirms the large-scale concentric thermal structure of the isotherms of Barrovian metamorphism, but shows that the high-grade isograds related to this event in the subdomes are separated from each other by a zone of lower Barrovian peak-T in the central Tauern depression.

4.3.3 Peak-P-T- and Timing Estimates for Subduction Metamorphism

Alpine subduction in the Tauern Window is evidenced by the occurrence of HP mineral parageneses in metabasites and metasediments with Mesozoic protolith ages. This HP event reached pressure conditions that indicate deep subduction to sub-crustal depths in tectonic units derived from the Alpine Tethys (Glockner Nappe s. str.) and the distal European margin (Rote Wand Nappe, Trögereck Nappe, Eclogite Zone). Several P-T estimates for these units exist, ranging from ca. 2.0-2.3 GPa and 600 °C in the continent-derived Eclogite Zone (Dachs, 1986, 1990; Frank et al., 1987; Hoschek, 2001; Kurz et al., 1998; Stöckhert et al., 1997; Zimmermann et al., 1994) to ca. 1.7 GPa and 570 °C in the oceanic Glockner Nappe s. str. (Dachs & Proyer, 2001). For the latter unit, Groß et al. (2020b) determined somewhat higher peak pressures of up to 2.3 GPa. Recent studies have also confirmed the widespread existence of this HP event (2 GPa, 500 °C) in the continental Rote Wand and Trögereck nappes (belonging to the Modereck nappe system) in the central Tauern Window (Groß et al., 2020b; Schmidt, 2015). For the uppermost Penninic nappe unit, the Matrei Zone, Koller & Pestal (2003) estimated conditions of subduction metamorphism to be ca. 0.9-1.0 GPa and 360-370 °C. For the Sub-Penninic Venediger nappe system, peak pressures of ca. 1.0 GPa at ca. 500 °C were reported (Droop, 1985; Selverstone, 1993; Selverstone et al., 1984). The tectonic units with a HP imprint experienced variable degrees of HT overprint during regional Barrovian metamorphism, depending on the locality. Previous mapping of peak-T concentrated

on the western and eastern Tauern subdomes to either side of the HP units mostly exposed in the central Tauern depression. Therefore, the thermal imprint of the subduction-related metamorphism has not yet been mapped as well as the Barrovian event, though in the Central Alps, it has been shown that at least parts of subduction-related peak-T patterns escaped later thermal overprint (e. g., Wiederkehr et al., 2011).

The age of the baric peak of subduction metamorphism is in debate. Studies that used Ar-Ar dating on phengite and hornblende found upper Eocene ages for peak-P conditions: ca. 39 Ma for the Rote Wand nappe (Kurz et al., 2008) and 45-38 Ma for the Eclogite Zone (Kurz et al., 2008; Ratschbacher et al., 2004). Abundant younger Ar-Ar ages in the range 36-32 Ma for the same units and the Glockner Nappe s. str. are commonly interpreted as cooling or deformation ages set during syn-deformational retrogression from peak-P condition (Kurz et al., 2008; Zimmermann et al., 1994). On the other hand, dating with high-retentivity isotopic systems using allanite (U-Pb, Smye et al., 2011) and garnet (Lu-Hf, Nagel et al., 2013) yielded similarly young ages of ca. 35-33 Ma for the prograde path and subsequent baric peak for metabasites of the Eclogite Zone and associated metasediments.

4.4 Raman Spectroscopy on Carbonaceous Material

Raman spectra of carbonaceous matter (RSCM) show two main intensity bands in the regions 1000-1500 cm^{-1} and 1500-1700 cm^{-1}, commonly named D- and G-band, respectively. Ideally, the G-band is the only band of perfectly ordered graphite in the first-order region (ca. 1100-1800 cm^{-1}), whereas the various D-bands are the result of double-resonant Raman scattering induced by disorder in the graphite crystal lattice (Reich & Thomsen, 2004). The relative intensities of these bands therefore depend on the crystallisation state of the carbonaceous matter (CM). The degree of ordering in the graphite crystal lattice gradually increases with increasing metamorphic temperature. Since the graphitization process of carbonaceous matter is irreversible, the temperatures obtained reflect the thermal peak of the whole metamorphic history of the investigated specimen (Beyssac et al., 2002). Several calibrations for this geothermometer have been proposed so far (e. g., Aoya et al., 2010; Beyssac et al., 2002; Kouketsu et al., 2014; Lahfid et al., 2010; Lünsdorf et al., 2017). These calibrations differ somewhat in terms of absolute temperatures derived from measuring the crystallisation state of CM. However, the relative temperature differences between samples — the information used in this study — is well-resolved irrespective of the calibration used. We chose the calibration of Lünsdorf et al. (2017) because it has the advantage of being applicable to a wide range of metamorphic temperatures (160-600 °C). Furthermore, their method provides a well-integrated automatic spectrum-fitting approach realised by their IFORS software that eliminates operator bias during curve fitting (Lünsdorf et al., 2017). Their method uses a statistical parameter ("scaled total area" = STA) that has been calibrated against the known metamorphic peak-T of a large number of reference samples.

Spectra of non-surface exposed CM particles in polished thin sections were obtained on a Horiba ISA Dilor Labram micro-confocal Raman spectrometer with a Nd-YAG laser (532.15 nm wavelength, 300 mm focal length) and a grating with 1800 grooves/mm. A high spatial resolution (ca. 1 µm spot size) was achieved by using a 400 µm wide confocal hole, a slit width of 100 µm and a 100x objective. The spectrometer was centered at 1100 or 1200 cm^{-1} to ensure sufficiently large background signal on both sides of the CM-band region. The acquisition time was 20 s with 2 accumulations. In order to avoid thermal destruction or photo-bleaching of the CM, the laser power was attenuated with a 0.3 filter to 2-3 mW of laser energy on the sample. In each sample we measured approximately 30 individual CM particles, preferentially as inclusions in transparent or translucent host phases (quartz, white mica, garnet, chloritoid, calcite, chlorite), in order to avoid alteration caused by sample preparation.

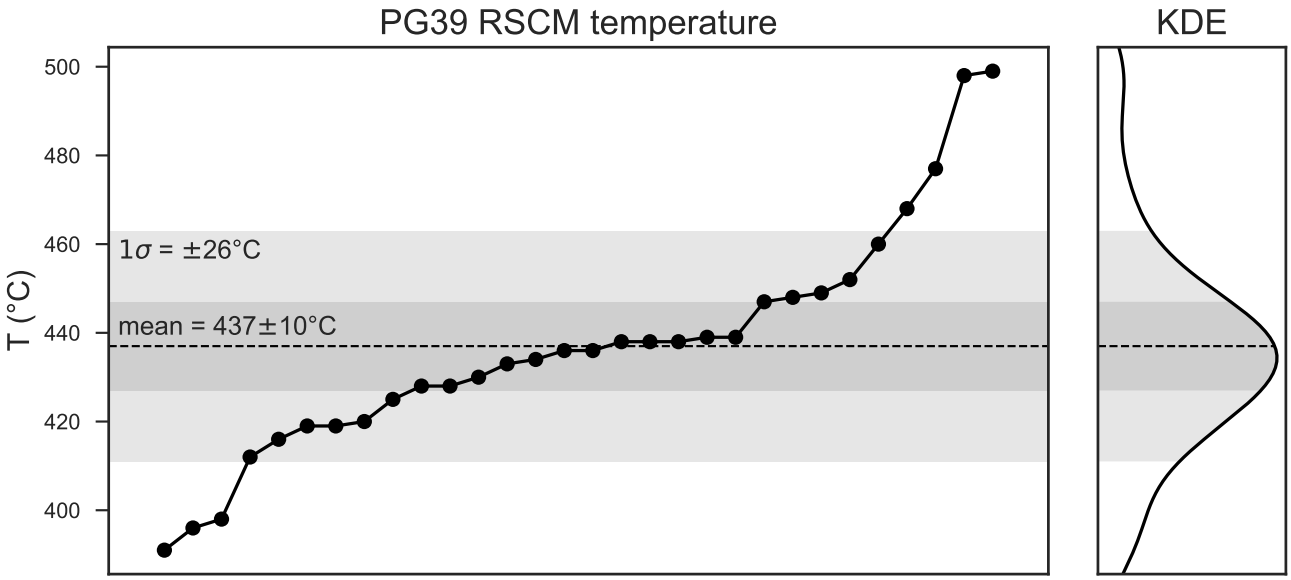

Figure 4.3: Exemplary summary of all RSCM temperature estimates from sample PG39. Individual measurements are on the x-axis. Sample mean (stippled line), 95% CI (dark shaded area) and one standard deviation (light shaded area) are also shown.

All spectra were fitted automatically with the IFORS software in the range of 1000-1900 cm^{-1} (= first order region of CM bands). Peaks and background were modelled simultaneously, with pseudo-Voigt functions for the peaks and a fifth-order polynomial as baseline correction. The results were manually checked for integrity (no spurious peaks, convergence of multiple runs, no strong fluorescence) so that those fittings with insufficient quality could be discarded from further evaluation. A temperature was calculated for each remaining spectrum by using the Lünsdorf et al. (2017) calibration, resulting in a range of temperatures for each sample. For graphical evaluation, the results of each sample are plotted in a diagram that shows the individual temperature measurements (Figure 4.3). The mean of this temperature range is assumed to represent the "true" sample temperature (e. g., Beyssac et al., 2002), with its uncertainty given by the 95% confidence interval (CI) of the mean. The within-sample heterogeneity is expressed as one standard deviation (1σ) of all temperature values obtained in the sample. Additionally, it is visualized with a kernel density estimate (KDE; Figure 4.3), making it easy to perceive non-unimodal or strongly skewed temperature distributions. The absolute geological uncertainty of each temperature estimate (compared with other methods, e. g., thermodynamic modelling) is in the order of ca. 30 °C (Aoya et al., 2010).

4.4.1 Robustness of the RSCM Temperature Estimates Regarding Amount of Analyses

Aoya et al. (2010) suggested that at least 25-30 individual measurements are required for each sample to assure that the scatter of the average of a statistical value (their R2 ratio) reduces to a narrow and reasonable range. In order to investigate the robustness of our temperature estimates, we expanded their approach by applying a simple bootstrapping analysis. For this purpose, we measured 60 CM grains in one specimen (PG25; 47.06106°N 12.79165°E), which is twice the number of 30 CM grains usually measured. This large sample dataset is randomly resampled (with replacement) to generate synthetic subsamples of variable size, n (3-60 CM; number of analyses per sample = n). This procedure is

repeated for 150 iterations. In each iteration, the most important statistical parameters (mean, median, standard deviation, confidence interval) are calculated. After all iterations, the scatter of these values is evaluated as a kernel density estimate for each *n* and the results are plotted (Figure 4.4).

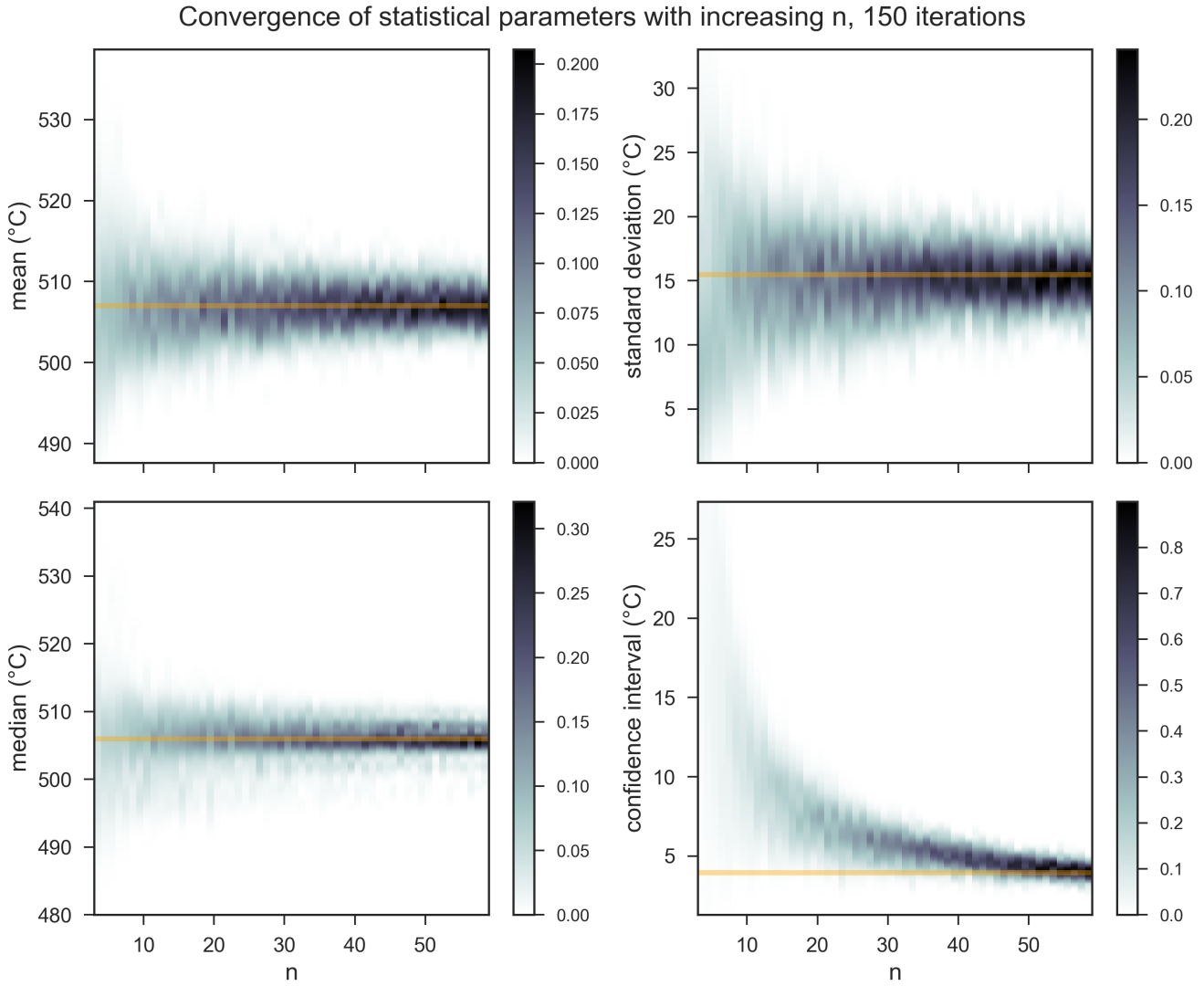

Figure 4.4: Bootstrapping analysis for increasing *n* shows that statistical parameters largely converge to sample average values (orange horizontal lines, calculated with actual data from sample PG25) for *n* of 3-60. The grey scale denotes the kernel density.

With increasing number of analyses per sample *n*, the scatter of mean, median and standard deviation strongly decreases until it stays nearly constant within a narrow range for *n* greater than about 20-25. The scatter of the confidence interval and its absolute value steadily decrease with increasing *n*, but the latter becomes reasonably low ($< 10\,°C$) at *n* of ca. 25-30. Given the overall uncertainty of the method, 30 analysed CM particles per sample is therefore sufficient to obtain precise, robust and reproducible results. The RSCM raw data, results from spectrum fitting with IFORS and the resulting RSCM-temperature data are available in the GFZ Data Services repository (Groß et al., 2020c).

4.5 Results

The results of RSCM-temperature analyses of all 104 samples are summarized in Table 4.2 and shown on a map (Figure 4.5) and several cross sections (Figure 4.6) of the study area. A map with sample locations (Appendix I.1) and enlarged, high-resolution versions of the RSCM map (Appendix I.2) and cross sections (Appendices I.4 and I.3) are provided in the Appendix. For details on cross-section construction and data projection, we refer to Appendix A.6 and Figure A.1. Our new peak-T data are in good agreement with the temperature estimates obtained by Frank et al. (1987) that are also shown on the map and cross sections.

Table 4.2: Results of RSCM-temperature analyses. Sample coordinates are in decimal degrees. n = number of analysed spectra per sample; CI = 95% confidence interval of the mean; 1σ = 1 standard deviation; Q1, Q3 = first and third quartile, respectively.

Sample	**Sample Coordinates**		**n**	**mean**	**CI**	**1σ**	**Q1**	**median**	**Q3**	**min**	**max**
	Lat	Lon		°C	°C	°C	°C	°C	°C	°C	°C
F15/17	47.09157	12.94475	27	**491**	**10**	26	482	497	508	426	544
PG13	47.06887	12.83963	30	**521**	**10**	26	508	516	534	475	582
PG18	47.06476	12.86976	32	**507**	**9**	25	500	508	524	420	543
PG21	47.08413	12.74363	43	**488**	**8**	27	468	482	504	439	544
PG25	47.06106	12.79165	60	**507**	**4**	15	496	506	512	478	550
PG29	47.08102	12.90041	31	**471**	**8**	22	452	468	478	440	528
PG32	47.08144	12.91461	37	**498**	**7**	20	484	498	511	462	565
PG39	47.20519	12.85492	30	**437**	**10**	26	421	436	448	391	499
PG41	47.17778	12.81980	31	**436**	**11**	29	417	431	448	383	516
PG48	47.08263	12.83997	31	**521**	**8**	21	506	519	534	488	565
PG50	47.08252	12.83879	31	**513**	**8**	21	498	512	528	465	555
PG59	47.08215	12.83455	33	**554**	**9**	25	546	560	570	468	581
PG60	47.08210	12.83445	30	**522**	**10**	26	505	522	542	470	560
PG61	47.08153	12.85327	40	**505**	**6**	20	490	506	520	462	550
PG70	47.01313	12.92355	31	**489**	**5**	15	482	489	500	456	519
PG89	46.99970	12.92027	32	**518**	**9**	24	503	522	536	456	577
PG93	47.00327	12.91583	33	**500**	**6**	17	491	503	515	462	524
PG102	47.02236	12.92846	35	**503**	**9**	26	493	505	518	428	559
PG117	47.08595	12.87196	31	**493**	**5**	13	485	494	500	469	522
PG119	47.01313	12.92362	27	**479**	**5**	13	469	475	484	460	511
PG126	47.02228	12.93056	32	**474**	**5**	13	468	472	479	448	509
PG130	47.11207	12.82534	30	**485**	**8**	21	474	487	498	441	538
PG133	47.08307	12.74402	34	**508**	**9**	27	492	511	523	444	561
PG139	47.13251	12.84119	30	**497**	**6**	17	487	496	507	461	537
PG141	47.13907	12.84402	28	**496**	**10**	27	483	496	513	447	557
PG143	47.12378	12.81980	31	**486**	**10**	28	471	480	500	442	558
PG144	47.13876	12.80937	31	**488**	**8**	23	474	488	508	436	527
PG145	47.19293	12.82843	29	**447**	**16**	43	411	428	489	393	523
PG150	47.16490	12.90585	30	**481**	**7**	20	467	480	497	447	517
PG155	47.12797	12.96785	30	**485**	**10**	28	462	479	504	441	541
PG157	47.18769	12.94088	31	**478**	**11**	30	454	477	501	410	527
PG159	47.18671	12.93966	32	**492**	**9**	26	474	500	513	437	523

Table 4.2: continued

Sample	Sample Coordinates		n	mean	CI	1σ	Q1	median	Q3	min	max
	Lat	Lon		°C	°C	°C	°C	°C	°C	°C	°C
PG161	47.11427	12.92652	31	**484**	**7**	20	467	488	495	444	524
PG163	47.10725	12.91453	30	**493**	**7**	19	482	488	497	471	552
PG167	47.11128	12.92077	30	**478**	**9**	24	462	474	492	430	539
PG176	47.21406	12.94204	29	**456**	**9**	23	438	450	463	426	507
PG178	47.19469	12.97066	31	**486**	**7**	20	475	487	501	439	523
PG180	47.19993	12.97218	33	**486**	**9**	25	468	491	507	434	518
PG182	47.21032	12.96617	30	**427**	**11**	28	416	432	440	337	490
PG185	47.20305	12.96998	30	**466**	**12**	31	435	469	487	408	520
PG188	47.23495	12.99888	36	**390**	**11**	33	368	377	418	339	480
PG189	47.23056	13.00392	33	**463**	**10**	28	439	465	484	419	505
PG190	47.27203	12.97922	32	**374**	**10**	27	360	372	380	335	468
PG192	47.27418	12.97755	30	**347**	**9**	25	336	344	353	301	415
PG194	47.20717	12.96765	30	**453**	**10**	27	436	450	469	386	509
PG195	47.20255	12.96635	35	**467**	**10**	28	449	463	492	420	537
PG206	47.19690	12.85223	30	**470**	**13**	36	452	468	496	390	535
PG208	47.08437	12.87841	29	**482**	**9**	24	465	482	505	442	524
PG214	47.01109	12.86035	22	**508**	**13**	29	489	509	527	431	555
PG216	47.01108	12.85454	23	**441**	**5**	11	437	440	448	418	471
PG220	47.06841	12.81982	25	**472**	**8**	20	463	469	477	411	514
PG223	47.16329	12.83337	29	**489**	**6**	16	482	492	500	454	522
PG228	47.16800	12.85818	30	**485**	**6**	15	478	488	492	451	528
PG229	47.16596	12.84674	22	**490**	**7**	17	480	488	496	465	529
PG233	47.15095	12.85413	30	**464**	**11**	28	452	462	476	379	521
PG235	47.09259	12.81526	22	**503**	**7**	16	493	498	508	468	534
PG238	47.09688	12.80421	30	**519**	**7**	18	507	520	530	486	552
PG242	47.18543	12.84582	29	**489**	**7**	17	479	491	498	452	522
PG243	47.18949	12.84968	27	**467**	**11**	27	450	458	496	424	509
PG247	47.19540	12.85067	28	**472**	**16**	40	442	465	514	393	530
PG250	47.21473	12.83527	32	**442**	**9**	26	427	436	451	393	502
PG251	47.17596	12.85750	30	**492**	**6**	15	479	490	504	466	517
PG254	47.17878	12.85954	30	**494**	**8**	22	479	497	508	429	532
PG256	47.18293	12.86215	29	**455**	**8**	21	440	452	469	408	516
PG258	47.18758	12.86514	29	**487**	**12**	30	469	489	506	433	541
PG260	47.12132	12.87562	32	**482**	**8**	23	469	475	498	434	538
PG261	47.11988	12.86785	30	**491**	**10**	27	481	493	506	414	534
PG262	47.10316	12.85082	29	**498**	**14**	37	488	504	521	371	560
PG264	47.09594	12.85090	21	**481**	**11**	25	466	478	494	427	551
PG267	47.16742	12.72921	30	**507**	**6**	16	500	506	515	479	541
PG268	47.16865	12.73390	31	**465**	**9**	25	452	465	472	410	522
PG270	47.16470	12.73638	30	**487**	**10**	27	472	491	503	433	541
PG275	47.25731	12.74228	29	**427**	**8**	21	419	427	437	379	468
PG277	47.14867	12.99552	31	**487**	**7**	19	476	492	502	436	509
PG278	47.14360	13.00195	30	**475**	**7**	19	462	476	484	438	526
PG280	47.13720	13.01402	22	**498**	**10**	22	481	500	517	454	530

Table 4.2: continued

Sample	Sample Coordinates		n	mean	CI	1σ	Q1	median	Q3	min	max
	Lat	Lon		°C	°C	°C	°C	°C	°C	°C	°C
PG282	47.13592	12.99925	29	**478**	**12**	30	453	475	494	424	541
PG283	47.03030	12.85314	23	**502**	**8**	19	490	498	518	464	537
PG285	47.06587	12.76461	30	**510**	**7**	19	494	511	524	478	549
PG288	47.06203	12.76904	41	**524**	**11**	36	497	515	553	464	585
PG291	47.22328	12.82085	31	**440**	**10**	26	422	440	456	394	504
PG293	47.23642	12.83177	27	**397**	**8**	20	386	401	410	350	432
PG295	47.14147	12.77297	30	**500**	**6**	16	486	498	514	476	533
PG299	47.13174	12.75609	30	**512**	**6**	16	499	512	521	489	552
PG301	47.15023	12.79487	30	**488**	**10**	27	466	485	506	443	544
PG302	47.11424	12.79357	32	**496**	**7**	19	483	498	507	460	530
PG303	47.10947	12.78826	30	**491**	**6**	16	478	494	501	462	522
PG304	47.10638	12.78808	30	**508**	**8**	20	496	511	523	462	543
PG305	47.11280	12.79372	31	**504**	**10**	29	494	505	518	397	579
PG334	47.17431	12.79483	28	**481**	**9**	23	468	478	497	437	534
PG335	47.16805	12.78938	26	**496**	**7**	18	480	494	511	469	526
PG336	47.17211	12.80316	30	**475**	**10**	27	458	468	497	433	533
PG337	47.17139	12.80800	27	**444**	**14**	36	426	434	454	384	519
PG338	47.05176	12.76148	30	**399**	**7**	18	388	395	411	371	444
PG340	47.05461	12.76606	28	**420**	**6**	16	412	420	428	392	469
YD003	47.04476	12.81100	27	**506**	**7**	18	493	507	522	463	535
YD005	47.04457	12.80834	28	**471**	**12**	32	452	479	494	386	530
YD006	47.04480	12.80639	28	**461**	**11**	29	442	455	480	407	535
YD007	47.04478	12.80628	27	**501**	**9**	23	488	502	518	435	541
YD010	47.04185	12.80246	28	**446**	**8**	19	437	440	456	402	511
YD011	47.03905	12.79922	29	**414**	**17**	44	403	417	437	281	490
YD012	47.03737	12.79731	30	**388**	**9**	23	371	382	398	360	437
YD014	47.03385	12.79360	28	**410**	**12**	32	393	410	427	306	487
YD017	47.03938	12.80034	28	**409**	**10**	25	393	406	423	370	475

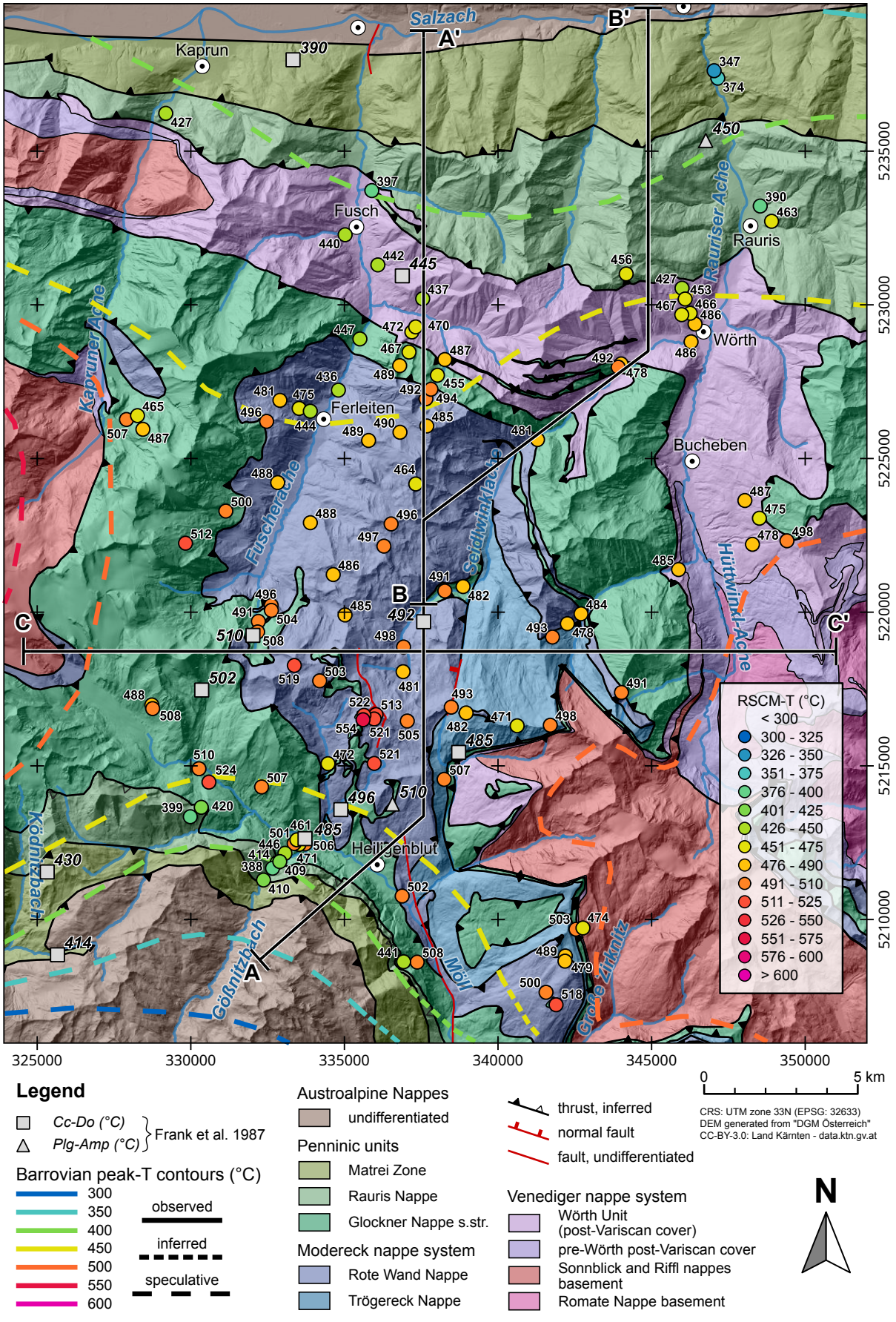
Salzach
Kaprun
Fusch
Rauris
Wörth
Bucheben
Ferleiten
Heiligenblut
Kapruner Ache
Fuscherache
Seidlwinklache
Rauriser Ache
Hüttwinkl-Ache
Ködnitzbach
Größnitzbach
Möll
Große Zirknitz
A
A'
B
B'
C
C'
RSCM-T (°C)
< 300
300 - 325
326 - 350
351 - 375
376 - 400
401 - 425
426 - 450
451 - 475
476 - 490
491 - 510
511 - 525
526 - 550
551 - 575
576 - 600
> 600
325000
330000
335000
340000
345000
350000
5235000
5230000
5225000
5220000
5215000
5210000
0
5 km
CRS: UTM zone 33N (EPSG: 32633)
DEM generated from "DGM Österreich"
CC-BY-3.0: Land Kärnten - data.ktn.gv.at
N
Legend
Cc-Do (°C)
Plg-Amp (°C)
Frank et al. 1987
Barrovian peak-T contours (°C)
300
350
400
450
500
550
600
observed
inferred
speculative
Austroalpine Nappes
undifferentiated
Penninic units
Matrei Zone
Rauris Nappe
Glockner Nappe s.str.
Modereck nappe system
Rote Wand Nappe
Trögereck Nappe
thrust, inferred
normal fault
fault, undifferentiated
Venediger nappe system
Wörth Unit (post-Variscan cover)
pre-Wörth post-Variscan cover
Sonnblick and Riffl nappes basement
Romate Nappe basement

Figure 4.5 ***(previous page)*****:** RSCM peak-temperature map of the central Tauern Window. Peak-T contours are displayed for the Barrovian metamorphic stage. A high-resolution version of this figure is available in Appendix I.2.

The highest temperatures of ca. 520 °C were obtained near the contact of the Rote Wand Nappe with the Glockner Nappe s. str. in the southern central part of the study area (Figures 4.5 and 4.6). From there, temperatures decrease in all directions except south, i. e., toward the "root" of the fold nappe. The lowest temperature estimates of ca. 350-400 °C are located along the northern border of the Tauern Window. For the lithologies with post-Variscan stratigraphic ages used in this study, peak-T was reached either during Alpine subduction or later regional Barrow-type thermal overprint (Tauernkristallisation). The relative uncertainty of the temperature estimates is generally on the order of ± 10 °C or even less, which is very low and facilitates resolution of even small temperature differences between samples.

4.5.1 3D Temperature Distribution in the Central Tauern Window in Map View and Cross Sections

Both normal and inverted peak-temperature gradients exist in the cross sections (Figure 4.6), i. e., trends in peak-T that increase both upwards and downwards. Gradual and more abrupt, fault-related transitions between these two modes also occur. Going upsection from the core of the Venediger basement where peak-T in excess of 550 °C is documented (Figure 4.5; e. g., Hoernes & Friedrichsen, 1974; Scharf et al., 2013b), we observe that temperatures first decrease to ca. 480 °C in the inverted lower limb of the Seidlwinkl sheath fold. Upsection from there, RSCM temperature increases again to ca. 520 °C along the contact between Glockner and Rote Wand nappes in the upper limb of the central part of the sheath fold. Further upsection towards the hanging wall of the Seidlwinkl sheath fold, RSCM temperature drops from ca. 520 °C to ca. 410 °C over a distance of only several hundred meters. East and west from the center of the Seidlwinkl fold, toward the western and eastern Tauern domes, the temperature inversion cannot be resolved unambiguously, either due to a lack of exposure of the Glockner and Rote Wand nappes or because it does not exist. North of the sheath fold, an inversion in the temperature gradient occurs at the contact of the Sub-Penninic Wörth Unit and the tectonically higher, Penninic Rauris Nappe, i. e., in the upper limb of the Wörth Antiform.

4.6 Discussion

4.6.1 Kinetic and Deformational Effects on the RSCM Thermometer

Kinetic and deformational effects were reported to potentially influence the RSCM thermometer. In cases that involve little deformation of the rocks containing CM, such as contact metamorphic settings, it has been shown that the graphitization process reaches steady state within several hundreds of years (Mori et al., 2017; Mori et al., 2015). This implies that on geological timescales, temperature is the main factor controlling the degree of graphitization of CM and kinetic effects are negligible. Kirilova et al. (2018) reported that brittle deformation decreases the degree of graphitization in CM by mechanical destruction of the crystal lattice. We avoided this effect by only analysing small isolated CM particles included in other mineral phases and clearly not affected by any brittle structures. On the other hand,

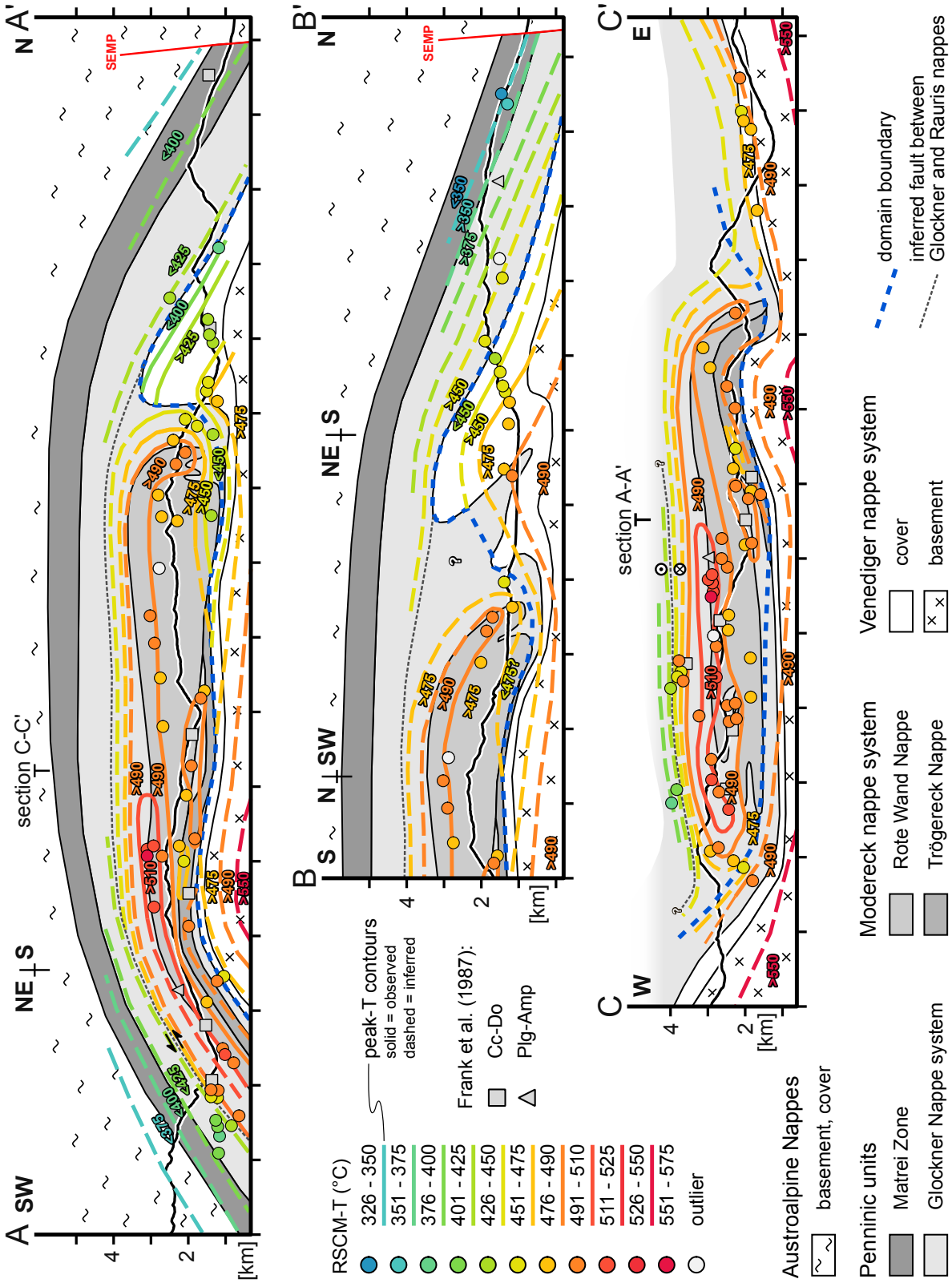

Figure 4.6: Profiles with RSCM temperatures of the central Tauern Window. Contours in these profiles are peak-T contours of both Barrovian and subduction-related metamorphic stages. See Figure 4.5 for traces of the section. A high-resolution version of this figure is available in Appendix I.4.

by comparing the crystallinity of large undeformed CM-flakes with CM aggregates in the schistosity

of a nearby shear zone, Barzoi (2015) showed that ductile strain can potentially increase the degree of graphitization in CM. Several observations indicate that such an effect did not substantially influence our results. First, we only measured unoriented CM inclusions and avoided CM aligned in shear zones or shear bands. Second, our results are well in line with other estimates on the peak-T conditions obtained with alternative methods (see above). Third, we observe a steady upward decrease of RSCM temperatures across the high-strain shear zone between the Glockner s. str. and Rauris nappes. This indicates that the degree of graphitization was not significantly affected by strain. Therefore, we see no evidence for any kinetic effects on our results.

4.6.2 Distinguishing Domains of Subduction- and Barrow-Related Metamorphism

Radiometric dating and thermobarometry (e. g., Dachs & Proyer, 2001; Kurz et al., 2008) show that the tectonic units in the Seidlwinkl sheath fold experienced a two-stage metamorphic evolution that is typical for subduction-collision orogens. In the map and cross sections (Figures 4.5 and 4.6), we distinguish parts of the Seidlwinkl sheath fold that still preserve subduction-related peak-T conditions from those where the peak-T are of the overprinting Barrovian metamorphism.

Discriminating between the subduction-related and the Barrovian metamorphic events in the central Tauern Window using thermometric data only is not easy. Both events reached very similar peak-T conditions of around 400-550 °C in different parts of the fold. Additionally, the peak-T pattern not only reflects the overprinting relationship of these two metamorphic events, but was also substantially modified by D5 deformation. RSCM data cannot discriminate between different metamorphic events in a single rock sample, since due to its irreversibility it yields peak-T only; in this sense it contrasts with geothermobarometry applied to multiple generations of minerals or mineral assemblages and their overprinting fabric relationships. In Figure 4.7, we sketch some potential overprinting patterns used in our interpretation of the RSCM data from the central Tauern Window. Note that unusual features, e. g., discontinuous or kinked iso-peak temperature lines (singularities), may occur in RSCM-temperature patterns (Figures 4.7b, c). These features reflect the irreversibility of the graphitization process. During a single metamorphic event, peak-T may have been reached diachronously, e. g., due to conductive heat flow from hotter to colder parts of the fold. Therefore, we refer to the isolines of peak-T as recorded by RSCM not as geotherms but as peak-T contours.

We base our distinction between subduction-related and Barrovian RSCM-temperature patterns on the following reasoning: The Barrovian event is younger than the subduction-related event, as proven by radiometric dating (e. g., Favaro et al., 2015; Zimmermann et al., 1994) and overprinting relationships (e. g., Dachs & Proyer, 2001). It is characterised by peak-T conditions that decrease with increasing distance from the cores of the western and eastern Tauern subdomes (Figure 4.1; e. g., Hoernes & Friedrichsen, 1974; Scharf et al., 2013b). We attribute inversions of this normal metamorphic gradient in the nappe stack to the inheritance of an older metamorphic event that was not overprinted by the Barrovian event (schematically shown in Figure 4.7b). Such an inversion occurs in the central Tauern Window in the lower limb of the Seidlwinkl sheath fold and at the base of the Rauris Nappe in the northern part of the study area (Figure 4.6). Therefore, we consider the RSCM temperature in the units below this inversion to reflect the peak-T during the Tauernkristallisation; the RSCM temperatures in the units above the inversion reflect the subduction-related peak-T pattern. Using this approach, we are able to define a metamorphic domain boundary between those areas of the central Tauern Window that were affected by the Barrovian overprint of the RSCM peak-T and those that still preserve the original subduction-related thermal peak conditions.

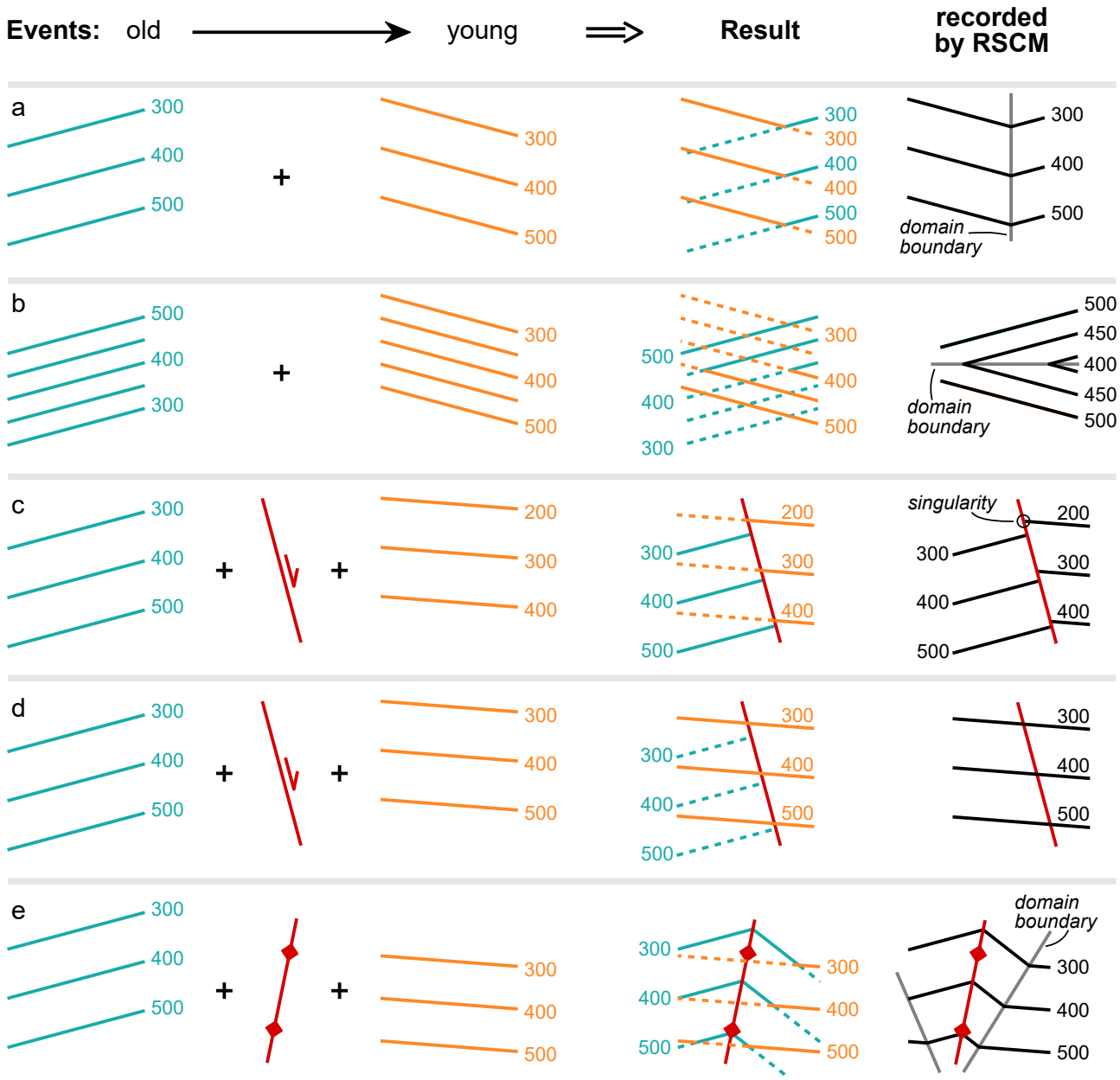

Figure 4.7: Hypothetical patterns of overlapping isotherms of two metamorphic stages and the associated peak-T contour patterns recorded by RSCM thermometry. (a) inclined T-fields of two metamorphic events are only partly recorded by RSCM thermometry; (b) inverted T-field partly overprinted by a normal-sense T-field. Inversion of apparent gradient in the RSCM-temperature pattern indicates boundary between old and young domain; (c) combination of metamorphism and faulting can lead to singularities in the RSCM-temperature pattern; (d) as in (c) but with more intense second metamorphic stage that erases the record of earlier stages; (e) combination of two-phase metamorphism and folding.

We projected RSCM-temperature estimates into cross sections (Figure 4.6) to construct peak-T contours highlighting the lateral and vertical variations in peak-T. Interpolating isolines involved some generalization of the RSCM results and the assumption that peak-T increased towards the cores of the WTD and ETD.

Very few temperature estimates had to be excluded from interpretation, mainly where their projection from the map into the cross section, e. g., due to strong non-cylindricity of the folds (Figure A.1) led to

outliers in the temperature pattern. However, we regard the first-order geometry and features of both peak-T domains summarized in Figure 4.8 as sufficiently robust for further interpretation.

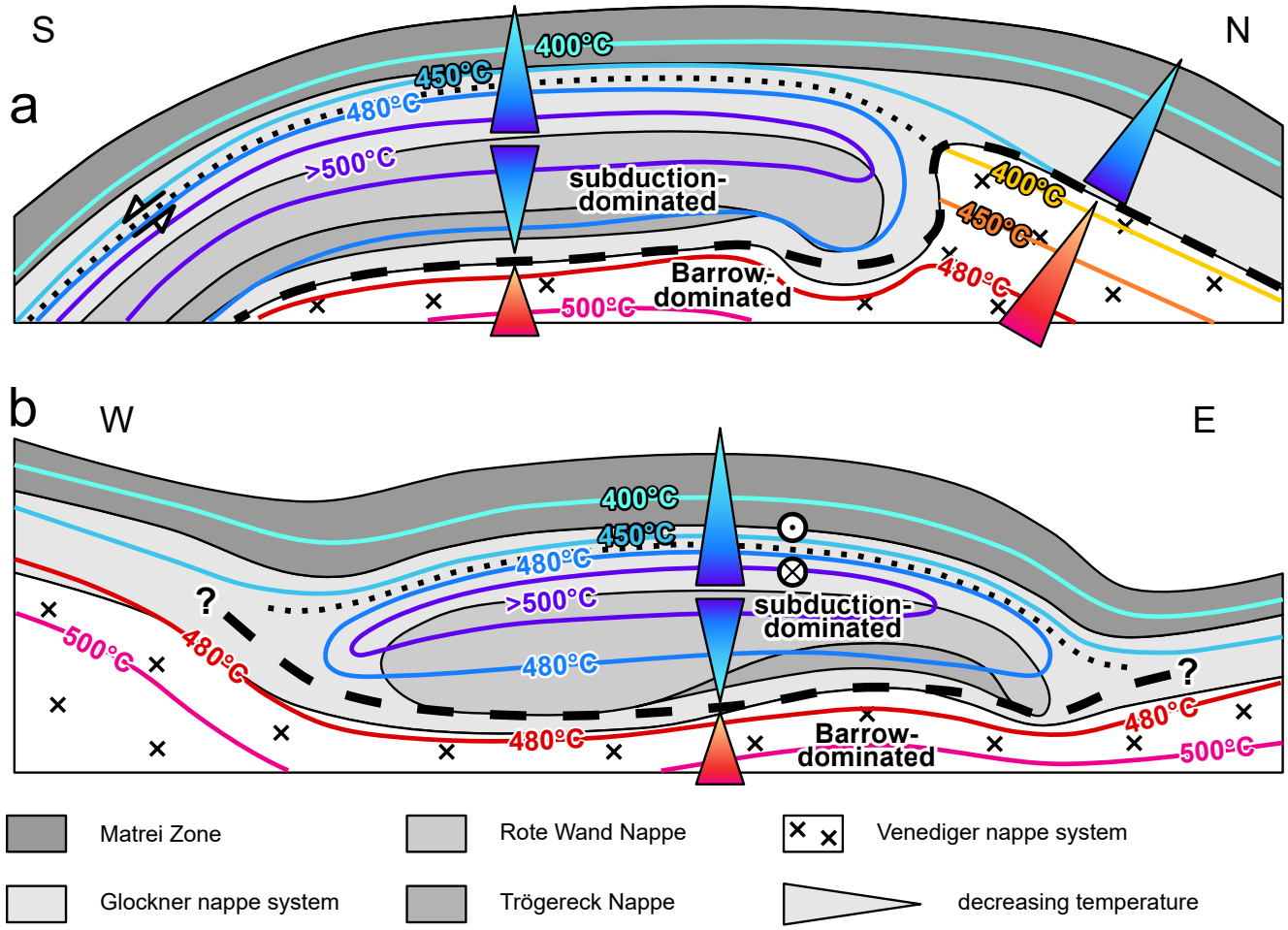

Figure 4.8: Sketch of the peak-T pattern in the Seidlwinkl sheath fold. The sections are parallel (a) and perpendicular (b) to the nappe transport direction. The boundary between subduction- and Barrow-related peak-T domains (dashed black line) is marked by inversion of the peak-T gradient. In the Barrovian domain, peak-T decreases away from the core of the basement domes. In the subduction domain, peak-T contours form a sheath-like pattern similar to the lithological layering.

4.6.3 Thermal Structure of the Barrovian Peak-T Domain

Over most of the study area, the Barrovian peak-T pattern is not observed in the RSCM data, since the older subduction-related peak-T were higher and their pattern is still preserved and exposed at the surface. An exception is the Wörth Unit (Figure 4.6). Large portions of the rocks belonging to this unit (mostly graphite-rich pelitic phyllites) are amassed in the Wörth Antiform, immediately north of the Seidlwinkl sheath fold (W. Frank, pers. comm August 2017; Groß et al., 2020b). In the Wörth Unit, the peak-T clearly decreases upwards, with peak values of ca. 490-500 °C (SE of Bucheben village, Figures 4.5 and Figure 4.8b) in the stratigraphically lowest part of the sedimentary cover sequence, close to the eastern Tauern subdome, where the Wörth Unit directly overlies the basement of the Venediger nappe system. Peak-T gradually decreases northward and upsection to ca. 430 °C in the upper (northern) limb of the Wörth Antiform, directly at the contact of the Wörth Unit with the overlying Rauris

Nappe. Where rocks above the metamorphic domain boundary are exposed at the surface, reconstruction of the Barrovian peak-T pattern relies on indirect evidence: The observed RSCM peak-T in the structurally lowest parts of the sheath fold provide an upper bound on the conditions reached during the Tauernkristallisation. In the central and northeastern part of the fold, the maximum estimate for the Barrovian temperature is ca. 480 °C as obtained on samples from the upper and lower Seidlwinkl Valley (Figure 4.5). At the base of the northwestern part of the sheath fold, exposed in the Fuscher Valley (near Ferleiten, Figure 4.5), the Barrovian peak-T is ca. 440 °C or less. At the southern border of the central Tauern Window near the town of Heiligenblut (Figure 4.5), where the Penninic nappes dip southwestward below the Austroalpine nappes, the RSCM data constrain the peak-T of Barrovian metamorphism to ca. 400 °C.

These observations are in line with the concentric pattern of Barrovian isograds in the Tauern Window (e. g., Hoinkes et al., 1999). Similar to the western and eastern Tauern subdomes, the metamorphic peak temperatures in the central Tauern depression decrease north- and southwards, nearly perpendicular to the east-west trend of the window. However, the structural depression in the central Tauern area coincides with a pronounced negative anomaly in the peak-T pattern. This is reflected by inwards-bending of lower-grade peak-T contours ($<$ ca. 450 °C) in the central Tauern depression, whereas higher-grade peak-T contours ($>$ ca. 500 °C) of the eastern and western Tauern domes do not connect across the depression. The peak-T contours are oblique to the main thrusts (e. g., D2 thrust fault between Glockner Nappe s. str. and Rote Wand Nappe) and large-scale D3 and D4 fold axes (e. g., fold axis of D4 Wörth Antiform) in the central Tauern depression. This indicates that the dominant structural imprint in this area predates the peak of the Barrovian "Tauernkristallisation" metamorphism. This is in line with independent microstructural observations (Figure 4.9), for example from the Wörth antiform, where the axial plane foliation defined by a prominent crenulation is overgrown by post-kinematic (post-D4) albite porphyroblasts, indicating heating after D4.

4.6.4 Thermal Structure of the Subduction-Related Peak-T Domain

The metamorphic domain boundary between peak-temperatures of the subduction-related and Barrovian domains is marked by an inversion in the direction of peak-T decrease (Figures 4.6 and 4.8). South of the Wörth Antiform, this inversion is located approximately in the lower limb of the Seidlwinkl sheath fold. In the northern limb of the Wörth Antiform, it is located at the base of the Rauris Nappe. There, peak-T decreases northward and upsection from ca. 460 °C to 350 °C, though details like the inclination of the peak-T contours cannot be resolved due to low sample coverage. The peak-T contours close to the northern margin of the central Tauern Window are more or less continuous with the iso-temperature contours reported for the western and eastern Tauern subdomes (Frank et al., 1987; Hoernes & Friedrichsen, 1974) that are thought to represent peak-T conditions of the Barrovian metamorphism (Scharf et al., 2013b). Therefore, the boundary between the subduction-related and the younger Barrow-related domain is poorly defined in the northernmost part of the central Tauern Window.

In the E-W cross-section (Figures 4.6 and 4.8) south of the Wörth Antiform, peak-T contours have an eye-shaped pattern in the inner part of the sheath fold and an omega-shaped pattern in its periphery. This pattern is well-resolved in the west but somewhat speculative in the east due to lower sample coverage. In the N-S cross-sections (Figures 4.6 and 4.8a), the peak-T contours are also curved and display a pattern very similar to the folded lithological layering. In essence, the high-grade peak-T contours in the Seidlwinkl sheath fold display a sheath-like pattern. This pattern is subparallel to the

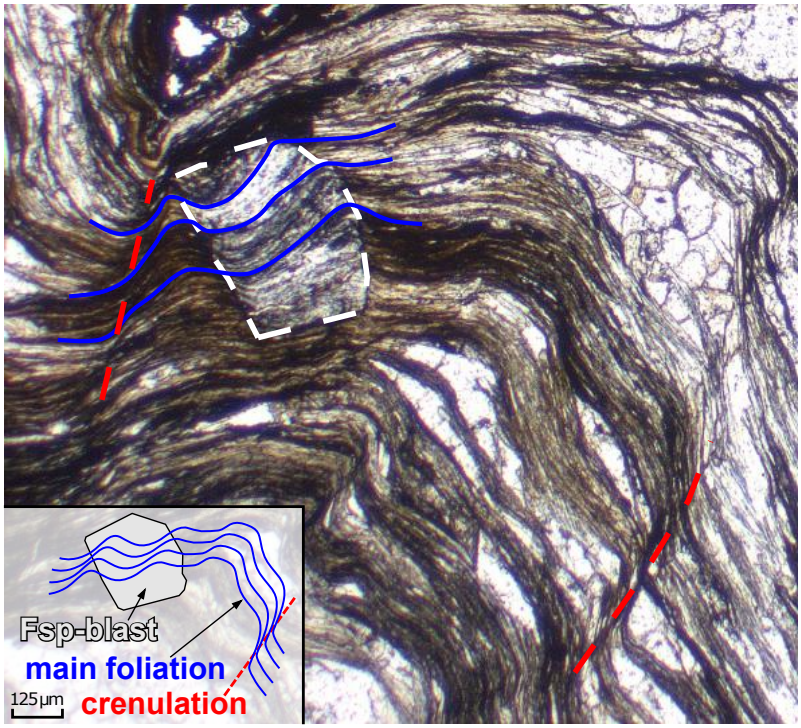

Figure 4.9: Post-kinematic feldspar porphyroblast in sample PG247 (47.19540°N 12.85067°E) overgrowing the axial plane foliation (i. e., crenulation) of the D4 Wörth antiform. The main foliation that is crenulated is the regional S3.

lithological layering that defines the sheath fold itself. However, the highest RSCM temperatures cluster along the D2 thrust boundary between the Glockner nappe s. str. and Rote Wand nappe.

In the south, towards the top of the Seidlwinkl sheath fold, the peak-T contours converge so that the 410 °C and 510 °C contours are only approximately one kilometer apart. This steep peak-T gradient of ca. 100 °C/km indicates post-peak-T tectonic thinning. This zone of thinning coincides with the nappe contact between the Glockner nappe s. str. and overlying Rauris nappe; it is a major D3 normal fault that partly accommodated the exhumation of the HP units in its footwall relative to the low-pressure units in its hanging wall (Groß et al., 2020b). The observation of narrowly spaced peak-T contours near the proposed contact is further independent evidence of this normal fault.

4.6.5 Formation of Sheath-Like Peak-T Pattern in the Alpine Subduction Zone

In an active subduction zone, the isotherm pattern is shaped by the rate of subduction, the temperature difference between the upper and lower plates bounding the zone, the length of the zone boundaries and by the characteristic heat diffusion length of rocks making up the subduction zone itself (Peacock, 1996). This pattern, schematically shown in Figure 4.10a, may be disturbed by varied thermal parameters of subducted rocks (e. g., Goffé et al., 2003) or when rock units start to move relative to its surroundings, e. g., when crustal nappes are sheared off from the downgoing slab and start to move relative to each other (Figure 4.10b). This was the case for D2 thrusting of the Glockner Nappe s. str. onto the Rote Wand Nappe and subsequent extrusion of the composite Rote Wand-Glockner s. str. Nappe during D3 (Groß et al., 2020b). However, the peak-T contours are not necessarily isotherms that were

"frozen in" at the moment when rocks in the Seidlwinkl fold began to ascend; individual RSCM temperatures are snapshots of the peak temperature when a rock started to cool. Rocks metamorphosed in settings dynamically changing from subduction to collision typically follow P-T-time paths where the temperature peak follows the maximum burial (highest P) with some delay (e. g., England & Thompson, 1984). P-T paths from the Rote Wand and Glockner s. str. nappes have shapes indicating that peak-T was reached after only a small decrease of pressure from maximum burial conditions and that further decompression was concomitant with slightly decreasing temperatures Dachs & Proyer, 2001; Groß et al., 2020b; Kurz et al., 2008. This suggests that during their exhumation, the Glockner s. str. and Rote Wand nappes were initially heated but then, during most of exhumation, cooled so that the peak-T contours behaved as passive markers during deformation.

The preservation of the highest peak-temperatures in the Seidlwinkl fold along the boundary between the Glockner s. str. and Rote Wand nappes can be explained by D2 thrusting of the former nappe onto the latter, assuming that upon attaining maximum depth immediately before D2, the Glockner Nappe s. str. was deeper and reached a higher peak-T than the Rote Wand Nappe. Another interpretation of the observed peak-T pattern is that it resulted from shear heating along the D2 thrust, i. e., the generation of heat due to viscous strain that caused a temperature rise (e. g., Molnar & England, 1990).

However, these two mechanisms, which are not mutually exclusive, cannot explain the decrease of peak-T to the east and west along the thrust plane, that is, towards the hinges of the Seidlwinkl Fold. Instead, the geometry of folded peak-T contours is similar to that of the D3 sheath fold pattern outlined by the lithological contacts, including the D2 thrust between the Glockner s. str. and Rote Wand nappes. This suggests that either the rocks within the Seidlwinkl sheath fold cooled below their peak-T between the D2 and D3 stages so that D3 folding of the contours was strictly passive, or that D3 started at temperatures close to the thermal peak and involved heat transported advectively by the exhuming Seidlwinkl fold. In that case, the D3 strain rates must have been high enough to maintain thermal disequilibrium, thus preventing smoothing of the contours due to heat loss (England & Molnar, 1993). In any case, the shear strain during D3 folding and mylonitic shearing was sufficiently high to rotate the initially oblique lithological contacts and peak-T contours into near-parallelism. In contrast, peak-temperature contours folded in shallower parts of an orogen are typically highly oblique to the lithological and nappe boundaries (e. g., Girault et al., 2020; Wiederkehr et al., 2011).

Classically, sheath folds are regarded to form by passive amplification of curved fold hinges in homogeneous simple shear (Cobbold & Quinquis, 1980). Domal structures on a surface subparallel to the shear plane will amplify into sheath folds that close in the direction of shear. Conversely, sheath folds closing in the opposite direction will form from depressions in the surface (Fossen & Rykkelid, 1990). Additionally, it has been shown that sheath folds also form by flow perturbation around weak (e. g., Exner & Dabrowski, 2010; Reber et al., 2012) or strong (e. g., Adamuszek & Dabrowski, 2017; Marques & Cobbold, 1995) inclusions in overall simple shear. While the initial geometry of the Rote Wand Nappe may have formed a domal perturbation in the D3 top-to-the-foreland shear zone (Groß et al., 2020b), the peak-T contours show an inverted temperature gradient throughout the Rote Wand nappe and any downward bulge in the contour pattern before shearing would have been transformed into a sheath fold closing opposite to the northward D3 shear direction. This is why in the light of our new thermometric data we favour strain variations perpendicular to the direction of transport (Alsop & Holdsworth, 2007; Xypolias & Alsop, 2014) as an alternative mechanism for the formation of the Seidlwinkl sheath fold. In sections through the fold that are close to the X-Z plane of D3 finite strain (Figures 4.6 and 4.8a), such variations exist between the top-to-the-south normal-sense shear zone along the top of the Glockner nappe s. str. and the top-to-the-north shear zone below. In the section perpendicular to the transport direction (Figures 4.6 and 4.8b), the eye- and omega-shaped patterns of the peak-T contours

can be explained by D3 top-to-the-north strain decreasing sideways from a maximum in the centre of the fold. In this interpretation, the D3 exhumation of the Glockner s. str. and Rote Wand nappes in the Seidlwinkl fold was diapiric in the purely kinematic sense of a tubular rock body that rises with respect to its wall rocks and that closes upwards in the direction of material flow (see also Kossak-Glowczewski et al., 2017). Unlike a classical pluton or salt diapir, however, the Seidlwinkl fold moved along bounding faults without disturbing the tectonostratigraphy of the surrounding rocks, i. e., as a pip-like extruding body (Wheeler et al., 2001).

Our observations are in line with a perturbation of the flow field in the subduction-exhumation zone with enhanced top-to-the-foreland flow in the core of the Seidlwinkl sheath fold. According to analogue and numerical models, flow perturbations may be caused by rheological heterogeneities in shear zones (Adamuszek & Dabrowski, 2017; Exner & Dabrowski, 2010; Marques & Cobbold, 1995; Reber et al., 2012). Such heterogeneities may well have been inherited along distal parts of continental passive margins where the continental crust is strongly segmented by normal faults (e. g., Boillot et al., 1989) and varies in composition and thickness. Therefore, Groß et al. (2020b) proposed that the Seidlwinkl fold originates from a promontory or extensional allochthon of the distal European margin that reached into the Alpine Tethys. If subducted, such isolated continental segments may provide first-order rheological and structural perturbations in the subduction channel where sheath folds can nucleate. We speculate that further amplification of the sheath fold happened at temperatures high enough to keep the viscosity contrast between different lithological layers < 10 which is the upper limit for sheath folding in analogue experiments (Marques et al., 2008). Strain localized in highly attenuated limbs of the exhuming fold nappe, while the hot ascending core preserved relics of HP assemblages from deeper parts of the subduction channel. So although D3 shearing affected the entire fold, its localization in the fold limbs with opposite-sense shearing (top-N thrusting in the footwall and top-S normal shearing in the footwall) enabled exhumation to shallower depths with a temperature of $\leq 400\,^{\circ}\mathrm{C}$. At that final stage, more proximal, less segmented parts of the European margin with more uniform thickness were underthrust below the Seidlwinkl sheath fold (Venediger nappe system) and the Wörth antiform developed in front of the Seidlwinkl sheath fold. This D4 deformation was highly cylindrical, indicating that during D4, lateral variations in the flow field had diminished and given way to more uniform flow. This style of deformation may be characteristic for more external and shallower parts of an orogen.

Sheath-fold formation is not a feature unique to deep parts of orogens or subduction channels (e. g., Alsop et al., 2007). However, large (i. e., nappe-scale) sheath folds require both a large initial perturbation and a shear zone that is even wider than the perturbation. Subduction of distal continental margins provides both ingredients for the formation of large sheath folds; a wide, high-strain shear zone in the subduction channel and structural-rheological perturbations in the form of subducted extensional allochthons and continental ribbons. As is suggested from the folded pattern of peak-temperature contours in the Seidlwinkl sheath fold, the formation of such large sheath folds can also partly involve diapir-like flow perturbations in an overall simple-shear dominated shear zone.

4.7 Summary and Conclusions

The distribution of peak-metamorphic temperatures in the central Tauern Window is consistent with a thermal history marked by two metamorphic events, each leaving behind a distinct peak-T pattern.

1. The younger event is the regional-scale, collision-related Barrovian metamorphic event known as Tauernkristallisation, characterised by a normal-sense geothermal gradient (i. e., upward-decreasing temperature) and peak-T decreasing away from the cores of the large subdomes towards the central depression and the surroundings of the Window.

2. The older metamorphic stage is related to Paleogene subduction. The area where the temperature pattern of this older event is still preserved corresponds with the areal extent of the Seidlwinkl sheath fold, an isoclinal and highly non-cylindrical fold nappe related to subduction and exhumation prior to collisional nappe stacking and Barrovian metamorphism. The peak-T contours of subduction-related metamorphism are folded and their geometry mimics that of the fold itself. The peak-T pattern is characterised by an inverted peak-thermal gradient in the fold's inverted lower limb and a normal gradient in the fold's upper limb. Peak-T contours close towards the northern, western and eastern parts of the fold, similar to lithological marker horizons marking the fold itself.

3. Narrowly spaced peak-T contours (100 °C drop over 1 km) at the top of the Seidlwinkl sheath fold are interpreted as independent evidence for the recently proposed substantial normal-sense offset within the Glockner nappe system (Groß et al., 2020b).

4. We propose that the sheath-like pattern of peak-T contours is the result of a change in the mode of nappe formation. During a first stage (Figure 4.10a), the hotter oceanic Glockner Nappe s. str. was thrust onto the colder continental Rote Wand Nappe. During the second stage (Figure 4.10b), the Rote Wand Nappe was then detached from the downgoing European lithosphere. Together with the overlying Glockner Nappe s. str., it started to exhume, cool and form a composite sheath fold nappe — the Seidlwinkl Fold. During this process, parts of the Glockner Nappe s. str. were wrapped around the Rote Wand Nappe. The previously established peak-T contours were deformed during exhumation and sheath folding. This second mode of nappe formation involving nappe folding is characterised by pervasive deformation of the whole fold nappe.

5. The sheath-like peak-T pattern can be explained by formation of the sheath fold as a diapir-like structure that formed during its ascent in the subduction channel. Such a diapir-like flow pattern requires lateral strain gradients, with the greatest amount of finite strain localized in the fold limbs with opposite-sense shear zones, and the greatest amount of exhumation in the centre of the sheath fold.

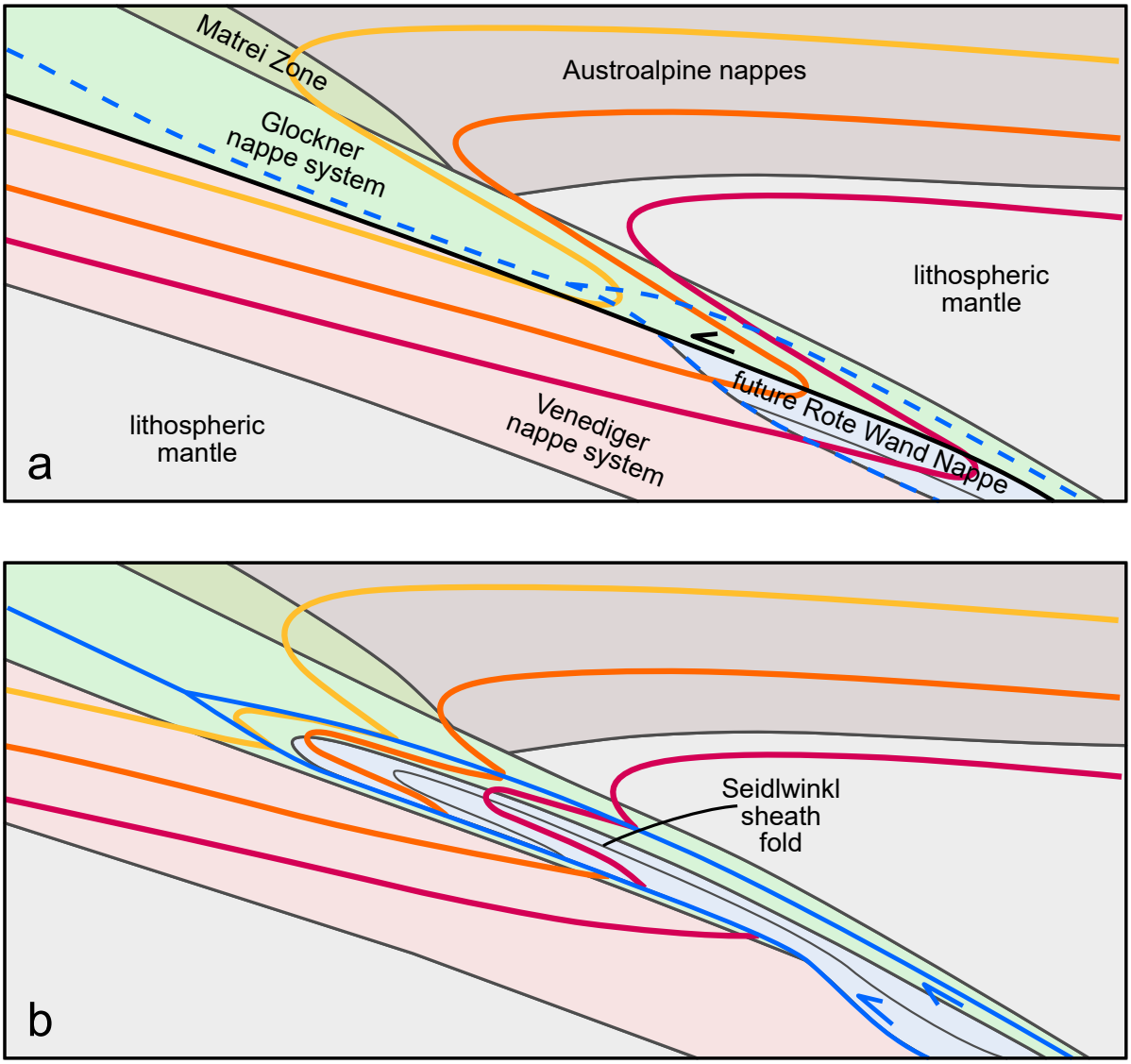

Figure 4.10: Schematic development of folded peak-T contours (red, orange and yellow lines) by formation of a sheath fold nappe during exhumation; inspired by Escher & Beaumont (1997). Before exhumation (a), isotherms in the subduction zone largely correspond to peak-T contours that are recorded by CM in the subducted rocks. These are largely subparallel to the lithological layering. With the onset of exhumation, the units start to cool and peak-T contours are preserved by CM. These lines act as markers that are passively deformed together with the folding rock. Further deformation during exhumation in an extrusion channel (b) leads to (sheath-) fold nappe formation and shearing of lithological markers and peak-T contours, resulting in a fold pattern that mimics that of the folded units. In the non-exhuming material, peak-T contours are constantly reset as peak-T increases in response to heat diffusion and advection.

Chapter 5

Conclusions

This study reveals that the central Tauern Window exhibits a multi-kilometer scale isoclinal sheath fold nappe, the Seidlwinkl sheath fold, that formed under high-pressure conditions in the Alpine subduction channel. It is a composite structure that folded an older thrust formed during subduction of the distal European margin in Cenozoic times. This thrust transported the oceanic Glockner Nappe s. str. onto the continental Rote Wand Nappe. The latter consists of a gneissic core covered by a Mesozoic sedimentary succession that traces the complex but well-ordered internal structure of the sheath fold. The fold shows pervasive top-to-the-foreland kinematics; only its top shows a top-to-the-hinterland shear zone. This shear zone marks the boundary of the high-pressure units in the fold to the low-pressure units in its hanging wall.

Thermobarometry on metasediments of the Glockner Nappe s. str., the Rote Wand Nappe and the Trögereck Nappe indicate peak-burial at conditions of around 2 GPa and 520 °C was followed by near-isothermal decompression to roughly 1 GPa. This decompression went along with the exhumation of the fold. It ascended inside of the subduction channel between two contemporaneous opposite-sense shear zones; normal-sense at the top of the fold and thrust-sense below.

By applying RSCM-thermometry on a large number of samples, the peak-temperature structure of the central Tauern Window was reconstructed. These results show that the peak-temperature structure in the Seidlwinkl sheath fold largely reflects the conditions attained during subduction metamorphism and was not substantially overprinted by later Barrovian metamorphism. The subduction-related thermal structure is characterised by a sheath-like geometry of peak-temperature contours. The highest peak-temperatures are located along the folded thrust of the Glockner nappe s. str. onto the Rote Wand Nappe, from where the temperatures decrease laterally and vertically. This reflects a change in the mode of nappe formation from (localised) thrusting to sheath fold nappe formation. The lateral decrease of peak-temperatures indicates that during exhumation and sheath fold formation, the amount of finite strain (i. e., top-to-the-foreland shearing) was greatest in the fold limbs of the sheath fold and decreased laterally (i. e., towards east and west). Therefore, together with the contemporaneous vertical strain gradients, the fold was shaped at least initially by diapir-like kinematics (Figure 5.1).

The correlation of the stratigraphy of the Rote Wand Nappe with other Europe-derived tectonic units in the central Tauern Window suggests that the distal European margin was strongly segmented after Mesozoic rifting. Here it is proposed that the Rote Wand Nappe originates from a small continental ribbon or extensional allochthon that was separated from the main margin by a zone of extremely thinned continental or transitional crust. The sedimentary infill of this rift basin is now mainly found in the Wörth Unit.

When this part of the European margin was subducted, the extensional allochthon was likely to have formed a first-order structural and rheological heterogeneity that substantially perturbed the flow in the subduction channel. Therefore, here it is proposed that the sheath fold may have nucleated at a rift-inherited crustal ribbon (i. e., extensional allochthon) in the subduction channel. It started to exhume as a diapir-like structure which was then subsequently amplified in the simple-shear dominated subduction channel. The driving force of the upward-directed flow may be forced channel flow, while positive buoyancy of the exhuming rock body is considered less plausible.

This study documents the existence of considerable along-strike heterogeneity in the deep part of a fossil subduction zone. Such heterogeneities may be significantly controlled by structures inherited from highly-segmented distal parts of continental margins. The example of the Seidlwinkl sheath fold illustrates how these inherited structures may evolve to large, highly non-cylindrical fold nappes during subduction and exhumation, in contrast to the classical model of largely cylindrical fold nappes. Considering that such structures can exist might be important in the interpretation of, e. g., seismic sections or numerical simulations of subduction zones. Such studies are often carried out in two dimensions, which might imply a higher degree of cylindricity than may be natural.

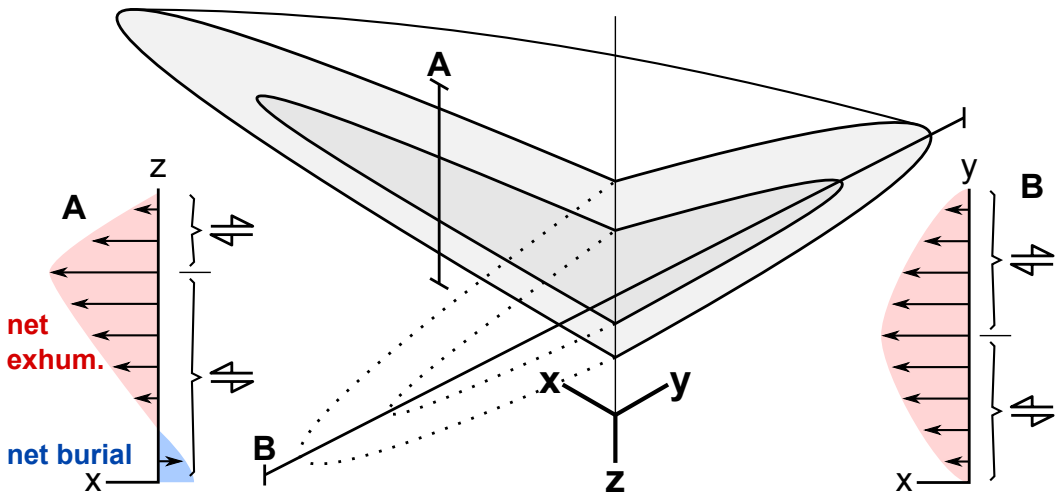

Figure 5.1: Strain gradients during an early stage of the formation of the Seidlwinkl sheath fold in the Alpine subduction channel, highlighting its diapiric character. Diagrams A and B schematically show displacement vectors (relative to a fixed upper plate) in the x-z- and x-y-plane, respectively. The relative positions of the sections are marked in the block diagram of the sheath fold, with hanging wall and footwall of the fold intentionally omitted.

Chapter 6

Outlook

From the research presented in this thesis, several new questions emerged, while others remain unanswered. The following lists some of those questions and topics, in the hope that they might inspire new lines of research.

- Are there structures similar to the Seidlwinkl sheath fold, in the Alps and elsewhere? How widespread is large-scale sheath folding in subduction-exhumation channels? When do they usually form with respect to the metamorphic peak? The recognition of similar structures might yield a more general understanding of the effects of distal margin subduction on the internal dynamics of subduction channels. A good candidate for such a comparative study might be the Adula Nappe in the Central Alps, which clearly shares many structural and metamorphic characteristics with the Seidlwinkl Fold.
- Thermo-mechanical modelling of subduction zones and exhumation in two dimensions is already challenging. However, sheath folds are inherently three-dimensional structures and modelling their evolution in a scenario similar to the one proposed in this study would require sophisticated three-dimensional numerical methods. Such simulations might give insights into the driving forces of the exhumation of small crustal ribbons and constrain the kinematics of sheath folding in such a scenario. Additionally, such models could explore the potential relevance of dynamic pressure, a topic shortly adressed in Chapter 3.
- Can structures similar to the Seidlwinkl sheath fold be imaged with geophysical methods (e. g., reciever functions). This question might be approached by, e. g., generating synthetic receiver function seismograms of internally well-structured (fold) nappes, a topic which is already partly adressed by the work of colleagues in the research project.
- Further constraining the rifting dynamics of the European continental margin now exposed in the central Tauern Window. This topic may be approached by a systematic, field-focussed study of facies variations in the Cretaceous (?) rift basin in the Tauern Window, especially concerning potential lateral transitions between the individual nappes. Similar studies in the Western and Central Alps were able to document, e. g., rift-related detachment faults and small extensional allochthons (e. g., Froitzheim & Manatschal, 1996; Ribes et al., 2020). Such a study might also provide more arguments for or against a Cretaceous age of rifting in these units.
- What is the age of oceanic crust formation in the Glockner nappe system? This is a critical question in the light of nappe correlations, paleogeographic reconstructions and convergence

estimates for the entire Alps. This subject could be addressed, e. g., by U-Pb-dating of magmatic zircon from oceanic basement rocks, a data set which is missing in the entire Tauern Window.

- What is the age of subduction and high-pressure metamorphism in the European margin? Previous attempts to answer this question focussed on the Eclogite Zone and produced contrasting results (e. g., Nagel et al., 2013; Zimmermann et al., 1994). In case of the Modereck Nappe system in the central Tauern Window, only one single Ar-Ar age is available (Kurz et al., 2008). This problem could potentially be tackled by using high-retentivity systems on refractory minerals like garnet, which are abundent in the Glockner Nappe s. str., Rote Wand Nappe and Trögereck Nappe.

Bibliography

Adamuszek, M. & Dabrowski, M. (2017). "Sheath folds as a strain gauge in simple shear". In: *Journal of Structural Geology* 102, pp. 21–36.

Agard, P., Plunder, A., Angiboust, S., Bonnet, G. & Ruh, J. (2018). "The subduction plate interface: rock record and mechanical coupling (from long to short timescales)". In: *Lithos* 320, pp. 537–566.

Agard, P., Monié, P., Jolivet, L. & Goffé, B. (2002). "Exhumation of the Schistes Lustrés complex: in situ laser probe 40Ar/39Ar constraints and implications for the Western Alps". In: *Journal of Metamorphic Geology* 20(6), pp. 599–618.

Agard, P., Yamato, P., Jolivet, L. & Burov, E. (2009). "Exhumation of oceanic blueschists and eclogites in subduction zones: timing and mechanisms". In: *Earth-Science Reviews* 92(1-2), pp. 53–79.

Alber, J. (1976). "Seriengliederung, Metamorphose und Tektonik des Hocharngebietes (Rauristertal/Salzburg)". PhD thesis. Universität Wien.

Alsop, G. & Carreras, J. (2007). "The structural evolution of sheath folds: A case study from Cap de Creus". In: *Journal of Structural Geology* 29(12), pp. 1915–1930.

Alsop, G., Holdsworth, R. & McCaffrey, K. (2007). "Scale invariant sheath folds in salt, sediments and shear zones". In: *Journal of Structural Geology* 29(10), pp. 1585–1604.

Alsop, G. I. & Holdsworth, R. (2006). "Sheath folds as discriminators of bulk strain type". In: *Journal of Structural Geology* 28(9), pp. 1588–1606.

– (2007). "Flow perturbation folding in shear zones". In: *Geological Society, London, Special Publications* 272(1), pp. 75–101.

Alsop, G. & Holdsworth, R. (2009). "Discussion of Sheath fold development with viscosity contrast: analogue experiments in bulk simple shear by Marques, FO, Guerreiro, SM, Fernandes, AR". In: *Journal of Structural Geology* 31(2), pp. 215–217.

– (2012). "The three dimensional shape and localisation of deformation within multilayer sheath folds". In: *Journal of Structural Geology* 44, pp. 110–128.

Angel, F. & Staber, R. (1952). "Gesteinswelt und Bau der Hochalm-Ankogel-Gruppe". In: *Wissenschaftliche Alpenvereinshefte* 13.

Angel, R. J., Alvaro, M., Miletich, R. & Nestola, F. (2017). "A simple and generalised P–T–V EoS for continuous phase transitions, implemented in EosFit and applied to quartz". In: *Contributions to Mineralogy and Petrology* 172(5), p. 29.

Aoya, M., Kouketsu, Y., Endo, S., Shimizu, H., Mizukami, T., Nakamura, D. & Wallis, S. (2010). "Extending the applicability of the Raman carbonaceous-material geothermometer using data from contact metamorphic rocks". In: *Journal of Metamorphic Geology* 28(9), pp. 895–914.

Argand, E. (1909). "L'exploration géologique des Alpes Pennines centrales". PhD thesis. Lausanne: Lausanne.

– (1911). "Les nappes de recouvrement des Alpes Pennines et leurs prolongements structuraux". In: *Beiträge zur geologischen Karte der Schweiz* 31, pp. 1–26.

– (1916). "Sur l'arc des Alpes occidentales". In: *Eclogae Geologicae Helvetiae* 14, pp. 145–191.

Ashley, K. T., Steele-MacInnis, M., Bodnar, R. J. & Darling, R. S. (2016). "Quartz-in-garnet inclusion barometry under fire: Reducing uncertainty from model estimates". In: *Geology* 44(9), pp. 699–702.

Ashley, K. T., Caddick, M. J., Steele-MacInnis, M. J., Bodnar, R. J. & Dragovic, B. (2014). "Geothermobarometric history of subduction recorded by quartz inclusions in garnet". In: *Geochemistry, Geophysics, Geosystems* 15(2), pp. 350–360.

Auzanneau, E., Schmidt, M., Vielzeuf, D. & Connolly, J. D. (2010). "Titanium in phengite: a geobarometer for high temperature eclogites". In: *Contributions to Mineralogy and Petrology* 159(1), pp. 1–24.

Babist, J., Handy, M., Konrad-Schmolke, M. & Hammerschmidt, K. (2006). "Precollisional, multistage exhumation of subducted continental crust: The Sesia Zone, western Alps". In: *Tectonics* 25(6).

Barzoi, S. C. (2015). "Shear stress in the graphitization of carbonaceous matter during the low-grade metamorphism from the northern Parang Mountains (South Carpathians) — Implications to graphite geothermometry". In: *International Journal of Coal Geology* 146, pp. 179–187.

Bauville, A. & Schmalholz, S. M. (2015). "Transition from thin-to thick-skinned tectonics and consequences for nappe formation: Numerical simulations and applications to the Helvetic nappe system, Switzerland". In: *Tectonophysics* 665, pp. 101–117.

Bayet, L., John, T., Agard, P., Gao, J. & Li, J.-L. (2018). "Massive sediment accretion at 80 km depth along the subduction interface: Evidence from the southern Chinese Tianshan". In: *Geology* 46(6), pp. 495–498.

Beaumont, C., Fullsack, P. & Hamilton, J. (1994). "Styles of crustal deformation in compressional orogens caused by subduction of the underlying lithosphere". In: *Tectonophysics* 232(1), pp. 119–132.

Beltrando, M., Rubatto, D. & Manatschal, G. (2010). "From passive margins to orogens: The link between ocean-continent transition zones and (ultra) high-pressure metamorphism". In: *Geology* 38(6), pp. 559–562.

Bertrand, M. (1884). "Rapports de structure des Alpes de Glaris et du bassin houiller du Nord". In: *Bulletin de la Société géologique de France* 3, pp. 318–330.

Beunk, F. & Page, L. (2001). "Structural evolution of the accretional continental margin of the Paleoproterozoic Svecofennian orogen in southern Sweden". In: *Tectonophysics* 339(1), pp. 67–92.

Beyssac, O., Goffé, B., Chopin, C. & Rouzaud, J. (2002). "Raman spectra of carbonaceous material in metasediments: a new geothermometer". In: *Journal of Metamorphic Geology* 20(9), pp. 859–871.

Bickle, M. & Powell, R. (1977). "Calcite-dolomite geothermometry for iron-bearing carbonates". In: *Contributions to Mineralogy and Petrology* 59(3), pp. 281–292.

Boillot, G., Mougenot, D., Girardeau, J. & Winterer, E. L. (1989). "Rifting Processes on the West Galicia Margin, Spain". In: *Extensional Tectonics and Stratigraphy of the North Atlantic Margins.* American Association of Petroleum Geologists.

Bonamici, C. E., Tikoff, B. & Goodwin, L. B. (2011). "Anatomy of a 10 km scale sheath fold, Mount Hay ridge, Arunta Region, central Australia: The structural record of deep crustal flow". In: *Tectonics* 30(6).

Borowicka, H. (1966). "Versuch einer stratigraphischen Gliederung des Dolomitmarmorzuges zwischen Dietersbach- und Mühlbachtal (Oberpinzgau, Salzburg)". In: *Unpublished report, Universität Wien.*

Bousquet, R., Goffé, B., Henry, P., Le Pichon, X. & Chopin, C. (1997). "Kinematic, thermal and petrological model of the Central Alps: Lepontine metamorphism in the upper crust and eclogitisation of the lower crust". In: *Tectonophysics* 273(1-2), pp. 105–127.

Bousquet, R., Oberhänsli, R., Schmid, S., Berger, A., Wiederkeher, M., Robert, C., Möller, A., Rosenberg, C., Koller, F., Molli, G. & Zeilinger, G. (2012). *Metamorphic framework of the Alps.* CCGM/CGMW.

Bousquet, R., Oberhänsli, R., Goffé, B., Wiederkehr, M., Koller, F., Schmid, S. M., Schuster, R., Engi, M., Berger, A. & Martinotti, G. (2008). "Metamorphism of metasediments at the scale of an orogen: A key to the Tertiary geodynamic evolution of the Alps". In: *Geological Society, London, Special Publications* 298(1), pp. 393–411.

Branney, M., Barry, T. & Godchaux, M. (2004). "Sheathfolds in rheomorphic ignimbrites". In: *Bulletin of Volcanology* 66(6), pp. 485–491.

Braumüller, E. (1939). "Der Nordrand des Tauernfensters zwischen dem Fuscher- und Rauristal". In: *Mitteilungen der Geologischen Gesellschaft Wien.*

Braumüller, E. & Prey, S. (1943). "Zur Tektonik der mittleren hohen Tauern". In: *Berichte des Reichsamts für Bodenforschung*, pp. 113–140.

Brun, J.-P. & Faccenna, C. (2008). "Exhumation of high-pressure rocks driven by slab rollback". In: *Earth and Planetary Science Letters* 272(1), pp. 1–7.

Brun, J. & Merle, O. (1988). "Experiments on folding in spreading-gliding nappes". In: *Tectonophysics* 145(1-2), pp. 129–139.

Burov, E., Jolivet, L., Le Pourhiet, L. & Poliakov, A. (2001). "A thermomechanical model of exhumation of high pressure (HP) and ultra-high pressure (UHP) metamorphic rocks in Alpine-type collision belts". In: *Tectonophysics* 342(1-2), pp. 113–136.

Carreras, J., Estrada, A. & White, S. (1977). "The effects of folding on the C-axis fabrics of a quartz mylonite". In: *Tectonophysics* 39(1). Fabrics, microstructures, and microtectonics, pp. 3–24.

Cavargna-Sani, M., Epard, J.-L. & Steck, A. (2014). "Structure, geometry and kinematics of the northern Adula nappe (Central Alps)". In: *Swiss Journal of Geosciences* 107(2-3), pp. 135–156.

Chapple, W. M. (1978). "Mechanics of thin-skinned fold-and-thrust belts". In: *Geological Society of America Bulletin* 89(8), pp. 1189–1198.

Chemenda, A. I., Mattauer, M., Malavieille, J. & Bokun, A. N. (1995). "A mechanism for syn-collisional rock exhumation and associated normal faulting: results from physical modelling". In: *Earth and Planetary Science Letters* 132(1), pp. 225–232.

Chetty, T., Yellappa, T., Mohanty, D., Nagesh, P., Sivappa, V., Santosh, M. & Tsunogae, T. (2012). "Mega sheath fold of the Mahadevi hills, Cauvery Suture Zone, southern India: Implication for accretionary tectonics". In: *Journal of the Geological Society of India* 80(6), pp. 747–758.

Chopin, C. (1984). "Coesite and pure pyrope in high-grade blueschists of the Western Alps: a first record and some consequences". In: *Contributions to Mineralogy and Petrology* 86(2), pp. 107–118.

Christensen, J. N., Selverstone, J., Rosenfeld, J. L. & DePaolo, D. J. (1994). "Correlation by Rb-Sr geochronology of garnet growth histories from different structural levels within the Tauern Window, Eastern Alps". In: *Contributions to Mineralogy and Petrology* 118(1), pp. 1–12.

Cliff, R. A., Droop, G. T. R. & Rex, D. C. (1985). "Alpine metamorphism in the south-east Tauern Window, Austria: 2. Rates of heating, cooling and uplift". In: *Journal of Metamorphic Geology* 3(4), pp. 403–415.

Cobbold, P. & Quinquis, H. (1980). "Development of sheath folds in shear regimes". In: *Journal of Structural Geology* 2(1), pp. 119–126.

Coggon, R. & Holland, T. (2002). "Mixing properties of phengitic micas and revised garnet-phengite thermobarometers". In: *Journal of Metamorphic Geology* 20(7), pp. 683–696.

Connolly, J. (2005). "Computation of phase equilibria by linear programming: a tool for geodynamic modeling and its application to subduction zone decarbonation". In: *Earth and Planetary Science Letters* 236(1), pp. 524–541.

Cornelius, H. P. & Clar, E. (1934). *Geologische Karte des Großglocknergebietes.* Wien: Geologische Bundesanstalt.

– (1935). *Erläuterungen zur geologischen Karte des Großglocknergebietes.* Wien: Geologische Bundesanstalt.

Cornelius, H. P. & Clar, E. (1939). *Geologie des Großglocknergebietes*. Wien: Zweigstelle Wien der Reichsstelle für Bodenforschung.

Cornish, S. & Searle, M. (2017). "3D geometry and kinematic evolution of the Wadi Mayh sheath fold, Oman, using detailed mapping from high-resolution photography". In: *Journal of Structural Geology* 101, pp. 26–42.

Dachs, E. (1986). "High-pressure mineral assemblages and their breakdown-products in metasediments South of the Grossvenediger, Tauern Window, Austria". In: *Schweizerische Mineralogische und Petrographische Mitteilungen* 66(1-2), pp. 145–161.

– (1990). "Geothermobarometry in metasediments of the southern Grossvenediger area (Tauern Window, Austria)". In: *Journal of Metamorphic Geology* 8(2), pp. 217–230.

Dachs, E., Kurz, W. & Proyer, A. (2005). "Alpine eclogites in the Tauern Window". In: *Mitteilungen der Österreichischen Mineralogischen Gesellschaft* 150, pp. 199–226.

Dachs, E. & Proyer, A. (2001). "Relics of high-pressure metamorphism from the Grossglockner region, Hohe Tauern, Austria". In: *European Journal of Mineralogy* 13(1), pp. 67–86.

Dahlen, F., Suppe, J. & Davis, D. (1984). "Mechanics of fold-and-thrust belts and accretionary wedges: Cohesive Coulomb theory". In: *Journal of Geophysical Research: Solid Earth* 89(B12), pp. 10087–10101.

Davies, J. H. & Blanckenburg, F. von (1995). "Slab breakoff: a model of lithosphere detachment and its test in the magmatism and deformation of collisional orogens". In: *Earth and Planetary Science Letters* 129(1-4), pp. 85–102.

Dell'Ertole, D. & Schellart, W. P. (2013). "The development of sheath folds in viscously stratified materials in simple shear conditions: An analogue approach". In: *Journal of Structural Geology* 56, pp. 129–141.

Desmurs, L., Manatschal, G. & Bernoulli, D. (2001). "The Steinmann Trinity revisited: mantle exhumation and magmatism along an ocean-continent transition: the Platta nappe, eastern Switzerland". In: *Geological Society, London, Special Publications* 187(1), pp. 235–266.

Diener, J. & Powell, R. (2012). "Revised activity–composition models for clinopyroxene and amphibole". In: *Journal of Metamorphic Geology* 30(2), pp. 131–142.

Diener, J., Powell, R., White, R. & Holland, T. (2007). "A new thermodynamic model for clino-and orthoamphiboles in the system Na2O–CaO–FeO–MgO–Al2O3–SiO2–H2O–O". In: *Journal of Metamorphic Geology* 25(6), pp. 631–656.

Dingeldey, C., Dallmeyer, R. D., Koller, F. & Massonne, H.-J. (1997). "P-T-t history of the Lower Austroalpine Nappe Complex in the "Tarntaler Berge" NW of the Tauern Window: implications for the geotectonic evolution of the central Eastern Alps". In: *Contributions to Mineralogy and Petrology* 129(1), pp. 1–19.

Droop, G. (1985). "Alpine metamorphism in the south-east Tauern Window, Austria: 1. P–T variations in space and time". In: *Journal of Metamorphic Geology* 3(4), pp. 371–402.

Eichhorn, R., Loth, G., Hoèll, R., Finger, F., Schermaier, A. & Kennedy, A. (2000). "Multistage Variscan magmatism in the central Tauern Window (Austria) unveiled by U/Pb SHRIMP zircon data". In: *Contributions to Mineralogy and Petrology* 139(4), pp. 418–435.

England, P. & Molnar, P. (1993). "The interpretation of inverted metamorphic isograds using simple physical calculations". In: *Tectonics* 12(1), pp. 145–157.

England, P. C. & Thompson, A. B. (1984). "Pressure—temperature—time paths of regional metamorphism I. Heat transfer during the evolution of regions of thickened continental crust". In: *Journal of Petrology* 25(4), pp. 894–928.

Escher, A. & Beaumont, C. (1997). "Formation, burial and exhumation of basement nappes at crustal scale: a geometric model based on the Western Swiss-Italian Alps". In: *Journal of Structural Geology* 19(7), pp. 955–974.

Evans, B. & Kohlstedt, D. L. (1995). "Rheology of rocks". In: *Rock Physics and Phase Relations: A Handbook of Physical Constants, AGU Ref. Shelf* 3, pp. 148–165.
Exner, C. (1956). *Geologische Karte der Umgebung von Gastein*. Wien: Geologische Bundesanstalt.
– (1957). *Erläuterungen zur geologischen Karte der Umgebung von Gastein*. Wien: Geologische Bundesanstalt.
Exner, C. (1949). "Tektonik, Feldspatausbildungen und deren gegenseitige Beziehungen in den östlichen Hohen Tauern". In: *Tschermaks mineralogische und petrographische Mitteilungen* 1(3), pp. 197–284.
– (1962). *Geologische Karte der Sonnblickgruppe*. Wien: Geologische Bundesanstalt.
– (1964). *Erläuterungen zur geologischen Karte der Sonnblickgruppe 1:50000*. Wien: Geologische Bundesanstalt.
Exner, U. & Dabrowski, M. (2010). "Monoclinic and triclinic 3D flanking structures around elliptical cracks". In: *Journal of Structural Geology* 32(12), pp. 2009–2021.
Favaro, S. (2016a). "Lithological map of the Sonnblick area. In: Response of orogenic crust to indentation by Adriatic continental lithosphere - Tauern Window, Eastern Alps (Austria)". PhD thesis. Freie Universität Berlin.
Favaro, S., Handy, M. R., Scharf, A. & Schuster, R. (2017). "Changing patterns of exhumation and denudation in front of an advancing crustal indenter, Tauern Window (Eastern Alps)". In: *Tectonics* 36(6), pp. 1053–1071.
Favaro, S. (2012). "Bericht 2012 über geologische Aufnahmen auf den Blättern 154 Rauris und 181 Obervellach". In: *Jahrbuch der Geologischen Bundesanstalt* 152(1-4), pp. 265–268.
– (2016b). "Response of orogenic crust to indentation by Adriatic continental lithosphere–Tauern Window, Eastern Alps (Austria)". PhD thesis. Freie Universität Berlin.
Favaro, S. & Schuster, R. (2012). "Bericht 2012 über geologische Aufnahmen auf den Blättern 154 Rauris, 155 Bad Hofgastein und 181 Obervellach". In: *Jahrbuch der Geologischen Bundesanstalt* 152(1-4), pp. 268–272.
Favaro, S., Schuster, R., Handy, M. R., Scharf, A. & Pestal, G. (2015). "Transition from orogen-perpendicular to orogen-parallel exhumation and cooling during crustal indentation — Key constraints from 147Sm/144Nd and 87Rb/87Sr geochronology (Tauern Window, Alps)". In: *Tectonophysics* 665, pp. 1–16.
Ferrando, S., Bernoulli, D. & Compagnoni, R. (2004). "The Canavese zone (internal Western Alps): a distal margin of Adria". In: *Schweizerische Mineralogische und Petrographische Mitteilungen* 84(1-20).
Fossen, H. & Rykkelid, E. (1990). "Shear zone structures in the Øygarden area, West Norway". In: *Tectonophysics* 174(3-4), pp. 385–397.
Frank, W., Höck, V. & Miller, C. (1987). "Metamorphic and tectonic history of the central Tauern Window". In: *Geodynamics of the Eastern Alps*, pp. 34–54.
Frank, W. (1965). "Zur Geologie des Guggernbachtales". PhD thesis. Universität Wien.
– (1969). "Geologie der Glocknergruppe". In: *Wissenschaftliche Alpenvereinshefte des Deutschen Alpenvereins* 21, pp. 95–111.
Frasl, G. & Frank, W. (1966). "Einführung in die Geologie des Penninikums im Tauernfenster mit besonderer Berücksichtigung des Mittelabschnittes im Oberpinzgau". In: *Der Aufschluß, Sonderheft* 15.
Frasl, G. (1958). "Zur Seriengliederung der Schieferhülle in den mittleren Hohen Tauern". In: *Jahrbuch der Geologischen Bundesanstalt* 101, pp. 323–472.
Frasl, G. & Frank, W. (1964). "Exkursion I/2: Mittlere Hohe Tauern". In: *Mitteilungen der Geologischen Gesellschaft in Wien* 57(1), pp. 17–31.
Frey, M., Desmons, J. & Neubauer, F. (1999). "The new metamorphic maps of the Alps: Introduction". In: *Schweizerische Mineralogische und Petrographische Mitteilungen* (79), pp. 1–4.

Frisch, W. (1979). "Tectonic progradation and plate tectonic evolution of the Alps". In: *Tectonophysics* 60(3-4), pp. 121–139.
– (1980). "Post-Hercynian formations of the western Tauern window: sedimentological features, depositional environment, and age". In: *Mitteilungen der Österreichischen Geologischen Gesellschaft* 71(72), pp. 49–63.
Frisch, W., Gommeringer, K., Kelm, U. & Popp, F. (1987). "The Upper Bündner Schiefer of the Tauern Window–A key to understanding Eoalpine orogenic processes in the Eastern Alps". In: *Geodynamics of the Eastern Alps*, pp. 55–69.
Frisch, W. (1976). "Ein modell zur alpidischen Evolution und Orogenese des Tauernfensters". In: *Geologische Rundschau* 65(1), pp. 375–393.
Froitzheim, N., Schmid, S. M. & Conti, P. (1994). "Repeated change from crustal shortening to orogen-parallel extension in the Austroalpine units of Graubünden". In: *Eclogae Geologicae Helvetiae* 87(2), pp. 559–612.
Froitzheim, N., Schmid, S. M. & Frey, M. (1996). "Mesozoic paleogeography and the timing of eclogite-facies metamorphism in the Alps: A working hypothesis". In: *Eclogae Geologicae Helvetiae* 89(1), p. 81.
Froitzheim, N. & Manatschal, G. (1996). "Kinematics of Jurassic rifting, mantle exhumation, and passive-margin formation in the Austroalpine and Penninic nappes (eastern Switzerland)". In: *Geological society of America bulletin* 108(9), pp. 1120–1133.
Fuhrman, M. L. & Lindsley, D. H. (1988). "Ternary-feldspar modeling and thermometry". In: *American Mineralogist* 73(3-4), pp. 201–215.
Gebauer, D. (1999). "Alpine geochronology of the Central and Western Alps: new constraints for a complex geodynamic evolution". In: *Schweizerische Mineralogische und Petrographische Mitteilungen* 79(1), pp. 191–208.
Gerya, T. (2015). "Tectonic overpressure and underpressure in lithospheric tectonics and metamorphism". In: *Journal of Metamorphic Geology* 33(8), pp. 785–800.
Ghosh, S., Hazra, S. & Sengupta, S. (1999). "Planar, non-planar and refolded sheath folds in the Phulad Shear Zone, Rajasthan, India". In: *Journal of Structural Geology* 21(12), pp. 1715–1729.
Girault, J., Bellahsen, N., Boutoux, A., Rosenberg, C., Nanni, U., Verlaguet, A. & Beyssac, O. (2020). "The 3-D Thermal Structure of the Helvetic Nappes of the European Alps: Implications for Collisional Processes". In: *Tectonics* 39(3), e2018TC005334.
Glodny, J., Ring, U., Kühn, A., Gleissner, P. & Franz, G. (2005). "Crystallization and very rapid exhumation of the youngest Alpine eclogites (Tauern Window, Eastern Alps) from Rb/Sr mineral assemblage analysis". In: *Contributions to Mineralogy and Petrology* 149(6), pp. 699–712.
Goffé, B., Bousquet, R., Henry, P. & Le Pichon, X. (2003). "Effect of the chemical composition of the crust on the metamorphic evolution of orogenic wedges". In: *Journal of Metamorphic Geology* 21(2), pp. 123–141.
Goscombe, B. (1991). "Intense non-coaxial shear and the development of mega-scale sheath folds in the Arunta Block, Central Australia". In: *Journal of Structural Geology* 13(3), pp. 299–318.
Grasemann, B., Wiesmayr, G., Draganits, E. & Fusseis, F. (2004). "Classification of Refold Structures". In: *The Journal of Geology* 112(1), pp. 119–125.
Green, E., Holland, T. & Powell, R. (2007). "An order-disorder model for omphacitic pyroxenes in the system jadeite-diopside-hedenbergite-acmite, with applications to eclogitic rocks". In: *American Mineralogist* 92(7), pp. 1181–1189.
Groß, P., Handy, M., John, T., Pestal, G. & Pleuger, J. (2020a). *Mineral Chemistry of Metapelites from the Modereck Nappe (central Tauern Window, Eastern Alps)*. DOI: 10.5880/fidgeo.2020.010.

Groß, P., Handy, M. R., John, T., Pestal, G. & Pleuger, J. (2020b). "Crustal-Scale Sheath Folding at HP Conditions in an Exhumed Alpine Subduction Zone (Tauern Window, Eastern Alps)". In: *Tectonics* 39(2).

Groß, P., Pleuger, J., Handy, M., Germer, M. & John, T. (2020c). *Raman spectroscopy of carbonaceous matter on metasediments from the central Tauern Window (Eastern Alps)*. DOI: 10.5880/fidgeo.2020.024.

Groß, P., Pleuger, J., Handy, M. R., Germer, M. & John, T. (2020d). "Evolving temperature field in a fossil subduction channel during the transition from subduction to collision (Tauern Window, Eastern Alps)". In: *Journal of Metamorphic Geology*.

Grujic, D., Casey, M., Davidson, C., Hollister, L. S., Kündig, R., Pavlis, T. & Schmid, S. (1996). "Ductile extrusion of the Higher Himalayan Crystalline in Bhutan: evidence from quartz microfabrics". In: *Tectonophysics* 260(1), pp. 21–43.

Grujic, D. & Mancktelow, N. S. (1995). "Folds with axes parallel to the extension direction: an experimental study". In: *Journal of Structural Geology* 17(2), pp. 279287–285291.

Hacker, B. R., Gerya, T. V. & Gilotti, J. A. (2013). "Formation and exhumation of ultrahigh-pressure terranes". In: *Elements* 9(4), pp. 289–293.

Handy, M. R., Herwegh, M., Kamber, B. S., Tietz, R. & Villa, I. M. (1996). "Geochronologic, petrologic and kinematic constraints on the evolution of the Err-Platta boundary, part of a fossil continent-ocean suture in the Alps (eastern Switzerland)". In: *Schweizerische Mineralogische und Petrographische Mitteilungen* 76(3), pp. 453–474.

Handy, M. R., Schmid, S. M., Bousquet, R., Kissling, E. & Bernoulli, D. (2010). "Reconciling plate-tectonic reconstructions of Alpine Tethys with the geological–geophysical record of spreading and subduction in the Alps". In: *Earth-Science Reviews* 102(3), pp. 121–158.

Handy, M. R., Ustaszewski, K. & Kissling, E. (2015). "Reconstructing the Alps–Carpathians–Dinarides as a key to understanding switches in subduction polarity, slab gaps and surface motion". In: *International Journal of Earth Sciences* 104(1), pp. 1–26.

Hanmer, S. & Greene, D. C. (2002). "A modern structural regime in the Paleoarchean (~3.64 Ga); Isua Greenstone Belt, southern West Greenland". In: *Tectonophysics* 346(3), pp. 201–222.

Haselton, H., Hovis, G. L., Hemingway, B. S. & Robie, R. A. (1983). "Calorimetric investigation of the excess entropy of mixing in analbite-sanidine solid solutions; lack of evidence for Na, K short-range order and implications for two-feldspar thermometry". In: *American Mineralogist* 68(3-4), pp. 398–413.

Heim, A. (1878). *Untersuchungen über den Mechanismus der Gebirgsbildung im Anschluss an die geologische Monographie der Tödi-Windgällen-Gruppe*. Vol. 1. Schwabe.

– (1922). *Geologie der Schweiz*. Vol. 2. 2.

Heinisch, H., Pestal, G., Stingl, V. & Hellerschmidt-Alber, H. (1995). *GK50 Blatt 123 Zell am See. Geologische Karte der Republik Österreich*. Wien: Geologische Bundesanstalt.

Henderson, J. R. (1981). "Structural analysis of sheath folds with horizontal X-axes, northeast Canada". In: *Journal of Structural Geology* 3(3), pp. 203–210.

Henk, A. (1993). "Subsidenz und Tektonik des Saar-Nahe-Beckens (SW-Deutschland)". In: *Geologische Rundschau* 82(1), pp. 3–19.

Hilty, L. (2013). "3D modeling of the Seidlwinkl-Nappe in the central Tauern Window, Austria". Bachelor Thesis. Universität Wien.

Höck, V. & Miller, C. (1987). "Mesozoic ophiolitic sequences and non-ophiolitic metabasites in the Hohe Tauern". In: *Geodynamics of the Eastern Alps*, pp. 16–33.

Höck, V. (1980). "Distribution maps of minerals of the Alpine metamorphism in the penninic Tauern window, Austria". In: *Mitteilungen der Österreichischen Geologischen Gesellschaft* 71(72), pp. 119–127.

Höck, V. & Pestal, G. (1994). *GK50 Blatt 153 Grossglockner. Geologische Karte der Republik Österreich.* Wien: Geologische Bundesanstalt.

Höck, V., Ślączka, A. & Uchman, A. (2006). "New biostratigraphic and palaeoenvironmental data on metamorphosed limestones from the northern margin of the Tauern Window (Eastern Alps, Austria)". In: *Austrian Journal of Earth Sciences* 99, pp. 42–56.

Hoernes, S. & Friedrichsen, H. (1974). "Oxygen Isotope Studies on Metamorphic Rocks of the Western Hohe Tauern Area (Austria)." In: *Schweizerische Mineralogische und Petrographische Mitteilungen* 54, pp. 769–788.

Höfer, C. & Tichy, G. (2005). "Fossilfunde aus dem Silbereckmarmor des Silberecks, Hafnergruppe (Hohe Tauern, Salzburg)". In: *Mitteilungen der Gesellschaft der Geologie- und Bergbaustudenten Österreichs* 47, pp. 145–158.

Hoinkes, G., Koller, F., Rantitsch, G., Dachs, E., Hock, V., Neubauer, F. & Schuster, R. (1999). "Alpine metamorphism of the Eastern Alps". In: *Schweizerische Mineralogische und Petrographische Mitteilungen* 79(1), pp. 155–181.

Holland, T. J. B. & Powell, R. (1998). "An internally consistent thermodynamic data set for phases of petrological interest". In: *Journal of Metamorphic Geology* 16(3), pp. 309–343.

Holland, T. (1979). "High water activities in the generation of high pressure kyanite eclogites of the Tauern Window, Austria". In: *The Journal of Geology* 87(1), pp. 1–27.

Hoschek, G. (2001). "Thermobarometry of metasediments and metabasites from the Eclogite zone of the Hohe Tauern, Eastern Alps, Austria". In: *Lithos* 59(3), pp. 127–150.

Hottinger, A. (1935). "Geologie der Gebirge zwischen der Sonnblick-Hocharn-Gruppe und dem Salzachtal in den östlichen Hohen Tauern". PhD thesis. ETH Zürich.

Houseman, G. A., McKenzie, D. P. & Molnar, P. (1981). "Convective instability of a thickened boundary layer and its relevance for the thermal evolution of continental convergent belts". In: *Journal of Geophysical Research: Solid Earth* 86(B7), pp. 6115–6132.

Inger, S. & Cliff, R. (1994). "Timing of metamorphism in the Tauern Window, Eastern Alps: Rb-Sr ages and fabric formation". In: *Journal of Metamorphic Geology* 12(5), pp. 695–707.

Jeřábek, P., Konopásek, J. & Žáčková, E. (2016). "Two-stage exhumation of subducted Saxothuringian continental crust records underplating in the subduction channel and collisional forced folding (Krkonoše-Jizera Mts., Bohemian Massif)". In: *Journal of Structural Geology* 89, pp. 214–229.

Jolivet, L., Faccenna, C., Goffé, B., Burov, E. & Agard, P. (2003). "Subduction tectonics and exhumation of high-pressure metamorphic rocks in the Mediterranean orogens". In: *American Journal of Science* 303(5), pp. 353–409.

Kiessling, W. (1992). "Palaeontological and facial features of the Upper Jurassic Hochstegen marble (Tauern window, Eastern Alps)". In: *Terra Nova* 4(2), pp. 184–197.

Kirilova, M., Toy, V., Rooney, J. S., Giorgetti, C., Gordon, K. C., Collettini, C. & Takeshita, T. (2018). "Structural disorder of graphite and implications for graphite thermometry". In: *Solid Earth* 9(1), p. 223.

Klebelsberg, R. V. (1940). "Ein Ammonit aus dem Hochstegen-Kalk des Zillertals (Tirol)". In: *Zeitschrift der Deutschen Geologischen Gesellschaft*, pp. 582–586.

Kleberger, J., Sägmüller, J. & Tichy, G. (1981). "Neue Fossilfunde aus der mesozoischen Schieferhülle der Hohen Tauern zwischen Fuschertal und Wolfbachtal (Unterpinzgau/Salzburg)". In: *Geologisch-Paläontologische Mitteilungen der Universität Innsbruck* 10, pp. 275–288.

Kohn, M. J. (2014). ""Thermoba-Raman-try": Calibration of spectroscopic barometers and thermometers for mineral inclusions". In: *Earth and Planetary Science Letters* 388, pp. 187–196.

Koller, F. & Pestal, G. (2003). "Die ligurischen Ophiolite der Tarntaler Berge und der Matreier Schuppenzone". In: *Geologische Bundesanstalt - Arbeitstagung 2003: Blatt 148 Brenner*, pp. 65–76.

Kossak-Glowczewski, J., Froitzheim, N., Nagel, T., Pleuger, J., Keppler, R., Leiss, B. & Régent, V. (2017). "Along-strike shear-sense reversal in the Vals-Scaradra Shear Zone at the front of the Adula Nappe (Central Alps, Switzerland)". In: *Swiss Journal of Geosciences* 110(2), pp. 677–697.

Kouketsu, Y., Mizukami, T., Mori, H., Endo, S., Aoya, M., Hara, H., Nakamura, D. & Wallis, S. (2014). "A new approach to develop the Raman carbonaceous material geothermometer for low-grade metamorphism using peak width". In: *Island Arc* 23(1), pp. 33–50.

Kreuss, O. (2013). *GK50 Blatt 124 Saalfelden am Steinernen Meer, preliminary Geofast map. Geologische Karte der Republik Österreich.* Wien: Geologische Bundesanstalt.

Kurz, W., Neubauer, F. & Genser, J. (1996). "Kinematics of Penninic nappes (Glockner Nappe and basement-cover nappes) in the Tauern Window (Eastern Alps, Austria) during subduction and Penninic-Austroalpine collision". In: *Eclogae Geologicae Helvetiae* 89(1), pp. 573–605.

Kurz, W., Neubauer, F., Genser, J. & Dachs, E. (1998). "Alpine geodynamic evolution of passive and active continental margin sequences in the Tauern Window (eastern Alps, Austria, Italy): a review". In: *Geologische Rundschau* 87(2), pp. 225–242.

Kurz, W. (2005). "Tectonic map and overall architecture of the Alpine orogen; Comment on an article by Stefan M. Schmid, Bernhard Fügenschuh, Eduard Kissling & Ralf Schuster 2004, Eclogae Geologicae Helvetiae, 97, 93–117". In: *Eclogae Geologicae Helvetiae* 98(1), pp. 97–98.

– (2006). "Penninic paleogeography from the Western toward the Eastern Alps—still open questions?" In: *International Geology Review* 48(11), pp. 996–1022.

Kurz, W., Handler, R. & Bertoldi, C. (2008). "Tracing the exhumation of the Eclogite Zone (Tauern Window, Eastern Alps) by 40Ar/39Ar dating of white mica in eclogites". In: *Swiss Journal of Geosciences* 101(1), pp. 191–206.

Lacassin, R. & Mattauer, M. (1985). "Kilometre-scale sheath fold at Mattmark and implications for transport direction in the Alps". In: *Nature* 315(6022), pp. 739–742.

Lahfid, A., Beyssac, O., Deville, E., Negro, F., Chopin, C. & Goffé, B. (2010). "Evolution of the Raman spectrum of carbonaceous material in low-grade metasediments of the Glarus Alps (Switzerland)". In: *Terra Nova* 22(5), pp. 354–360.

Lambert, R. S. J. (1970). "A Potassium-Argon Study of the Margin of the Tauernfenster at Döllach, Austria". In: *Eclogae Geologicae Helvetiae* 63, pp. 197–205.

Lammerer, B. (1986). "Das Autochthon im westlichen Tauernfenster". In: *Jahrbuch der Geologischen Bundesanstalt* 129(1), pp. 51–67.

Lammerer, B. & Weger, M. (1998). "Footwall uplift in an orogenic wedge: the Tauern Window in the Eastern Alps of Europe". In: *Tectonophysics* 285(3), pp. 213–230.

Lanari, P., Wagner, T. & Vidal, O. (2014). "A thermodynamic model for di-trioctahedral chlorite from experimental and natural data in the system MgO–FeO–Al2O3–SiO2–H2O: applications to P–T sections and geothermometry". In: *Contributions to Mineralogy and Petrology* 167(2), pp. 1–19.

Laubscher, H. (1969). "Mountain building". In: *Tectonophysics* 7(5-6), pp. 551–563.

Laubscher, H. (1971). "The large-scale kinematics of the western Alps and the northern Apennines and its palinspastic implications". In: *American Journal of Science* 271(3), pp. 193–226.

Ledoux, H. (1984). "Paläogeographie und tektonische Entwicklung im Penninikum des Tauern-Nordwestrandes im oberen Tuxer Tal". In: *Jahrbuch der Geologischen Bundesanstalt* 126, pp. 359–368.

Lemoine, M. (2003). "Schistes lustrés from Corsica to Hungary: back to the original sediments and tentative dating of partly azoic metasediments". In: *Bulletin de la Société géologique de France* 174(3), pp. 197–209.

Lemoine, M., Bas, T., Arnaud-Vanneau, A., Arnaud, H., Dumont, T., Gidon, M., Bourbon, M., Graciansky, P.-C. de, Rudkiewicz, J.-L., Megard-Galli, J., et al. (1986). "The continental margin of the Mesozoic Tethys in the Western Alps". In: *Marine and petroleum geology* 3(3), pp. 179–199.

Linner, M., Reitner, J. & Pavlik, W. (2013). *GK50 Blatt 179 Lienz. Geologische Karte der Republik Österreich*. Wien: Geologische Bundesanstalt.

Loprieno, A., Bousquet, R., Bucher, S., Ceriani, S., Dalla Torre, F. H., Fügenschuh, B. & Schmid, S. M. (2011). "The Valais units in Savoy (France): a key area for understanding the palaeogeography and the tectonic evolution of the Western Alps". In: *International Journal of Earth Sciences* 100(5), pp. 963–992.

Lugeon, M. (1902). "Les grandes nappes de recouvrement des Alpes du Chablais et de la Suisse". In: *Bulletin de la Société géologique de France* 4, pp. 723–825.

Lünsdorf, N. K., Dunkl, I., Schmidt, B. C., Rantitsch, G. & Eynatten, H. von (2017). "Towards a Higher Comparability of Geothermometric Data Obtained by Raman Spectroscopy of Carbonaceous Material. Part 2: A Revised Geothermometer". In: *Geostandards and Geoanalytical Research*.

Luth, S. W. & Willingshofer, E. (2008). "Mapping of the post-collisional cooling history of the Eastern Alps". In: *Swiss Journal of Geosciences* 101(1), pp. 207–223.

Manatschal, G. & Müntener, O. (2009). "A type sequence across an ancient magma-poor ocean–continent transition: the example of the western Alpine Tethys ophiolites". In: *Tectonophysics* 473(1-2), pp. 4–19.

Mancktelow, N. S. (1995). "Nonlithostatic pressure during sediment subduction and the development and exhumation of high pressure metamorphic rocks". In: *Journal of Geophysical Research: Solid Earth* 100(B1), pp. 571–583.

– (2008). "Tectonic pressure: theoretical concepts and modelled examples". In: *Lithos* 103(1), pp. 149–177.

Mancktelow, N. (1993). "Tectonic overpressure in competent mafic layers and the development of isolated eclogites". In: *Journal of Metamorphic Geology* 11(6), pp. 801–812.

Marques, F. O. (2009). "Reply to discussion by G.I. Alsop and R.E. Holdsworth of "Sheath fold development with viscosity contrast: analogue experiments in bulk simple shear" by Marques et al., Journal of Structural Geology, 30, 1348–1353." In: *Journal of Structural Geology* 2(31), pp. 218–219.

Marques, F. O. & Cobbold, P. (1995). "Development of highly non-cylindrical folds around rigid ellipsoidal inclusions in bulk simple shear regimes: natural examples and experimental modelling". In: *Journal of Structural Geology* 17(4), pp. 589–602.

Marques, F. O., Guerreiro, S. M. & Fernandes, A. R. (2008). "Sheath fold development with viscosity contrast: analogue experiments in bulk simple shear". In: *Journal of Structural Geology* 30(11), pp. 1348–1353.

Massonne, H.-J. & Willner, A. P. (2008). "Phase relations and dehydration behaviour of psammopelite and mid-ocean ridge basalt at very-low-grade to low-grade metamorphic conditions". In: *European Journal of Mineralogy* 20(5), pp. 867–879.

Maxelon, M. & Mancktelow, N. S. (2005). "Three-dimensional geometry and tectonostratigraphy of the Pennine zone, Central Alps, Switzerland and Northern Italy". In: *Earth-Science Reviews* 71(3-4), pp. 171–227.

Mies, J. W. (1993). "Structural analysis of sheath folds in the Sylacauga Marble Group, Talladega slate belt, southern Appalachians". In: *Journal of Structural Geology* 15(8), pp. 983–993.

Milnes, A. G. (1974). "Structure of the Pennine Zone (Central Alps): a new working hypothesis". In: *Geological society of America bulletin* 85(11), pp. 1727–1732.

Minnigh, L. (1979). "Structural analysis of sheath-folds in a meta-chert from the Western Italian Alps". In: *Journal of Structural Geology* 1(4), pp. 275–282.

Mohn, G., Manatschal, G., Beltrando, M. & Haupert, I. (2014). "The role of rift-inherited hyper-extension in Alpine-type orogens". In: *Terra Nova* 26(5), pp. 347–353.

Molnar, P. & England, P. (1990). "Temperatures, heat flux, and frictional stress near major thrust faults". In: *Journal of Geophysical Research: Solid Earth* 95(B4), pp. 4833–4856.

Mori, H., Mori, N., Wallis, S., Westaway, R. & Annen, C. (2017). "The importance of heating duration for Raman CM thermometry: evidence from contact metamorphism around the Great Whin Sill intrusion, UK". In: *Journal of Metamorphic Geology* 35(2), pp. 165–180.

Mori, N., Wallis, S. & Mori, H. (2015). "Graphitization of carbonaceous material in sedimentary rocks on short geologic time-scales: An example from the Kinsho-zan area, central Japan". In: *Island Arc* 24(2), pp. 119–130.

Moulas, E., Podladchikov, Y., Aranovich, L. Y. & Kostopoulos, D. (2013). "The problem of depth in geology: When pressure does not translate into depth". In: *Petrology* 21(6), pp. 527–538.

Nagel, T., Herwartz, D., Rexroth, S., Münker, C., Froitzheim, N. & Kurz, W. (2013). "Lu–Hf dating, petrography, and tectonic implications of the youngest Alpine eclogites (Tauern Window, Austria)". In: *Lithos* 170, pp. 179–190.

Neubauer, F. (2014). "The Structure of the Eastern Alps: From Eduard Suess to present-day Knowledge". In: *Austrian Journal of Earth Sciences* 107(1).

Newton, R., Charlu, T. & Kleppa, O. (1980). "Thermochemistry of the high structural state plagioclases". In: *Geochimica et Cosmochimica Acta* 44(7), pp. 933–941.

Nirrengarten, M., Mohn, G., Kusznir, N., Sapin, F., Despinois, F., Pubellier, M., Chang, S., Larsen, H. & Ringenbach, J. (2020). "Extension modes and breakup processes of the southeast China-Northwest Palawan conjugate rifted margins". In: *Marine and Petroleum Geology* 113, pp. 104–123.

Oberhänsli, R., Bousquet, R., Engi, M., Goffé, B., Gosso, G., Handy, M., Höck, V., Koller, F., Lardeaux, J., Polino, R., et al. (2004). "Metamorphic Structure of the Alps." In: *CCGM (Commission of the Geological Maps of the World), Paris.*

Okay, A. I., Xu, S. & Sengor, A. C. (1989). "Coesite from the Dabie Shan eclogites, central China". In: *European Journal of Mineralogy* 1(4), pp. 595–598.

Oxburgh, E., Lambert, R. S. J., Baadsgaard, H. & Simons, J. (1966). "Potassium argon age studies across the south-east margin of the Tauern Window, the Eastern Alps". In: *Verhandlungen der Geologischen Bundesanstalt* 1966, pp. 17–33.

Peacock, S. M. (1996). "Thermal and petrologic structure of subduction zones". In: *Subduction: top to bottom* 96, pp. 119–133.

Peer, H. & Zimmer, W. (1980). "Geologie der Nordrahmenzone der Hohen Tauern (Gasteiner Ache bis Saukarkopf-Großarltal)". In: *Jahrbuch der Geologischen Bundesanstalt* 123(2), pp. 411–466.

Péron-Pinvidic, G. & Manatschal, G. (2010). "From microcontinents to extensional allochthons: witnesses of how continents rift and break apart?" In: *Petroleum Geoscience* 16(3), pp. 189–197.

Pestal, G., Hejl, E., Braunstingl, R., Schuster, R., Draxler, I., Egger, H., Heinrich, M., Lenhardt, W., Letouze-Zezula, G., Linner, M., et al. (2009). *Geologische Karte von Salzburg 1:200000: Erläuterungen.* Ed. by R. Braunstingl. Wien: Geologische Bundesanstalt.

Pestal, G. (2014). *GK50 Blatt 154 Rauris, unpublished manuscript map. Geologische Karte der Republik Österreich.* Geologische Bundesanstalt.

Pestal, G. (2008). "Bericht 2006 und 2007 über geologische Aufnahmen auf Blatt 154 Rauris". In: *Jahrbuch der Geologischen Bundesanstalt* 148(2), pp. 262–264.

– (2009). "Bericht 2008 über geologische Aufnahmen auf Blatt 154 Rauris". In: *Jahrbuch der Geologischen Bundesanstalt* 149(4), pp. 545–546.

Pestal, G., Hejl, E., Egger, H., Van Husen, D., Linner, M., Mandl, M., Moser, M., Reitner, J., Rupp, C. & Schuster, R. (2005). *Geologische Karte von Salzburg 1:200000.* Ed. by R. Braunstingl. Wien: Geologische Bundesanstalt.

Pestal, G. & Hellerschmidt-Alber, J. (2011). "Bericht 2009 und 2010 über geologische Aufnahmen auf Blatt 154 Rauris". In: *Jahrbuch der Geologischen Bundesanstalt* 151(1+2), pp. 142–147.

Petrini, K. & Podladchikov, Y. (2000). "Lithospheric pressure-depth relationship in compressive regions of thickned crust". In: *Journal of Metamorphic Geology* 18(1), pp. 67–78.

Platt, J. (1986). "Dynamics of orogenic wedges and the uplift of high-pressure metamorphic rocks". In: *Geological society of America bulletin* 97(9), pp. 1037–1053.

Pleuger, J., Froitzheim, N. & Jansen, E. (2005). "Folded continental and oceanic nappes on the southern side of Monte Rosa (western Alps, Italy): Anatomy of a double collision suture". In: *Tectonics* 24(4).

Pleuger, J. & Podladchikov, Y. Y. (2014). "A purely structural restoration of the NFP20-East cross section and potential tectonic overpressure in the Adula nappe (central Alps)". In: *Tectonics* 33(5), pp. 656–685.

Prey, S. (1964). "Die Matreier Zone in der Sadniggruppe". In: *Erläuterungen zur geologischen Karte der Sonnblickgruppe*. Ed. by C. Exner. Wien: Geologische Bundesanstalt, pp. 131–151.

Proyer, A., Dachs, E. & Kurz, W. (1999). "Relics of high-pressure metamorphism from the Großglockner region, Hohe Tauern, Austria: Textures and mineral chemistry of retrogressed eclogites". In: *Mitteilungen der Österreichischen Geologischen Gesellschaft* (90), pp. 43–55.

Ramberg, H. (1964). "Selective buckling of composite layers with contrasted rheological properties, a theory for simultaneous formation of several orders of folds". In: *Tectonophysics* 1(4), pp. 307–341.

Ramsay, J. G. & Huber, M. I. (1987). *The Techniques of Modern Structural Geology. Volume 2: Folds and Fractures*. Vol. 2. Academic Press, pp. 309–700.

Ratschbacher, L., Dingeldey, C., Miller, C., Hacker, B. R. & McWilliams, M. O. (2004). "Formation, subduction, and exhumation of Penninic oceanic crust in the Eastern Alps: time constraints from 40 Ar/39 Ar geochronology". In: *Tectonophysics* 394(3), pp. 155–170.

Ratschbacher, L., Frisch, W., Linzer, H.-G. & Merle, O. (1991). "Lateral extrusion in the Eastern Alps, part 2: structural analysis". In: *Tectonics* 10(2), pp. 257–271.

Reber, J. E., Dabrowski, M. & Schmid, D. W. (2012). "Sheath fold formation around slip surfaces". In: *Terra Nova* 24(5), pp. 417–421.

Reddy, S., Cliff, R. & East, R. (1993). "Thermal history of the Sonnblick Dome, south-east Tauern Window, Austria: implications for heterogeneous uplift within the Pennine basement". In: *Geologische Rundschau* 82(4), pp. 667–675.

Reich, S. & Thomsen, C. (2004). "Raman spectroscopy of graphite". In: *Philosophical Transactions of the Royal Society of London. Series A: Mathematical, Physical and Engineering Sciences* 362(1824), pp. 2271–2288.

Reitz, E., Höll, R., Hupak, W. & Mehltretter, C. (1990). "Palynologischer Nachweis von Unterkreide in der Jüngeren (Oberen) Schieferhülle des Tauernfensters (Ostalpen)". In: *Jahrbuch der Geologischen Bundesanstalt* 133(4), pp. 611–618.

Ribes, C., Ghienne, J.-F., Manatschal, G., Dall'Asta, N., Stockli, D. F., Galster, F., Gillard, M. & Karner, G. D. (2020). "The Grès Singuliers of the Mont Blanc region (France and Switzerland): stratigraphic response to rifting and crustal necking in the Alpine Tethys". In: *International Journal of Earth Sciences*, pp. 1–28.

Ribes, C., Manatschal, G., Ghienne, J.-F., Karner, G. D., Johnson, C. A., Figueredo, P. H., Incerpi, N. & Epin, M.-E. (2019). "The syn-rift stratigraphic record across a fossil hyper-extended rifted margin: the example of the northwestern Adriatic margin exposed in the Central Alps". In: *International Journal of Earth Sciences* 108(6), pp. 2071–2095.

Roberts, A. (1989). "Fold and thrust structures in the Kintradwell 'Boulder beds', Moray Firth". In: *Scottish Journal of Geology* 25(2), pp. 173–186.

Rockenschaub, M., Kolenprat, B. & Nowotny, A. (2003). "Das westliche Tauernfenster". In: *Arbeitstagung*, pp. 7–38.

Rosas, F., Marques, F. O., Luz, A. & Coelho, S. (2002). "Sheath folds formed by drag induced by rotation of rigid inclusions in viscous simple shear flow: nature and experiment". In: *Journal of Structural Geology* 24(1), pp. 45–55.

Rosenberg, C., Brun, J.-P., Cagnard, F. & Gapais, D. (2007). "Oblique indentation in the Eastern Alps: insights from laboratory experiments". In: *Tectonics* 26(2).

Rosenberg, C. L., Schneider, S., Scharf, A., Bertrand, A., Hammerschmidt, K., Rabaute, A. & Brun, J.-P. (2018). "Relating collisional kinematics to exhumation processes in the Eastern Alps". In: *Earth-Science Reviews* 176, pp. 311–344.

Rutland, R. (1965). "Tectonic overpressures". In: *Controls of metamorphism*, pp. 119–139.

Sander, B. (1914). "Geologische Studien am Westende der Hohen Tauern". In: *Denkschriften der Kaiserlichen Akademie der Wissenschaften* 82, pp. 257–320.

Schaltegger, U., Desmurs, L., Manatschal, G., Müntener, O., Meier, M., Frank, M. & Bernoulli, D. (2002). "The transition from rifting to sea-floor spreading within a magma-poor rifted margin: Field and isotopic constraints". In: *Terra Nova* 14(3), pp. 156–162.

Schardt, H. (1893). "Sur l'origine des Préalpes romandes". In: *Eclogae Geologicae Helvetiae* 4, pp. 129–142.

– (1898). "Les régions exotiques du versant nord des Alpes suisses". In: *Bulletin de la Société vaudoise des sciences naturelles* 34, pp. 114–219.

Scharf, A., Handy, M., Favaro, S., Schmid, S. M. & Bertrand, A. (2013a). "Modes of orogen-parallel stretching and extensional exhumation in response to microplate indentation and roll-back subduction (Tauern Window, Eastern Alps)". In: *International Journal of Earth Sciences* 102(6), pp. 1627–1654.

Scharf, A., Handy, M., Ziemann, M. & Schmid, S. (2013b). "Peak-temperature patterns of polyphase metamorphism resulting from accretion, subduction and collision (eastern Tauern Window, European Alps)–a study with Raman microspectroscopy on carbonaceous material (RSCM)". In: *Journal of Metamorphic Geology* 31(8), pp. 863–880.

Scharf, A., Handy, M. R., Schmid, S. M., Favaro, S., Sudo, M., Schuster, R. & Hammerschmidt, K. (2016). "Grain-size effects on the closure temperature of white mica in a crustal-scale extensional shear zone—Implications of in-situ 40Ar/39Ar laser-ablation of white mica for dating shearing and cooling (Tauern Window, Eastern Alps)". In: *Tectonophysics* 674, pp. 210–226.

Schenker, F., Schmalholz, S., Moulas, E., Pleuger, J., Baumgartner, L., Podladchikov, Y., Vrijmoed, J., Buchs, N. & Müntener, O. (2015). "Current challenges for explaining (ultra) high-pressure tectonism in the Pennine domain of the Central and Western Alps". In: *Journal of Metamorphic Geology* 33(8), pp. 869–886.

Schmid, S. M., Fügenschuh, B., Kissling, E. & Schuster, R. (2004). "Tectonic map and overall architecture of the Alpine orogen". In: *Eclogae Geologicae Helvetiae* 97(1), pp. 93–117.

– (2005). "Reply to Comment by W. Kurz on "Tectonic map and overall architecture of the Alpine orogen"". In: *Eclogae Geologicae Helvetiae* 98(1), pp. 99–101.

Schmid, S. M., Pfiffner, O.-A., Froitzheim, N., Schönborn, G. & Kissling, E. (1996). "Geophysical-geological transect and tectonic evolution of the Swiss-Italian Alps". In: *Tectonics* 15(5), pp. 1036–1064.

Schmid, S. M., Rück, P. & Schreurs, G. (1990). "The significance of the Schams nappes for the reconstruction of the paleotectonic and orogenic evolution of the Penninic zone along the NFP-20 East traverse (Grisons, eastern Switzerland)". In: *Mémoires de la Société géologique de France (1833)* 156, pp. 263–287.

Schmid, S. M., Scharf, A., Handy, M. R. & Rosenberg, C. L. (2013). "The Tauern Window (Eastern Alps, Austria): a new tectonic map, with cross-sections and a tectonometamorphic synthesis". In: *Swiss Journal of Geosciences* 106(1), pp. 1–32.

Schmidt, C. & Ziemann, M. A. (2000). "In-situ Raman spectroscopy of quartz: A pressure sensor for hydrothermal diamond-anvil cell experiments at elevated temperatures". In: *American Mineralogist* 85(11-12), pp. 1725–1734.

Schmidt, K. (2015). "Microstructural and thermobarometric investigations of high-pressure mineral assemblages in metapelites of the Modereck Nappe Complex (Tauern Window, Austria)". MA thesis. Freie Universität Berlin.

Schmidt, K., Handy, M. R., Scharf, A., Milke, R., John, T. & Oberhänsli, R. (2014). "First evidence of subduction-related metamorphism in the most distal European continental margin unit of the Eastern Alps (Modereck Nappe, Tauern Window)". In: *TSK15 Potsdam 2014 Abstract Volume*.

Schuster, R. (2015). "Zur Geologie der Ostalpen". In: *Abhandlungen der Geologischen Bundesanstalt* 64, pp. 143–165.

Searle, M. & Alsop, G. (2007). "Eye-to-eye with a mega–sheath fold: A case study from Wadi Mayh, northern Oman Mountains". In: *Geology* 35(11), pp. 1043–1046.

Selverstone, J. (1993). "Micro- to macroscale interactions between deformational and metamorphic processes, Tauern Window, Eastern Alps". In: *Schweizerische Mineralogische und Petrographische Mitteilungen* 73(2), pp. 229–239.

Selverstone, J., Spear, F. S., Franz, G. & Morteani, G. (1984). "High-pressure metamorphism in the SW Tauern Window, Austria: PT paths from hornblende-kyanite-staurolite schists". In: *Journal of Petrology* 25(2), pp. 501–531.

Skjernaa, L. (1989). "Tubular folds and sheath folds: definitions and conceptual models for their development, with examples from the Grapesvare area, northern Sweden". In: *Journal of Structural Geology* 11(6), pp. 689–703.

Smye, A. J., Bickle, M. J., Holland, T. J., Parrish, R. R. & Condon, D. J. (2011). "Rapid formation and exhumation of the youngest Alpine eclogites: A thermal conundrum to Barrovian metamorphism". In: *Earth and Planetary Science Letters* 306(3-4), pp. 193–204.

Spear, F. (2014). "The duration of near-peak metamorphism from diffusion modelling of garnet zoning". In: *Journal of Metamorphic Geology* 32(8), pp. 903–914.

Stampfli, G. M. & Borel, G. D. (2004). "The TRANSMED Transects in Space and Time: Constraints on the Paleotectonic Evolution of the Mediterranean Domain". In: *The TRANSMED Atlas. The Mediterranean Region from Crust to Mantle*. Ed. by W. Cavazza, F. Roure, W. Spakman, G. Stampfli & P. Ziegler. Springer, pp. 53–80.

Staub, R. (1924). "Der Bau der Alpen". In: *Beiträge zur geologischen Karte der Schweiz* 52, p. 107.

Steck, A., Epard, J.-L. & Masson, H. (2019). "The Maggia nappe: an extruding sheath fold basement nappe in the Lepontine gneiss dome of the Central Alps". In: *International Journal of Earth Sciences*, pp. 1–14.

Steck, A. & Hunziker, J. (1994). "The Tertiary structural and thermal evolution of the Central Alps—compressional and extensional structures in an orogenic belt". In: *Tectonophysics* 238(1-4), pp. 229–254.

Stöckhert, B., Massonne, H.-J. & Nowlan, E. U. (1997). "Low differential stress during high-pressure metamorphism: the microstructural record of a metapelite from the Eclogite Zone, Tauern Window, Eastern Alps". In: *Lithos* 41(1-3), pp. 103–118.

Suess, E. (1909). *Das Antlitz der Erde*. Vol. 3. 2. Wien: Tempsky, p. 789.

Tajčmanová, L., Connolly, J. A. D. & Cesare, B. (2009). "A thermodynamic model for titanium and ferric iron solution in biotite". In: *Journal of Metamorphic Geology* 27(2), pp. 153–165.

Tajčmanová, L., Podladchikov, Y., Powell, R., Moulas, E., Vrijmoed, J. C. & Connolly, J. A. D. (2014). "Grain-scale pressure variations and chemical equilibrium in high-grade metamorphic rocks". In: *Journal of Metamorphic Geology* 32(2), pp. 195–207.

Takashima, R., Nishi, H., Huber, B. T. & Leckie, R. M. (2006). "Greenhouse World and the Mesozoic Ocean". In: *Oceanography*.

Talbot, C. J. & Jackson, M. P. (1987a). "Salt tectonics". In: *Scientific American* 257(2), pp. 70–79.

Talbot, C. & Jackson, M. (1987b). "Internal kinematics of salt diapirs". In: *AAPG Bulletin* 71(9), pp. 1068–1093.
Termier, P. (1904). "Les nappes des Alpes orientales et la synthèse des Alpes". In: *Bulletin de la Société géologique de France*.
– (1906). *La synthèse géologique des Alpes*. Liège.
Thiele, O. (1980). "Der Geologische Aufbau Österreichs". In: ed. by R. Oberhauser. Springer. Chap. Das Tauernfenster, pp. 300–314.
Thiele, O. (1974). "Tektonische Gliederung der Tauernschieferhülle zwischen Krimml und Mayrhofen". In: *Jahrbuch der Geologischen Bundesanstalt* 117, pp. 55–74.
Thiessen, R. (1986). "Two-dimensional refold interference patterns". In: *Journal of Structural Geology* 8(5), pp. 563–573.
Thomas, J. B. & Spear, F. S. (2018). "Experimental study of quartz inclusions in garnet at pressures up to 3.0 GPa: evaluating validity of the quartz-in-garnet inclusion elastic thermobarometer". In: *Contributions to Mineralogy and Petrology* 173, pp. 1–14.
Tinkham, D. K., Zuluaga, C. A. & Stowell, H. H. (2001). "Metapelite phase equilibria modeling in MnNCKFMASH: the effect of variable Al2O3 and MgO/(MgO+ FeO) on mineral stability". In: *Geological Materials Research* 3(1), pp. 1–42.
Tollmann, A. (1965). "Die Fortsetzung des Briançonnais in den Ostalpen". In: *Mitteilungen der Geologischen Gesellschaft Wien* 57(1964), pp. 469–478.
Tollmann, A. (1977). *Geologie von Österreich: Die Zentralalpen*. Vol. 1. Deuticke.
Trümpy (1988). "A possible Jurassic-Cretaceous transform system in the Alps and the Carpathians". In: *GSA Special Paper*.
Trümpy, R. (1975). "Penninic-Austroalpine boundary in the Swiss Alps: a presumed former continental margin and its problems". In: *American Journal of Science* 275(A), pp. 209–238.
– (1992). "Ostalpen und Westalpen - Verbindendes und Trennendes". In: *Jahrbuch der Geologischen Bundesanstalt* 135(4), pp. 875–882.
– (2001). "Why plate tectonics was not invented in the Alps". In: *International Journal of Earth Sciences* 90(3), pp. 477–483.
Van der Wateren, F. M. (1999). "Structural geology and sedimentology of the Heiligenhafen till section, Northern Germany". In: *Quaternary Science Reviews* 18(14), pp. 1625–1639.
Vannay, J.-C. & Grasemann, B. (2001). "Himalayan inverted metamorphism and syn-convergence extension as a consequence of a general shear extrusion". In: *Geological Magazine* 138(03), pp. 253–276.
Veselá, P., Lammerer, B., Wetzel, A., Söllner, F. & Gerdes, A. (2008). "Post-Variscan to Early Alpine sedimentary basins in the Tauern window (eastern Alps)". In: *Geological Society, London, Special Publications* 298(1), pp. 83–100.
Veselá, P., Söllner, F., Finger, F. & Gerdes, A. (2011). "Magmato-sedimentary Carboniferous to Jurassic evolution of the western Tauern window, Eastern Alps (constraints from U-Pb zircon dating and geochemistry)". In: *International Journal of Earth Sciences* 100(5), pp. 993–1027.
Vollmer, F. (1988). "A computer model of sheath-nappes formed during crustal shear in the Western Gneiss Region, central Norwegian Caledonides". In: *Journal of Structural Geology* 10(7), pp. 735–743.
Warren, C. (2013). "Exhumation of (ultra-) high-pressure terranes: concepts and mechanisms". In: *Solid Earth* 4(1), p. 75.
Weissert, H. J. & Bernoulli, D. (1985). "A transform margin in the Mesozoic Tethys: evidence from the Swiss Alps". In: *Geologische Rundschau* 74(3), pp. 665–679.
Wheeler, J., Reddy, S. & Cliff, R. (2001). "Kinematic linkage between internal zone extension and shortening in more external units in the NW Alps". In: *Journal of the Geological Society* 158(3), pp. 439–443.

Wheeler, J. (2014). "Dramatic effects of stress on metamorphic reactions". In: *Geology* 42(8), pp. 647–650.

Wiederkehr, M., Bousquet, R., Ziemann, M. A., Berger, A. & Schmid, S. M. (2011). "3-D assessment of peak-metamorphic conditions by Raman spectroscopy of carbonaceous material: an example from the margin of the Lepontine dome (Swiss Central Alps)". In: *International Fournal of Earth Sciences* 100(5), pp. 1029–1063.

Xypolias, P. & Alsop, G. (2014). "Regional flow perturbation folding within an exhumation channel: a case study from the Cycladic Blueschists". In: *Journal of Structural Geology* 62, pp. 141–155.

Zhong, X., Moulas, E. & Tajčmanová, L. (2018). "Tiny timekeepers witnessing high-rate exhumation processes". In: *Scientific reports* 8(1), p. 2234.

Zimmermann, R., Hammerschmidt, K. & Franz, G. (1994). "Eocene high pressure metamorphism in the Penninic units of the Tauern Window (Eastern Alps): evidence from 40Ar-39Ar dating and petrological investigations". In: *Contributions to Mineralogy and Petrology* 117(2), pp. 175–186.

Appendix A

Methods

A.1 Compilation of Lithological Map and Cross-Section Construction

The cross sections of the central Tauern Window (Appendix G) are based on a new geological/lithological map (Appendix F) that was compiled from existing and manuscript 1:50000 maps of the Geological Survey of Austria (Geologische Bundesanstalt (GBA); full references given on the map), the 1:200000 geological map of Salzburg (Pestal et al., 2005), the 1:50000 geological maps of the Goldberggruppe (Exner, 1962) and the area of Gastein (Exner, 1956), as well as a lithological map of the Mallnitz synform (Favaro, 2016a). Gaps were filled by our own field work. We also strongly acknowledge fruitful discussions with colleagues from the GBA (W. Frank, B. Huet, R. Schuster, C. Iglseder) and have also tried to reference contributions made verbally in the main text. The cross sections are oriented both parallel (Appendix G, profile A) and perpendicular (Appendix G, profiles B-G) to the D3 nappe transport direction. Profile A passes through the nose of the Seidlwinkl fold nappe. Due to the non-cylindricity of the folds, the projection from the map into the plane of section could only be performed approximately.

A.2 RSQI-Barometry

This method exploits the fact that the elastic strain in quartz inclusions can be measured directly with Raman spectroscopy, since the Raman shift of quartz peaks is a function of pressure (and to a lesser extent a function of temperature; Schmidt & Ziemann, 2000). Quartz (Qz) crystals that were enclosed in newly grown garnet (Grt) at elevated pressure conditions will, after the pressure has decayed, still retain a portion of this pressure, since the enclosing garnet acts as a strong elastic container that substantially prevents the relaxation of the quartz inclusion, at least at low temperatures (Zhong et al., 2018). By applying an elastic model on the system quartz-inclusion-in-garnet-host, the pressure during entrapment of the inclusion can be calculated from the quartz-peak-shift measured at ambient conditions, assuming no non-elastic relaxation has occurred (e. g., viscous relaxation, cracking). The applicability of the quartz Raman shift in geobarometry has been successfully shown in the past (e. g., Ashley et al., 2016, 2014; Bayet et al., 2018; Kohn, 2014; Spear, 2014; Thomas & Spear, 2018).

Spectra of quartz inclusions in garnets in microprobe-quality thin and thick sections were obtained on a Horiba ISA Dilor Labram micro confocal Raman spectrometer with a Nd-YAG laser (532.15 nm

wavelength, 300 mm focal length) and a grating with 1800 grooves/mm. A high spatial resolution (ca. 1 µm spot size) was achieved by using a 400 µm wide confocal hole, a slit width of 100 µm, and a 100x objective. The spectrometer was usually centered at 900 cm^{-1} (sometimes also at 1000, 1050 or 1100 cm^{-1}). The acquisition time was 20 s or longer, depending on the peak-to-noise ratio, with 2 accumulations. For quartz measurements we did not use a filter, resulting in 20-40 mW of laser energy on the sample. A synthetic unstrained quartz crystal was measured every hour as reference for the ideal unstrained 464 cm^{-1} quartz peak. Linear interpolation between these reference spectra allowed to correct the inclusion spectra for machine drift during one day of continuous measurements.

Every inclusion measured yields one P estimate for the P-T conditions at the moment of enclosure. This is always a minimum estimate due to the persistent possibility of partial relaxation of the inclusion. To get a robust estimate on the P conditions of garnet growth, we measured as many inclusions as feasible. Usually, they all together give a relatively large range in pressures, but ideally some converge at the upper end of this range. Therefore, the highest pressure estimate in one sample is assumed to be the best minimum estimate for the pressure during garnet growth.

The uncertainty of this method is mainly controlled by two factors: First the uncertainty resulting from measuring the peak position of the 464 cm^{-1} quartz peak and second the uncertainty introduced by the assumption of a fixed model garnet composition. The peak position uncertainty is a combination of the uncertainty of the measurement itself and of the quality of curve fitting. Combined it is estimated to be ca. ± 0.2 cm^{-1}, which propagates to ca. ± 0.02 GPa for the inclusion pressure uncertainty and results in ca. ± 0.05 GPa for the entrapment pressure uncertainty. The elastic properties of garnet depend on its composition, which in turn has an impact on the calculated entrapment pressures. The maximum difference between highest and lowest pressures calculated for pure garnet endmembers is between grossular and pyrope (apart from spessartine, which is highly unlikely for Mn-poor lithologies). We assumed an intermediate model garnet composition (Alm = 65 mol%, Prp = 15 mol%, Grs = 15 mol%, Sps = 5 mol%) which is realistic for a garnet formed from metapelites during regional metamorphism and is confirmed by our own garnet measurements (Tables B.1 and B.2). The entrapment pressure calculated from the model composition is bracketed by the pressures calculated for the pure endmembers. The deviation in entrapment pressure between model and endmembers is always smaller than ± 0.05 GPa. Therefore, the overall uncertainty of the entrapment pressure estimate is ± 0.1 GPa or less. These considerations do not account for the error introduced by using a strongly simplified elastic model, for a detailed discussion of this issue see Angel et al. (2017). Thomas & Spear (2018) found that this simplification is unproblematic for the range of metamorphic conditions relevant to this study.

A.3 Thermodynamic Modeling

Thermodynamic modeling was performed with the Perple_X software package (version 6.8.1, Connolly, 2005) using the Holland & Powell (1998) dataset (with 2004 revision; Thermocalc dataset "tcds55") and associated solution models (biotite ("Bio(TCC)", Tajčmanová et al., 2009; Tinkham et al., 2001), carpholite ("Carp(M)", Massonne & Willner, 2008), chlorite ("Chl(LWV)", Lanari et al., 2014), chloritoid ("Ctd(HP)", Holland & Powell, 1998), clinopyroxene ("Omph(GHP)", Diener & Powell, 2012; Green et al., 2007), clinoamphibole ("cAmph(DP)", Diener & Powell, 2012; Diener et al., 2007), cordierite ("hCrd", ideal), feldspar ("feldspar", Fuhrman & Lindsley, 1988; after Newton et al., 1980 and Haselton et al., 1983), garnet ("Gt(HP)", Holland & Powell, 1998), ilmenite ("IlGkPy", ideal), staurolite ("St(HP)", Holland & Powell, 1998), stilpnomelane ("Stlp(M)", Massonne & Willner, 2008), white mica ("Mica+(CHA)", Auzanneau et al., 2010; Coggon & Holland, 2002).

All samples were modeled in the P-T range of 0.5-2.5 GPa and 300-600 °C, assuming water-saturated conditions. Bulk chemical analyses for the samples were obtained by X-ray fluorescence analysis following a standard procedure. The data are reported in Appendix C. From the bulk chemical analysis, a model composition was extracted by a) removing all components with < 0.1 wt% to only account for major elements, b) recalculating the Fe-content (measured as Fe_2O_3) as completely ferrous ($FeO = Fe_2O_3 * 0.899$), c) correcting the Ca-content for Ca-in-apatite by using the measured P_2O_5-content. The renormalisation of the model composition to a total of 100% is performed in Perple_X automatically.

A.4 Mineral Composition Measurements

The compositions of rock forming minerals (white mica, garnet, chloritoid and chlorite are shown in Tables B.1 and B.2 in Appendix B) were aquired on a JEOL JXA 8200 SuperProbe at Freie Universität Berlin, Institut für Geologische Wissenschaften. Measurement conditions for spot analyses and element maps were 15 kV acceleration voltage, 20 nA beam current and < 1 µm beam diameter. We used natural and synthetic reference materials for instrument calibration. Structural formulae were calculated from microprobe results using standard procedures. The representative mineral composition data can also be obtained in spreadsheet format from the GFZ Data Services (Groß et al., 2020a; http://doi.org/10.5880/fidgeo.2020.010).

A.5 Compilation of Barrovian Peak-Temperature Contours

We recompiled available datasets containing information on temperature (T) conditions during Barrovian metamorphism in the Tauern Window region in order to create an updated peak-T contour map for the central Tauern Window. Doing so, we largely adopted the results from previous compilations without modifications in the eastern and western Tauern domes (Bousquet et al., 2012; Hoernes & Friedrichsen, 1974; Rosenberg et al., 2018; Scharf et al., 2013b). Only in the central Tauern Window, we updated the existing compilations based on our new RSCM data and a re-evaluation of some datasets.

We used two kinds of datasets: a) direct temperature estimates from mineral equilibria and stability (Dachs, 1990; Droop, 1985; Frank et al., 1987), RSCM-thermometry (Scharf et al., 2013b; own data) and isotope fractionation (Hoernes & Friedrichsen, 1974). b) indirect temperature estimates from published radiometric ages obtained with low-retentivity isotopic systems using the closure temperature of the respective isotopic system (Favaro et al., 2015; Inger & Cliff, 1994; Lambert, 1970; Oxburgh et al., 1966; Reddy et al., 1993). In this approach we assume that ages greater than 32 Ma mean that the respective isotopic system was not reset during Barrovian metamorphism, which means that the Barrovian peak-T was lower than the closure temperature of the respective system.

A.6 Cross-Section Construction, Data Projection and Contour Interpolation

As basis for cross-section construction, we used our own lithological and tectonic map compilations of the central Tauern Window (Groß et al., 2020b). In the cross-sections presented here, the geometries of the lithological and tectonic boundaries were slightly simplified in order to highlight the main

features relevant to this study. The positions of the sections were chosen to give a good representation of the large scale structure and to allow for projection of as much RSCM-data as possible. The RSCM-data can be obtained in raw and processed form from the GFZ Data Services (Groß et al., 2020c; http://doi.org/10.5880/fidgeo.2020.024).

At least two perpendicular cross sections are needed to adequately illustrate sheath-fold geometries; one parallel and one perpendicular to the transport direction. Due to the substantial non-cylindricity of these structures, quantitatively correct projection of data points from the map to the cross sections is practically impossible. Therefore, we applied a semi-quantitative approach that is illustrated in Figure A.1. First, data points were projected horizontally into the line of section, either perpendicularly to the section trace or parallel to the overall structural trend. Then, the vertical position of the data points in the tectono-stratigraphy was determined based on the outcrop context, local structural information and topographic elevation. This approach is unproblematic for data points located close to a section. For far-projected data points, however, it means that the absolute localisation of the points in the section may be inexact; nevertheless, they will be located in a plausible tectono-stratigraphic setting and therefore be a good representation of the "true" situation. In any case, we only considered data for projection that are not too far from the sections and with only mild disturbance arising from non-cylindricity.

Based on the projected data, we interpolated peak-T contours in the cross sections. Contouring was performed manually under the prerequisite that, first, the Barrovian event is younger than the subduction-related event, as proven by radiometric dating (e. g., Favaro et al., 2015; Zimmermann et al., 1994) and overprinting relationships (e. g., Dachs & Proyer, 2001) and second, the Barrovian event is characterised by peak-T conditions that concentrically decrease with increasing distance from the structurally lowest parts of the western and eastern Tauern domes (e. g., Hoernes & Friedrichsen, 1974; Scharf et al., 2013b).

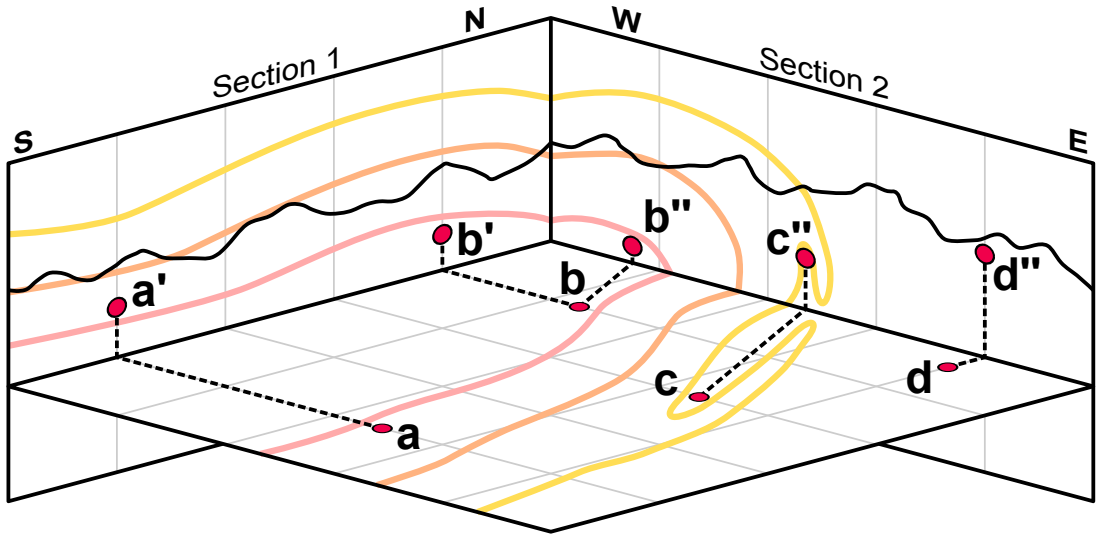

Figure A.1: Examples of semi-quantitative projection of RSCM-data into cross sections. The depiction of the data points in map view does not consider topography effects. Point *a* can be projected perpendicularly into section 1, because of minor effect of non-cylindricity along the projection line. The relative elevation of point *a'* is estimated based on the local information that point a is located just above the red marker layer. Point *b* is close to both sections. It is projected perpendicularly into section 1 to point *b'* and parallel to the structural trend into section 2 to point *b''*, with relative elevation of the points indicated by the red marker layer. Point *c* is projected parallel to the structural trend into section 2 to point *c''*, with its elevation given by its position inside the hinge of a minor fold of the yellow marker layer. Projection to section 1 is impossible due to strong non-cylindricity along the potential projection line. Point *d* is lacking reliable information on local structure, but being very close to section 2, it can be projected perpendicularly to this section to point *d''*. Its elevation can be estimated from the topographic context.

Appendix B

Characterisation of selected samples

B.1 Garnet Micaschist

Sample PG89 is an example of garnet micaschist used for thermodynamic P-T modelling. It comes from the very south of the investigated area, in the Stanziwurten summit region (location on map in Appendix F, UTM Zone 33N 341888 5207230). The sample is of a garnet-rich layer within a dark micaschist of the Brennkogel Formation. Its matrix minerals are quartz, phengite, garnet, chlorite, albite, tourmaline and rutile (often with ilmenite margins). No lawsonite, paragonite, glaucophane or omphacite was found. Quartz-, mica- and chlorite-SPO define the S3 foliation (Fig. 3.5). The sample also contains an older S2 schistosity defined by relict chloritoid- and rutile-inclusions in garnet, usually near its core; this internal foliation is oblique to the main S3 schistosity in the matrix (Fig. 3.5c). White mica oriented parallel to S3 has a variable phengite content, with Si ranging from 3.06-3.42 p.f.u. and Mg+Fe ranging from 0.16-0.46 p.f.u. which is mainly controlled by Tschermak substitution (muscovite to phengite); pyrophyllite substitution has a minor effect (K+Na always $>$ 0.85 p.f.u.). Element maps (Fig. 3.5d-f) document that the cores of these micas are phengite-rich (high Mg content in map in Fig. 3.5d). Along grain boundaries and cleavage fractures, however, these micas are partly replaced by a younger generation of phengite-poor mica (low Mg content in map in Fig. 3.5d). Cross-micas oblique to S3 also tend to have low phengite contents. S3 phengite is commonly intergrown with synkinematic chlorite, especially near the strain shadows of garnet. Garnet shows a prograde growth zoning, with Mn and Ca decreasing from core to rim and Mg decreasing in the opposite sense (Fig. 3.5d-f). The lack of the Mg-rich and Ca-poor rims at opposite faces of the garnet grain in Figures 3.5d and 3.5f indicates pronounced resorption at the contact with the S3 matrix schistosity. See Table B.1 for representative mineral composition data of garnet micaschist sample PG89.

Table B.1: Representative mineral compositions of garnet micaschist PG89. Measurements are for phengite (Ph), garnet core (Grt-c.), garnet mantle (Grt-m.), garnet rim (Grt-r.), chloritoid (Cld) and chlorite (Chl). Oxides in weight percent, site occupancies in atoms per formula unit.

meas. No.	**4**	**8**	**11**	**36**	**192**	**224**	**254**	**260**	**276**	**283**	**182**	**303**	**183**	**187**
Mineral	**Ph**	**Ph**	**Ph**	**Ph**	**Ph**	**Ph**	**Grt-c.**	**Grt-m.**	**Grt-m.**	**Grt-r.**	**Cld**	**Cld**	**Chl**	**Chl**
SiO_2	46.41	50.35	47.76	50.78	48.35	50.68	37.27	37.49	38.53	37.92	24.97	24.82	25.91	24.39
TiO_2	0.43	0.25	0.13	0.15	0.54	0.36	0.11	0.18	0.01	0.07	0.02	0.12	0.05	0.10
Al_2O_3	34.83	29.21	33.37	28.15	31.39	28.41	22.04	22.50	22.62	22.93	40.27	40.53	20.86	22.36
Cr_2O_3	0.14	0.00	0.10	0.12	0.03	0.27	0.00	0.00	0.02	0.01	0.00	0.06	0.04	0.00
FeO(tot)	2.01	1.96	1.79	2.15	2.81	2.01	33.08	33.40	32.98	34.98	22.51	23.96	25.56	25.06
MgO	0.86	2.58	1.25	2.42	2.26	3.25	0.95	1.03	2.21	3.12	3.47	2.30	13.85	14.05
MnO	0.03	0.05	0.00	0.04	0.01	0.01	3.65	2.21	1.43	0.67	0.13	0.23	0.42	0.35
CaO	0.00	0.00	0.00	0.00	0.01	0.03	3.20	3.42	3.03	1.17	0.04	0.02	0.07	0.05
Na_2O	0.70	0.51	0.58	0.35	0.44	0.40	0.03	0.10	0.04	0.06	0.05	0.01	0.02	0.02
K_2O	10.01	9.82	9.83	9.56	9.95	9.66	0.00	0.00	0.00	0.01	0.00	0.00	0.01	0.02
Total	*95.41*	*94.72*	*94.81*	*93.73*	*95.78*	*95.08*	*100.32*	*100.33*	*100.88*	*100.94*	*91.45*	*92.05*	*86.78*	*86.40*
Si	3.09	3.36	3.18	3.42	3.21	3.37	6.01	6.01	6.07	5.98	2.06	2.05	2.76	2.61
Ti	0.02	0.01	0.01	0.01	0.03	0.02	0.01	0.02	0.00	0.01	0.00	0.01	0.00	0.01
Al	2.73	2.30	2.62	2.23	2.46	2.22	4.19	4.25	4.20	4.26	3.92	3.95	2.62	2.82
Cr	0.01	0.00	0.01	0.01	0.00	0.01	0.00	0.00	0.00	0.00	0.00	0.00	0.00	0.00
Fe(tot)	0.11	0.11	0.10	0.12	0.16	0.11	4.46	4.48	4.35	4.61	1.55	1.66	2.28	2.25
Mg	0.09	0.26	0.12	0.24	0.22	0.32	0.23	0.25	0.52	0.73	0.43	0.28	2.20	2.24
Mn	0.00	0.00	0.00	0.00	0.00	0.00	0.41	0.24	0.16	0.07	0.01	0.01	0.03	0.03
Ca	0.00	0.00	0.00	0.00	0.00	0.00	0.55	0.59	0.51	0.20	0.00	0.00	0.01	0.01
Na	0.09	0.07	0.07	0.05	0.06	0.05	0.01	0.03	0.01	0.02	0.01	0.00	0.00	0.00
K	0.85	0.84	0.84	0.82	0.84	0.82	0.00	0.00	0.00	0.00	0.00	0.00	0.00	0.00
XMg	0.43	0.70	0.55	0.67	0.59	0.74	0.04	0.05	0.11	0.14	0.22	0.15	0.49	0.50

B.2 Chloritoid Micaschist

Sample PG61 serves as example for chloritoid micaschists from the Piffkar formation. It was collected in the central part of the investigated area, ca. 1 km east of Hochtor on the Rossköpfl summit (location on map in Appendix F, UTM Zone 33N 337044 5216460). The matrix mineral assemblage of this sample is quartz, phengite, chloritoid, some chlorite, ilmenite (mix of ilmenite, geikielite, Fe-oxide) and relicts of sceletal garnet (as palisades along quartz grain boundaries) and accessory allanite. Rutile occurs as inclusions in quartz and no lawsonite, kyanite or carpholite were found. The main foliation is defined by a SPO of phengite, quartz, chloritoid, chlorite and ilmenite. Chloritoid occasionally forms aggregates consisting of aligned crystals. Quartz has a strong CPO indicating a top-NNW shear sense. The garnet relicts are interpreted to be largely pseudomorphosed by randomly oriented chloritoid-laths; however, sparse remains of the original garnet are partly preserved. The matrix foliation wraps around the pseudomorphs with former pressure shadows being preserved as well. White mica shows a variable phengite content, with Si ranging from 3.04-3.33 p.f.u. and Mg+Fe ranging from 0.14-0.34 p.f.u. which is mainly controlled by Tschermak substitution (muscovite to phengite); pyrophyllite substitution has a minor effect (K+Na always $>$ 0.90 p.f.u.). See Table B.2 for representative mineral composition data of chloritoid micaschist sample PG61.

Table B.2: Representative mineral compositions of chloritoid micaschist PG61. Measurements are for phengite (Ph), chloritoid (Cld) and garnet (Grt). Oxides in weight percent, site occupancies in atoms per formula unit.

meas. No.	**18**	**74**	**78**	**84**	**86**	**89**	**10**	**361**	**349**	**363**	**365**	**340**	**354**	**359**
Mineral	**Ph**	**Ph**	**Ph**	**Ph**	**Ph**	**Ph**	**Cld**	**Cld**	**Cld**	**Cld**	**Cld**	**Grt**	**Grt**	**Grt**
SiO_2	50.04	49.13	47.77	47.28	47.23	45.82	24.44	24.45	24.13	24.44	24.71	37.38	37.57	37.51
TiO_2	0.15	0.17	0.23	0.18	0.22	0.23	0.01	0.06	0.00	0.00	0.03	0.02	0.00	0.01
Al_2O_3	29.94	30.71	31.90	33.19	34.74	36.27	39.88	39.76	39.44	40.25	40.29	21.08	21.32	21.02
Cr_2O_3	0.00	0.01	0.01	0.10	0.07	0.04	0.00	0.04	0.00	0.01	0.01	0.08	0.01	0.02
FeO(tot)	3.11	3.38	2.90	2.50	1.91	1.65	25.32	26.50	27.95	27.13	26.52	38.52	38.99	39.15
MgO	1.65	1.23	1.08	0.98	0.75	0.55	1.25	0.97	0.54	0.89	1.21	0.47	0.41	0.42
MnO	0.00	0.02	0.00	0.00	0.00	0.00	0.07	0.02	0.02	0.04	0.06	0.48	0.31	0.27
CaO	0.01	0.00	0.00	0.00	0.00	0.00	0.01	0.00	0.01	0.01	0.01	2.24	2.08	1.94
Na_2O	0.16	0.10	0.19	0.21	0.23	0.35	0.02	0.02	0.00	0.06	0.00	0.04	0.05	0.02
K_2O	10.33	10.45	10.48	10.75	10.38	10.64	0.00	0.00	0.00	0.00	0.00	0.00	0.01	0.00
Total	*95.39*	*95.19*	*94.57*	*95.18*	*95.52*	*95.54*	*91.00*	*91.82*	*92.09*	*92.81*	*92.85*	*100.29*	*100.76*	*100.36*
Si	3.33	3.29	3.22	3.17	3.13	3.05	2.06	2.05	2.04	2.03	2.05	6.07	6.07	6.09
Ti	0.01	0.01	0.01	0.01	0.01	0.01	0.00	0.00	0.00	0.00	0.00	0.00	0.00	0.00
Al	2.35	2.42	2.53	2.62	2.72	2.84	3.96	3.93	3.92	3.95	3.94	4.03	4.06	4.02
Cr	0.00	0.00	0.00	0.01	0.00	0.00	0.00	0.00	0.00	0.00	0.00	0.01	0.00	0.00
Fe(tot)	0.17	0.19	0.16	0.14	0.11	0.09	1.78	1.86	1.97	1.89	1.84	5.23	5.27	5.31
Mg	0.16	0.12	0.11	0.10	0.07	0.05	0.16	0.12	0.07	0.11	0.15	0.11	0.10	0.10
Mn	0.00	0.00	0.00	0.00	0.00	0.00	0.00	0.00	0.00	0.00	0.00	0.05	0.04	0.03
Ca	0.00	0.00	0.00	0.00	0.00	0.00	0.00	0.00	0.00	0.00	0.00	0.39	0.36	0.34
Na	0.02	0.01	0.03	0.03	0.03	0.05	0.00	0.00	0.00	0.01	0.00	0.01	0.01	0.01
K	0.88	0.89	0.90	0.92	0.88	0.90	0.00	0.00	0.00	0.00	0.00	0.00	0.00	0.00
XMg	0.49	0.39	0.40	0.41	0.41	0.37	0.08	0.06	0.03	0.06	0.08	0.02	0.02	0.02

Appendix C

XRF Data

Table C.1: Whole rock major and trace element abundances of samples from the central Tauern Window obtained by XRF analysis. Oxides in wt%, elements in ppm.

Sample	**F15/17**	**PG36**	**PG60**	**PG61**	**PG70**	**PG75**	**PG89**	**PG109**	**PG117**	**PG119**
Lat	47.09157	47.11521	47.08210	47.08153	47.01313	47.00636	46.99970	47.08204	47.08595	47.01313
Lon	12.94475	12.82437	12.83445	12.85327	12.92355	12.92570	12.92027	12.83439	12.87196	12.92362
Lithology	Cld-ms.	phyllite	Grt-ms.	phyllite	Ky-phyllite	gneiss	Grt-ms.	Grt-ms.	Cld-Ky-ms.	Cld-Ky-ms.
SiO_2	63.04	67.41	58.79	67.43	76.57	66.29	80.51	56.86	66.81	57.17
TiO_2	1.40	1.04	0.72	0.85	0.99	0.62	0.32	0.76	1.57	1.10
Al_2O_3	20.05	18.03	18.73	16.13	14.19	14.91	7.58	19.79	23.05	29.61
Fe_2O_3	8.38	4.88	5.94	9.68	1.38	5.01	5.56	9.07	2.61	2.98
FeO	7.53	4.39	5.34	8.70	1.24	4.50	5.00	8.15	2.35	2.68
MnO	0.02	<0.01	0.14	0.03	0.02	0.06	0.24	0.24	0.02	0.04
MgO	0.80	0.41	2.44	0.61	0.24	1.22	1.64	2.95	0.49	0.65
CaO	0.12	0.13	2.90	0.13	0.04	1.08	0.41	1.26	0.09	0.18
Na_2O	<0.01	<0.01	0.40	<0.01	<0.01	0.06	0.10	0.86	<0.01	<0.01
K_2O	2.34	4.76	4.70	1.51	1.49	6.50	1.27	3.70	1.80	5.05
P_2O_5	0.05	0.06	0.06	0.06	0.02	0.14	0.10	0.03	0.06	0.07
H_2O		2.98	3.34	3.21	1.47	2.54	1.92	3.72		
CO_2										
LOI	4.07								3.73	3.01
SUM	**100.27**	**99.74**	**99.71**	**99.83**	**99.94**	**99.72**	**99.88**	**99.55**	**100.23**	**99.85**
Ba	561	413	488	121	238	268	240	392	215	783
Cr	212	118	84	98	86	28	79	92	168	154
Ga	24	21	23	20	17	21	11	24	31	42
Nb	35	30	15	20	21	17	<10	19	37	37
Ni	52	24	62	32	<10	13	62	79	48	45
Rb	191	281	199	90	106	316	61	155	117	324
Sr	56	87	96	20	54	106	41	85	93	144
V	126	99	138	88	80	37	97	157	126	161
Y	33	25	27	74	30	42	20	17	54	61
Zn	22	20	93	68	<10	80	57	139	<10	<10
Zr	268	285	125	316	502	286	74	129	610	217

Table C.1: continued

Sample	**PG123**	**PG130**	**PG131**	**PG136**	**PG137**	**PG139**	**PG141**	**PG142**	**PG151**	**PG152**
Lat	47.02261	47.11207	47.11206	47.08650	47.08885	47.13251	47.13907	47.14150	47.10787	47.10801
Lon	12.92827	12.82534	12.82532	12.73868	12.73426	12.84119	12.84402	12.85275	12.87641	12.87692
Lithology	Grt-ms.	Cld-ms.	Cld-Bt-schist	Grt-prasinite	Grt-ms.	Cld-Ky-ms.	Cld-Ky-ms.	Cld-ms.	Cld-ms.	Bt-gneiss
SiO_2	43.93	59.70	47.33	43.09	79.24	76.63	57.44	67.52	58.88	73.93
TiO_2	0.77	1.02	0.64	0.92	0.33	1.26	1.11	0.82	0.92	0.34
Al_2O_3	18.57	21.42	15.25	16.53	7.88	14.23	24.13	16.36	22.52	13.65
Fe_2O_3	8.54	12.98	28.30	9.67	4.22	2.68	8.61	6.17	8.83	2.82
FeO	7.68	11.67	25.44	8.69	3.79	2.41	7.74	5.55	7.94	2.54
MnO	0.41	0.06	0.06	0.25	0.08	0.03	0.04	0.04	0.03	0.05
MgO	1.89	0.90	3.26	7.85	1.36	0.58	1.27	0.84	1.18	1.11
CaO	1.37	0.08	0.13	9.98	1.85	0.05	0.13	0.60	0.18	0.51
Na_2O	0.71	<0.01	<0.01	3.60	<0.01	<0.01	<0.01	<0.01	<0.01	0.71
K_2O	3.39	0.80	<0.01	0.17	1.94	2.59	3.49	4.83	4.00	4.40
P_2O_5	0.09	0.03	0.06	0.08	0.05	<0.01	0.04	0.05	0.04	0.09
H_2O										
CO_2										
LOI	20.16	3.33	4.70	7.47	3.70	2.24	3.90	3.04	3.33	2.13
SUM	**99.82**	**100.31**	**99.73**	**99.62**	**100.65**	**100.29**	**100.15**	**100.27**	**99.91**	**99.74**
Ba	631	109	<10	60	235	367	634	1060	1499	561
Cr	91	147	102	236	84	126	142	127	149	23
Ga	24	28	27	15	14	22	31	22	36	25
Nb	15	28	23	15	20	38	29	21	28	20
Ni	44	88	90	106	72	32	35	73	67	<10
Rb	139	67	29	23	108	172	255	329	265	158
Sr	152	41	16	265	45	97	74	138	102	77
V	104	115	68	128	75	58	133	76	129	14
Y	38	32	39	25	20	32	42	49	36	44
Zn	58	98	170	57	65	16	20	14	35	22
Zr	96	237	167	50	36	622	211	191	133	280

Table C.1: continued

Sample	**PG161**	**PG226**	**PG228**	**PG231**	**PG237**	**PG265**	**PG286**	**PG288**	**PG299**	**PG304**	**PG306**
Lat	47.11427	47.16897	47.16800	47.14560	47.09692	47.09641	47.06330	47.06203	47.13174	47.10638	47.06326
Lon	12.92652	12.85127	12.85818	12.85267	12.80422	12.84890	12.76519	12.76904	12.75609	12.78808	12.76522
Lithology	Grt-ms.	ms.	ms.	ms.	ms.	ms.	ms.	ms.	ms.	ms.	ms.
SiO_2	59.43	59.52	57.60	64.93	73.27	65.88	48.61	71.62	88.67	72.10	58.87
TiO_2	0.52	1.07	1.02	1.01	0.76	0.91	1.33	0.51	0.20	0.57	0.65
Al_2O_3	12.22	20.80	23.36	17.86	14.44	18.30	18.66	12.41	4.57	12.19	17.66
Fe_2O_3	5.10	12.38	8.88	7.44	3.48	7.30	10.80	5.15	2.30	4.22	7.13
FeO	4.58	11.13	7.98	6.69	3.13	6.56	9.71	4.63	2.07	3.79	6.41
MnO	0.23	0.07	0.07	<0.01	0.01	<0.01	0.36	0.29	0.26	0.07	0.12
MgO	1.97	0.86	1.68	0.46	0.95	0.69	2.38	1.58	1.02	1.12	2.53
CaO	8.14	0.06	0.11	0.06	0.08	0.05	7.89	2.29	0.98	0.55	2.41
Na_2O	<0.01	<0.01	0.01	0.05	0.07	<0.01	0.09	0.11	<0.01	0.47	0.08
K_2O	2.00	1.20	2.78	4.87	3.72	3.95	3.72	2.09	0.46	2.26	4.99
P_2O_5	0.09	0.07	0.09	0.03	0.04	0.03	0.18	0.07	0.05	0.09	0.05
H_2O		3.91	4.12	3.04	2.78	2.57	2.79	2.55	0.97	2.70	3.14
CO_2		<0.01	<0.01	0.04	0.20	0.05	2.60	1.04	0.63	3.38	1.56
LOI	10.21										
SUM	**99.91**	**99.94**	**99.71**	**99.79**	**99.81**	**99.73**	**99.42**	**99.70**	**100.12**	**99.72**	**99.19**
Ba	366	140	238	439	338	669	381	244	96	445	467
Cr	92	122	108	116	96	105	304	73	35	92	78
Ga	18	22	30	23	16	22	16	13	<10	15	20
Nb	16	25	20	25	12	21	<10	10	<10	11	11
Ni	77	31	41	51	17	55	143	76	32	25	103
Rb	109	72	183	271	186	245	139	100	29	112	177
Sr	206	38	53	71	25	44	135	108	15	166	38
V	109	111	118	102	79	93	189	117	47	103	142
Y	29	56	69	30	24	35	35	24	13	18	34
Zn	102	55	51	23	24	42	121	93	67	87	137
Zr	78	344	254	271	318	317	112	80	31	162	105

Appendix D

Shear Sense Indicators

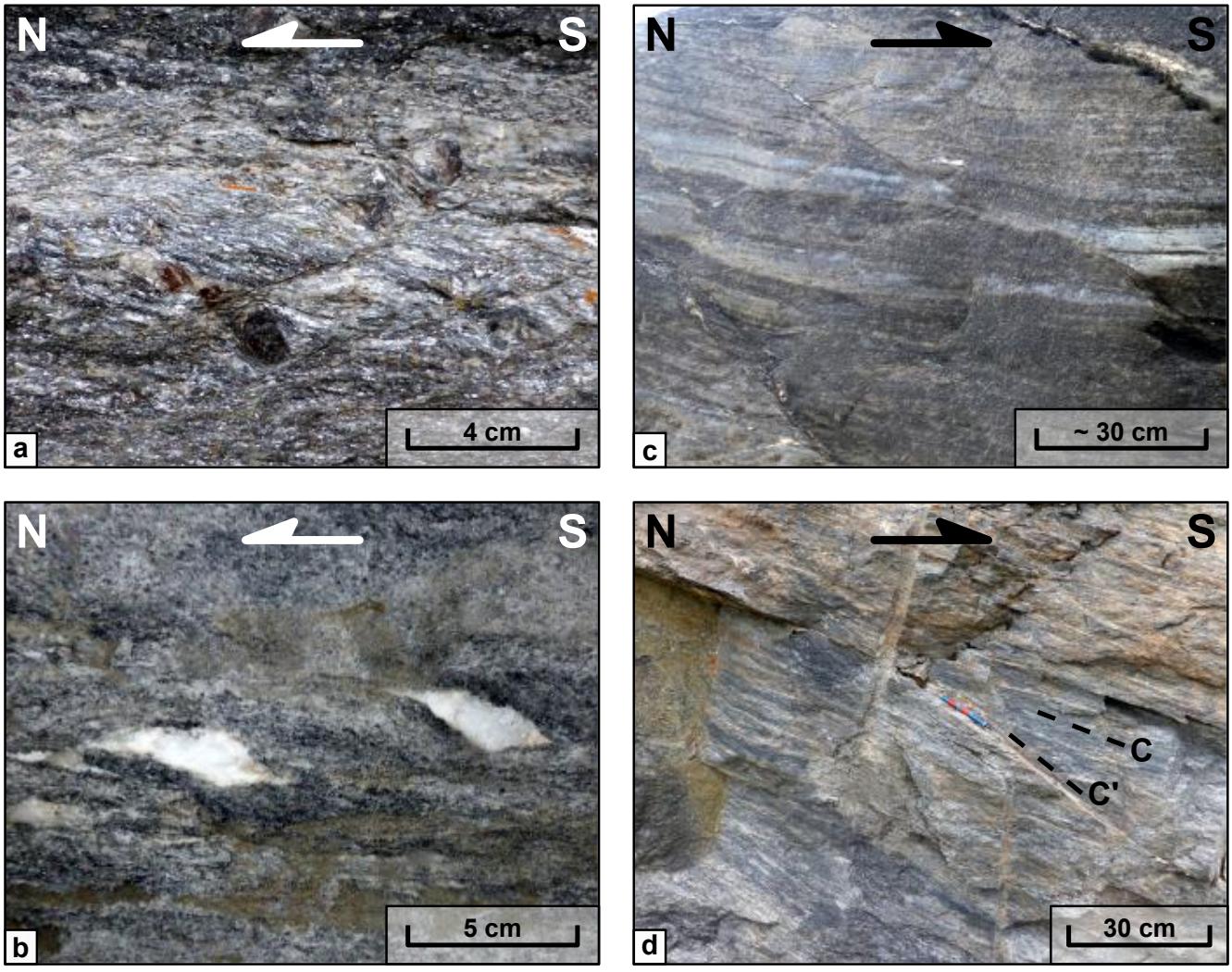

Figure D.1: Examples of outcrop-scale thrusting (top-N; a-b) and normal-faulting (top-S; c-d) shear sense indicators. (a) S-C' fabric in garnet-micaschist (UTM 33N 330266 5214896). (b) sigmoidal calcite clasts in calcareous micaschist (ca. UTM 33N 329190 5216380, in Gamsgrube tunnel). (c-d) C-C' fabric in marble (c: UTM 33N 330284 5214981; d: UTM 33N 330266 5214896).

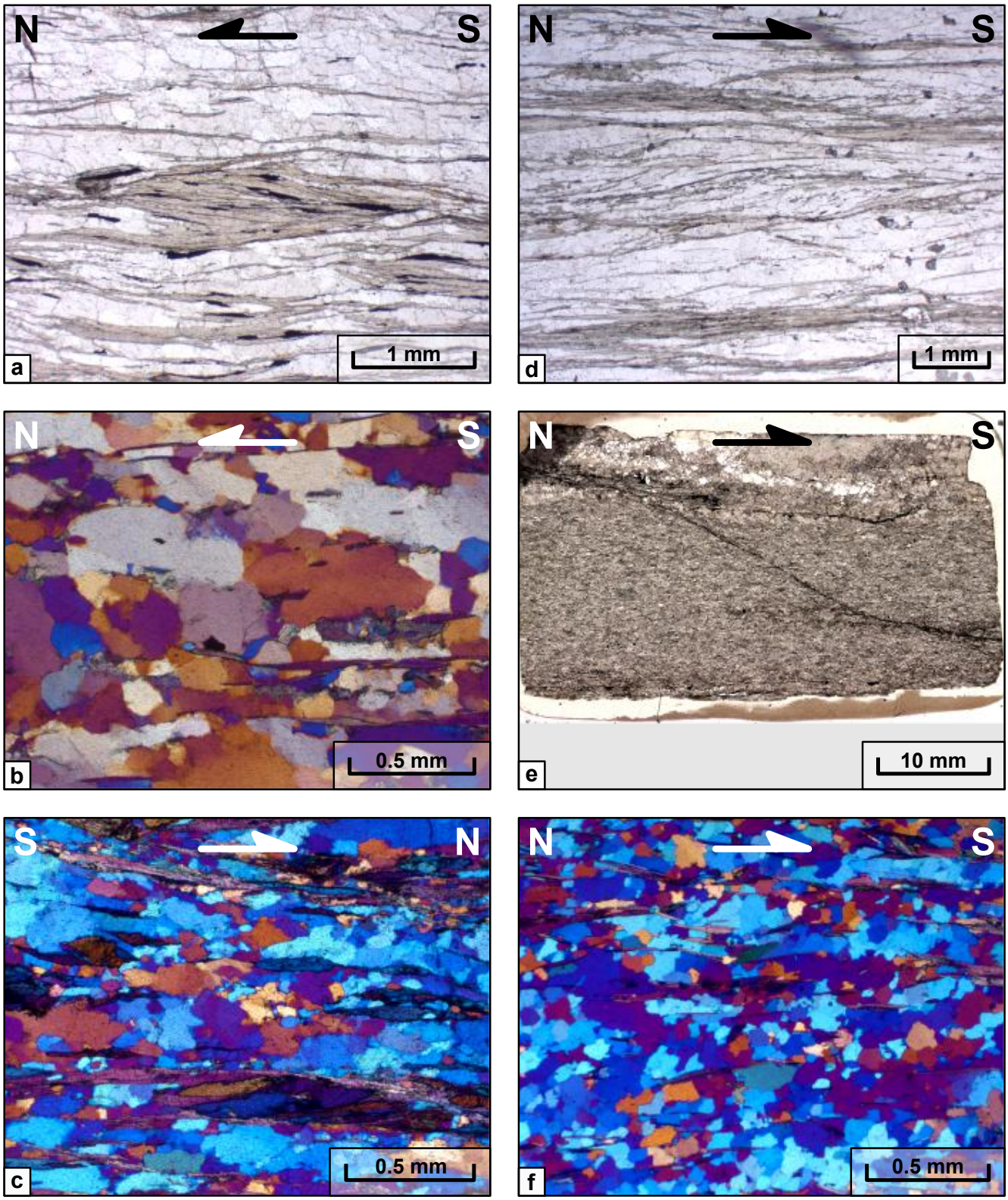

Figure D.2: Examples of microscale thrusting (top-N; a-c) and normal-faulting (top-S; d-f) shear sense indicators. (a) S-C fabric indicated by a mica fish in impure quartzite (sample PG118, UTM 33N 342183 5208701). (b-c) qualitative Qz-CPO in quartzite (b: sample PG239, UTM 33N 335206 5217582; c: sample PG120, UTM 33N 342184 5208715). (d) S-C fabric in impure quartzite (sample T2, UTM 33N 330341 5213651). (e) S-C' fabric in impure marble (sample PG343; UTM 33N 332661 5211664). (f) qualitative Qz-CPO in quartzite (sample PG341, UTM 33N 329574 5215111).

Appendix E

Peak-Pressure estimates

Table E.1: Peak-pressure P-T data for all samples. * denotes a sample where the temperature was estimated based on the measured temperature of immediately neighboring samples. Tectonic units denoted as M=Modereck nappe system and G=Glockner nappe system.

Sample	**UTM coordinates** *(Zone 33N)*		**Unit**	**Lithology**	**RSQI-P** *in GPa*	**Si-in-Ph P** *in GPa*	**RSCM-T** *in ℃*	
	X	*Y*			*∼ ±0.1 GPa*	*∼ ±0.1 GPa*	*∼ ±30℃*	
F15/17	344404	5217279	M	Cld-micaschist		1.43	491	
PG21	328730	5216984	G	Grt-quartzschist	1.87		488	
PG25	332304	5214316	G	Grt-calcmicaschist	2.31		511	
PG29	340621	5216306	M	Grt-micaschist	1.33		471	
PG32	341700	5216324	M	Grt-Fsp-micaschist	1.97		498	
PG59	335626	5216568	M	Grt-micaschist	2.25		554	
PG60	335618	5216563	M	Grt-micaschist	1.94		522	
PG61	337045	5216461	M	Grt-Cld-micaschist		1.60	505	
PG89	341888	5207230	M	Grt-micaschist	1.94	1.99	518	
PG93	341562	5207636	M	Grt-Cld-calcmicaschist	2.20		500	
PG102	342578	5209732	G	Grt-quartzschist	1.76		503	
PG109	335613	5216557	M	Grt-micaschist		2.19	500	*
PG130	335019	5219912	M	Cld-micaschist		1.32	485	
PG137	328035	5217528	G	Grt-quartzschist	2.12	1.70	500	*
PG139	336284	5222151	M	graphitic Cld-micaschist		1.76	497	
PG141	336519	5222873	M	Cld-micaschist		1.77	496	
PG142	337188	5223126	M	Cld-Ep-micaschist		1.34	490	*
PG161	342701	5219948	M	Grt-calcmicaschist	1.60		484	
PG254	337817	5227254	M	graphitic Grt-micaschist	1.91		494	
PG286	330301	5214622	G	Grt-Ep-micaschist	2.12		520	*
PG288	330589	5214473	G	Grt-calcmicaschist	2.30		524	
PG299	329828	5222246	G	Grt-micaschist	2.02		512	
PG304	332175	5219360	G	Grt-micaschist	2.02		508	
PG305	332622	5220061	G	Grt-calcmicaschist	2.16		504	

Appendix F

Geological Map of the Central Tauern Window

GEOLOGICAL MAP OF THE CENTRAL TAUERN WINDOW (AUSTRIA)

compilation by
Philip Groß, 2019

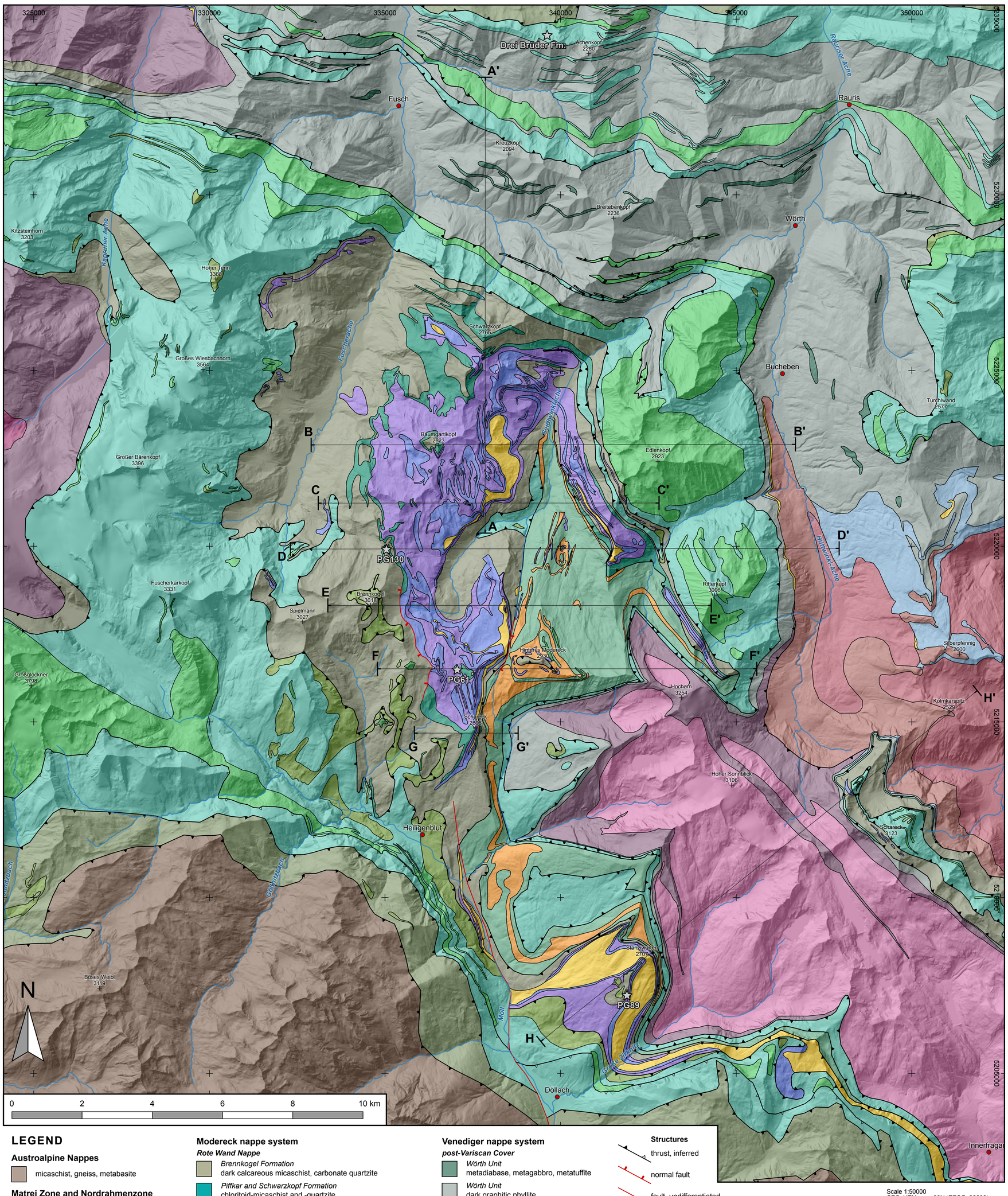

LEGEND

Austroalpine Nappes

- micaschist, gneiss, metabasite

Matrei Zone and Nordrahmenzone

- calcareous micaschist with blocks of prasinite, marble, serpentinite, slivers of Austroalpine
- serpentinite

Glockner nappe system

- bright calcareous micaschist, with garnet-bearing layers in Glockner Nappe
- prasinite, greenschist, metabasite
- garnet-prasinite, eclogite relics
- serpentinite

☆ PG89 sample locality

Modereck nappe system

Rote Wand Nappe

- *Brennkogel Formation*
  dark calcareous micaschist, carbonate quartzite
- *Piffkar and Schwarzkopf Formation*
  chloritoid-micaschist and -quartzite
- *Seidlwinkl Formation*
  dolomitic marble
- *Seidlwinkl Formation*
  calcitic marble
- *Wustkogel Formation*
  fine-grained phengite-augengneiss, green quartzite, metaarkose

Trögereck Nappe

- dark calcareous micaschist, carbonatic metaarkose, garnet-micaschist layers
- garnet-prasinite, eclogite relics
- calcitic and dolomitic marble
- *Trögereck-Gneiss*
  feldspar micaschist, augengneiss

Venediger nappe system

post-Variscan Cover

- *Wörth Unit*
  metadiabase, metagabbro, metatuffite
- *Wörth Unit*
  dark graphitic phyllite
- *Silbereck Marble (upper Jurassic)*
  bright marble with corals and ammonites (Perisphinctidae)
- *Wustkogel Formation (Permian-Triassic)*
  fine-grained phengite-augengneiss, green quartzite, metaarkose
- *Woisgenschiefer (Post-variscan?)*
  biotite-porphyroblast schist, bright garnet-micaschist

late-Variscan intrusives - Zentralgneise

- *Sonnblick Nappe Zentralgneis*
  coarse grained granite gneiss
- *Riffl Nappe Zentralgneis*
  alkali feldspar gneiss
- *Romate Nappe Zentralgneis*
  fine-grained granite and syenite gneiss

pre-Variscan basement

- *Altes Dach and Altkristallin*
  diverse gneisses, micaschists and metabasites

Structures

- thrust, inferred
- normal fault
- fault, undifferentiated

Scale 1:50000
CRS: UTM zone 33N (EPSG: 32633)

DEM generated from "DGM Österreich"
CC-BY-3.0: Land Kärnten - data.ktn.gv.at

Distribution of base maps used in this compilation

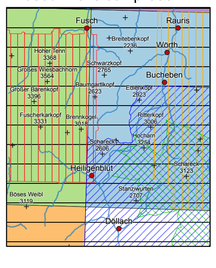

Cornelius, H.P. & Clar, E. (1934). Geologische Karte des Grossglocknergebietes. Wien: Geologische Bundesanstalt and D. u. Ö. Alpenverein.

Exner, C. (1956). Geologische Karte der Umgebung von Gastein. Wien: Geologische Bundesanstalt.

Exner, C. (1962). Geologische Karte der Sonnblickgruppe. Wien: Geologische Bundesanstalt.

Favaro, S. (2016). Lithological map of the Sonnblick area. In: Response of orogenic crust to indentation by Adriatic continental lithosphere – Tauern Window, Eastern Alps (Austria). PhD dissertation, Freie Universität Berlin, Germany, pp. 164.

Heinisch, H., Pestal, G., Stingl, V. & Hellerschmidt-Alber, H. (1995). GK50 Blatt 123 Zell am See. Geologische Karte der Republik Österreich. Wien: Geologische Bundesanstalt.

Höck, V., & Pestal, G. (1994). GK50 Blatt 153 Grossglockner. Geologische Karte der Republik Österreich. Wien: Geologische Bundesanstalt.

Kreuss, O. (2013). GK50 Blatt 124 Saalfelden am Steinernen Meer, preliminary Geofast map. Geologische Karte der Republik Österreich. Wien: Geologische Bundesanstalt.

Linner, M., Reitner, J.M. & Pavlik, W. (2013). GK50 Blatt 179 Lienz. Geologische Karte der Republik Österreich. Wien: Geologische Bundesanstalt.

Pestal, G. (2014). GK50 Blatt 154 Rauris, unpublished manuscript map. Geologische Karte der Republik Österreich. Wien: Geologische Bundesanstalt.

Pestal, G., Hejl, E., Egger, H., Van Husen, D., Linner, M., Mandl, G.W., Moser, M., Reitner, J., Rupp, C. & Schuster, R. (2005). Geologische Karte von Salzburg 1: 200000. Wien: Geologische Bundesanstalt.

Complementary reconaissance work and small-scale mapping was conducted by the authors in several parts of the map (2015-2019).

Appendix G

Cross Sections of the Seidlwinkl Sheath Fold

Cross-sections of the Seidlwinkl sheath fold, central Tauern Window

Scale 1:25000. Legend is on the Geological map of the central Tauern Window.

by Philip Groß (October 2019)

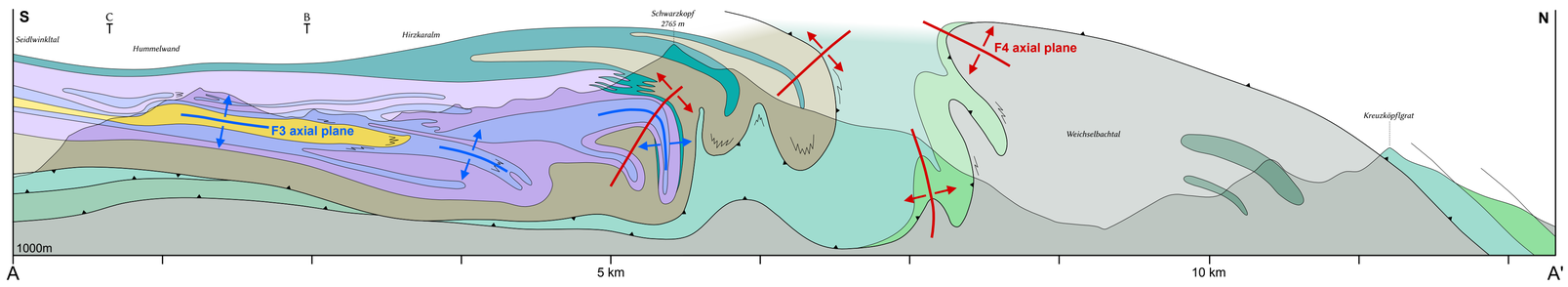

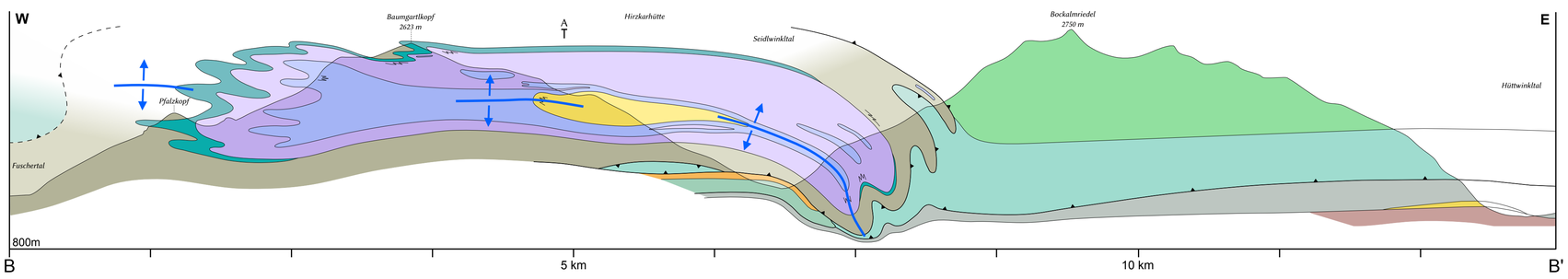

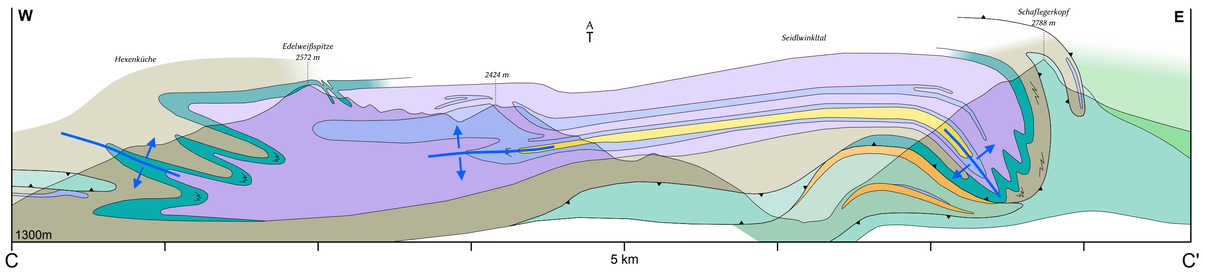

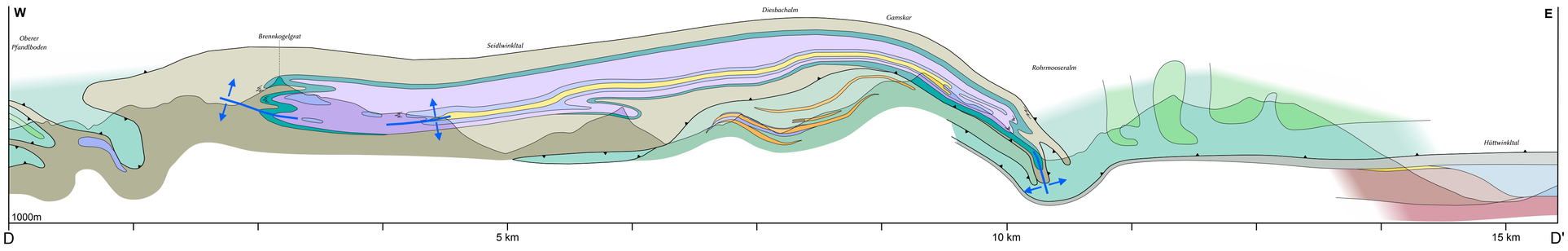

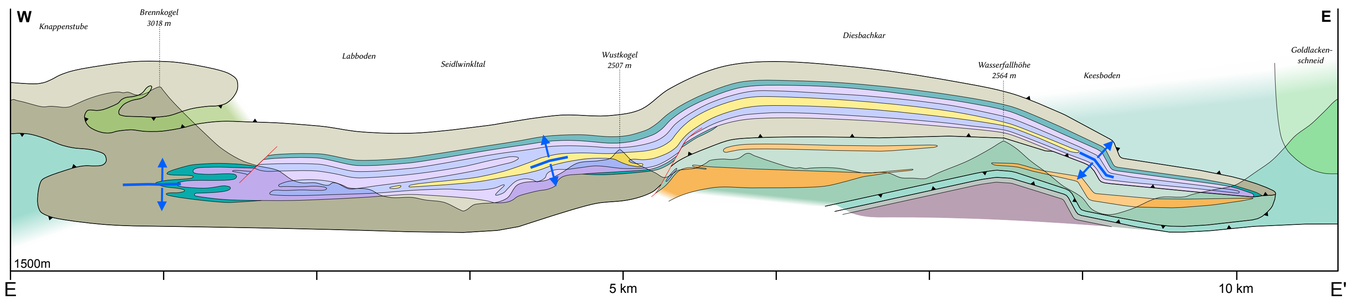

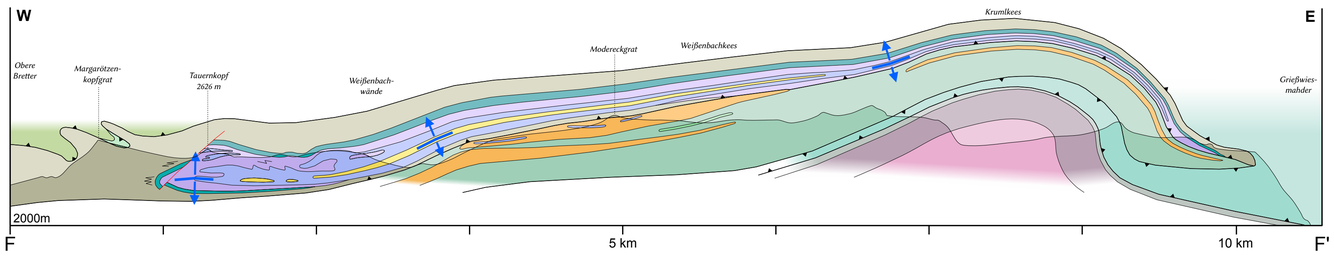

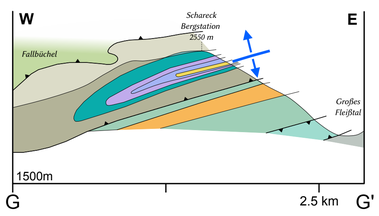

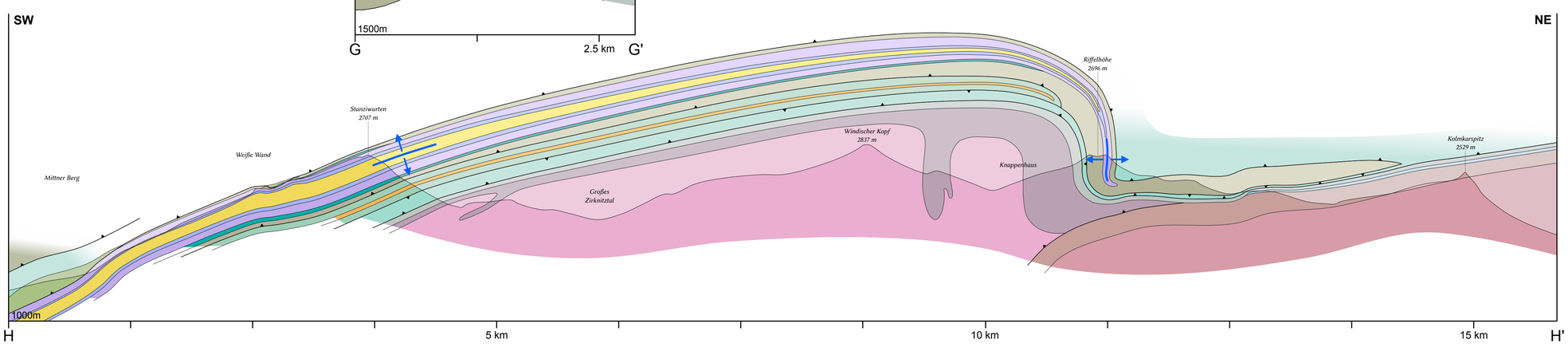

Appendix H

Lithostratigraphic Columns of the Central Tauern Window

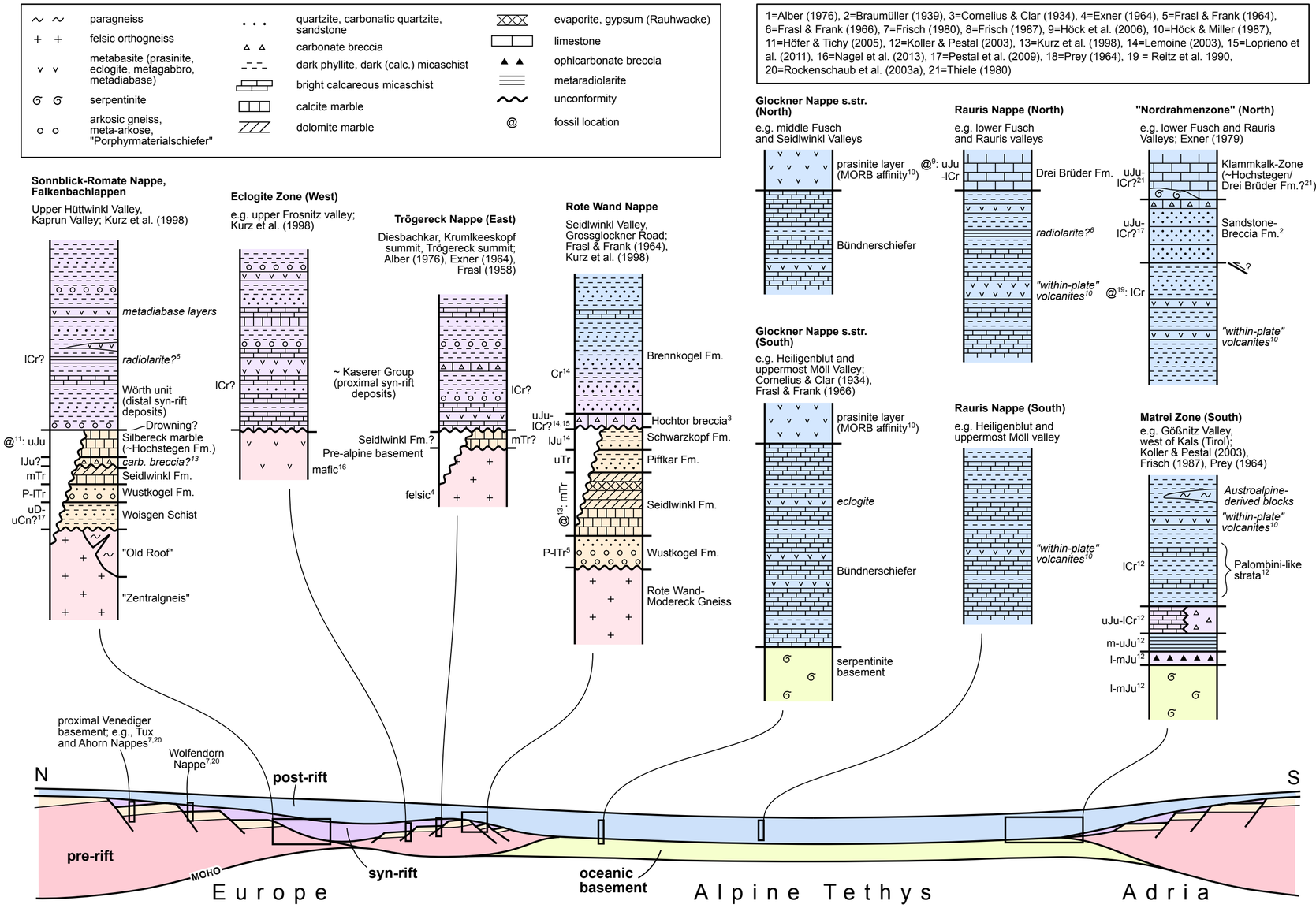
paragneiss
felsic orthogneiss
metabasite (prasinite, eclogite, metagabbro, metadiabase)
serpentinite
arkosic gneiss, meta-arkose, "Porphyrmaterialschiefer"
quartzite, carbonatic quartzite, sandstone
carbonate breccia
dark phyllite, dark (calc.) micaschist
bright calcareous micaschist
calcite marble
dolomite marble
evaporite, gypsum (Rauhwacke)
limestone
ophicarbonate breccia
metaradiolarite
unconformity
fossil location
1=Alber (1976), 2=Braumüller (1939), 3=Cornelius & Clar (1934), 4=Exner (1964), 5=Frasl & Frank (1964), 6=Frasl & Frank (1966), 7=Frisch (1980), 8=Frisch (1987), 9=Höck et al. (2006), 10=Höck & Miller (1987), 11=Höfer & Tichy (2005), 12=Koller & Pestal (2003), 13=Kurz et al. (1998), 14=Lemoine (2003), 15=Loprieno et al. (2011), 16=Nagel et al. (2013), 17=Pestal et al. (2009), 18=Prey (1964), 19 = Reitz et al. 1990, 20=Rockenschaub et al. (2003a), 21=Thiele (1980)
Sonnblick-Romate Nappe, Falkenbachlappen
Upper Hüttwinkl Valley, Kaprun Valley; Kurz et al. (1998)
metadiabase layers
lCr?
radiolarite?6
Wörth unit (distal syn-rift deposits)
Drowning?
@11: uJu
Silbereck marble (~Hochstegen Fm.)
lJu?
carb. breccia?13
mTr
Seidlwinkl Fm.
P-lTr
Wustkogel Fm.
uD-uCn?17
Woisgen Schist
"Old Roof"
"Zentralgneis"
Eclogite Zone (West)
e.g. upper Frosnitz valley; Kurz et al. (1998)
lCr?
mafic16
Trögereck Nappe (East)
Diesbachkar, Krumlkeeskopf summit, Trögereck summit; Alber (1976), Exner (1964), Frasl (1958)
~ Kaserer Group (proximal syn-rift deposits)
lCr?
Seidlwinkl Fm.?
Pre-alpine basement
felsic4
mTr?
Rote Wand Nappe
Seidlwinkl Valley, Grossglockner Road; Frasl & Frank (1964), Kurz et al. (1998)
Cr14
Brennkogel Fm.
uJu-lCr?14,15
Hochtor breccia3
lJu14
Schwarzkopf Fm.
uTr
Piffkar Fm.
@13: mTr
Seidlwinkl Fm.
P-lTr5
Wustkogel Fm.
Rote Wand-Modereck Gneiss
Glockner Nappe s.str. (North)
e.g. middle Fusch and Seidlwinkl Valleys
prasinite layer (MORB affinity10)
Bündnerschiefer
Glockner Nappe s.str. (South)
e.g. Heiligenblut and uppermost Möll Valley; Cornelius & Clar (1934), Frasl & Frank (1966)
prasinite layer (MORB affinity10)
eclogite
Bündnerschiefer
serpentinite basement
Rauris Nappe (North)
e.g. lower Fusch and Rauris valleys
@9: uJu-lCr
Drei Brüder Fm.
radiolarite?6
"within-plate" volcanites10
Rauris Nappe (South)
e.g. Heiligenblut and uppermost Möll valley
"within-plate" volcanites10
"Nordrahmenzone" (North)
e.g. lower Fusch and Rauris Valleys; Exner (1979)
uJu-lCr?21
Klammkalk-Zone (~Hochstegen/ Drei Brüder Fm.?21)
uJu-lCr?17
Sandstone-Breccia Fm.2
@19: lCr
"within-plate" volcanites10
Matrei Zone (South)
e.g. Gößnitz Valley, west of Kals (Tirol); Koller & Pestal (2003), Frisch (1987), Prey (1964)
Austroalpine-derived blocks
"within-plate" volcanites10
lCr12
Palombini-like strata12
uJu-lCr12
m-uJu12
l-mJu12
l-mJu12
proximal Venediger basement; e.g., Tux and Ahorn Nappes7,20
Wolfendorn Nappe7,20
N
S
post-rift
pre-rift
syn-rift
MOHO
oceanic basement
Europe
Alpine Tethys
Adria

Appendix I

RSCM Maps and Profiles

I.1 Map of RSCM Sample Locations

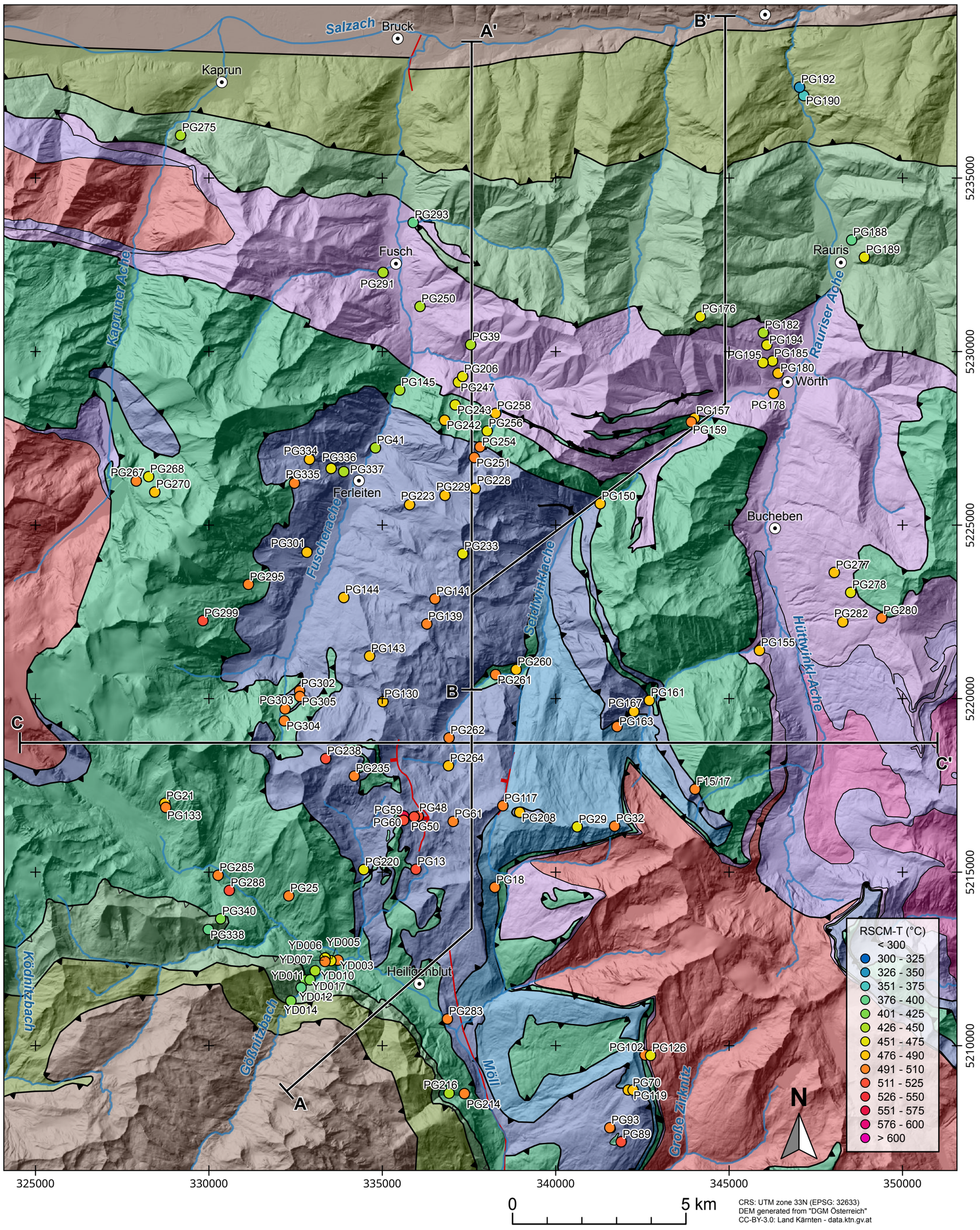
Salzach
Bruck
A'
B'
Kaprun
PG275
PG192
PG190
PG293
Fusch
PG291
PG250
PG188
Rauris
PG189
PG176
PG182
PG194
PG195
PG185
PG180
Wörth
PG178
PG157
PG159
PG39
PG206
PG247
PG145
PG243
PG258
PG242
PG256
PG254
PG251
PG41
PG334
PG336
PG337
PG335
PG267
PG268
PG270
Ferleiten
PG223
PG229
PG228
PG150
Bucheben
PG301
PG233
PG295
PG144
PG141
PG139
PG299
PG143
PG260
PG261
PG302
PG303
PG305
PG304
PG130
PG262
PG161
PG167
PG163
PG277
PG278
PG282
PG280
PG155
B
C
C'
PG238
PG235
PG264
PG21
PG133
PG59
PG60
PG48
PG50
PG61
PG117
PG208
PG29
PG32
F15/17
PG220
PG13
PG285
PG288
PG25
PG340
PG338
PG18
YD006
YD005
YD007
YD003
YD011
YD010
YD017
YD012
YD014
Heiligenblut
PG283
PG102
PG126
PG70
PG119
PG216
PG214
PG93
PG89
A
Salzach
Kaprun
Fuscherache
Seidlwinklache
Hüttwinkl-Ache
Rauriser Ache
Ködnitzbach
Gößnitzbach
Möll
Große Zirknitz
RSCM-T (°C)
< 300
300 - 325
326 - 350
351 - 375
376 - 400
401 - 425
426 - 450
451 - 475
476 - 490
491 - 510
511 - 525
526 - 550
551 - 575
576 - 600
> 600
N
5235000
5230000
5225000
5220000
5215000
5210000
325000
330000
335000
340000
345000
350000
0
5 km
CRS: UTM zone 33N (EPSG: 32633)
DEM generated from "DGM Österreich"
CC-BY-3.0: Land Kärnten - data.ktn.gv.at

I.2 Map of RSCM Peak-Temperatures

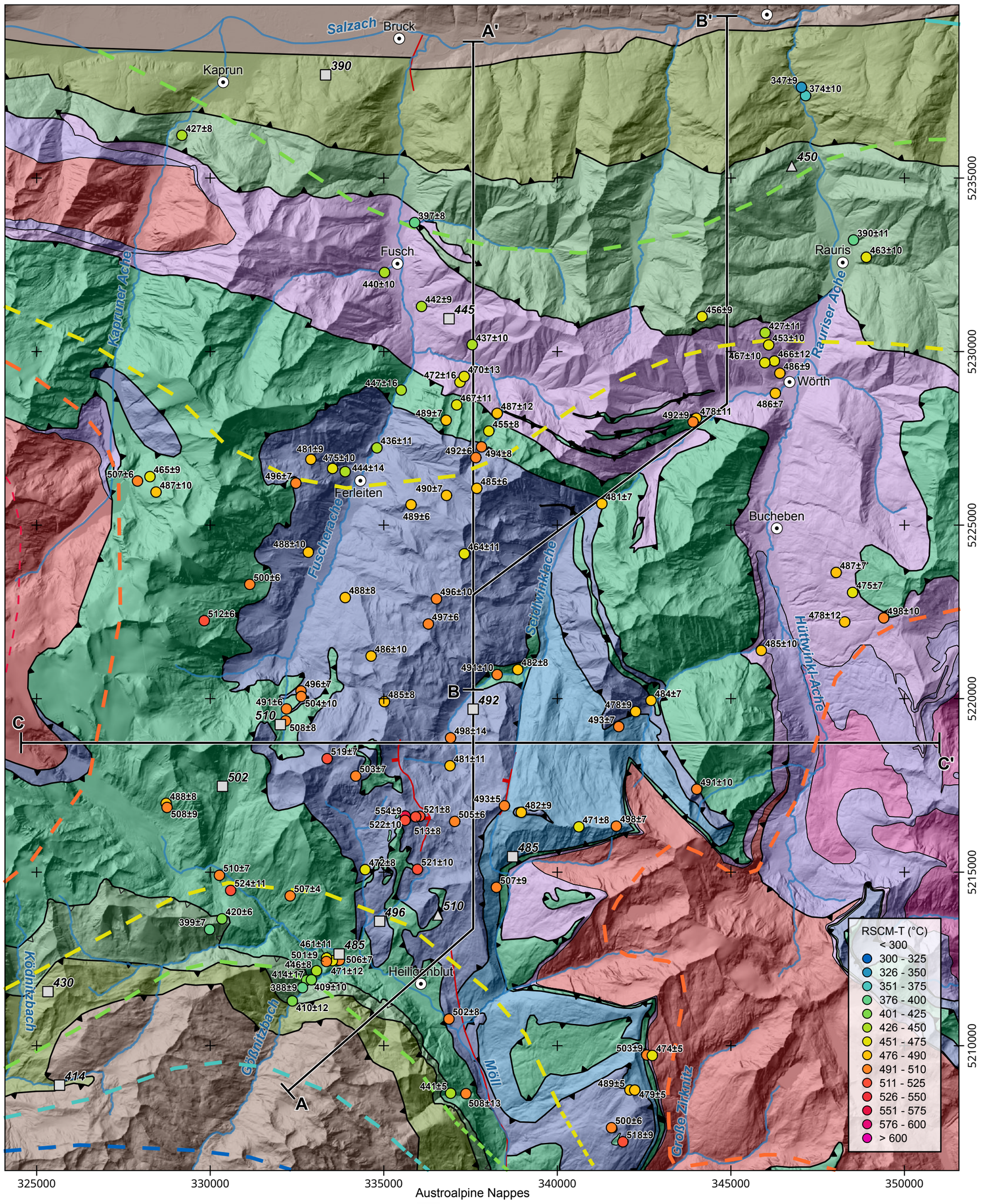
Salzach
Bruck
Kaprun
Fusch
Ferleiten
Rauris
Wörth
Bucheben
Heiligenblut
Kaprunner Ache
Fuscherache
Seidlwinklache
Hüttwinkl-Ache
Rauriser Ache
Ködnitzbach
Gößnitzbach
Möll
Große Zirknitz
A
A'
B
B'
C
C'
390
445
492
450
485
496
510
502
430
414
347±9
374±10
427±8
397±8
390±11
463±10
440±10
442±9
456±9
437±10
427±11
453±10
467±10
466±12
486±9
486±7
472±16
470±13
447±16
467±11
487±12
489±7
492±9
478±11
455±8
436±11
481±9
475±10
444±14
492±6
494±8
507±6
465±9
487±10
496±7
485±6
490±7
481±7
489±6
488±10
464±11
487±7
500±6
488±8
496±10
475±7
512±6
497±6
478±12
498±10
486±10
485±10
491±10
482±8
496±7
491±6
504±10
485±8
484±7
478±9
493±7
508±8
498±14
519±7
503±7
481±11
491±10
488±8
508±9
493±5
482±9
554±9
521±8
505±6
471±8
498±7
522±10
513±8
472±8
521±10
507±9
510±7
524±11
507±4
420±6
399±7
461±11
501±9
506±7
446±8
471±12
414±17
388±9
409±10
410±12
502±8
503±9
474±5
441±5
508±13
489±5
479±5
500±6
518±9
325000
330000
335000
340000
345000
350000
5235000
5230000
5225000
5220000
5215000
5210000
RSCM-T (°C)
< 300
300 - 325
326 - 350
351 - 375
376 - 400
401 - 425
426 - 450
451 - 475
476 - 490
491 - 510
511 - 525
526 - 550
551 - 575
576 - 600
> 600
Legend
Barrovian peak-T contours (°C)
300
350
400
450
500
550
600
observed
inferred
speculative
Cc-Do (°C)
Plg-Amp (°C)
Frank et al. 1987
thrust, inferred
normal fault
fault, undifferentiated
Austroalpine Nappes
undifferentiated
Penninic units
Matrei Zone
Rauris Nappe
Glockner Nappe s.str.
Modereck nappe system
Rote Wand Nappe
Trögereck Nappe
Venediger nappe system
Wörth Unit (post-Variscan cover)
pre-Wörth post-Variscan cover
Sonnblick and Riffl nappes basement
Romate Nappe basement
0
5 km
CRS: UTM zone 33N (EPSG: 32633)
DEM generated from "DGM Österreich"
CC-BY-3.0: Land Kärnten - data.ktn.gv.at
N

I.3 Profiles with RSCM Sample Locations

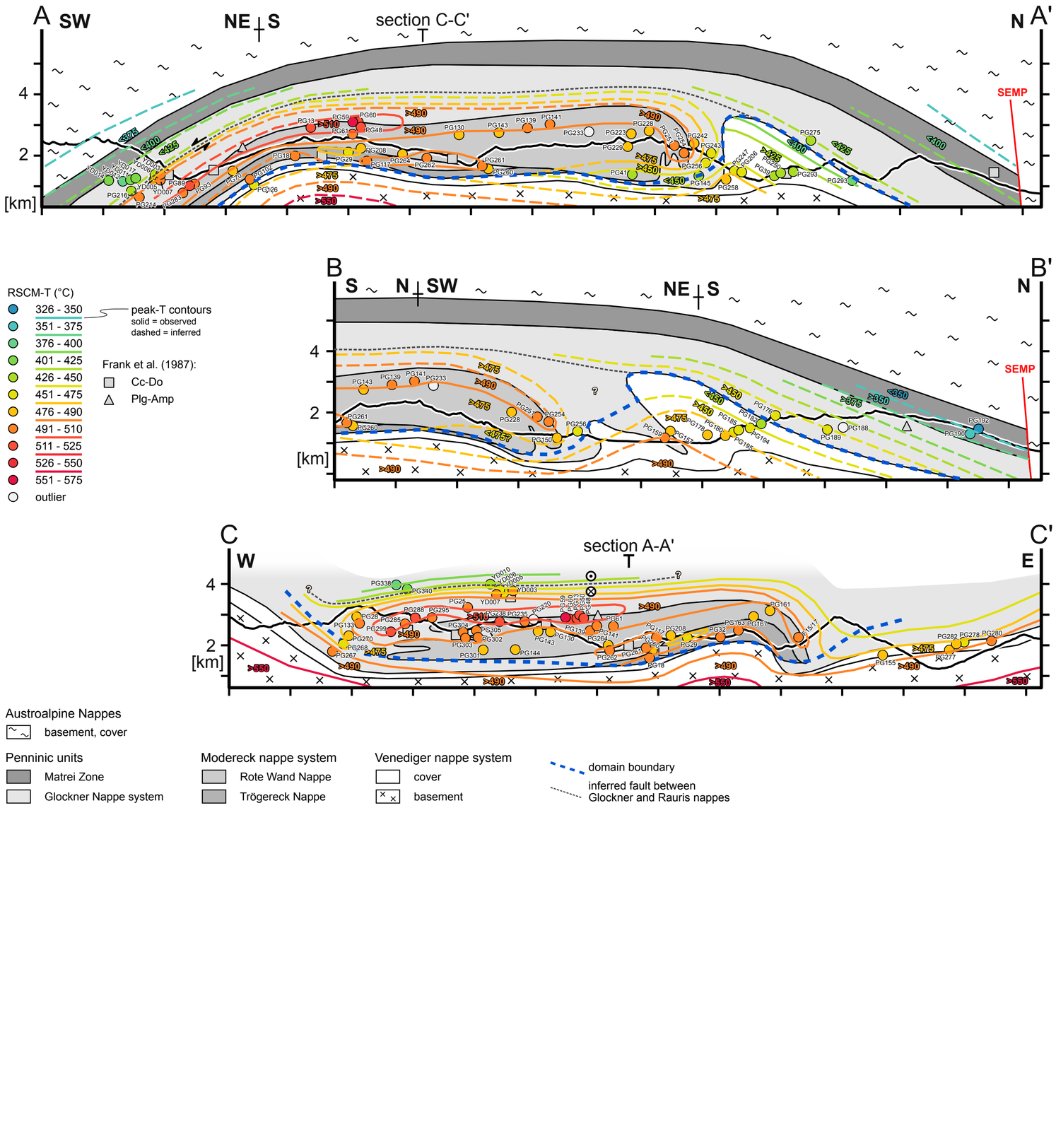
A SW
NE S
section C-C'
T
N A'
SEMP
[km]
B S N SW
NE S
B' N
C W
section A-A'
T
E C'
RSCM-T (°C)
326 - 350
351 - 375
376 - 400
401 - 425
426 - 450
451 - 475
476 - 490
491 - 510
511 - 525
526 - 550
551 - 575
outlier
peak-T contours
solid = observed
dashed = inferred
Frank et al. (1987):
Cc-Do
Plg-Amp
Austroalpine Nappes
basement, cover
Penninic units
Matrei Zone
Glockner Nappe system
Modereck nappe system
Rote Wand Nappe
Trögereck Nappe
Venediger nappe system
cover
basement
domain boundary
inferred fault between
Glockner and Rauris nappes

I.4 Profiles with RSCM temperatures

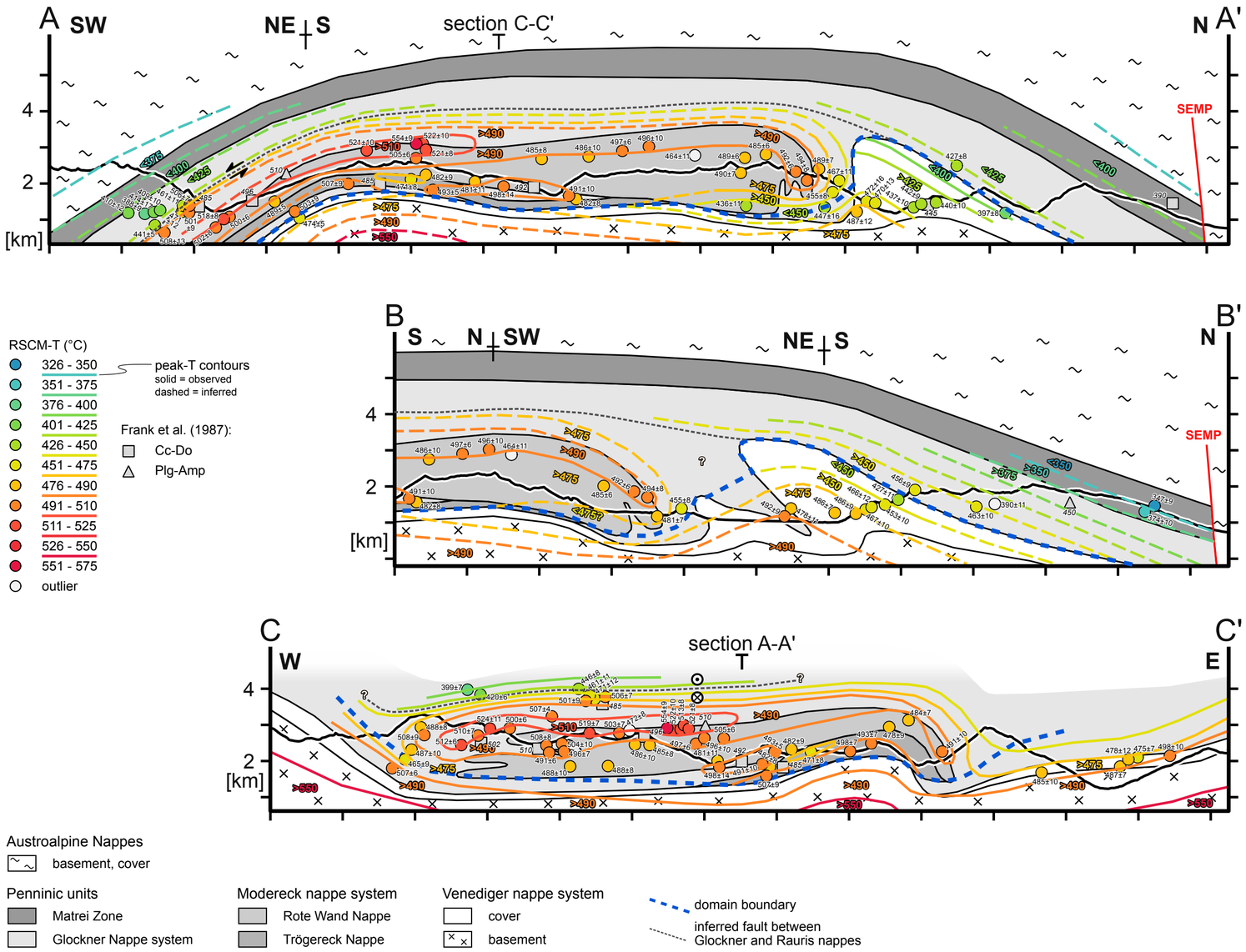
A SW
NE S
section C-C'
T
N A'
SEMP
[km]
B S N SW
NE S
B'
C W
section A-A'
T
E C'
RSCM-T (°C)
326 - 350
351 - 375
376 - 400
401 - 425
426 - 450
451 - 475
476 - 490
491 - 510
511 - 525
526 - 550
551 - 575
outlier
peak-T contours
solid = observed
dashed = inferred
Frank et al. (1987):
Cc-Do
Plg-Amp
Austroalpine Nappes
basement, cover
Penninic units
Matrei Zone
Glockner Nappe system
Modereck nappe system
Rote Wand Nappe
Trögereck Nappe
Venediger nappe system
cover
basement
domain boundary
inferred fault between
Glockner and Rauris nappes